

---

# Sensitivity analysis of single storm surges in the Jade-Weser Estuary

---

Von der Fakultät für Bauingenieurwesen und Geodäsie  
der Gottfried Wilhelm Leibniz Universität Hannover

Zur Erlangung des Grades

Doktor der Ingenieurwissenschaften

Doktoringenieur (Dr.-Ing.)

genehmigte Dissertation

von

Dipl.-Ing. (FH) Oliver Lojek, M.Sc.

geboren am 22. Mai 1986

in Siegburg

Hannover, 2020

---

Referent: Prof. Dr.-Ing. habil. Torsten Schlurmann  
Koreferent: Prof. Dr.-Ing. habil. Jürgen Jensen  
Tag der Promotion: 03. Juni 2019

---







## Abstract

Coastal engineering is tasked with designing, constructing and maintaining hydraulic works in the coastal zone. Coastal dikes form a first hard line of defense against impending storm surges, developed waterways ensure safe navigation and developed terminals facilitate maritime trade and are classified as critical coastal infrastructure depending on their individual turnover and criticality.

European Windstorms, intrinsic to Europe, impact the German Bight ten times a year on average, inducing storm surges, eroding coastline stretches and obstructing navigation due to agitated sea states causing large monetary losses, endangering livelihoods and necessitating ensuing repairs. These extra-tropical cyclones develop on the Atlantic Ocean and follow a westward storm trajectory through the North Sea. The German Bight, with its relatively shallow water depth and intricate coastline is located at the impact end of these storm trajectories. Due to the geographic nature this coastline exerts a funneling effect on storm systems with northern or western incident angles. Ubiquitous environmental changes impact atmospheric and hydrospheric processes, which control the formation and evolution of extreme system states such as storm surges. Consequently, the assessment of individual coastal key drivers is an integral part of coastal engineering and research investigating impacts on critical coastal infrastructure and coasts against the background of environmental change.

In this thesis, potential impacts stemming from changes in sea level, estuarine discharge, sea state and aeolian quantities as well as sediment transport, are investigated for the Jade-Weser estuary. Identified changes are simulated employing a numerical open source software suite and evaluated for the transshipment complex Wilhelmshaven lining the Inner Jade, comprising several critical terminals. A comprehensive model quality assessment is carried out and demonstrates the well-suited character of the model to reproduce the complex hydrodynamics, sea states, atmospheric conditions and induced morphological changes. Storm research scenarios are developed around permutations of coastal key drivers with three different intensity levels for a Scandinavian and a Jutland type storm, which constitute the two major storm types impacting the German Bight. Impacts on hydrodynamics, waves and morphodynamics are evaluated and residual current and transport patterns compiled.

A juxtaposition of results reveals non-linear amplification effects. Regional sea level rise is attributed as the largest single driver contribution, the second largest impact magnitude is exerted by changes in atmospheric conditions and tertiary effects are attributable to changes in wave conditions. The smallest changes on storm impacts are induced by estuarine discharge. Hydraulic development of the European Container Terminal Wilhelmshaven, a critical coastal infrastructure, induces distinct impacts on current and transport residuals under storm conditions.

**Keywords:** *European Windstorm, Storm surge, Compound event  
Numerical simulation, Critical coastal infrastructure*



## Kurzfassung

Küsteningenieurwesen ist mit der Planung, Errichtung und Erhaltung von Bauwerken in der Küstenzone betraut. Seedeiche bieten Hochwasserschutz vor anbrandenden Sturmfluten, während ausgebaute Fahrwasser die Sicherheit der Küsten- und Seeschifffahrt gewährleisten und Hafenanlagen (Über-)Seehandel ermöglichen und je nach Umschlagmenge und Güterart als kritische Infrastrukturen klassifiziert werden.

Europäische Sturmzyklone treffen die Deutsche Bucht im Durchschnitt zehn Mal pro Jahr und verursachen Sturmfluten, erodieren Küstenvorländer und beeinträchtigen die Schifffahrt. Sturmschäden belaufen sich jährlich auf Milliarden Euro und erfordern Ertüchtigungen von Küstenbauwerken. Diese Sturmzyklone entstehend über dem Atlantik und folgen einer Westzugbahn, die sie über Nordeuropa und die Nordsee ziehen lässt, wo sie die Deutsche Bucht mit ihrer geringen Wassertiefe und verwinkelten Küstenlinie treffen. Sich ändernde Umweltbedingungen beeinflussen atmosphärische sowie hydrosphärische Prozesse gleichermaßen, die für die Entwicklung und Zugbahn extremer Systemzustände wie Orkane und Sturmfluten entscheidend sind. Folgerichtig ist die Identifikation und Erforschung von individuellen Schlüsselprozessen, die maßgeblich zur Küstenentwicklung beitragen und potentielle Auswirkungen auf systemkritische Küsteninfrastruktur aufweisen, ein integraler Bestandteil der Forschung im Küsteningenieurwesen.

Im Rahmen dieser Arbeit werden Auswirkungen untersucht, die sich durch Meeresspiegelanstieg, erhöhten Binnenlandabfluss, verstärkten Seegang sowie intensivierten Wind und Druckfelder für das Jade-Weser Ästuar ergeben. Identifizierte Änderungen werden mit einem quelloffenen numerischen prozessbasierten Modell berechnet und für den Hafenkomples Wilhelmshaven in der Innenjade, der teilweise kritische Infrastrukturen umfasst, ausgewertet. Ein umfassender Vergleich mit Beobachtungsdaten zeigt, dass das Modell in der Lage ist, komplexe hydrodynamische Prozesse aber auch Seegang, Atmosphärische Prozesse und induzierten Sedimenttransport abzubilden. Sturmszenarien mit drei unterschiedlichen Amplifikationsniveaus für die Schlüsselprozesse werden entwickelt und Einzel- sowie Kombinationswirkung untersucht. Auswirkungen auf die Hydromechanik, Wellenausbreitung und Morphodynamik werden untersucht und Residuale Strömungs- und Transportmuster der zwei Sturmtypen studiert.

Eine Gegenüberstellung der Ergebnisse zeigt nicht-lineare Wechselwirkungen der einzelnen Prozesse auf, die z.T. verstärkend wirken. Lokaler Meeresspiegelanstieg weist die größte Wirkamplitude auf, Atmosphärische Änderungen zeigen die zweitstärksten Auswirkungen und Wellen die drittstärkste. Den kleinsten Einfluss auf die Sturmflutparameter zeigt der Binnenlandabfluss. Wasserbauliche Änderungen durch den geplanten Ausbau des Europäischen Container Terminals Wilhelmshaven, einer kritischen Küsteninfrastruktur, weist einen starken Einfluss auf Residuale Strömungs- und Transportmuster unter Sturmbedingungen auf.

**Schlagworte:** *Orkan, Sturmflut, Zusammengesetztes Ereignis, Numerische Simulation, kritische Küsteninfrastruktur*







## Acknowledgements

This study bears no administrative framework but is the synthesis of numerous previous research assignments along the German North Sea coast as well as personal experiences of storm surges, which lead to the formulation of the research questions within this thesis.

I am very thankful to my supervisor, Prof. Dr. habil. Torsten Schlurmann, who gave me the chance to freely develop the research questions and approaches of this thesis. I greatly appreciate the years of coastal engineering research across various projects I was granted, which provided a broad view on a multifaceted discipline covering exclusive, sometimes laborious but always extremely rewarding field campaigns as well as challenging numerical modelling of coastal processes including the acquisition and installment of electronic data processing infrastructure as well as field instrumentation and deployment.

I would also like to express my gratitude to Prof. Dr. Jürgen Jensen for agreeing to becoming the second reviewer.

The coastal engineering research staff at the Ludwig-Franzius-Institute constitutes a very ambitious and inspiring team of coastal researches working in many different fields, creating a very diverse and easily enjoyable working environment. I am especially thankful to my colleagues and friends for always having an open ear, giving feedback, insights and ideas as well as lively and invigorating discussions on scientific as well as societal topics. I will never have to look up the definition of team in a dictionary again.

The most wholehearted and warm gratitude go to my family, who had to cope with me missing a lot of events and family life as I set out on a way into the fascinating world of research and scholarship unraveling the mysteries of the land-water interface.

Special thanks go to Christina who endured my near constant preoccupation with this thesis and chaperoned and motivated me finalizing it.



## Contents

<b>Abstract</b>	<b>i</b>
<b>Kurzfassung</b>	<b>iii</b>
<b>List of Figures</b>	<b>x</b>
<b>List of Tables</b>	<b>xiii</b>
<b>Symbols</b>	<b>xiv</b>
<b>Acronyms</b>	<b>xv</b>
<b>1 Introduction</b>	<b>1</b>
1.1 Motivation . . . . .	2
1.2 Objectives . . . . .	4
1.3 Outline . . . . .	6
<b>2 State of science on climate change research</b>	<b>7</b>
2.1 Global Climate Change and Impact Research . . . . .	8
2.1.1 Modeling climate change related impacts . . . . .	9
2.1.2 Main drivers for coastal regions . . . . .	10
2.1.3 Impact study types . . . . .	12
2.2 Extreme event definition . . . . .	12
2.2.1 Examples . . . . .	14
2.2.2 European Windstorm . . . . .	15
2.2.3 Storm surge events . . . . .	19
2.2.4 Event attribution . . . . .	21
2.2.5 Attribution frameworks . . . . .	21
2.3 Modes of variability and related impacts . . . . .	24
2.3.1 Sea level . . . . .	25
2.3.2 Tidal dynamics . . . . .	28
2.3.3 Storms . . . . .	29
2.3.4 Wind . . . . .	34
2.3.5 Waves . . . . .	36
2.3.6 Extreme sea level . . . . .	38
2.3.7 Discharge . . . . .	41
2.3.8 Sediment delivery . . . . .	44
2.3.9 Hydraulic works . . . . .	47
2.4 Research focus area . . . . .	55
2.4.1 Jade Weser Estuary . . . . .	55



2.4.2	Brief hydraulic history . . . . .	58
2.4.3	Recent hydraulic development . . . . .	61
2.4.4	Critical coastal infrastructure . . . . .	62
2.4.5	Climate impact research . . . . .	65
<b>3</b>	<b>Methodology</b>	<b>71</b>
3.1	Storm reference scenarios . . . . .	71
3.1.1	European Windstorm Christian . . . . .	73
3.1.2	European Windstorm Xaver . . . . .	74
3.2	Storm research scenarios . . . . .	76
3.2.1	Mean sea level change . . . . .	78
3.2.2	Wind speed change . . . . .	78
3.2.3	Wave changes . . . . .	78
3.2.4	Extreme Sea Level changes (external surge) . . . . .	79
3.2.5	Discharge changes . . . . .	81
3.2.6	Constructive changes . . . . .	81
3.3	Atmospheric Reanalysis Data . . . . .	83
3.4	Numerical modeling . . . . .	85
3.4.1	Processes and scales . . . . .	86
3.4.2	Model . . . . .	88
3.5	Jade-Weser-Model . . . . .	90
3.5.1	Active boundary conditions . . . . .	92
3.5.2	Computational sediment inventory . . . . .	94
3.6	Base model configuration . . . . .	97
3.6.1	Initial sediment distribution and transport . . . . .	97
3.6.2	Bed roughness coefficient . . . . .	99
3.6.3	Chosen time steps . . . . .	101
3.7	Calibration and Validation . . . . .	102
3.7.1	Water Levels . . . . .	104
3.7.2	Tidal characteristics . . . . .	105
3.7.3	Current velocities . . . . .	108
3.7.4	Atmospheric parameters . . . . .	111
3.7.5	Wave . . . . .	112
3.7.6	Sediments . . . . .	114
<b>4</b>	<b>Results</b>	<b>119</b>
4.1	Hydrodynamic impact . . . . .	119
4.1.1	Water levels . . . . .	120
4.1.2	Storm surge volume . . . . .	122
4.1.3	Current velocities along the Jade . . . . .	127

4.1.4	Residual current velocities . . . . .	133
4.2	Wave impact . . . . .	140
4.2.1	Significant wave height impact . . . . .	141
4.2.2	Wave steepness impact . . . . .	144
4.2.3	Wave reach impact . . . . .	147
4.3	Morphologic impact . . . . .	151
4.3.1	Net sediment volume changes . . . . .	151
4.3.2	Morphologic bed evolution . . . . .	156
4.3.3	Hydraulic development scenario . . . . .	166
4.4	Coastal key driver impacts . . . . .	167
<b>5</b>	<b>Summary and Conclusion</b>	<b>171</b>
5.1	Summary . . . . .	171
5.2	Coastal key driver impacts . . . . .	172
5.3	Concluding remarks . . . . .	175
5.4	Outlook . . . . .	179
	<b>References</b>	<b>181</b>
<b>A</b>	<b>Appendix</b>	<b>213</b>
A.1	Curriculum Vitae . . . . .	214
A.2	Model in- and outputs and featured resolutions . . . . .	215
A.3	Reclassified sediment sample distribution . . . . .	216
A.4	Decomposition of tide gauge signal for storm surge events . . . . .	217
A.5	Barometric deep sea surge potential . . . . .	218
A.6	Sectional Weser fairway . . . . .	219
A.7	Multibeam survey of Wilhelmshaven New Outer Harbour . . . . .	220
A.8	Scour measurement between the ECTW and the BTW . . . . .	221
A.9	Simulation results for Wilhelmshaven . . . . .	222
A.10	Summary terms for evidence and agreement . . . . .	222
A.11	KRITIS threshold definitions . . . . .	223
A.12	Residual storm surge currents . . . . .	224
A.13	Hydraulic intervention scenario . . . . .	241



## List of Figures

1.1	European Windstorm statistics . . . . .	3
1.2	German Bight with the Jade-Weser Region . . . . .	5
2.1	Global mean surface temperature anomaly . . . . .	7
2.2	Conceptual IMLAST extra tropical cyclone (ETC) model . . . . .	17
2.3	ETC Xaver induced surge levels in the focus region . . . . .	19
2.4	Atlantic multidecadal oscillation (AMO) signal . . . . .	24
2.5	Trends in storm related research studies . . . . .	33
2.6	Wave related Frequencies and Periods . . . . .	36
2.7	Extreme sea levels (ESLs) at the tide gauge Wilhelmshaven Alter Vorhafen . . . . .	39
2.8	Intschede monthly discharge stages and Weser catchment area. . . . .	43
2.9	North Sea sediment influx and Anglian plume . . . . .	45
2.10	Coastal defense spending of Lower Saxony . . . . .	48
2.11	Research focus region . . . . .	55
2.12	The Jade Weser Estuary . . . . .	56
2.13	Jade fairway with hydraulic works a) and associated tidal parameters b) . . . . .	57
2.14	Current velocities observed in the Jade . . . . .	59
2.15	Historic coastal evolution of the German North Sea coast . . . . .	60
2.16	Development of the Mean Tidal highwater (MHW) between 1900 to 2017 . . . . .	62
2.17	Hydraulic works along the Jade Fairway . . . . .	63
2.18	Potential flood extent for extreme surge event . . . . .	67
3.1	Hydro-meteorologic quantities & magnitudes of ETC Christian . . . . .	73
3.2	Hydro-meteorologic quantities & magnitudes of ETC Xaver . . . . .	75
3.3	Literature based ranges of Coastal main drivers . . . . .	76
3.4	Xaver related surge levels a) and gauge locations b) . . . . .	79
3.5	Tidal water level observation during Xaver . . . . .	80
3.6	Planned hydraulic works and development of the Weser fairway . . . . .	82
3.7	Planned hydraulic works and development of the Jade fairway . . . . .	83
3.8	CoastDat2 data for European Windstorm Xaver . . . . .	84
3.9	Morphologic units with associated temporal and spatial scales . . . . .	87
3.10	Conceptual flow chart of Delft3D-FLOW/WAVE/MOR . . . . .	89
3.11	Delft3D FLOW/MOR and WAVE model domain . . . . .	91
3.12	Salinity and Temperature boundary condition . . . . .	93
3.13	Sediment data for the Model domain . . . . .	95
3.14	Sediment sample distributions . . . . .	96
3.15	Morphologic domain response dependant on reclassification pattern . . . . .	98
3.16	Bed roughness coefficients . . . . .	100
3.17	Observation data network . . . . .	103

3.18	Observation and Simulation values for water levels . . . . .	104
3.19	Simulated partial tidal constituents . . . . .	106
3.20	Tidal water levels & currents observed at the tidal gauging station Schillig and D5 respectively . . . . .	108
3.21	Tidal current velocities and directions simulated at D5 . . . . .	109
3.22	Simulated and observed ebb and flood current magnitudes and duration . .	110
3.23	Observed and simulated wind direction (a) and speed (b) . . . . .	111
3.24	Observed and simulated significant wave height $H_{1/3}$ . . . . .	113
3.25	Observed and simulated peak wave period $T_p$ . . . . .	113
3.26	Morphodynamic signal analysis polygon I . . . . .	115
3.27	Morphodynamic signal analysis polygon V . . . . .	116
4.1	Mean tidal high and low water . . . . .	119
4.2	Evolution of storm surge water levels for Windstorm Christian . . . . .	120
4.3	Evolution of storm surge water levels for Windstorm Xaver . . . . .	121
4.4	Simulated storm surge volume under European Windstorm Christian . . . .	123
4.5	Envelope of simulated surge volume changes under Windstorm Christian .	124
4.6	Envelope of simulated surge volume changes under Windstorm Xaver . . . .	126
4.7	Simulated tidal velocities under European Windstorm Christian . . . . .	128
4.8	Simulated tidal velocities under European Windstorm Xaver . . . . .	131
4.9	Simulated residual storm surge currents - Christian - Outer Jade . . . . .	133
4.10	Simulated residual storm surge currents - Xaver - Outer Jade . . . . .	136
4.11	Residual currents in the hydraulic intervention scenario . . . . .	138
4.12	Residual currents in the hydraulic intervention scenario . . . . .	139
4.13	Simulated significant wave heights for reference Windstorm Christian . . .	140
4.14	Simulation results for sig. wave height for ETC Christian . . . . .	141
4.15	Simulation results for sig. wave height for ETC Xaver . . . . .	143
4.16	Wave steepness development for Windstorm Christian . . . . .	145
4.17	Wave steepness development for Windstorm Xaver . . . . .	146
4.18	Simulation results along wave transect for ETC Christian . . . . .	148
4.19	Simulation results along wave transect for ETC Christian . . . . .	149
4.20	Simulation results along wave transect for ETC Xaver . . . . .	150
4.21	Net sediment changes for European Windstorm Christian. . . . .	151
4.22	Net sediment changes for European Windstorm Christian. . . . .	152
4.23	Net sediment changes for European Windstorm Christian. . . . .	153
4.24	Net sediment changes for European Windstorm Xaver. . . . .	154
4.25	Net sediment changes for European Windstorm Xaver. . . . .	155
4.26	Net sediment changes for European Windstorm Xaver. . . . .	156
4.27	Morphological impact reference scenario Christian. . . . .	157
4.28	Morphological impact medium scenario Christian. . . . .	159



4.29 Morphological impact extreme scenario Christian. . . . .	160
4.30 Morphological impact reference scenario Xaver. . . . .	162
4.31 Morphological impact medium scenario Xaver. . . . .	163
4.32 Morphological impact extreme scenario Xaver. . . . .	164
4.33 Morphological impact under hydraulic development. . . . .	166
4.34 Impacts of coastal key drivers for storm Christian . . . . .	167
4.35 Impacts of coastal key drivers for storm Christian . . . . .	169
A.1 Sediment sample distributions . . . . .	216
A.2 Tidal water level observation during Christian . . . . .	217
A.3 Tidal water level observation during Elon . . . . .	217
A.4 Barometric pressure and external surge potential . . . . .	218
A.5 Outer and Lower Weser fairway . . . . .	219
A.6 Wilhelmshaven New Outer Harbour survey . . . . .	220
A.7 European Container Terminal Wilhelmshaven survey . . . . .	221
A.8 New Outer Harbour Wilhelmshaven simulation results for Xaver . . . . .	222
A.9 IPCC terminology for trend description . . . . .	222
A.10 Simulated residual storm surge currents - Christian - Outer Jade . . . . .	224
A.11 Simulated residual storm surge currents - Christian - Outer Jade . . . . .	225
A.12 Simulated residual storm surge currents - Christian - Outer Jade . . . . .	226
A.13 Simulated residual storm surge currents - Christian - Outer Jade . . . . .	227
A.14 Simulated residual storm surge currents - Christian - Outer Jade . . . . .	228
A.15 Simulated residual storm surge currents - Christian - Outer Jade . . . . .	229
A.16 Simulated residual storm surge currents - Christian - Outer Jade . . . . .	230
A.17 Simulated residual storm surge currents - Christian - Outer Jade . . . . .	231
A.18 Simulated residual storm surge currents - Xaver - Outer Jade . . . . .	232
A.19 Simulated residual storm surge currents - Xaver - Outer Jade . . . . .	233
A.20 Simulated residual storm surge currents - Xaver - Outer Jade . . . . .	234
A.21 Simulated residual storm surge currents - Xaver - Outer Jade . . . . .	235
A.22 Simulated residual storm surge currents - Xaver - Outer Jade . . . . .	236
A.23 Simulated residual storm surge currents - Xaver - Outer Jade . . . . .	237
A.24 Simulated residual storm surge currents - Xaver - Outer Jade . . . . .	238
A.25 Simulated residual storm surge currents - Xaver - Outer Jade . . . . .	239
A.26 Simulated residual storm surge currents - Xaver - Outer Jade . . . . .	240
A.27 Residual currents in the hydraulic intervention scenario . . . . .	241
A.28 Residual currents in the hydraulic intervention scenario . . . . .	242
A.29 Residual currents in the hydraulic intervention scenario . . . . .	243
A.30 Residual currents in the hydraulic intervention scenario . . . . .	244



## List of Tables

2.1.1 Main drivers for coastal regions . . . . .	10
2.2.1 Storm surge definition according to the BSH . . . . .	13
2.2.2 Very heavy storm surge levels at the German North Sea Coast . . . . .	20
2.3.1 Projected global mean sea level changes . . . . .	26
2.3.2 Overview over different sea level rise analysis. . . . .	27
2.3.3 Overview of projected changes in wind speed. . . . .	35
2.3.4 Wave evolution related processes . . . . .	37
2.3.5 Overview of projected changes in wind waves. . . . .	38
2.3.6 Overview of projected changes in Weser flood discharge. . . . .	44
2.4.1 Critical infrastructure in the Jade . . . . .	65
2.4.2 KRITIS-V storm surge impact classification . . . . .	68
3.1.1 Reference Storm events . . . . .	72
3.2.1 Storm research scenarios . . . . .	77
3.5.1 Reclassified sediment fractions . . . . .	97
3.7.1 Delft3D Hydrodynamic calibration & validation coefficients . . . . .	105
3.7.2 Delft3D Hydrodynamic calibration & validation coefficients . . . . .	107
3.7.3 Delft3D Hydrodynamic calibration & validation coefficients . . . . .	110
3.7.4 Delft3D wind calibration & validation parameters . . . . .	112
3.7.5 Delft3D SWAN wave calibration & validation parameters . . . . .	114
3.7.6 Delft3D morphodynamic calibration & validation parameters . . . . .	116
4.1.1 Surge levels for the New Outer Harbor Wilhelmshaven tide gauge . . . . .	122
4.1.2 Process related surge volumes for reference European Windstorm Christian . . . . .	124
4.1.3 Process related surge volumes for European Windstorm Xaver . . . . .	126
4.1.4 Process related hydrodynamic impacts for EU Windstorm Christian . . . . .	129
4.1.5 Process related hydrodynamic impacts for EU Windstorm Xaver . . . . .	132
4.2.1 Wave steepness during Windstorm Christian . . . . .	146
4.2.2 Wave steepness during Windstorm Xaver . . . . .	147
A.2.1 Model in- and outputs . . . . .	215



## Symbols

$H_{1/3}$	Significant wave height (m)
$T_p$	Wave period (s)
$kt$	knot ( $\text{ms}^{-1}$ )
$MSS$	Murphy Skill Score (0 – 1)
$C_d$	drag coefficient as a measure for hydraulic roughness (real)
$D_{50}$	mean grain size diameter (mm)
$H$	local water depth (m)
$P_e$	Probability of exceedance (real)
$RI$	return interval (yrs)
$c_{amp}$	amplitude of tidal constituent $c$ (m)
$\omega_c$	frequency of tidal constituent $c$ (Hz)
$\phi_c$	phase of tidal constituent $c$ ( $^\circ$ )
$c$	tidal constituent (–)
$\delta$	difference (real)
$\delta t$	time step (s)
$\Delta x$	grid cell extent in x direction (m)
$\Delta y$	grid cell extent in y direction (m)
$\eta$	observed tidal water level time series (–)
$\gamma_{amp}$	relative sea surface distortion (m)
$g$	gravity constant ( $\text{ms}^{-1}\text{m}$ )
$h$	water level (m)
$\mu\text{m}$	micro meter ( $1 \times 10^{-6}\text{m}$ )
$m$	realizations (real number)
$n_c$	number of used tidal constituents (real)
$n$	sample size (real number)
$\phi_{asy}$	relative surface phase of tidal constituent ( $^\circ$ )
$\Phi$	porosity parameter (%)
$\rho_s$	specific density ( $\text{kgm}^{-3}$ )
$t$	single time step (s)
$u_{10}$	wind speed measured 10 m above ground ( $\text{ms}^{-1}$ )
$L_{wave}$	wave length (m)
$T_{wave}$	wave period (s)

## Acronyms

ACE	accumulated cyclone energy (10e4kt)
AMO	Atlantic multidecadal oscillation
AMOC	Atlantic meridional overturning circulation
AR5	5th Assessment Report (Stocker et al., 2013)
BBK	Federal Office for Civil Protection and Disaster Assistance ( <i>Ger.: Bundesamt für Bevölkerungsschutz und Katastrophenhilfe - BBK</i> )
BC	before Christ
Bft	Beaufort
BMI	Federal Ministry of the Interior ( <i>Ger.: Bundesministerium des Inneren</i> )
BSH	Federal Maritime and Hydrographic Agency ( <i>Ger.: Bundesamt für Seeschifffahrt und Hydrographie</i> )
BSS	Brier Skill Score
BTW	Bulk Terminal Wilhelmshaven
CD	chart datum
CFL	Courant-Friedrichs-Lewy
CJ	Cold Jet
CMIP	Coupled Model Intercomparison Project
DAO	decadal Atlantic Oscillation
DIN	German Institute for Standardization ( <i>Ger.: Deutsches Institut für Normierung</i> )
DRR	disaster risk reduction
DTMW	Digital terrain model of the waterbody
DWD	German Weather Service ( <i>deut.: Deutscher Wetterdienst</i> )
ECMWF	European Centre for Medium-Range Weather Forecasts
ECTW	European Container Terminal Wilhelmshaven
ENSO	El Nino Northern Oscillation
ESL	extreme sea level
ETC	extra tropical cyclone



fkM	fairway kilometer
GCM	general circulation model
GHG	green house gas
GMSL	geocentric mean sea level
GMSLR	global mean sea level rise
GMST	global mean surface temperature
HZG	Helmholtz Zentrum Geesthacht
IMLAST	Intercomparison of MID-LAtitude STorm diagnostics
IPCC	International Panel on Climate Change
MHW	mean high water
MLW	mean low water
MSL	mean sea level
MSLR	mean sea level rise
MWH	mean wave height
NAO	North Atlantic oscillation
NHN16	standard elevation zero of 2016 ( <i>Ger.: Normal Höhen Null 2016</i> )
OHC	ocean heat content
PDO	Pacific decadal oscillation
PE	presonal equivalent
PPE	perturbed physics ensemble
RCM	regional climate model
RCP	Representative Concentration Pathway
RI	return interval
RMSE	root mean square error
RMSL	relative mean sea level
RSLR	regional sea level rise
SJ	Sting Jet
SKEB	stochastic kinetic energy backscatter scheme
SLP	sea level pressure

SLR	sea level rise
SNR	signal to noise ratio
SPPT	stochastically perturbed physics ensemble
SRES	special report on emission scenarios
SSC	suspended sediment concentration
SSL	storm surge level
SSR	storm surge residual
SST	sea surface temperature
SWH	significant wave height
TC	tropical cyclone
UNEP	United Nations Environmental Program
UNFCCC	United Nations Framework Convention on Climate Change
WCRP	World Climate Research Program
WHV	Wilhelmshaven
WJ	Warm Jet
WMO	World Meteorological Organization
WRT	Wilhelmshaven Refinery Terminal
WSV	Water and Shipping Directive



## 1 Introduction

Hydromorphology describes the interaction between bedforms present in a water body influencing the local and global fluid mechanics and vice versa. These bedforms can be of natural or anthropogenic origin, covering sand ripples and tidal channels as well as navigational channels, harbors and other components of coastal infrastructure. Natural bedforms, if exposed to tides and waves, are susceptible to dynamic changes in their form and possibly their sedimentological composition. Anthropogenically induced bedforms such as navigational channels and harbor basins predominantly represent subaqueous depressions in the terrain allowing for the draft of vessels, naturally capturing sediments.

Presently, over 40 harbors with adjacent navigational channels located at the German North Sea coast require constant, and expensive maintenance operations due to siltation constituting a man-made problem. The repetitive tidal cycle transports sediments into those siltation prone areas giving rise to the continuous need of dredging operations to guarantee safe navigation. In contrast to regular conditions given over the course of spring-neap tide cycles, single storm events constitute extreme hydrodynamic conditions impacting coastal systems upon landfall.

European Windstorms, intrinsic to Europe, reach wind speeds above 64 knots. These storm systems develop on the Atlantic Ocean and move across Europe. Due to its geographic nature the German Bight, with its relatively shallow water depth and intricate coastline, has a funneling effect on storm systems often amplifying their impact. The detailed relationship of single storm events on siltation and back-filling rates remains an important question to researchers, planners and operators but also for refurbishing and blueprinting coastal structures and especially harbors. Physical or numerical modelling of planned layouts is an established method to investigate possible impacts and deduce implications and financial consequences.

Nevertheless, accurate and detailed observations during storm events are difficult to acquire and few systematic collections of such data are available. Moreover, severe effects are reported from various harbors, which often are faced with non-navigable waters after a storm season. Against the background of climate change and possible connected alterations of storm climate the research question of possible implications for the bed forming characteristics of storm surges gains even more relevance for stakeholders.

## 1.1 Motivation

Critical infrastructure is defined by the Federal Ministry of the Interior (*Ger.: Bundesministerium des Inneren*) (BMI) as:

*"Organizations and institutions of special importance for the country and its people where failure or functional impairment would lead to severe supply bottlenecks, significant disturbance of public order or other dramatic consequences"* (BMI, 2009).

According to the BMI critical infrastructure is classified into nine main sectors, with (nautical) traffic and logistics as well as energy being of focal interest to the objectives of this study (BMVI, 2015a). Consequently, functionality has to be ensured and is of outmost interest to shareholders and responsible managing institutes alike. Engineered structures such as shipping channels, harbor access channels or harbors and marinas impose bathymetric imbalances in the subaquatic geometry of coastal systems. These unnaturally deepened regions provide safe navigation and facilitate maritime trade as well as naval sovereignty. However, given their artificial nature - the environment strives to restore an equilibrium void of anthropogenic sub aquatic structures giving rise to the constant need for dredging and maintenance to keep up the imbalance. Sea ports and marinas as well as their respective naval and terrestrial auxiliary infrastructure constitute thriving land-sea transport-interfaces between countries, which are usually located in sheltered areas along coasts and estuaries (Bray et al., 1997; PIANC, 2004, 2008).

Coastal environments as such are exposed to external driving forces including tidal waves, wind waves, wind and pressure systems, resulting in complex non-linear hydrodynamics, which initiate sediment mobilization and redistribution altering the sea bed and forming a feedback loop onto the hydrodynamic conditions (Bosboom and Stive, 2015).

Vicissitude in external driving forces such as water level or storm patterns due to climate change affect global coastal infrastructure in that the environment for which it was designed and constructed slowly but surely transforms. Man made structures and interventions, i.e. training walls or dredging operations and river bed incisions, additionally influence and transform the hydrosphere. Extreme conditions, given during energy intense storm surge events, challenge not only coastal defenses due to higher wind-waves and wind induced set-up but also impact the sea bed directly - mobilizing and transporting bed material.

European Windstorms are the most loss-relevant natural hazards affecting Central Europe - damaging infrastructure, disrupting nautical traffic and potentially causing loss of life. Given the meteorological extent of storm systems, vast areas and stretches of coastline are impacted, resulting in an average loss and damage of 4 bn. € every season across



Europe, with Germany related data given in figure 1.1.

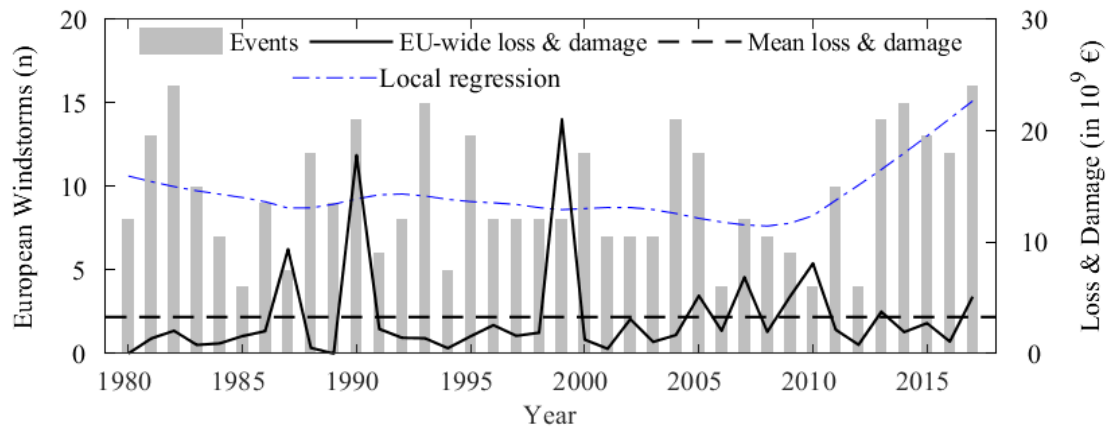


Figure 1.1: European Windstorm statistics giving an overview over the annual occurrence between 1980 and 2018 with inflation-adjusted associated loss and damage volumes (GDV, 2014, 2015, 2016, 2017; statista, 2018; NatCatSERVICE, 2018; MunichRe, 2014, 2017, 2018b).

For Germany, nine out of the ten most expensive natural disasters are European Windstorms (MunichRe, 2018a) - with an average of 9.4 storms forming per year, statistically inflicting 850 mio. € per storm with individual events rivaling tropical hurricane losses ranging from 1.4 to 4.7 bn., € (Xaver, 2013, Christian 2013, Kyrill, 2007) with catastrophic events such as Lothar (1999), costing 5.3 bn., €. Among the globally 40 most expensive natural disasters on record to date 16 are Hurricanes, 6 EU Windstorms, 3 Typhoons and 3 convective thunderstorms all 28 of which occurred during the last decade (SwissRe Sigma, 2017).

The International Panel on Climate Change (IPCC) stated in the most recent report that there is robust evidence for an increase in frequency and intensity in tropical and extra-tropical cyclones forming in the northern Atlantic over the last 50 years (Kossin and Vimont, 2007). Namely hurricanes of category 4 and 5 exhibit a 75% increase since 1970. Furthermore, a distinct pole and eastward shift for ETC tracks is found in observations and this phenomenon is supported by studies based on reanalysis data, which also predict an increase in frequency and intensity (Schneidereit et al., 2007; Vilibić and Šepić, 2010). Dikes and flood protection works constitute the first engineered risk reduction measures with regard to storm surge impacts. Firstly developed centuries ago (Kramer and Rohde, 1992) they are nowadays designed according to national methodologies (KFKI 2002; pp. 12-15) as a first line of defense against local storm surge impacts. However, increasing mean sea level rise (MSLR) rates due to green house gas (GHG) emissions represent a ma-

major challenge for low lying coastlines and coastal infrastructure alike, reducing freeboard of defensive structures as well as amplifying wave and surge related impact levels (Arns et al., 2015, 2017). Accordingly, earth system sciences develop approaches to decipher and project system responses related to minor changes in key drivers such as sea surface temperature (SST) or ocean heat content (OHC) which in turn are used by other science fields, such as hydraulic or coastal engineering, to perform impact studies on smaller and more complex scales emulating physical processes under changing boundary conditions.

Recent winter storm Herwart (2017) impacted the German coast and caused widespread erosion, removing 80 % of the island coastline of Wangerooge and impacting the coastline resulting in beach nourishment measures costing 400.000 € on Wangerooge alone culminating 8 Mio. € (NLWKN, 2018; NDR, 2017). Consequently, assessment and management of coastal systems in response to extreme conditions against the background of climate change constitutes a complex and multifaceted problem. Planning and maintenance of anthropogenic structures within such dynamically evolving systems often requires overarching strategies based on, or influenced by, research and development. Henceforth, potential impacts of selected storm events upon critical coastal infrastructure are investigated combining numerical modelling with field data and scientific projections of future climate scenarios.

## 1.2 Objectives

This thesis focuses on potential impacts of storm surge events on the Jade-Weser Estuary in the light of climate change. Initially formed by storm surges and reshaped by man-made land reclamation, the estuary constitutes a prime-example for storm surge impact research.

The Jade-Weser region is located in the German Bight (see figure 1.2). Given the vast and severe impacts extreme weather events can cause, they draw public and scientific attention alike and give rise to questions such as, whether such events are attributable to climate change and to what extent anthropogenic emissions potentially alter event frequency and magnitude, and what potential impacts might look like. Consistent with societal requirements, science undertakes research efforts to ultimately yield insightful advice to policy makers facilitating decisions and disaster risk reduction (DRR) alike.

Impact assessment studies are a very useful tool for transferring projected changes in climatic drivers from a global or regional to a local scale, elucidating potential socioeconomic as well as environmental ramifications. Initially scenarios with different combinations of potential climate change impacts were employed to investigate regional and local scale effects. Nevertheless, ongoing research calls into question previously established hypothesis such as a linearly increasing tidal range connected to MSLR or changes in storm

surge patterns within the North Sea. More recent findings point to an increasing MSLR, potentially affecting coastal storm surge impacts (Arns et al., 2017; Nerem et al., 2018). Whereas the storm surge climate itself constitutes a very elusive and complex field and potential changes appear vexed by contradictory findings.

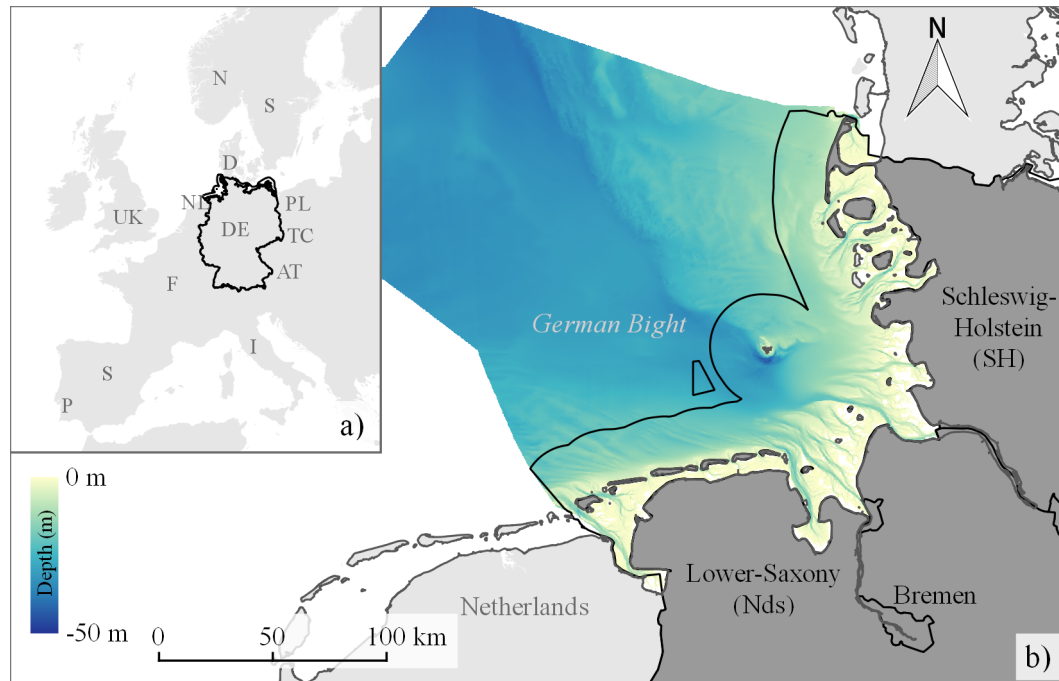


Figure 1.2: German Bight with the Jade-Weser Region in relation to Europe. Bathymetric information is based on Federal Maritime and Hydrographic Agency (Ger.: *Bundesamt für Seeschifffahrt und Hydrographie*) (BSH) data from 2017.

Consequently, headstone of this study forms a literature review focusing on climate change impact research potentially affecting the Jade-Weser estuary, Germany. To gauge confidence and likelihood associated with projected impacts attributable to climate change, the globally accepted methodology developed by the IPCC is employed (Mastrandrea et al., 2011). Evaluating previous impact studies and research findings for the focus region, different scenarios are going to be outlined, comprising different parameter settings to investigate potential impacts under altered storm surge conditions. Impact scenarios defined comprise (1) a Jutland type storm event, (2) a Scandinavian type storm event (3) constructive bathymetry alterations.

Considering varying degrees of confidence and likelihood associated with individual key drivers and projected impacts, constructed storm surge scenarios naturally will exhibit different levels of relevance for practitioners. Given the complexity and highly controversial discussion associated with long term projections of individual parameters for the



end of this century, the study at hand investigates rather short to medium term scenarios with temporal horizons between 2030 to 2050.

The primary objective constitutes the numerical quantification of potential storm surge impacts upon the coastal environment, especially upon morphology and sedimentology of the focus region and its bed forming characteristics. Especially to elucidate morphological impacts in the light of critical coastal infrastructure represented as parametric functions, specifically harbors and different terminals located along the west coast of the inner Jade Bay.

The secondary objective focuses on a possible detection, differentiation and attribution of impacts to individual key drivers. This is achieved conducting driver specific simulations and a subsequent permutation of scenario boundary parameters to conduct sensitivity studies for the Jade-Weser Estuary on processes and effects (i.e. sea states, morphological changes, hydrodynamics) and their non-linear interactions.

The third objective comprises the projection and analysis of potential storm surge impacts related to climate change associated variations in key drivers. Amplification factors for represented processes (i.e. sea state) are researched and integrated into the model simulations to subsequently assess impacts related to climate change and sea level rise (SLR).

### 1.3 Outline

The study at hand is structured as follows, Chapter 2 commences with an introduction to climate change research and developed methodologies, discerns coastal key drivers and closes with a short introduction to the focus region. Chapter 3 draws on the main findings of chapter 2 in combination with field observation data, impact scenarios are derived. Furthermore, the methods employed for numerically simulating the episodic events and evaluating results are given. The ensuing chapter 4 presents results obtained for the various scenarios and discusses them in contrast to findings given in chapter 2. Finally, chapter 5 summarizes the main findings of this study and gives an outlook on potential future research questions.

## 2 State of science on climate change research

A technical stipulation the state of science resembles the third and highest level of scientifically proven and technically realizable aspects (BMJV, 2008). However, the vast increasing quantity of published research articles globally on the topic renders a holistic description of a research topic virtually impossible and translates into an approximation strongly dependant on the access to knowledge limited by journal access regulations, language barriers and temporal resources of the individual researcher. A thermodynamic indicator of present day science for climate change is the global surface temperature anomaly given in figure 2.1.

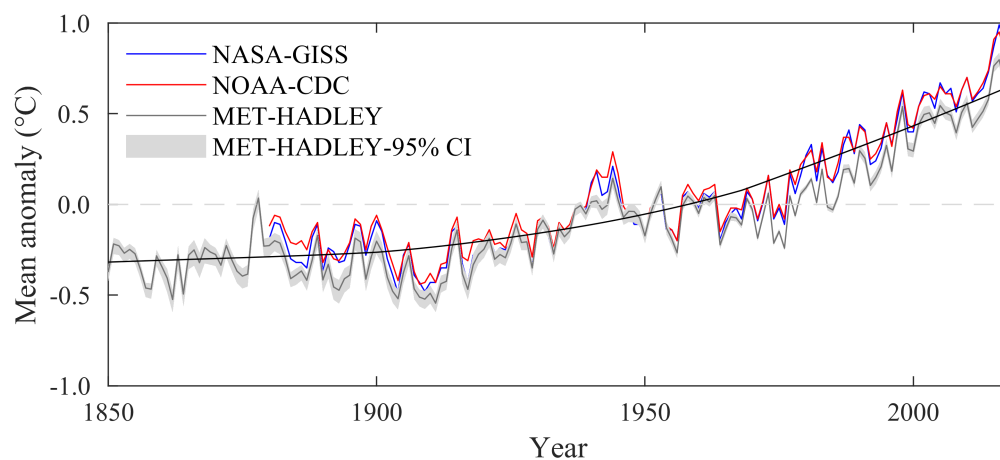


Figure 2.1: Global mean surface temperature anomaly based on data provided by the NASA (Hansen et al., 2010; GISTEMP Team, 2018), the NOAA (Smith et al., 2008; Huang et al., 2018) and the Hadley Center (Brohan et al., 2006).

Earth's climate has been at the attention of early researchers such as Robert Hook (1670) (Davies, 1964) or Wilhelm Gottfried Leibniz (1692) (Leibniz et al., 2014), both investigated fossil records and found they pointed towards warmer climate periods. Leibniz became a co-founder of paleontology, a major sub-field of current climate research investigating i.e. drill cores of arctic ice reconstructing climates of past millennia proving an ubiquitous climate change.

Coming a long way, climate research reached a lot of major milestones throughout the centuries, i.e. John Tyndall (1892) discovered the green house effect and responsible gases or James Croll (1864) described the Ice-Albedo-feedback, both are crucial mechanisms and a focus of earth system sciences (John Tyndall, 1873; Croll, 2009). A physical basis for understanding earth's energy budget was formulated by Max Planck (1900) known as Planck's law paving the way for quantitative calculations as well as simulations (Planck, 1899).

Gilbert Plass (1956) used early computers to calculate atmospheric warming based off atmospheric emission increases and projected anthropogenic increase of  $1^{\circ}\text{C}$  by the year 2000 resembling a 30% increase in  $\text{CO}_2$ , quantifying anthropogenic impact on a warming trend (Plass, 1956). The calculations were commented on by Roger Revelles famous words: "Human beings are now carrying out a large-scale geophysical experiment of a kind that could not have happened in the past nor be reproduced in the future. Within a few centuries we are returning to the atmosphere and oceans the concentrated organic carbon stored in sedimentary rocks over hundreds of millions of years. This experiment, if adequately documented, may yield a far-reaching insight into the processes determining weather and climate." Since then earth system science and research of change related impacts has experienced an unmatched scientific development, culminating in the formation of the IPCC by the United Nations Environmental Program (UNEP) and the World Meteorological Organization (WMO) in order to assimilate the state of science regarding climate change into assessment reports which serve as information basis for policy makers (United Nations, 1988).

## 2.1 Global Climate Change and Impact Research

A review of scientific literature on climate change research published between 1980 to 2014 identified a sharp increase of research output doubling every 5 to 6 years with over  $2 \times 10^5$  articles totally, exhibiting an extraordinary development given an average doubling-time of 24 years for literature on research fields (Haunschild et al., 2016).

Engineering represents the research field showing strongest relative field-specific research increase with impact research and modelling being the focal points. Oceanic waters and impact research are both ranked third regarding the increase of publications summarized by the IPCC classifications, clearly discerning the importance of sciences at the land-water interface (Haunschild et al., 2016).

As the most prominent assessment body the IPCC publishes Assessment Reports with the fifth (AR5) being the current one (Stocker, 2014). The aim of the assessment reports by the IPCC are threefold. Firstly to condense available observations on earth climate system to provide an estimate on trends and changes. Secondly, to develop an attribution framework to identify the anthropogenic share of observed changes. Lastly scientific tools, i.e. general circulation models (GCMs), are developed to project possible future developments and consequences. Projections are modeled along the lines of pre-defined Representative Concentration Pathway (RCP) scenarios. These are physically based as they incorporate possible civilization driven developments of GHG concentrations, in turn amplifying the green house effect accumulating radiation energy within the atmosphere. RCP scenarios are categorized by their projected radiative forcing in 2100 referenced to a pre-industrialized world of 1750.

### 2.1.1 Modeling climate change related impacts

GCMs represent a type of climate model simulating the atmospheric and/or oceanic planetary circulation processes. Typically GCMs are based off the Navier-Stokes equations complimented by thermodynamic formulae for sources and sinks. First developments date back to the 1950's (Phillips, 1956) with significant improvements made by coupling ocean and atmosphere models (Manabe and Bryan, 1969; Ruttimann, 2006). Further advancements were made adding soil and vegetation type parameters (Xue et al., 1996) and gravity waves (Lott and Millet, 2009).

The most prominent example representing the state of science is the Coupled Model Intercomparison Project (CMIP) by the World Climate Research Program (WCRP) currently in its 5<sup>th</sup> iteration (Taylor et al., 2012) with CMIP6 in development endorsing 21 different working groups to contribute through numerical modelling (Eyring et al., 2016). CMIP-results of multi-model ensemble experiments are evaluated and findings compiled in the IPCC Assessment Reports for decision makers. The approach employs multiple numerical models with different parametrizations, which are used to simulate sets of RCPs with slightly varying start conditions to acquire a bandwidth of projections to arrive at more robust trends.

GCMs usually follow a risk-based approach, trying to identify changes in likelihood of occurrence and respective return period, thus resemble a frequency approach with exceedance levels and thresholds. A key feature of GCMs lies in the simulation of counterfactual scenarios, i.e. void of anthropogenic emission impacts, to identify the potential role of the Anthropocene. GCM-approaches are associated with higher confidence levels for changes in lower return periods of events (1/10a) given the length of observations compared to changes in high impact events typically featuring large return periods (1/100a-1/1000a) (Otto et al., 2017).

Finally, perturbed physics ensembles are an emerging trend for climate modelling. Observation based constraints of physical parameters in models do not apply to all functions due to insufficient knowledge. As a potential solution, systematic perturbation of model parameters identify other potential combinations, which yield identical and physically plausible climate projections allowing for further refinement of process based models (Shutts, 2005; Shutts et al., 2011; Sparrow et al., 2018).

### 2.1.2 Main drivers for coastal regions

Main drivers for certain regions are identified by the IPCC and future developments of these drivers are investigated and projected results assessed regarding their likelihood and confidence. Main drivers affecting coastal regions are compiled in table 2.1.1 from the 5th Assessment Report (Stocker et al., 2013) (AR5) adopting the terminology on trends from Mastrandrea et al. (2011) illustrated in figure A.9.

Table 2.1.1: Main drivers for coastal regions, their trends, and main physical and ecosystem effects due to climatic change and anthropogenic interventions according to the IPCC (Wong et al. 2014, table 5-1, p.368).

Driver	Physico-Chemical effect	Trend	Projections	Since AR4
Sea level	Submergence, flooding, erosion, salinization	Very likely increase	Very likely increase, regional variability	Improved confidence
Storms <sup>1</sup>	Storm surges, storm waves, erosion, coastal infrastructure damage & flood defense failure	Likely pole-ward shift, low confid. in intensity changes	Low confid. in intensity increase	Low confid. in intensity increase, more basin specific information
Winds	Wind waves, storm surges, coastal currents, land coastal infrastructure damage	Low conf. in trends of mean and extreme wind speeds	Likely increase in tropical cyclone (TC) extremes, low conf. in mean increase	Not addressed in AR4
Waves	Coastal erosion, overtopping and coastal flooding	Likely pos. trend in $H_{1/3}$ in high lat.	Low conf. in projections overall	Large increase in number of projections
Extreme Sea Levels	Coastal flooding, erosion, salinization	High conf. of increase	High, conf. due to MSLR, low conf. due to storms	Subsidence is an important local factor
Freshwater Input	Altered flood risk in coastal areas, changing salinities, altered fluvial sediment supply	Medium conf. i net decline of annual discharge	Medium conf. general increase in high lat.	Emerging information for changes
Sediment Delivery	Coastline retreat, stability of tidal areas, barrier islands & fairways, loss of habitats	Global decrease by 25% to 32% since 1950	Reduced natural recovery after storm impacts, loss of coastal areas, loss of dunes	Not specifically addressed

<sup>1</sup> Select information presented for ETC only for TC the reader is referred to (Wong et al., 2014)



Trends are observation based, whereas projections are mainly based on GCMs simulations. However, both entail a rather high degree of uncertainty. Reliable observations date back a few decades to a hundred years yielding comparatively short data series for trend analysis of a complex climate system. Projections conducted with GCMs rely on mathematical descriptions of physical processes found in nature. What is more, a lot of multidecadal processes and phenomena distributing radiative energy are not yet fully understood or even still to be discovered due to a lack of observations. Consequently, changes in storm systems and their inherent dynamics pertaining to seemingly chaotic non-linear interactions, are still very difficult to predict with GCMs, and thus are often associated with low confidence in projections. Further impacts arise from constructive interventions through port and fairway development along coasts and estuaries.

Uncertainty associated to modelling climate change related impacts and its quantification can be categorized into the two categories of either aleatoric uncertainty or epistemic uncertainty (Matthies, 2007).

Aleatoric uncertainty constitutes non-measurable or unknown effects, which result in different results every time the same experiment is repeated. Aleatoric uncertainty is also known as statistic uncertainty. Epistemic uncertainty is induced through systematic approaches, which can neglect certain known influences preferring simplification over exactness. Epistemic uncertainty is also known as systematic uncertainty. In science uncertainty quantification is tasked with reducing aleatoric uncertainty to epistemic uncertainty by developing adequate methods such as e.g. Monte Carlo experiments (Kroese et al., 2011). Epistemic uncertainty can be evaluated using fuzzy-logic or more generalized Bayesian theory derivatives (Kennedy and O'Hagan, 2001).

Time and infrastructural constraints limit the number of experiments within this study and thereby precludes the application of Monte Carlo method, which requires an abundant number of realizations (Kroese et al., 2011). Therefore, an ensemble-like approach is chosen, which contrasts different storm surge types and intensity levels.

Furthermore, uncertainty quantification is confronted with a twofold problem. One being the forward propagation of uncertainty, where variables and coefficients are input into a model or a system to obtain results and assess the overall uncertainty in the system response (Cole, 2001). The second one is the inverse assessment of model uncertainty, obtained through simultaneous parameter calibration on test data. The first problem is addressed through techniques reducing parametric variability, ensuring a representative data set. This is achieved in this study through careful selection of individual storm surge events (see section 3.1), an exhaustive literature research on coastal drivers and their variations (see section 2.3) as well as homogenization of input time series. The latter problem is addressed by a thorough parameter calibration of the numerical model and adjacent validation with parameter evaluation (see section 3.7).

### 2.1.3 Impact study types

Against the background of ubiquitous climate change, regardless of potential anthropogenic amplifications, a changing environment brings forth new challenges for planners and practitioners and with it the need for estimations of potential impacts they will bring about to meet them on a constructive level. Three main types of impact studies can be differentiated, namely:

1. Classical **Impact Study** is based on climate simulations run with GCMs. They span long time spans often encompassing centuries and allow for deriving general trends. However, they do not account for a high degree of internal variability required for realistic representation of extreme events due to scale.
2. **Sensitivity studies** employ idealized boundary conditions to force impact models in order to filter out main drivers and system eminent sensitivities towards certain parameters, when these are unknown.
3. **Time Slice** studies simulate projected impacts on a short time scale with high resolution due to computational efficiency. These are not suitable to derive general trends but represent snapshots and are conditional on climate study projections. They allow for testing extreme hypotheses combining MSLR with augmented mean wave height (MWH) and overall increased accumulated cyclone energy (10e4kt) (ACE).

Given the above definitions, storm surge modelling under projected climate changes falls within the third category. Employing an ensemble-like approach within this study, by contrasting different main storm surge types on different intensity levels, reduces the uncertainty within the time slice study, giving multiple realizations instead of one per storm surge. Furthermore, a permutation of physical processes (wind, waves, discharge) helps to reveal non-linear interactions and identify and reduce epistemic uncertainty.

## 2.2 Extreme event definition

The definition of an extreme event is not unequivocal since every observed extreme event is uniquely dependent on external climatic drivers as well as internal dynamics and therefore non-repetitive. Notwithstanding, uniqueness renders the assessment of its recurrence interval or magnitude impossible and prevents statistical event-prediction or identifying key-parameters contributing to the event in question. Therefore, classification and abstraction are inevitable although no clear dichotomy exists between a unique extreme event and a class of extreme events (Otto et al., 2017). Consequently, the definition is highly case sensitive and dependent on the methodology and assessment body. Generally events can be classified according to their frequency and/or magnitude (Ross,

2014). Frequency of occurrence or recurrence interval is an estimate of likelihood of event realization and can be determined as follows:

$$\text{recurrence interval} = \frac{n + 1}{m} \quad (2.2.1)$$

with  $n$  = sample size and  $m$  = realizations. The return period is defined as the inverse probability of any event being exceeded any one year, i.e. a 100-year flood features a chance of  $\frac{1}{100}$  or 1 % chance of being exceeded any one year. Nevertheless, a 100-year storm-surge event does not automatically occur once every 100-years, but actually features a probability of exceedance ( $P_e$ ) of 63.4 % according to the hydraulic risk definition (Salas et al., 2013) to occur once or more-often during any 100-year period.

The German Institute for Standardization (*Ger.:Deutsches Institut für Normierung*) (DIN) defines storm surges for the North Sea according to their respective annual mean exceedance values at high tide, i.e. water levels exceeded along the coast 10-0.5 tides a year are categorized as storm surge, heavy storm surges and severe storm surges feature 0.5 (one in 10 years) and 0.05 (one in 20 years) respectively (DIN 1992, p. 36; DIN 1992, pp. 9).

Magnitudes often compliment frequency analysis and serve as physical classification directly related to their respective recurrence intervals given their exceedance of defined thresholds, i.e. table 2.2.1 gives the storm surge definition according to the BSH for the German North Sea coast (Jensen and Müller-Navarra, 2008).

Table 2.2.1: Storm surge definition according to the BSH based on analysis of data from the tidal gauges Emden, Bremen and Hamburg inside the three Estuaries on the German North Sea coast.

storm surge	1.5-2.5 m above mean high water (MHW)
severe storm surge	2.5-3.5 m above MHW
very severe storm surge	≥3.5 m above MHW

Applying the DIN or the BSH definitions yield marginally different results. However, this exemplifies how different methodologies can lead to fundamentally different questions being answered by individual approaches; i.e. *to what degree has anthropogenic climate change altered the frequency and magnitude of an extreme event occurring today in contrast to the inquiry of its respective evolution in time based on observations*. Similarly, applying an identical approach can yield contradicting results considering the qualitative and quantitative role of individual external drivers in turn dependant on event definition

(Rahmstorf and Coumou, 2011; Dole et al., 2011; Otto et al., 2012).

Rahmstorf and Coumou (2011) show that temperature data sets with increased standard deviation (satellite-derived lower-troposphere) obscure trends and decrease extreme event numbers versus ground based observations featuring smaller variability - building a strong argument that with increasing signal variations record event occurrences decrease and become near zero given very large signal amplitudes of investigated parameters. Also they show, that a simple shift of a random distribution towards warmer climate significantly increases the number of expected record events. They conclude that an increase in extremes depends on climatic signal trends to short-term data variability: for records this relationship is linear, for extremes exceeding a threshold it is highly non-linear.

Independent of different methodologies and assessment bodies every study investigating extreme events should explicitly formulate an event definition including climatic variables, thresholds, geographic region and scales.

### 2.2.1 Examples

Hurricane Sandy, often referred to as super or hybrid storm, was a TC that originated south of Jamaica on October 22<sup>nd</sup> of 2012 and made landfall in New Jersey, flooding large parts of New York City. Hurricane Sandy initially recorded as a category 3 TC crossing Cuba and the Caribbean, weakened to a category 2 hurricane off the coast of the Northeastern United States. However, traversing a coastal band of abnormally elevated SST at 1.5 °C above climatological records, the TC drew on energy and water vapor, growing the low pressure system to the largest recorded in the north Atlantic with a diameter of 1800 km, impacting vast stretches of coast. Furthermore, the increase in moisture resulted in a 35% precipitation increase, the added latent energy increased overall wind speeds by 3.6 ms<sup>-1</sup> resulting in sustained wind speeds of 185 km h<sup>-1</sup> and the storm eye pressure decreased by an additional 7.6 hPa dropping the central pressure to 940 hPa (Magnusson et al., 2014). Additionally, the U.S. east coast experienced a MSLR of 0.19 m, increasing the reach and amplifying the dynamic impact (Trenberth et al., 2015). Sandy impacted vast coastal stretches, flooded parts of New York City, caused power outage to over five million homes, cancelling of all rail services along the north east seaboard for two days and a lay off for nearly 20.000 flights as well as a closure of the stock market. Infrastructural damage amounted to 50.5 × 10<sup>9</sup>€ (NOAA, 2018; U.S. Department of Energy, 2012; Kaufmann et al., 2012). European Centre for Medium-Range Weather Forecasts (ECMWF) investigations clearly discerned that Temperature as thermodynamic indicator shows anthropogenic liability (Magnusson et al., 2014).

Taiphoon Haiyan (*chin.: storm-petrel*) is a particular significant extreme storm event of recent history, which occurred in November 2013. With sustained wind speeds of 315 km h<sup>-1</sup>

and  $378 \text{ km h}^{-1}$  gusts, Haiyan devastated the Philippines. The low pressure system measured 895 hPa storm eye depression and was suggested to be rated as a category 6 storm (Lin et al., 2014). Riding on a significantly increased mean sea level (MSL) due to the negative Pacific decadal oscillation (PDO) phase augmented the water levels by 0.3 m since 1993. Increased OHC supported the typhoon throughout its course and prevented energy dissipation and cooling through vertical mixing of the ocean – maintaining storm intensity (Captain Evans and Director Falvey, 2013; Trenberth et al., 2014). Research concluded, that the event was governed by natural variability but that impact amplification was increased due to climate change driven thermodynamic effects (Trenberth et al., 2014).

Scoring a cumulative ACE of 224 the hyperactive hurricane season of 2017 ranks 5<sup>th</sup> since 1851 and established terrifying records. It was one of only six seasons which have seen multiple category 5 TCs. Figuring at  $225.7 \times 10^9 \text{ €}$  in damage it is the most expensive storm season on record (NHC, 2018), with individual storms causing as much as  $100 \times 10^9 \text{ €}$  (Harvey). It is the only season ever recorded with three individual storm events surpassing an individual ACE of 40 namely, Irma 64.9, Maria 44.8, Jose 43.3. Simultaneous occurrence of TCs Katia (category 2), Irma (category 5) and Jose (category 5) led to a rarely observed clustering of events, but unprecedented for two category 5 storms (Blake et al., 2013; Blake and Zelinsky, 2018; Avila, 2017; Berg, 2018).

### 2.2.2 European Windstorm

A basic problem is that there is no universally accepted definition for a cyclone or a storm; in fact most research groups define their own set of parameters and thresholds in order to analyze storm or cyclone related data (Hewson and Neu, 2015). The German Weather Service (*deut.: Deutscher Wetterdienst*) (DWD) defines storm cyclones as mid-latitude low pressure systems under which either a 10-minute mean of at least Beaufort (Bft) 8 has been measured (especially ship based observations) or equivalent wind speeds can be derived from observed pressure fields for any given system. Such low pressure systems can occur all year round, but tend to be more frequent during winter months. Their formation consequently requires a strong pole-ward temperature gradient complimenting a strongly barotropic atmosphere (DWD, 2018b). Synoptic definitions are most frequent and describe European Windstorms as large synoptic-scale mid-latitude low pressure systems with diameters ranging from 500 km to 5000 km (Weisse et al., 2012; Coco and Ciavola, 2018). European Windstorms constitute a type of ETC, with cyclogenesis located over the North Atlantic, where they originate either from (i) a diminutive atmospheric wave, (ii) a frontal wave or (iii) as a barotropic low (Eady, 1949; Shapiro and Keyser, 1990; Coco and Ciavola, 2018). Their storm track follows the northeast coast of the continental US and extends east from the tip of Newfoundland across the Atlantic where it curves northward

affecting northern Europe and Scandinavia (Hoskins and Hodges, 2002). Nevertheless, if atmospheric conditions are favourable given a more southerly Jet-Stream location, the storm track redirects southward through Spain, Portugal and France (Liberator et al., 2013). European Windstorms can cause large damage to infrastructure (e.g. Schultz and Browning 2017), hence correct detection, tracking and prediction are of paramount interest to stakeholders such as the insurance industry, building industry and disaster risk agencies alike. However, given the vast variety of studies on individual storm related aspects, processes and impacts, most of the research is rather incomparable due to varying definitions and methodologies - consequently the Intercomparison of Mid-Latitude Storm diagnostics (IMLAST) project was initiated 2009, today encompassing over 20 research groups across Europe (Neu et al., 2013; Ulbrich et al., 2013; Rudeva et al., 2014; Simmonds and Rudeva, 2014; Lionello et al., 2016). To form a common basis of understanding, a conceptual cyclone model was developed describing seven stages of cyclone development and differentiating three different wind phenomena, as well as their respective damage swathes (Hewson and Neu, 2015). These three wind storm zones are delineated using pattern matching and air mass flows, which relates strong wind field locations relative to the frontal systems of a cyclone. Therefore, the zones are physically based since the air masses delineating the different cyclone fronts exhibit very different stability characteristics<sup>1</sup>.

---

<sup>1</sup>Stability of air mass here defines the level of resistance air has to overcome to propagate downwards, in turn amplifying surface wind gusts, which are paramount in terms of damage swathes, impact research and resilience building, closely followed by areal extend, temporal duration and occurrence (Hewson and Neu, 2015)

The conceptual model developed within IMLAST is shown in figure 2.2, together with the ETC tracks of recent storm events Xaver and Christian (Roberts et al., 2014).

Figure 2.2: Conceptual IMLAST ETC model a) showing the ETC track associated with European Windstorms and its respective phases 1 to 7 marked equidistant in time along the track as well as tracks of Xaver and Christian; b) shows the meteorologic cyclone development phases and c) showcases the three different wind storm zones, their respective phases and associated wind gust speeds.

Numbered phase markers are equidistant in time. Phase 1 characterizes the cyclogenesis over the eastern North Atlantic, starting as i-iii (see above). Phase 2 circumscribes the initially slow moving phase 1 phenomenon, which crosses a strong cross-Atlantic jet stream and is accelerated. Phases 2 to 3 show a rapid translation and allow first wind-storm traits to develop, as the warm conveyor belt induces minimal vertical friction. A strong upper jet propels the air mass towards Europe reaching  $70 \text{ kt}$ , with no directional friction. Approaching the European coast, the mainland during winter is usually cold and forms a natural deceleration zone, counteracting downward winds and momentum transfer due to its relatively high stability. This holds especially true, for stable inland zones during cold winters. For example, gusts from ETC Oratia reduced from  $70$  to  $40 \text{ kt}$  within

100 km of the coastal zone (Hewson and Neu, 2015).

Phases four and five see the most rapid deepening of the ETC and associated intensification. During these phases Warm Jet (WJ) and Cold Jet (CJ) may coexist and Sting Jet (SJ) form due to low level atmosphere instabilities. 33 % to 50 % of the maximum cyclone deepening (phase five) are contributed by latent heat and thus are driven by SST, exhibiting a clear thermodynamic driver for storm amplification (Hewson and Neu, 2015). During phases six and seven the storm system tends to follow a trajectory bending northward, progressively losing intensity due to a decrease in thermal gradient until it dissolves.

The three main wind storm zones distinguishable are:

- *WJs* develop the strongest wind gusts during early phases two to four with wind speeds of 50 kts to 70 kts. The Warm Jet is usually stronger on the open sea and the coastal regions, as the warm air conveyor belt provides an ideal trajectory with minimal vertical friction. Intensity is reduced by 30 % to 50 % upon landfall, as continental air masses in winter are usually cold and dampen the warm jet, inducing friction on downward directed wind gusts. Warm Jets on average last 24 h to 48 h with damage footprints between 200 km to 500 km wide and up to 1000 km long.
- *SJs* are a relatively recent discovery (Browning, 2004; Schultz and Browning, 2017) and are a rare phenomenon, typically forming between phases four and five. *SJs* have been reported to reach wind gust speeds of 70 kts to 90 kts, lasting between 1 h to 12 h. Their respective damage footprint extends over 20 km to 200 km width and up to 800 km in length. Due to their short duration, high intensity and small scale, the phenomenon is very difficult to measure, represent in re-analysis data or even model and predict (Hewson and Neu, 2015). However, they constitute a high impact process, with large damage and loss quantities associated. Moreover, the physics of the *SJ* are not exhaustively explained, nor is the phenomenon confined to the open sea or experiences any intensity reduction within the coastal zone.
- *CJs* constitute a transition taking place during phase five, on the northwest cyclone flank. A *CJ* may coexist with *WJ*, on the opposite side of the cyclone as well as a *SJ*, but usually encircles and replaces or underflows and elevates the *SJ*. The *CJ* usually lasts 12 h to 36 h and reaches wind speeds between 60 kts to 80 kts. The strongest gusts and winds are generated in coastal waters, due to elevated SST causing convective destabilization of the lower atmosphere, allowing downward wind gusts with relatively low vertical shear and friction. The *CJ* has the most extensive damage footprint of the three types with a typical width of 100 km to 800 km and a length of up to 2500 km.

European Windstorms have become a major research topic driven by associated damage and loss footprints, striving to understand governing physical processes to readily assimilate atmospheric observation data, detect and forecast ETCs and prepare for impacts. A



conceptual model has been developed to classify and compare events, segregating three storm wind zones and seven developmental stages. It is noteworthy that, the WJ intensity exhibits strong linkage to SST and changes therein, driving the destabilization of the low atmosphere pressure fields through thermal convection.

### 2.2.3 Storm surge events

Storm surge is a coastal flood phenomenon, induced by low pressure weather systems (i.e. tropical cyclones or extratropical cyclones). The surge is a measure of the rise of water beyond the expected tidal water level due to wind surge. Its intensity depends mainly on the fetch length for the winds spiraling inward towards the storm inducing surface friction on the sea, the low-pressure-induced dome of water, which trails the storm center and the overall storm duration. Additional known processes influencing the overall surge water level at the coast are the Coriolis force, near-shore waves and the rainfall effect as well as the coastal geometry and degree of development (Holthuijsen, 2007; Cavaleri et al., 2016; Gönnert, 2003).

European windstorms can cause storm surges along the North Sea coast, depending on their track as described in chapter 2.2.2. During the recent winter seasons 2016/2017, six storm surges were observed, two of them heavy ( $\leq 2.5$  m MHW). During the ensuing season 2017/2018, eleven storm surges occurred with one heavy event (BSH, 2018a). The most severe *very heavy storm surges* result in coastal water levels exceeding  $\leq 3.5$  m above MHW. This type has been rarely observed at the German North sea coast, culminating in 13 events since 1949 (MUSE, 2005). The last one being the ETC Xaver (4/12/2013-10/12/2013), with coastal water levels for the focus region given in figure 2.3.

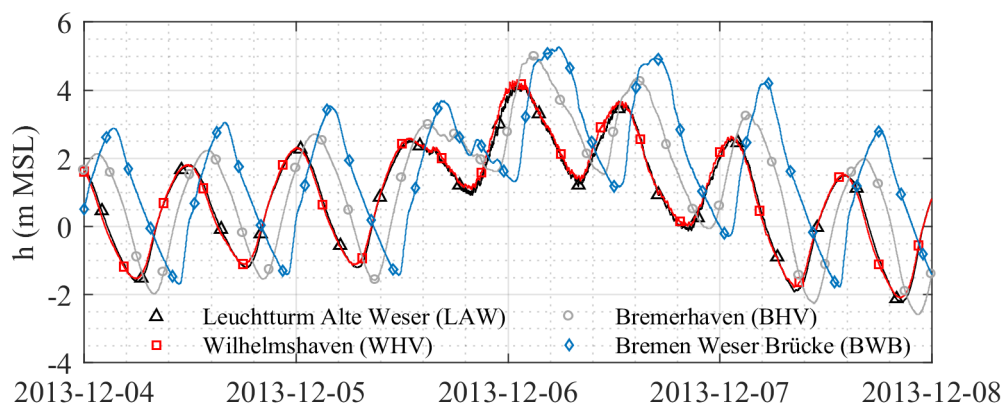


Figure 2.3: ETC Xaver induced surge levels in the focus region.

The very heavy storm surge events are described in table 2.2.2 for the three large German

estuaries Ems, Weser and Elbe as well as the Jade bight based on peak water levels observed at tide gauges seaward and landward. Values are referenced to standard elevation zero of 2016 (*Ger.: Normal Höhen Null 2016*) (NHN16). The observed values show that very heavy storm surges ( $h_{\text{surge}} \geq \text{MHW}+3.5$ ) induce storm surge water levels all along the German Bight. What is more, water levels are lower at the open coast compared to estuarine ones. Island based tide gauges so far did not record a single storm surge with  $\leq \text{MHW}+3.5$ . Furthermore, the recorded events contain one clustering of very heavy storm surges during the winter 1976. Such a clustering results in potential devastation, if flood defenses fail or are damaged during the first encounter, the consecutive event may extend inundation areas and have a larger impact as repairs are still ongoing (Zitscher et al., 1979). The observation pairs allow for deriving a stowage coefficient *sto* relating the two peak water levels to show the event related stowage for the four regions given in the columns ensuing the pairs. The stowage coefficients for all four regions show increasing tendencies over time, with mean values for the focus region of 1.18 (Jade) and 1.21 (Weser). Hydraulic development of the coastal waters as well as MSLR influence the development of the surge levels as is shown in chapter 2.3 and especially in 3.2.1 and 2.3.9, showcasing the anthropogenic impact on surge development along the German North Sea coast for three estuaries.

Table 2.2.2: Very heavy storm surge levels at the German North Sea Coast.  
Data is compiled from Deutscher Bundestag (2014); Jensen (2005).

	Estuary	EMS			JADE			WESER			ELBE		
		NDY	EMD	sto	LAW	WHV	sto	LAW	BHV	sto	CUX	STP	sto
MHW to NHN16 (m)		1.2	1.5		1.4	1.8		1.4	1.9		1.5	2.1	
No.	Date and Time	peak water level above MHW (m)											
1	16/02/1962 23:38	2.9	3.4	1.17	2.9	3.5	1.21	2.9	3.7	1.28	3.5	3.9	1.11
2	03/01/1976 14:19	2.7	2.9	1.07	2.8	3.1	1.11	2.8	3.5	1.04	3.7	4.5	1.22
3	21/01/1976 03:36	2.7	3.0	1.11	2.7	3.2	1.19	2.7	3.2	1.19	3.3	3.6	1.09
4	24/11/1981 11:41	2.4	2.8	1.17	2.5	2.6	1.04	2.5	2.6	1.04	3.1	3.8	1.23
5	28/02/1990 02:48	2.4	2.8	1.13	2.4	2.7	1.13	2.4	2.7	1.13	2.7	3.7	1.28
6	23/01/1993 01:16	2.1	2.3	1.10	2.3	2.5	1.09	2.3	2.9	1.26	2.9	3.7	1.28
7	28/01/1994 13:50	2.5	3.2	1.28	2.5	2.8	1.12	2.5	3.0	1.20	3.0	4.0	1.33
8	10/01/1995 07:02	2.3	2.9	1.26	2.3	3.0	1.30	2.3	3.0	1.30	3.0	4.0	1.33
9	05/02/1999 03:52	2.2	2.4	1.09	2.3	2.2	0.96	2.3	2.7	1.17	2.8	3.7	1.32
10	03/12/1999 22:10	2.0	2.4	1.20	2.2	2.4	1.23	2.2	2.7	1.18	3.0	3.9	1.30
11	01/11/2006 08:13	2.6	3.7	1.42	2.2	3.1	1.41	2.2	2.8	1.27	2.4	2.8	1.17
12	09/11/2007 12:41	2.6	3.3	1.27	2.4	3.0	1.25	2.4	2.9	1.21	2.9	3.6	1.24
13	06/12/2013 02:52	2.6	3.5	1.35	2.5	3.3	1.32	2.5	3.2	1.28	3.1	4.0	1.29

$\geq \text{MThw}+1.5\text{m}$  storm surge  
 $\geq \text{MThw}+2.5\text{m}$  heavy storm surge  
 $\geq \text{MThw}+3.5\text{m}$  very heavy storm surge

Until now no mean wind conditions<sup>2</sup> of  $Bft \geq 12$  have been observed during storm surge events along the North Sea (Deutscher Bundestag, 2014). Consequently, higher storm surge events are physically possible, plausible and subject of current research. Details are given in chapter 2.4.5.

### 2.2.4 Event attribution

Over the course of the preceding decade extreme event attribution has emerged from theory into a sub-field of climate science, which aims to provide scientific evidence for a potential anthropogenic influence on climate change specifically in extreme events. Science has developed different attribution and framing approaches, which are discussed in detail in the ensuing section 2.2.5, resulting in very different and even contradictory results. In literature the ongoing development and debate of appropriate scientific methodologies is well documented on how to address various needs brought forward by policy makers and stakeholders as well as scientific limitations. Limitations and constraints are overcome and pushed-further by technological advancements, increasing computer and processing resources, as well as methodological developments of new tools - knowing that the research of full impacts of extreme events poses a major challenge for the scientific community within the near future (Otto et al., 2017).

### 2.2.5 Attribution frameworks

Extreme events, especially heat waves and hurricanes as well as associated societal impacts draw the attention of the public and science sectors alike. The fifth iteration of the IPCC assessment report (Wong et al., 2014), much like its predecessors, predominantly focused on the detection and attribution of long-term trends in existent temperature observations. However, individual event attribution was deemed impossible until a first methodology was described by Allen (2003) and subsequently applied to a first extreme event a year later. Results implicate an increase of likelihood of at least 100 % due to anthropogenic influence (Stott et al., 2004).

Nevertheless, event attribution does not automatically quantify trends consistent with global warming research results.

A recent example for this constitutes the meteorological flooding in the United Kingdom during the winter of 2000/2001. First attempts to differentiate between natural variation and emission showed no clear correlation (Met Office, 2011), which was expected. However, applying statistical and hydrological modelling of industrial and non-industrial emission scenarios it could be shown that: the probability of occurrence of heavier rain

---

<sup>2</sup>mean wind speed here is defined as 10 min (DWD, 2018b) mean within any hour

fall in summer and subsequent extreme discharge and flooding in autumn/winter exhibit a decrease in likelihood, due to a shift in various parameters, i.e. snow-melt and weather-pattern shifts (Pall et al., 2011; Kay et al., 2011). This is contrasted by a large increase of rain-fall across northern and central Europe (Pfahl et al., 2017). Moreover, individual attribution analysis can either indicate that the event in question cannot be attributed clearly due to a lack of understanding and methods, or attributions could show that the event has not been affected by climate change. If the event in question can however successfully be assessed – results show whether anthropogenic emissions have or have not altered the likelihood of an event to occur (Otto et al., 2017).

1. The **Oxford approach** constitutes one of two main attribution schemes currently debated. This risk-based approach aims to quantify changes in likelihood of any given extreme event, adding or subtracting the potential influence of man made emissions. It is therefore conditional towards GHG emission scenarios, which force either a GCM or a regional climate model (RCM) and depends highly on individual model sensitivity towards atmospheric aerosol processes. The method entails a broad spectrum of statistical tools to evaluate industrial climate scenarios against synthetic counterfactual scenarios (Keller et al., 2017; Shepherd, 2016; Easterling et al., 2016; Parker et al., 2016).
2. The **Boulder Approach** represents the second major attribution scheme in development. This approach attempts to structure individual events and attribute individual contributions to single processes, i.e. climate change or natural variability. In contrast to the Oxford approach, this method does not envisage statistical analysis but a circulation pattern based predictability of the individual event (Hoerling et al., 2006; Seager et al., 2015). Climate change statements can be made applying the Clausius-Clapeyron equation, which describes the atmospheric water-holding-capacity and is based on thermodynamics. This yields good results for extreme events governed by temperature and is generally associated with high confidence.
3. Finally, a **Circulation-Based Approach** classifies each event according to its circulation state. Subsequently, analogue states of circulation are obtained either from reanalysis data or model simulations and evaluated for elapsed time between occurrences. Increased numbers of analogs in the recent past indicate a climate change sensitivity. Trenberth et al. (2015) developed the concept further and propose separating out thermodynamics from inherent dynamics in order to arrive at higher levels of confidence regarding the attribution of potential human induced climate change acceleration within extreme event impacts.

Methodologically the conventional attribution framework, encompassing the Boulder and the Oxford Approach, struggles with dynamically driven extremes due to small signal to noise ratio (SNR) associated with circulation-related extremes in observed records. Thus

even if anthropogenic impacts are modelled and identified, the reliability of such findings is not very trustworthy due to their immanent lack of reproducing physical dynamics, which in part are yet to be understood, as well as effects causing changes in turn driving the extreme (Shepherd, 2015; Trenberth et al., 2015).

Henceforth, Trenberth et al. (e.b.d.) suggest evaluating whether known changes in the thermodynamic state of a climatic system affected any impact(s) of a given event. Thermodynamics can be modelled unlike dynamic non-linear effects obscuring the governing processes, thus a separation might be more useful to arrive at different sets of equations and conclusions to form a basis for communicating climate change less contradictory in public and more productive with stakeholders and policy makers.

#### **Summary of chapters 1 & 2.1-2.2:**

Critical coastal infrastructure, encompassing fairways and ports, is challenged by extreme events under changing environmental conditions. Earth system sciences use numerical models to project possible future changes and identify key drivers for the coastal zone. Different impact study types exist, with time slice studies facilitating the research of single (extreme) events under projected varying key drivers within this study. European Windstorms are identified as synoptic extreme events impacting the North Sea coast, with two main cyclone pathways to be investigated. Attribution frameworks, currently under development, aim to discern potential human liabilities for environmental changes but are highly case sensitive and contraindicatory. Therefore, this study aims to investigate key driver liability for extreme events under changing conditions. Changes in key drivers are investigated in the following chapters and findings used to derive research scenarios in chapter 3.2.

### 2.3 Modes of variability and related impacts

Dynamics are much more difficult to simulate and predict with GCMs and RCMs but are essential for successfully projecting climate change related extreme events, mainly occurring due to small shifts in circulation patterns. However, instrumental records cover mostly the last century with some exceptions reaching back until the mid 19<sup>th</sup> century (e.g. Church and White 2011; Stewart et al. 2017), making statistical assessments of long periodic cycles and mechanisms difficult.

The complex and often non-linear combination and interaction of different modes can result in extreme events such as European Windstorms or Hurricanes. Importantly, chaotic weather elements, immanent to the earth's atmosphere, preclude long-term statements regarding regional patterns as they are not solely externally forced by thermodynamics but reflect an internal variability. This degree of complexity is not yet represented by GCMs or RCMs, mostly due to a lack of understanding in physics and insufficient observations (Trenberth et al., 2015).

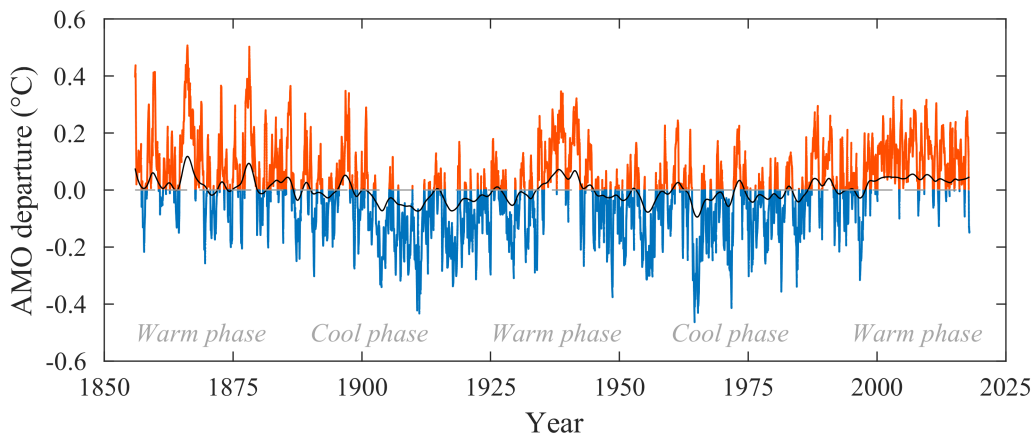


Figure 2.4: AMO signal based on data provided by the NOAA (2018) showing the fluctuation between warm and cold phases, modulating the storm activity (Enfield et al., 2001).

Such modes of variability cover large-scale effects on longer time-periods like the renowned El Niño Northern Oscillation (ENSO) but also less prominent mechanisms such as the AMO shown in figure 2.4, the North Atlantic oscillation (NAO) and the decadal Atlantic Oscillation (DAO) affecting the Atlantic basin, which in turn affect the OHC and SST directly impacting atmospheric circulation patterns and cyclone formation. In accordance with coastal key drivers given in table 2.1.1 the ensuing chapters cover recent findings regarding key drivers.

### 2.3.1 Sea level

Climate related impact assessment in coastal zones to a high degree depends on projected MSL change, as the assumed water level directly impacts flooding risks, coastal erosion and amplifies wave and surge impacts. Science differentiates between *eustatic* and *relative* sea level changes. Eustatic changes pertain to variations in mass or volume of the oceans, while relative changes refer to coast line changes regarding the land water boundary. Eustatic sea level changes are often referred to as geocentric mean sea level (GMSL), which is referenced to the center of earth and corrected for plate tectonics (Rovere et al., 2016). GMSL is mostly used for GCM simulations due to global model scales. Eustatic sea level changes are induced through physical mass changes from melting ice sheets, tectonic sea floor changes and includes steric sea level changes. Steric or thermostatic sea level changes are induced through thermal and salinity related density changes. (Bamber et al., 2019). According to current research, the largest single contribution to SLR constitutes thermal expansion (41 %) followed by mass-addition from melting glaciers (21 %), the Greenland ice-shield (15 %) and Antarctica (8 %). The research group compared altimetry with ground based (tide gauge) data and reduced the remaining discrepancy between the data sets to 0.3 mm (WCRP, 2018).

However, for coastal planning and impact research on a local scale the relative MSL rise is of higher importance (Nicholls et al., 2011). Relative sea level can be impacted by (i) temperature induced ice mass changes, (ii) tectonic responses to ice mass changes, (iii) thermostatic sea level changes, (iv) tectonic activity and (v) regional subsidence due to compaction and drainage (Rovere et al., 2016). Changes in GMSL have been investigated repeatedly within many different studies. The majority of investigations relies on tide gauge data series, which are available for relatively long time periods of over 100 years (e.g. Wahl et al. 2017). GMSL trends for the period 1900 to 1990 vary slightly between different studies, depending on employed methodologies  $1.2 \pm 0.2 \text{ mm yr}^{-1}$  (Hay et al., 2015)  $1.5 \pm 0.2 \text{ mm yr}^{-1}$  (Church and White, 2011) but result in a GMSL of about 0.11 m to 0.15 m. Table 2.3.2 gives an overview over SLR values and rates, researched by different groups using different methods and data sets for varying time periods.

Tide gauge data indicate a significant rate increase since 1993 of  $3 \text{ mm yr}^{-1}$  (Hay et al., 2015; Church and White, 2011) which was recently supported by altimeter data analysis confirming a trend of  $3.0 \pm 0.4 \text{ mm yr}^{-1}$  (Nerem et al., 2018) – resulting in an additional 0.07 m GMSL since 1993 and about 0.16 m to 0.21 m since 1900. For the German Bight an increase of about 0.3 m was identified (Weisse et al., 2014a). About one third is attributed to thermostatic expansion whereas two thirds stem from mass addition to the oceans mainly from ice mass changes (Church et al., 2014; Leuliette, 2015). For the period 1993 to 2009 Wahl et al. (2013) found an above average increase of GMSL for the inner North Sea of  $4.59 \pm 1.82 \text{ mm yr}^{-1}$  which relates to global GMSL of  $2.80 \pm 0.47 \text{ mm yr}^{-1}$  according

to Church and White (2011). According to recent findings, a rather large portion of GMSL can be attributed to anthropogenic impacts (Slangen et al., 2014; Dangendorf et al., 2015; Kopp et al., 2016). Kopp et al. (2016) state that GMSL rise would extremely likely have been 30 % lower compared to observations, in absence of 20<sup>th</sup> century global warming. Similarly, Slangen et al. (2014) found that about 80 % of simulated GMSL between 1970 and 2005 and about 50 % for the period 1900 to 2005 was attributable to anthropogenic forcing.

Additionally, satellite altimetry data revealed an accelerating trend of  $0.084 \pm 0.025 \text{ mm yr}^{-1}$ , which is in agreement with IPCC assessment model predictions of AR5 (Nerem et al., 2018). At this accelerating rate the MSL could rise by  $0.65 \pm 0.12 \text{ m}$  by 2100. Based on gauge time series from 1900 to 2011 the North Sea exhibited a trend for GMSL change above the global mean with  $1.6 \pm 0.1 \text{ mm}$  and a relative rise for the German Bight of  $2.3 \pm 0.2 \text{ mm}$  (Wahl et al., 2013).

Several impact studies investigating the German coast used a SLR value of 0.79 m (Grabemann and Weisse, 2008; Gaslikova et al., 2012), which is based on AR4 projections with 0.59 m pertaining to projected SLR of the most severe emission scenario and an additional 0.2 m for potential increase due to linearly extrapolated ice mass changes based on observed fluxes. Recent climate projections assessed by the IPCC within their RCPs scenarios and associated uncertainties regarding global mean sea level rise (GMSLR) for 2100 are summarized in table 2.3.1. For the North Sea, these variations mainly pertain to postglacial subsidence and will potentially result in MSLR surpassing the global average (Brasseur et al. 2017, pp.97). Vousdoukas et al. (2017) recently presented the first pan-European assessment study integrating all major components of Extreme Sea Levels (RSLR, tidal dynamics, waves, wind) and project a mean RSLR for Europe of 0.57 m by 2100, with regional differences.

Table 2.3.1: Projected global mean sea level changes and associated uncertainties from the CMIP5 assessed by the IPCC AR5 (Church et al., 2014).

RCP	likely ranges	median projections
2.6	0.28-0.61 m	0.44 m
4.5	0.36-0.71 m	0.53 m
6.0	0.38-0.73 m	0.55 m
8.5	0.52-0.98 m	0.74 m

The North Sea and especially the German Coast exhibits the highest increase with 0.98



m for RCP8.5 by 2100. Regardless of observation method GMSL has risen nearly linearly over the last century and exhibits a recent acceleration since 2006 (Wahl et al., 2013; Nerem et al., 2018). Furthermore, future projections indicate a continuous increase until at least 2100 (Church et al., 2014).

Table 2.3.2: Overview over different sea level rise analysis between different studies with varying methods, data sets and time periods.

Period	Type	Range	Reference	Note
1900-1990	GMSLR	1.2±0.2 mm yr <sup>-1</sup>	Hay et al. (2015)	
		1.5±0.2 mm yr <sup>-1</sup>	Church and White (2011)	
1900-2011	RMSLR	1.6±0.1 mm yr <sup>-1</sup>		North Sea
		2.3±0.1 mm yr <sup>-1</sup> 0.11 m to 0.15 m	Wahl et al. (2013)	German Bight
1993-2009	GMSLR	4.54±1.82 mm yr <sup>-1</sup>	Wahl et al. (2013)	German Bight
		2.8±0.47 mm yr <sup>-1</sup>	Church and White (2011)	
since 1903	GMSLR	3.0±0.7 mm yr <sup>-1</sup>	Hay et al. (2015)	
		2.8±0.5 mm yr <sup>-1</sup>	Church and White (2011)	
		2.8±0.5 mm yr <sup>-1</sup>	Rhein and Wang (2013)	
		3.1±0.6 mm yr <sup>-1</sup>	Jevrejeva et al. (2017)	
		3.1±1.4 mm yr <sup>-1</sup>	Dangendorf et al. (2017)	
		3.0±0.4 mm yr <sup>-1</sup>	Nerem et al. (2018)	+0.1 mm yr <sup>-1</sup>
		3.1±0.3 mm yr <sup>-1</sup>	Legeais et al. (2018)	+0.1 mm yr <sup>-1</sup>
	RMSLR	0.3 mm yr <sup>-1</sup>	Weisse et al. (2014a)	German Bight
By 2100	RMSLR	0.77 m	Vousdoukas et al. (2017)	North Sea
By 2100	RMSLR	0.79 m	Gaslikova et al. (2012)	North Sea
1800-2100	RMSLR	1.6 mm yr <sup>-1</sup>	Brasseur et al. (2017)	North Sea
By 2100	RMSLR	0.79 m	Grabemann et al. (2015)	North Sea
1993-2016	GMSLR	3.5 mm yr <sup>-1</sup>	Wahl et al. (2017)	North Sea
1900-2000	GMSLR	1.5±0.2 mm yr <sup>-1</sup>	Kopp et al. (2016)	
1900-2011	RMSLR	1.76 mm yr <sup>-1</sup>	Dangendorf et al. (2015)	Cuxhaven
1900-2011	RMSLR	1.84 mm yr <sup>-1</sup>	Dangendorf et al. (2015)	Norderney
1957-2005	GMSLR	0.026±0.021 mm	Slangen et al. (2014)	Thermostatic
1901-1990	GMSLR	1.5±0.21 mm yr <sup>-1</sup>	Leuliette (2015)	Steric
1900-2010	GMSLR	1.5 mm yr <sup>-1</sup>	Rovere et al. (2016)	Eustatic
1993-2018	GMSLR	3.1±0.3 mm yr <sup>-1</sup>	WCRP (2018)	+0.1 mm yr <sup>-1</sup>

### 2.3.2 Tidal dynamics

Tides describe periodic water level changes induced by a combination of gravitational forces exerted by the earth, moon and sun and their respective orientation to one another as well as the rotation of earth. Tidal waves are distorted due to interactions with the sea floor in shallow (coastal waters) and reflections at coastlines, resulting in complex patterns of tidal characteristics. The North Sea, part of the European continental shelf, is a shallow coastal sea with an average depth of 80 m (Sündermann and Pohlmann, 2011). Predominant North Sea tidal characteristics comprise semi-diurnal components with an average tidal period of 12.5 h as well as three amphidromic points (Malcherek, 2010). The mean tidal range along the German coast ranges from 2.25 m on Borkum in the East, up to 3.69 m at Wihlhelmshaven New Outer Harbor inside the Jade Bay and 4.12 m at the Weser Bridge in Bremen (WSV, Pegel Online; Accessed Jan. 2018).

Distorting the tidal wave are both local effects such as for example dredging and the construction of coastal infrastructure as well as meteorological changes and non-local effects such as resonance changes (Woodworth, 2010; Pickering et al., 2012).

In the recent past several modelling studies for the North Sea have been conducted, which produced consistent results for comparable scenarios or uniform SLR. Based on a modelling study, Idier et al. (2017) analyzed SLR impacts on tidal characteristics for the North Sea. They report good agreement with observational studies by Woodworth (2010) and Mawdsley et al. (2015) regarding changes in tidal constituents and spatial distribution pattern with increases for the German Bight. Nevertheless, no spatial correlation was found for uniform SLR scenarios and related impacts. The ratio of change in tidal range to SLR exhibited  $\pm 15\%$ , presuming a proportional ratio of SLR to tidal range changes at a SLR rate of  $3.0 \text{ mmyr}^{-1}$  (Church et al., 2014), results in  $0.9 \text{ mmyr}^{-1}$  that could be attributed to effects of uniform global SLR. Similar effects were reported by Arns et al. (2015) investigating a SLR scenario of 0.54 m, which resulted in an extra 0.1 m augmentation of regional water levels due to non-linear and spatially incoherent changes in main tidal constituents.

Pickering et al. (2012) and Pelling et al. (2013) as well as Idier et al. (2017) show comparable modelling results for uniform SLR scenarios of 2 m and 5 m in case of non-floodable coastal areas for the M2 with amplitude changes of 10 % to 15 %. Pelling and Idier show proportional increases dependent on SLR, whereas Pickering finds no proportionality. Idier et al. (2017), Ward et al. (2012) and Pelling et al. (2013) consistently show an increase for the German Bight. Inconsistencies between spatial patterns are traced back to differences in utilized bathymetry data (Idier et al., 2017). All studies that investigated a flood scenario, which allowed the flooding of coastal areas, show a decrease of proportionality regarding SLR related amplitude impacts (Pelling et al., 2013; Ward et al., 2012; Idier et al., 2017). For non-flood scenarios, a high proportionality between SLR and

tidal impacts is observed. The German Bight exhibits a high degree of increase with a non-proportional response to SLR. Remaining uncertainties within the studies pertain to non-uniform SLR scenario development, which show sensitivity of 8 % for tidal flats and especially the German Bight, coastal defense adaptation measures as well as geomorphological changes. The latter shall be investigated within this study for the case of ESL.

### 2.3.3 Storms

A synonym for images of destruction, storms represent the natural environment in one of its most energetic states with large waves eroding beaches and rapid storm surges inundating vast low-lying coastal stretches. Storms are one of the deadliest natural hazards on earth, being second only to tsunamis (IRFC, 2016; MunichRe, 2018b). Coastal zones present the environment most vulnerable to coastal storm impacts representing a land-sea interface, with its morphology constantly being reworked by currents, waves and wind (van Rijn, 1993; Holthuijsen, 2007). Inbound energy is dissipated and translated into morphodynamic changes, which under average conditions exhibit minimal short-term effects. Storm related energy levels on the other hand can well surpass the capacity of coastal zones to dissipate these, potentially resulting in severe erosion and exposure or even inundation of coastal hinterland areas, which are densely populated around the world with an estimated 23 % of the world's population living at the coast and 40 % living within 100 km of it (Small and Nicholls, 2003; United Nations, 2017). Hurricane Katrina impressively demonstrated in 2005, that despite scientific advancements, satellite technology and computer forecasts – nations can still be caught off-guard causing the loss of more than 1800 lives, insured losses of 62.3 bn.\$ and a total damage of 125 bn.\$ exemplifying single event impacts.

Coastal storms can be defined as:

*“Meteorologically-induced disturbance to the local maritime conditions (i.e. waves and/or water levels) that has the potential to significantly alter underlying morphology and expose the backshore to waves, currents and/or inundation.”*

(Coco and Ciavola 2018, p. 7)

Storm induced disturbances to the maritime conditions significantly alters the underlying morphology (sandbars, tidal flats, dunes and fairways) from its modal form in such a way, that a recovery period ensues where the coastal system balances out the impacts and strives for a morphologic equilibrium. In case of severe storm events, coastal zones may not recover at all but indeed develop a new equilibrium. Coastal storminess is a focal point in assessing storm impacts and integrates the frequency of events, timing, trends,

impacts of large scale phenomena such as ENSO and potential climate change impacts. Storminess can be assessed either statistically or synoptically (this study). Two main synoptic systems are responsible for most coastal storms, namely TCs and ETCs. TCs are intense low-pressure systems rotating around a warm core and follow regional typology, commonly tropical storms reach wind speeds between  $17\text{-}32\text{ ms}^{-1}$  whereas above,  $32\text{ ms}^{-1}$  Hurricanes (North Atlantic), Typhoons (Northwestern Pacific), TC everywhere else. Typical TCs are 650 km in diameter with 80 to 90 events per year (Marks, 2003). ETCs represent a broad class of cold-core systems induced by atmospheric temperature gradients and form between  $30^\circ$  and  $60^\circ$  latitude and genuinely exhibit west-east tracks. ETCs are much larger and slow moving systems compared to TCs with scales of 2000 km. With over 3000 events annually, ETCs are much more frequent and have equivalent and even more severe coastal impacts than TCs. Most prominent ETCs are the nor-easters along the eastern coast of the USA, European Windstorms, and east-coast lows in Australia.

Coastal storm impacts can lead to severe erosion (Ciavola et al., 2011). In 2007 an ETC hit Australia and eroded 29 m of coastline, with a ten month recovery period (Harley et al., 2017). European windstorms can have similar impacts, for example the ETC Barbara in 2016 eroded  $50.000\text{ m}^3$  of beach on Wangerooge (cost: 350.000 €) and again in 2017 Herwart removed 80 % of the islands coastline with reinstatement costs of 400.000 € (NL-WKN, 2018).

Coastal storm impacts show a disproportionate impact on society and ecosystems compared to changes in mean climate signals (Wong et al., 2014). The assessment by the IPCC special report on managing the risks of extreme events and disasters to advance climate change adaptation (SREX) (Field et al., 2014) revealed that data availability, quality and consistency affect statistics of extreme event analysis, as cyclone reports vary for different ocean basins. Similar problems are reported for wind extremes due to sensitivity of measurements to changing instruments and observation methods (Smits et al., 2005; Wan et al., 2010). The IPCC observed regional trends in TC frequency and intensity for the North Atlantic which are considered robust (very high confidence) since 1970. However, no robust trends in annual numbers have been identified for the last 100 years. An increase is still highly debated and only documented for the satellite era (Kossin and Vimont, 2007; Elsner et al., 2008). Recent hurricane seasons appear to consolidate this assumption, with record setting events nearly every storm season since 2006 and increasing damage and loss amounts. ETCs show a pole-ward shift of storm tracks (AR5) since 1950 with evidence that supports more frequent and more intense winter cyclones (AR5). European Windstorms according to the AR5 show no clear picture, due to inconsistencies in data series and derived proxies as well as potential artifacts in re-analysis products (Stocker 2014, p.217).

European Windstorms can be classified into the fast-moving Jutland-Type originating over Newfoundland moving east and a Scandinavian-Type forming over Greenland/Iceland, which move slow towards South East. A third type is the Skagerrak-Type, which represents a mixture of both types.

Storm surges constitute a main component contributing to ESLs along with tidal oscillations and wind waves (Losada et al., 2013). Wind drives the water masses towards the coast, inducing setup and surge. Sea level pressure (SLP) gradients also promote this motion of mass, contributing to the change in water level at the coast, also referred to as the inverse barometric effect (Doodson, 1924; WMO, 2011). Size, track, speed and intensity of the individual storm system as well as its interaction with the nearshore bathymetry and coastline contribute to the surge magnitude (Arns et al., 2015).

Results for cyclone assessment and simulation vary considerably depending on approach and input data (Brasseur et al. 2017, pp.67).

Potential dynamics of future storm surge level (SSL) and related parameters have been investigated by several studies under climate change conditions for Europe. For the Mediterranean an overall decrease is projected with an increase in interannual variability and an increase in extremes (Conte and Lionello, 2013; Jordà et al., 2012; Marcos et al., 2011; Androulidakis et al., 2015). Similar findings are reported for the Atlantic coast (Lowe and Gregory, 2005; Lowe, 2009; Church et al., 2010; Marcos et al., 2012). The Baltic Sea exhibits increase of the 99 percentile or  $Q_{0.99}$  of wind by 3-5 % which are projected to increase surge levels by 0.2 m. Increase in 30yr RI events by 0.4 m to 0.6 m (A1B,B1) (Gräwe and Burchard, 2012; Meier et al., 2004; Meier, 2006).

North Sea storm surge climate and potential climate change impacts have been investigated by several studies:

Observation based studies investigate tide gauge data as well as pressure readings or derived storm-precursor indicators (Carter and Draper, 1988; Coco and Ciavola, 2018; Cornes and Jones, 2011; Cornes, 2014; Cusack, 2013; de Kraker, 1999; Hanna et al., 2008; Schmidt and von Storch, 1993; Weisse and Meinke, 2011; Gönnert, 2003; Jensen et al., 2006b; Brooks et al., 2016; Santo et al., 2016; Stewart et al., 2017; Weisse et al., 2012; Stendel et al., 2016; Brasseur et al., 2017; Howard et al., 2010; Santo et al., 2016). The majority of the observational based studies ( 66.7 % ) concludes that no long term trend could be identified based on their mostly regional, data. Only two studies each found an increasing or a decreasing trend for frequency and intensity. Nevertheless, 22.2 % of the studies identified a shift in storm climate over the North Sea towards more pronounced westerly winds.

Studies based around hind-casts or investigating re-analysis data on the other hand show a different picture, with 61.5 % of the studies indicating an increased storm frequency and duration and 30.8 % finding a shift within the storm climate towards more westerly

winds and increased extreme events (Brönnimann, 2015; Donat et al., 2009; Donat, 2010; Siegismund and Schrum, 2001; Smits et al., 2005; Weisse and Plüess, 2006; von Storch and Weisse, 2008; Vousdoukas et al., 2016; Brown et al., 2012; Sterl et al., 2015; Befort et al., 2015).

Finally, simulation based studies for future scenario projections comprise by far the largest group (Andersen et al., 2001; Bengtsson et al., 2006; Beersma et al., 2016; Beniston et al., 2007; de Winter et al., 2013; Della-Marta et al., 2009; Donat, 2010; Knippertz et al., 2000; Leckebusch et al., 2006, 2008; Pinto et al., 2007, 2009; Rockel and Woth, 2007; Sterl et al., 2009; Ulbrich et al., 2008; Vousdoukas et al., 2016; Weisse and Storch, 2010; Debernard and Roed, 2008; Loewe, 2009; Howard et al., 2010; Brown et al., 2012; Gaslikova et al., 2012; Howard et al., 2014; Arns et al., 2015; Harvey et al., 2012; Woollings et al., 2012; Harvey et al., 2014, 2015; Befort et al., 2015; Stewart et al., 2017). Most of the studies are based on GCM or RCM simulations and in some cases use dynamic down-scaling to transfer results to local study sites. Predominant across 82.4 % of the studies is a trend of increasing storm intensity for the extremes ( $Q_{0.99}$ ) as well as a decrease in mean events regarding intensity. A main finding of more recent investigations pertains to a shift of the storm track not only pole-ward but also an eastward extension towards Europe (Harvey et al., 2015; Vousdoukas et al., 2016; Befort et al., 2015; Callies et al., 2017; Quante and Colijn, 2016).

All studies emphasize that storm associated parameters exhibit a large natural variability (i.e. Arns et al. 2015; Dangendorf et al. 2015; Feser et al. 2015; Weisse et al. 2012), which at this point in research preclude the possibility to discern a potential trend due to the large SNR. Recent investigations show that the storm track and intensity are closely related to large scale atmospheric changes, for example, but not limited to, the NAO, the ENSO as well as the Atlantic meridional overturning circulation (AMOC) (Huthnance et al. 2016, pp.94). Furthermore, investigations by Donat (Donat et al., 2009; Donat, 2010) have revealed, that a characteristic process of European Windstorms is the *Sting jet* (SJ). Sting jets are responsible for the large wind-speeds and gusts across Europe, thus are a crucial element of most ETCs. However, due to their comparably small scale of 150 km across and their transient nature they are not resolved by all type of re-analysis data. Consequently, projected climatologies are flawed (Martínez-Alvarado et al., 2014). Trends identified within reviewed storm research literature are shown in figure 2.5. While the majority of observation based studies finds little evidence of a changing storm climate across Europe, hindcast based studies show a more mixed pattern with a clear intensification and internal shift.

Simulation based projections of the future climate finally show a prevalent trend towards increased storm intensity as well as a shift towards more westerly events. Model sensitivity towards certain parameters or processes currently receives a lot of attention and is

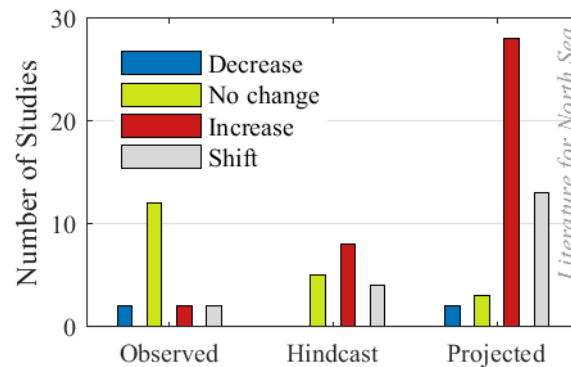


Figure 2.5: Trends in storm related research studies categorized into observation, hindcast and future projection based studies.

investigated using the perturbed physics ensembles (PPEs) method and pre-defined filter techniques to reduce the computational cost (i.e. Sparrow et al. 2018). PPEs are mainly designed to systematically sample uncertainties within a model framework by perturbing poorly constrained parameters within physically plausible ranges, thereby greatly increasing the experiment control compared to the common ensemble results. The key limitation is that structural or stochastic modeling uncertainties are not assessed within a single model framework. Accordingly, multi-model ensembles in combination with PPEs allow for identifying missing or structurally deficient representations of processes in models. Computational efficiency can be tweaked by the application of observational constraints limiting the physically plausible range of the PPE. More elaborate schemes include the stochastically perturbed physics ensemble (SPPT) and the stochastic kinetic energy backscatter scheme (SKEB) (Shutts, 2005; Shutts et al., 2011).

Consequently, further advancement of science and technology is required and currently in development to reduce the large uncertainties associated with projecting dynamic non-linear components of extreme events such as storms. Regardless of large uncertainties in storm projections, three major findings are identified across the majority of storm research studies for the North Atlantic and adjacent North Sea:

- Research projects a likely increase in intensity for the most extreme events as well as a more westerly wind direction
- A pole-ward shift of the north Atlantic storm track is very likely
- Recent findings show an alarming eastward extension of the storm track across Europe (i.e. Feser et al. 2015; Romero and Emanuel 2017; Michaelis et al. 2017)

### 2.3.4 Wind

Wind (*greek: anemos*) describes the relocation of air particles regarding their direction and speed and is typically represented as a vector. Meteorology differentiates several wind types, with the ground wind being the international reference, which is measured 10 m above ground. Windspeed can also be classified according to the well-renowned Beaufort-Scale. Initially developed by civil engineer John Smeaton to classify wind impacts on structures (Smeaton, 1759), it was further developed to classify wind speeds according to sea states and finally published in 1837 by Sir Francis Beaufort (Huler, 2004). The Beaufort scale ranges from 0 Bft *calm* to 12 Bft *Hurricane force*, with 9 Bft resembling the threshold for *Storm* with windspeeds of  $20.8 \text{ ms}^{-1}$  to  $24.4 \text{ ms}^{-1}$ . Winds are mainly driven by gradients in air-pressure, with air masses streaming from high-pressure systems to low-pressure systems, with the earth rotary motion inducing circular wind-trajectories. Air pressure is defined as the pressure an air mass between the ground surface and the outer atmosphere exerts onto a defined surface area due to gravity. Mean SLP is 1013.25 hPa (DWD, 2018b).

Wind constitutes a major component of storm surge generation, as onshore winds exert drag onto the water surface, thereby elevating water levels at the coast (Gönnert, 2003). For the German Coast, wind directions generating severe storm surges are West-South-West to North-North-West from  $247.5^\circ$  to  $337.5^\circ$  (Jensen et al., 2006b). The European continental shelf sea atmosphere is strongly influenced by large-scale atmospheric patterns over the North Atlantic and inherent changes. Studies investigating the occurrence of strong low pressure systems ( $<950 \text{ hPa}$ ) show an increase between 1990 and 2000 with a decrease until 2006 and a surge since then, with the record number of 18 events taking place in 2013/2014 (Franke 2009 extended in Quante and Colijn 2016, fig. 1.19, p. 22).

Projected changes in extreme wind speeds for the North Sea region and the German Bight are compiled in table 2.3.3 from different sources, described hereafter.

Wind climatology of the North Sea region is mainly characterized by a large variability present across multiple time-scales. Prior to satellite observations, in-situ wind observations (mainly land-based) were employed, which represent a poor geographic sampling grid and are partially homogeneous (i.e. Lindenberg et al. 2012), driving the need for homogenous areal wind-data, giving rise to re-analysis data sets, i.e. ERA-Interim, 20CR, coastDat2. Reanalysis products are derived assembling all available data into state-of-the-art GCMs, which are then used to hind-cast areal atmospheric patterns, while making use of observational data for calibration purposes. Based on reanalysis data, several studies found a strong increase in wind speeds observed over the North Sea between 1948 to 2014 and a decrease in recent years (Donat et al., 2011). Siegismund and Schrum (2001) found an increase of 10 % for winter periods in the 1960's and 1980's but no robust trend using NCEP data for the period 1958 to 1997. Also using NCEP data for scenario simulations,



Weisse et al. (2005) found an increase in storminess with a positive trend for the southern North Sea with  $12\% \text{yr}^{-1}$  for the period 1958 to 2001. Recent projections of wind climatology for the North Sea show regional differences due to higher resolution simulations, with areas of likely decrease (Feser et al., 2015), unaffected areas (Sterl et al., 2015) as well as areas with high sensitivity and likely increase (Vousdoukas et al., 2016) of high wind speeds. The German Bight with its intricate coastline shows a strong regional variation and high overall sensitivity towards changes in wind patterns.

Table 2.3.3: Overview of projected changes in wind speed for the southern North Sea.

time period	wind speed change ( $u_{10} \text{m s}^{-1}$ )	Reference
1961-2100	$0.2\text{-}0.5 \text{ m s}^{-1}$	Gaslikova et al. (2012)
1961-2100	$0.55\text{-}1.1 \text{ m s}^{-1}$	
1961-2100	$1.19 \text{ m s}^{-1}$	Groll et al. (2014)
1999-2050	$1.02 \text{ m s}^{-1}$	Grabemann et al. (2004)
2071-2100	$1\text{-}2 \text{ m s}^{-1}$	Grabemann and Weisse (2008)
2000-2100	$0.35\text{-}0.68 \text{ m s}^{-1}$	Lowe (2009)
1977 event	$0.85\text{-}1.7 \text{ m s}^{-1}$	Brown et al. (2010)
2071-2100	$0.3\text{-}0.40 \text{ m s}^{-1}$	Weisse et al. (2012)

Increases in extreme wind speeds related to the 99<sup>th</sup> percentile have been reported by various research groups, ranging from 6% to 8% (Gaslikova et al., 2012; Rockel and Woth, 2007; Debernard and Roed, 2008; Grabemann et al., 2004; Grabemann and Weisse, 2008; Grabemann et al., 2015; Groll et al., 2014; Winter et al., 2012; de Winter et al., 2013; Brown et al., 2010). A research group around Vousdoukas et al. (2016) projected strong increases in westerly winds for the North Sea based on RCP scenarios simulating tidal dynamics as well as wind waves forced with atmospheric re-analysis data. Their findings are in agreement with previous results based on RCP as well as special report on emission scenarios (SRES) (Rockel and Woth, 2007; Debernard and Roed, 2008; Gaslikova et al., 2012). Furthermore, they found a potential increase in inter-annual variability, which was previously reported by other researchers as well (e.g. Dangendorf et al. 2014; Weisse et al. 2012). Moreover, several studies project a change of direction to more frequent westerly winds (Grabemann et al., 2015; Vousdoukas et al., 2016; Gaslikova et al., 2012; Groll et al., 2014; Sterl et al., 2015). Based on observations, storm surge and related wind influence for the German Bight and their respective evolution in time have been investigated (Gönnert, 2003). Results show a statistical increase in wind surge duration due to single extreme events as well as elongated storm surge events. Furthermore, an

increase of annual mean wind speeds of 10% was found for the period 1960 to 2000 for the winter months within re-analysis data (Siegismund and Schrum, 2001).

### 2.3.5 Waves

Waves<sup>3</sup> are vertical motions of the ocean surface and occur on many scales, ranging from wind induced surface gravity waves to tides or storm surges (Holthuijsen, 2007). Tidal waves have been elaborated on in section 2.3.2, while the occurrence and development of surge is described in section 2.3.6. This section focuses on surface gravity waves induced by wind with periods of 1/4-30s and corresponding wave lengths of 0.1-1500 m (see figure 2.6). Surface gravity waves are typically characterized by statistical parameters such as  $H_{1/3}$  and the  $T_p$  or energy density spectrum. Processes affecting the wave evolution in coastal waters and their respective importance is given in table 2.3.4.

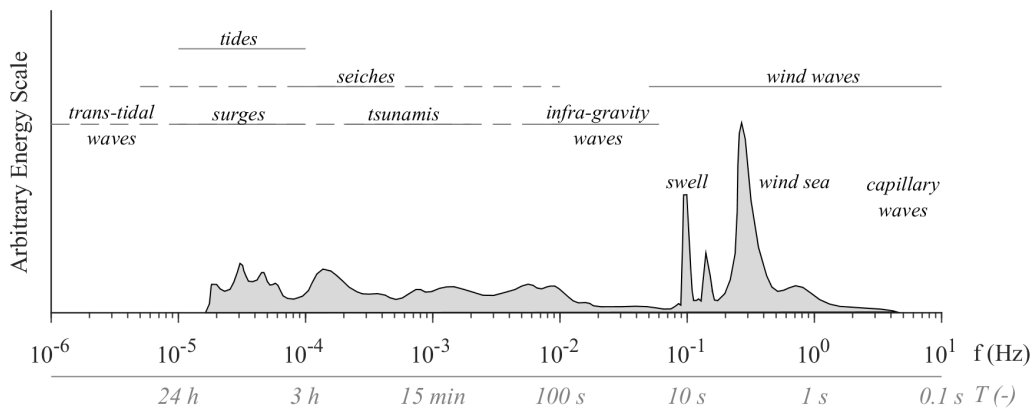


Figure 2.6: Wave related Frequencies and Periods of the vertical motions of the ocean. Redrawn/Adapted after Munk (2005).

Extreme ocean waves in the North Sea are induced by strong ETC winds coming either from the North or the South-West. Events coming from the North feature the larger waves, as the winds wrap around the south-west side of the storms and form sting-jets (see section 2.3.4), which run across a longer fetch, generating the largest waves for the North Sea (Ponce de León and Guedes Soares, 2014). An additional growth effect can occur, when the ETC moves at the same speed as the wave-group celerity, resulting in *trapped-fetch* (Reistad et al., 2005).

The North Sea is characterized by dominant wave directions of W-SW and N, occurring

<sup>3</sup>Waves are considered disturbances of the equilibrium state in any given body of material, which propagate through that body over distances and times much larger than the characteristic wave lengths and periods of the disturbance

Table 2.3.4: Wave evolution related processes and their relative importance for the coastal zone (updated and redrawn after Holthuijsen 2007).

Process	Coastal waters		
	Shelf seas	Nearshore	Infrastructure
Wind generation	•••	•	○
Quadruplets	•••	•	○
White-capping	•••	•	○
Bottom-friction	••	••	○
Current refraction	•	••	••
Bottom refraction/shoaling	••	•••	••
Depth induced breaking	•	•••	○
Triads	○	••	•
Reflections	○	•/••	•••
Diffraction	○	•	•••

••• = dominant, •• = significant, • = minor importance, ○ = negligible

for 60% of the time (Groll et al., 2014). For the central North Sea Bell et al. (2017) examined the 97.8 percentile of wind wave data recorded at the Fortis Platform from 1974 to 2015. They found a bi-modal distribution of wave direction as well with 47% pertaining to southerly events and 53% to northerly events and 6 m to 9 m resembling the majority of events for both directions, with extremes of up to 11 m.

Value ranges of projected changes in surface wind waves for the North Sea region and the German Bight are compiled in table 2.3.5.

Future projections of North Sea wave climate based on GCM or RCM simulations are genuinely forced with atmospheric re-analysis data. A comparative study of future wave climate projections for the North Sea showed a consistent upward trend for  $H_{1/3}$  for the south-eastern North Sea and a decrease for the North-Western North Sea (e.g. Schrum et al. 2016, pp.184). Increases in extreme surface waves considered as the 99<sup>th</sup> percentile exhibit a range of 6% to 8% or 0.26 m to 0.35 m (Debernard and Roed, 2008; Grabemann and Weisse, 2008; Groll et al., 2014; Grabemann et al., 2015; Vousdoukas et al., 2017). Results are based on various modelling tools and a range of IPCC scenarios.

However, all studies emphasize that the wave climate is strongly controlled by the atmospheric forcing, which is associated with a high degree of uncertainty regarding future changes (cmp. section 2.3.4) and that projected changes in wave climate remain within the natural variability (e.g. Weisse et al. 2012).

Nevertheless, increased relative mean sea level (RMSL) trends result in a reduction of depth limited breaking due to increased water levels during storm surges. Consequently, the high-pass filter effect of tidal flats, ebb-deltas and foreshores is significantly reduced, allowing higher and longer waves to travel further inland and finally impact coastal structures (Niemeyer et al. 2016, pp. 457). In recent years the clustering of ETCs caused increasing wave impact damage (Bell et al., 2017). Clustering of storm events can result in increased  $H_{1/3}$ , when an incoming storm affects a disturbed sea surface from a previous event (Cavaleri et al., 2016).

Table 2.3.5: Overview of projected changes in wind waves for the southern North Sea.

Sig. wave height increase (m)	Reference	Note
0.25-0.35 m	Grabemann and Weisse (2008)	
0.0 m	Sterl et al. (2009)	
0.35 m	Vousdoukas et al. (2017)	
0.30 m	Weisse et al. (2012)	
0.35 m	Groll et al. (2014)	
0.25 m	Groll N. (2014)	
0.26-0.35 m	Debernard and Roed (2008)	
0.25-0.50 m	Grabemann et al. (2015)	
0.10 m	Weisse et al. (2012)	

### 2.3.6 Extreme sea level

Extreme Sea Levels pose a significant threat for coastal flooding and erosion. Composed of MSL (cmp. section 2.3.1), tides (cmp. section 2.3.2), waves (cmp. section 2.3.5) and storm surge levels ESLs represent one of the most energetic and violent states of nature (Coco and Ciavola, 2018). Storm surges are a societal risk, which has impacted the lives of hundred-thousands of people. Increasing urbanization lead to the construction of flood protection works, greatly reducing floodplains and thus increasing coastal flood levels and potential impacts and dangers from dike failures (von Storch, 2014). A major milestone constitute the modern national weather and storm surge forecast systems, which issue warnings and allow for impact preparations (DWD, 2018a; BSH, 2018b).

Water levels associated with ESLs have constantly increased over the last 100 years given the underlying influence of SLR (Weisse et al., 2014a). For the German Bight a collective of over 200 storm surges has been recorded over the last century (Gönnert, 2003; Gönnert

and Thumm, 2010). Based on the time series of the gauge Wilhelmshaven Alter Vorhafen, a total of 195 ESLs has been identified (according to BSH classification) with one extreme storm surge event and are shown in figure 2.7.

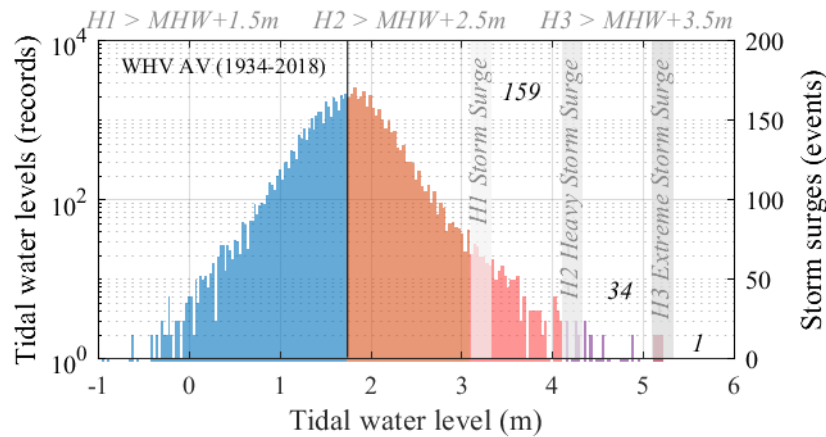


Figure 2.7: ESLs for the tide gauge of Wilhelmshaven Alter Vorhafen from 1940 to 2018 classified according to the BSH criterion presented in chapter 2.2 with century based adaption of MHW and indicated moving reference levels (gray shadowed bars) for surge classification.

Previous studies stated that based on tide gauge data, changes in ESL are likely not to surpass MSLR and that associated uncertainties are of the same magnitude (Church et al. 2010, pp. 326). However, ensuing research findings showed that ESL exhibits pronounced short-term variations, associated with seasonal and nodal tidal cycles. Identified long-term trends correspond to MSLR, with high natural variability due to single events (Weisse et al., 2014a).

Coastal engineering and research alike investigate ESLs for deriving design water levels for coastal (defense) structures using deterministic or statistic approaches (e.g. KFKI 2002, pp.19). Given the need for practicality and applicability for extensive stretches of coastline, Germany has adopted the single value method as well as the comparative value method, both are based on linear superposition of empirical values whereas the extreme value analysis is the third option, which includes statistically extrapolated values. However, ESL-components have been shown to exhibit non-linear interactions, which affect the overall ESL related water level (e.g. Arns et al. 2015; Vousdoukas et al. 2017).

Observation based statistical extreme value analysis was recently performed for global ESL using GESLA-2<sup>4</sup> data. Findings show that statistical return periods for e.g. a 100 year event is significantly reduced to a once per year event by 2050, assuming a linear

<sup>4</sup><http://gesla.org>

SLR as well as no changes in storm climate. Furthermore, an analysis of the recently published GTSR-data set (Muis et al., 2016; Muis, 2016) was performed and revealed a general underestimation by the model but an overall better performance than point based statistical approaches. Combined ESL associated mean uncertainties for events featuring return intervals (RIs) equal to 10, 100 and 1000 years are 0.27 m, 0.4 m and 0.74 m. The results show the large range of uncertainties associated with future ESL projections, which are an order of magnitude larger than, for example, projections of SLR (cmp. section 2.3.1) (Jensen et al., 2017).

Several studies have investigated possible changes in ESL due to climate change using dynamic modelling (i.e. Debernard and Roed 2008; Weisse et al. 2014a; Jensen et al. 2017; Wahl et al. 2017; Vousdoukas et al. 2017; Rasmussen et al. 2018).

Debernard and Roed (2008) found an 8% to 10% increase for Storm surge residuals (SSRs) based on dynamic modelling. Schrum et al. (2016) identified ESL changes of  $-0.08$  m to  $0.18$  m with a predominant increase for Europe's coasts, which were confirmed by Gaslikova et al. (2012). Weisse et al. (2014a) found marginal increases of  $<5\%$  using a combined approach of dynamic and statistical modelling. The research group around Jensen, showed a significant increase and present high uncertainty ranges for ESL values in northern Europe and the world's coasts.

Dynamic modelling of MSL impact on surge levels under atmospheric forcing was reported to additionally amplify the overall water level by  $0.15$  m for the Wadden Sea especially for shallow coastal areas. Furthermore, the impact of SLR was three times larger than the effect of increased wind, leading to the conclusion that the main effect occurs due to non-linear shifts in tidal components arising from interactions with the bathymetry. High waters were shown to establish earlier due to a decreased run-up time. Atmospheric forcing showed a dampening effect for the high water levels due to a water-depth related surge reduction (Arns et al., 2015). Exceedance probabilities for all considered SLR scenarios were surpassed by  $0.07$  m to  $0.1$  m.

Recent advances made in a pan-European coastal impact assessment study combined dynamic modelling of tides, waves and storm surges to project climate change impacts on ESLs along Europe's coasts. Results show an RMSL driven average increase of ESL amounting to  $0.57$  m and  $0.81$  m for RCP4.5 and RCP8.5 respectively. The largest values were found for the German Bight with  $0.98$  m. Projected changes in storm and wave climate are shown to contribute  $22.1\%$  to the overall changes in ESL. Estimates for 100-year ESL threatening  $5 \times 10^6$  Europeans, show an alarming trend towards becoming an annual ESL (within RCP8.5) (Vousdoukas et al., 2017).

Results obtained by applying a similar method investigating changes in ESL frequency and intensity oriented along guidelines published by the United Nations Framework Convention on Climate Change (UNFCCC) project an increase in frequency and intensity. It

is noteworthy that, the study defines a set of scenarios for projecting future changes, considering and redefining the Paris agreement goal of a stabilized global mean surface temperature (GMST) 2.0 °C warming threshold to 1.5 °C aligned with UNFCCC documents (United Nations 2015, §2 a). Accounting for stabilized GMST of 1.5 °C to 2.5 °C, ESL changes exhibit strong regional differences. For Cuxhaven Germany the  $ESL_{500}$  is projected to occur 0.01 yr<sup>-1</sup> for the 1.5 °C scenario, 0.03 yr<sup>-1</sup> and 0.01 yr<sup>-1</sup> for the 2.0 °C and 2.5 °C scenarios respectively. Results showcase the long term impact environmental policies have affecting a global coastal population of  $>6.25 \times 10^6$  inhabiting low-lying coastal areas (<10 m MSL) (Rasmussen et al., 2018).

Advancements regarding ESL process understanding and drivers clearly show, that initial assumptions of intensity or frequency being largely unaffected by climate change were revised as methods become more refined with ongoing research. Current research presents strong evidence for increasing ESL intensity and frequency with great spatial differences. Uncertainties associated with ESL estimates are still an order of magnitude larger than those associated with MSLR projections. Nevertheless, estimates are crucial for coastal impact assessments and long term planning, given their relative importance for flood protection. Furthermore, current research investigates non-linear effects of ESL components as these may further amplify the overall surge level employing dynamic numerical models on small to medium scales.

### 2.3.7 Discharge

River runoff is mainly controlled by precipitation and drainage characteristics of individual catchment areas, providing the available water volume. Changes to the overall volume or seasonal shifts in distribution have been linked to global climate change as well as constructive and river engineering measures (Stocker, 2014; Bormann et al., 2011). River discharge and especially extreme high flow resembles an additional factor, potentially leading to increased ESL within estuaries, if they occur together with a storm surge, forming compound events (Petroliagkis et al., 2016).

Changes within river flood discharge due to climatic impacts on components of the hydrological cycle such as precipitation and evapotranspiration have been investigated using ensemble forced hydrological models as well as statistical time series analysis (Bormann, 2010; Bormann et al., 2011; Fangmann et al., 2013; Hattermann et al., 2014a,b, 2017; Roudier et al., 2016; Donnelly et al., 2017; Lobanova et al., 2018).

Europe wide research studies based on hydrological modelling primarily project a prevalent north-south gradient for precipitation and high flow discharge, with decreasing values for southern Europe and increasing trends for the northern parts including Germany. Studies report a shift of spring high flows towards earlier occurrences as well as increased

winter discharge volumes, although amplitudes are associated with uncertainties of the same order of magnitude as for storm projections (Roudier et al., 2016; Donnelly et al., 2017; Hattermann et al., 2017; Lobanova et al., 2018).

A first cross-scale inter-model comparison study for hydrological models revealed that both GCM and RCM exhibit a similar sensitivity towards climate variability regarding river basins (Hattermann et al., 2017). The study concludes that large uncertainties still persist and that more ensemble runs are needed to reproduce natural variability. Furthermore, related processes need to be investigated and integrated into the models in more detail, which is in line with current research focusing on improving physical process based models (Shutts, 2005; Shutts et al., 2011).

A study employing different warming scenarios ranging from 1.5 °C to 3.0 °C within RCP ensembles, investigated changes in the hydrological cycle using 5 different hydrological models forced by ensemble data (Donnelly et al., 2017). The authors report a robust trend for increases in both precipitation and winter discharge for northern Germany. Nevertheless, they conclude that ensemble data is insufficient to account for natural variability of the hydrological cycle and suggest the usage of more ensembles. Furthermore, they state that RCP scenarios do not realistically account for time-lagged responses of the oceans to an increase in GMST of 2.0 °C within simulation time spans; thus ignoring potential impacts arising from slow changing biogeochemical processes controlling CO<sub>2</sub> and therewith vegetation and evapotranspiration with direct feedback onto the hydrological system. This statement was also observed within storm surge research (Rasmussen et al., 2018). Impacts differ between the scenarios, in that the 1.5 °C scenario shows the weakest impacts on regional scales. The 2.0 °C variation significantly intensifies previously found changes and 3.0 °C show an alarming spatial extension of affected catchments multiplying impact magnitudes. They summarize that environmental policy and technological advances have a large and profound significance for mitigating climate change impact through legislation. Substantial GHG reductions are crucial to prevent severe changes in Europe's water cycle (Donnelly et al., 2017).

The estuarine focus area of this study encompasses the Weser a major river in Germany with an associated catchment area of 46.306 km<sup>2</sup> and a total length of 432 km (NLWKN, 2014a). The Weser barrage in Bremen constitutes the tidal boundary for the Lower and Outer Weser. The highest high tide water level occurred in conjunction with the ETC Xaver and measured 2.67 m and 3.15 m above MHW in Bremen and Bremerhaven. Longterm mean monthly discharge values are given in figure 2.8(a) together with future projections of discharge changes.

Weser catchment precipitation analyses for the last 50 years reveals a significant increase in winter precipitation and flood discharge volumes between 1950 to 2005. Winter is characterized by increased maximum precipitation of 24 h and 5 d events, hence an intensifica-



tion of extreme precipitation events due to a shift in seasonal distribution with a decrease in summer and an increase in winter as well as an overall volume increase (Haberlandt et al., 2010; Fangmann et al., 2013). Analysis of annual maximum flood discharge and stage values for the Weser gauge Intschede from 1850 to 2010 revealed a decrease in annual extremes from  $1800 \text{ m s}^{-3}$  to  $1150 \text{ m s}^{-3}$  and 7.3 m to 5.8 m respectively. Decreases in discharge are linked to changes in land use and spreading urbanization, whereas flood stage levels have fallen due to the ongoing incision of the Weser and river engineering measures, directly attributing changes in river regime to anthropogenic activity (Bormann et al., 2011).

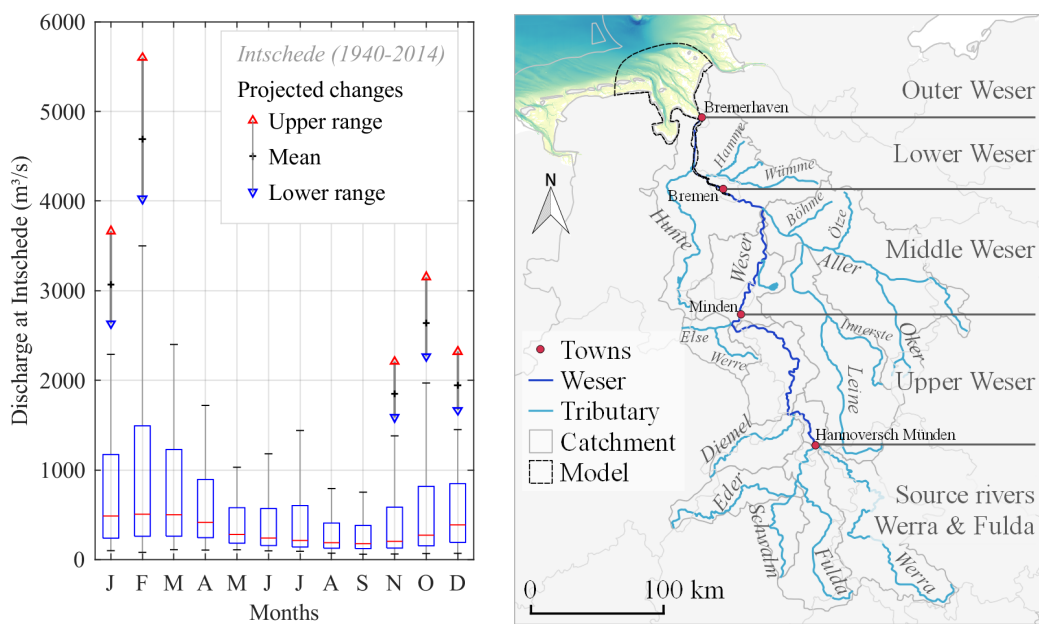


Figure 2.8: Intschede monthly discharge stages and Weser catchment area.

However, only one annual maximum was considered within the study, excluding possible shifts in frequencies. A significant discharge increase of 40 % to 60 % for winter peak discharge within A1B and RCP8.5 scenarios respectively was projected for the Weser across a model range of 4 GCMs and 12 RCMs for the period 2031 to 2060 excluding effects of vegetation and soil composition (Hattermann et al., 2014b). Winter related increase of extreme discharge regimes was linked to increased melt-water (Bormann, 2010). Similar orders of magnitude have been projected by catchment related studies for the Weser as well as sub-catchments (Hölscher et al., 2012; Kreye et al., 2010). Other studies project an increase of 2 % and 15 % for winter discharge volumes for 2100 (Hölscher et al., 2012; Huang et al., 2013). Projected changes in winter discharge volume for the Weser river are given in table 2.3.6.

Table 2.3.6: Overview of projected changes in Weser flood discharge volume for the winter season.

time period	discharge change (%)	Reference
2031-2060	+20-80 %	Hattermann et al. (2014b)
2071-2100	+2-47 %	Hölscher et al. (2012)
2000-2100	+50 %	Kreye et al. (2010)
2061-2100	-5- +50 %	Huang et al. (2013)
1951-2005	+49- +50 %	Fangmann et al. (2013)

### 2.3.8 Sediment delivery

Global estimates of river borne sediment discharge to the oceans ranges from  $9 \text{ Gtyr}^{-1}$  to  $58 \text{ Gtyr}^{-1}$  (Judson and Ritter, 1964; Fournier, 1960) with a majority of studies estimating  $15 \text{ Gtyr}^{-1}$  to  $20 \text{ Gtyr}^{-1}$  (Walling, 1983; Milliman and Meade, 1983; Milliman and Syvit-ski, 1992; Ludwig and Probst, 1998). Global dam construction is estimated to retain 28 % of suspended sediments, potentially reducing global sediment transport to the oceans by  $4 \text{ Gtyr}^{-1}$  to  $5 \text{ Gtyr}^{-1}$  and suggest a profound anthropogenic impact on the sedimentary cycle (Vörösmarty et al., 2003). Total sediment flux reduction based on a database maintained by the International Commission on Large Dams (ICOLD) was conservatively estimated at  $60 \text{ Gtyr}^{-1}$  (Basson, 2008; Walling, 2009). Particulate matter, mainly C, N and P, are main drivers for biogeochemical processes controlling coastal sediment inventories and are estimated to have been reduced by anthropogenic activities by as much as 13 % globally (Beusen et al., 2005). Sediment delivery to the coastal zone by rivers and long shore transport is vital for natural shore development and sustains a morphodynamic equilibrium. A distortion by insufficient supply can easily lead to erosive tendencies destabilizing ebb deltas, barrier islands and beaches alike (Bakker et al., 2008).

A first comprehensive analysis of beaches on a global scale revealed that sandy beaches cover 31 % of the world's coastline. Out of these 24 % exhibit erosive trends, 28 % show accretion and the remaining 48 % appear to be in stable equilibrium states over a 33 year timeseries of satellite images. Main coastline changes have been attributed to anthropogenic impacts and coastal works obstructing long- and cross-shore sediment transport resulting in coastal squeeze (Luijendijk et al., 2018). Coastal squeeze imposes major constraints on the adaptability of coastal systems and reduces the resilience towards storm driven impacts (Pontee, 2013). Moreover, climate change will exacerbate coastal squeeze induced losses and stresses given the intensification of the earth system energy fluxes

(Ranasinghe, 2016).

Europe comprises 100.925 km shoreline with 40.7 % classifying as sandy of which 25 % are reported to erode, 12 % are protected by coastal works and 5.6 % are eroding despite being protected (EU 2004b,a, p.5 Table 2). Germany has 3524 km of coastline (5 % soft rock; 64 % beaches; 13 % tidal mudflats; 18 % artificial/engineered) of which 30 % are eroding (12.8 % unprotected, 22 % protected, 4.2 % eroding despite protection).

The sandy shores and dune fields of the North Sea constitute a regional complex developed out of sediment discharged by the Rhine-Meuse delta into the coastal zone (Quante and Colijn, 2016). In the North Sea the material is transported via long shore currents following the anti-clockwise flow of the semi-diurnal tide around the south-eastern coastline of the North Sea with westerly winds driving the sediments inland. Main sediment influx sources are 12 major river systems given in figure 2.9 a) with a cumulative annual sediment supply of  $23.5 \times 10^6 \text{ t yr}^{-1}$  as well as storm related coastal erosion of cliffs on the Atlantic coasts of Great Britain and France.

Figure 2.9: North Sea sediment influx and Anglian plume with the major sediment delivering river systems given in a) and the storm driven monthly extend of the East Anglian Plume based on data given in Pietrzak et al. (2011), Huthnance et al. (2016) and the NLWKN (2014a).

A major transport phenomenon conveying as much as 6.6 Gt of sediments into the southern North Sea is the East Anglian Plume, exemplary extends are given in figure 2.9 b), which originates off the east coast of southern England and transports sediments from major rivers and the Norfolk cliffs south-eastward entrained by the anticlockwise circulation pattern of the North Sea, merging with the Rhine Delta plume (Huthnance et al., 2016; EU, 2004b).

The German Bight coastline classifies as mixed wave- and meso- to macrotidal environment; comprising barrier islands with interjacent tidal inlets as well as three large estuaries all embedded in open and back-barrier tidal flats (Winter and Bartholomä, 2006; Hadley, 2009; Winter, 2011a; Kösters and Winter, 2014). Based on 22.000 sea bed samples collected throughout the German shelf sea, sedimentological characteristics were analyzed and driving morphodynamic processes inferred (Valerius et al., 2015). The German shelf sea exhibits bed dominated areas, limited to the Borkum and Norderney reefs along the south-west coast and all along the north-east coast, as well as flow formed zones found elsewhere. Flow formed areas are characterized by well graded mobile fine-sand (125  $\mu\text{m}$  to 177  $\mu\text{m}$ ) with shares in excess of >50 %, whilst bed formed areas are identified by poorly graded medium to coarse sand fractions (177  $\mu\text{m}$  to 500  $\mu\text{m}$ ). The German Bight is an accumulation area for sediments, with annual import estimates of  $1.3 \times 10^6 \text{ ty}^{-1}$  (Puls et al., 1997) with high annual fluctuations depending on storm events (Quante and Colijn 2016; pp.110). High morphodynamic activity is found throughout the German Bight, with tidally driven morphodynamics governing the deeper tidal channels in Estuaries and inlets between barrier islands, with wind waves shaping the island foreshores and open tidal areas of the estuaries (Kösters and Winter, 2014). Mobile sand fractions consist of medium sand, being transported as suspended and bedload by the tidally driven conveyor belt into the German Bight, mainly covering the shoreline and tidal areas; and a highly mobile fine sand fraction (63  $\mu\text{m}$  to 177  $\mu\text{m}$ ), which is transported off-shore and settles with increasing water depth where it remains (Valerius et al., 2015).

Large changes are found on barrier-island coasts with rates ranging  $1 \text{ myr}^{-1}$  to  $8 \text{ myr}^{-1}$  and is mainly storm surges driven which also reshaped barrier and back-barrier morphology (Kelletat, 1992). Over the last 120 yr an acceleration of erosion is evident; an increase at Sylt from  $0.9 \text{ myr}^{-1}$  (1870-1952) to  $1.5 \text{ myr}^{-1}$  (1952-1984) despite increasing protection measures with both MSLR and increase in storminess drive it. However, no evidence of a regionally coherent response to large-scale forcing in history (MSLR) was identified to date, which could mainly be due to insufficient data (Quante and Colijn 2016; pp.116).

Abiotically-induced climate related morphologic changes are mainly expected to be found in the German Bight, as climate related change is more likely where benthic organisms control the development of bedforms as so-called *ecosystem engineers*. However, no comprehensive field studies have been conducted until now. Numeric simulations for climate change impacts on *ecosystem engineers* on the Dutch continental shelf suggest a strong impact (Borsje et al., 2013) and signifies an important future research subject. If sediment import into the Wadden Sea can compensate for the MSLR is a major subject of discussion; higher temperatures are expected to enhance the organic matter turnover with yet unknown effects on the Wadden Sea food web and associated soil-mechanics (ecosystem engineers). Large scale processes as the AMO shows a high variability with no discernible trend, whereas the NAO is clearly correlated to North Sea characteristics. Currents are

highly variable due to atmospheric components and a single storm can be significant compared for a year's integrated transport (Quante and Colijn, 2016). Research findings regarding sediment dynamics and delivery for the North Sea and German Bight can be summarized as follows:

### 2.3.9 Hydraulic works

Coastal engineering, a special branch of civil engineering, is engaged to plan, design, and construct as well as maintain works in the coastal zone. Actions can be attributed to soft or hard measures, with both often related to sediment transport and/or stabilization. Soft measures encompass beach nourishment or bioengineering measures, e.g. dune stabilization with vegetation. Constructions such as jetties, training walls, ports or storm surge barriers, seawalls and revetments are considered hard measures. They are designed to purposefully control shorelines, defend them against floods, storm surges and wave attack. Equally important are the design and development of ports and harbours as well as nautical fairways or off-shore industries. Additionally, coastal engineering strives to develop coastal ecosystem services to employ natural synergies and reduce constructive constraints, e.g. coastal squeeze, negatively impacting natural resilience and adaptation of the coastal zone. Coastal structures and infrastructure is typically designed for lifespans between 1 yr to 100 yr during which they have to maintain their structural integrity being exposed to a highly energetic and dynamic environment. Coastal energies coming from waves, tides as well as wind and atmospheric pressure systems or fresh water discharge all permanently shape the morphology of the environment around the structure(s). Naturally, changes in external forces will induce changes in the coastal shoreline and morphology. Vice versa, structures can be designed to influence hydrodynamic processes and favorably modify sediment dynamics (Bosboom and Stive, 2015).

Hydraulic works have reshaped coasts globally, resulting in 14 % of the United States coast exhibiting concrete structures while along the North Sea coast of France, the Netherlands and Germany 15 %, 60 % and 18 % are engineered. The German North Sea coast runs 1300 km, the main countries are Schleswig-Holstein and Lower-Saxony with 466 km and 750 km of coastline respectively. Schleswig-Holstein maintains 262.5 km of dikes, whilst Lower-Saxony has to maintain 610 km of coastal dikes (LKNSH, 2013; NLWKN, 2011b, 2018). Those coastal structures are the result of a long history full of transgressive relocations dating back centuries.

A decisive turning point in European coastal engineering marked the storm surge of 1953, which caused widespread destruction and flooding along the Dutch, Belgian, English and German coasts, initiating the development of large scale coastal defense strategies like the *Delta-Plan* (Deltawerken, 2004) (NL) or the *Sigma-Plan* (Vlaamse Overheid, 2018) (BE) and the *Lower-Saxon Coastal Program* later *General Coastal Defense Plan* (DE)

(Gierloff-Emden and Hans, 1954; NLWKN, 2011b) and sparking research activities regarding forecast and early warning systems, sorely missed during impact preparation and crises management (see section 2.3.4), as well as hydraulic engineering (Hensen, 1959; NLWKN, 2011b; von Storch, 2014). The second Julian-Flood of 1962 caused widespread destruction of infrastructure and loss of life along the German coasts and led to an intensification of hydraulic construction of coastal defense systems (NLWKN, 2011b).

Dikes in Lower Saxony were erected and existing ones consequently elevated, resulting in a 610 km long main coastal dike line as well as over 1000 km dike lines along estuaries and barrier islands varying in height from 5.6 m to 9.5 mMSL. Furthermore, 14 storm surge barriers are operating in Lower Saxony (NLWKN 2011b, pp.19).

Today the southern North Sea coastal zone is comprised of barrier islands, off-shore reefs and the back-tidal areas, which dissipate marine energy from coastal storms and represent a major component of coastal flood protection, lined by dikes in many regions to protect the hinterlands. Along with hard defense measures such as dikes, breakwaters or storm surge barriers, soft measures in the form of inter-annual beach nourishments are realized along the sandy shores of the barrier islands (NLWKN, 2011b; Quante and Colijn, 2016; Bosboom and Stive, 2015).

Figure 2.10 depicts the annual budget of Lower Saxony together with the number of storm surge events. Storm surges are classified according to the BSH methodology (see section 2.2).

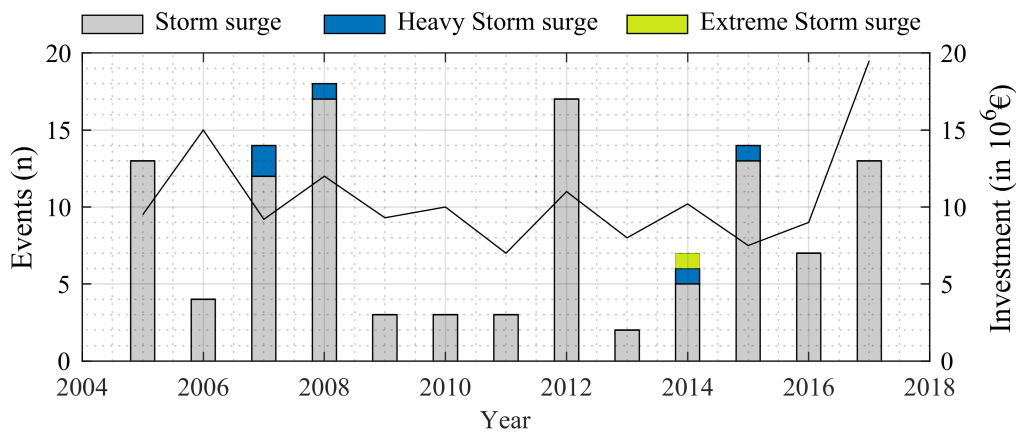


Figure 2.10: Coastal defense spending of Lower Saxony for the barrier islands against the number of events, based on data given in NLWKN (2004-2018).

Storm impact driven beach erosion along the barrier island chain of Lower Saxony during the winter 2016/2017 required beach nourishment volumes in excess of 800.000 m costing 8 Mio. € to reset the previous states, culminating in 19.5 Mio. € barrier islands reinstatement.

ment and defense spending alone contributing over 30 % of the total investment volume of 64.7 Mio. € for coastal defense projects along the coasts of Lower Saxony. Similar effects are reported for the collective of the North Frisian Barrier islands for the last 14 years, strongly correlating with storm surge intensity as shown in figure 2.10 (LKNSH, 2013; NLWKN, 2004, 2005, 2006, 2007b, 2008, 2009, 2010, 2011b, 2012, 2013, 2014b, 2015, 2016, 2018). Annual construction and maintenance for coastal protection along the German North Sea coast amounts to 6.7 Bn. € since 1962 with current annual investments of 150 Mio. € (NLWKN, 2018; LKNSH, 2013; LSBG, 2012).

Storm surge related coastal impacts have been a major driver of hydraulic development throughout history; coastal erosion and flooding of inhabited areas sparked the development of land reclamation techniques as well as flood protection works (Brahms, 1989), changing the human role from a reactive to a proactive one. At present, dikes are being reinstated and elevated to compensate for a projected MSLR of 0.5 m by 2100, which are linearly superimposed on design water levels (NLWKN, 2011b, 2018; LKNSH, 2013; LSBG, 2012; KFKI, 2002).

### Summary of chapter 2.4 | Coastal Key Drivers

#### ▪ Sea level

For practical applications, case sensitive regional RMSL is relevant. Recent findings show that RMSL is not increasing linearly but exhibits a stark acceleration of increase over the last decade and that RMSL in the North Sea ranges above the global average with  $2.3 \pm 0.2 \text{ mmyr}^{-1}$ . Under-laying a lot of processes, above average rates will result in considerable impact amplification of wave heights and surge levels. Accordingly, this study investigates RMSL scenarios deriving a mean and an extreme water level based on literature values ranging from 0.15-2.0 m from 21 studies. These are summarized in figure 3.3 a for deriving research scenario values in chapter 3.2.1.

#### ▪ Tidal dynamics

Recent studies have shown that engineered coasts and waterways exhibit a clear impact on local tidal dynamics, as the tidal waves are distorted by local shallow water bathymetry and are reflected at the coastline, potentially resulting in additional non-linear augmentation of tidal water levels by up to 0.1 m at the German North Sea coast. Consequently, tidal dynamics and planned constructive changes within the focus region are an integral part of this study.

Numerical simulations for the North Sea illustrated that uniform as well as non-uniform SLR exhibits a non-linear potential to additionally increase tidal water levels at the southern North Sea coast. Furthermore, a study comparison has revealed that the model setup near the coast (flood-able/non-flood-able) as well as used bathymetric data quality has a non-negligible impact on results. As a consequence this study strives for spatiotemporal data homogeneity.

#### ▪ Storms

Their disproportional and possibly system disrupting impact on coastal zone morphology and inherent infrastructure compared to slow changes in mean-conditions greatly elevates the importance of storm impact assessment for coastal engineering. Earth system sciences currently compose a largely inhomogeneous picture of future European Windstorm climate above the North Sea due to inherent dynamics as well as the multitude and degree of complexity of processes involved.



▪ **Storms (continued)**

Consequently, applied sciences are well-implemented to research potential consequences on a more deterministic basis to assess possible impacts. Large scale processes spanning the North Atlantic influence the formation, trajectory and intensity of storm systems. Recent research agrees that parameter ranges, and inherent dynamics preclude a successful prediction of future storm climate with current GCM systems. The relative recent discovery of sting jets as a principal and highly energetic and disruptive component of European Windstorms and their respective small-scale high intensity character exemplify the spatiotemporal discrepancy between the complex atmosphere and schematized numerical modelling systems. Emphasizing the need for further research and development.

▪ **Wind**

Wind speed, direction and duration may induce wind surge, as the wind shear drags water masses towards the shore elevating local water levels. Recent findings show, that wind induced setup is not linearly superimposed onto tidal storm water levels but may be larger during low tide and is reduced during high tide. Observation based statistical analysis showed that storm wind duration and peak values increased over time since 1900, amplifying European Windstorm impacts. Values for the southern North Sea project an increase of  $0.2\text{-}2.0\text{ ms}^{-1}$  based on eight studies. Findings are visualized in figure 3.3 b. These values are used to derive wind related research scenarios in chapter 3.2.2.

Atmospheric sciences project a decrease in mean wind velocities over the North Sea but an increase in extremes. Furthermore, westerly winds prevail in most projections. Projections are associated with rather large degrees of uncertainty due to the degree of complexity and the transient nature of atmospheric extreme states. Atmospheric historic records render rather inconclusive for climate projections, due to low observation density and inhomogeneous methods changing over time, generating inconsistent records leading to potential artifacts in re-analysis products used to force GCM simulations. The study at hand uses coastDat2 products, further described in chapter 3.3.

▪ **Waves**

Traversing shelf seas and entering the near-shore area, wind waves constitute a significant energy input into the coastal region, exerting loads onto structures, tidal flats and the coast. Storm wave conditions re-mobilize coastal sediments, which are then transported off-shore and settle in deeper waters, inaccessible for further coastal morphological processes. Exacerbated by RMSL, depth induced breaking of waves is reduced, changing reach and dissipation patterns as well as erosion potential. Thus, wind waves are crucial for investigating morphological storm impacts in changing conditions as part of this study. Projected values range from  $0.1\text{-}0.5\text{ m}$  based on eight different studies and are summarized in figure 3.3 for deriving research scenarios in chapter 3.2.3 around wind waves as a key driver.

▪ **Waves (continued)**

The North Sea wave climate is characterized by two predominant incident angles for waves during storm conditions being W-SW (southerly ETC) and N-NW (northerly ETC), both investigated within this study. Most wave simulations under climate projections show strong indications of increased wave heights along the German North Sea coast in the future, elevating energy levels which are dissipated at the coast. Climate change related augmentation in conjunction with increased water levels, tidal dynamics and elevated wind-speeds could have a profound impact on wave related parameter dynamics under storm surge conditions with morphologic impacts associated. Therefore, this study investigates changes in wave parameters along the line of storm research scenarios described in 3.2.

▪ **Extreme sea levels**

Aggregated from RMSL, tidal dynamics, wind waves and wind surge, storm surges constitute extreme sea levels which challenge coastal infrastructure and potentially threaten lives. ESLs are assessed by national laws and methods to arrive at design water levels, mostly by linear superposition, a methodology which has been indicated might be insufficient, as ESLs have been shown to exhibit non-linear interactions and related amplifications putting into question the practice to-date. Historic records show that ESLs have constantly increased driven by SLR. Furthermore, ESL levels are influenced by seasonal and nodal tidal cycles correcting previous assumptions that ESL levels increase linearly and will not surpass MSLR rates. Dynamic ESL processes are being investigated by means of numerical modelling to attain information along the coast in between point based observations through tide gauges. Recent research indicates a future reduction of return intervals.

▪ **Discharge**

Civil engineering influences the hydrologic water cycle on a catchment wide scale, increasing discharge volumes and reducing runoff times through urbanization and spreading of impervious surfaces, precluding a slow percolation of rain. Hydraulic engineering develops rivers into navigable waterways, greatly reducing their cross section simultaneously increasing their depth and removing river islands, meanders and bends to facilitate navigation. Therefore, heavily engineered waterways and their estuaries are more prone to inland winter peak discharge events coinciding with storm surges forming compound events. Five different hydrologic studies for the focus region project an increase of 2% to 60% in winter peak discharge, which are summarized in figure 3.3 and used in 3.2.5 to derive research scenarios. Changes in atmospheric conditions impact the hydrologic water cycle, resulting in overall volume changes of available water mass as well as seasonal redistribution of precipitation and evapotranspiration through changing ambient temperature and atmospheric compositions. Research within this area is associated with levels of uncertainty equaling atmospheric storm studies. Notwithstanding, Meteorologists project precipitation and runoff distributions by means of numerical and statistical modelling; results indicate a seasonal shift towards reduced summer runoff-discharge and increased winter and spring peak discharge events for the focus region.

### ▪ **Sediment delivery**

Sediment discharge into the oceans is reduced by an estimated 28 % through dam construction related retainment, impacting morphologic equilibria downstream and at the coast. Satellite based time series analysis revealed that 31 % of the earth's coasts are sandy with 24 % showing erosion, traceable to constructive interventions obstructing long- and/or cross-shore transport of sediments, resulting in a lack of material. 64 % of Germany's coasts are comprised of sandy beaches, of which 30 % are eroding. Single events like European Windstorms can significantly influence annual suspended budgets within the North Sea and easily erode vast stretches of coastline, resulting in expensive nourishment. Accordingly, one of the objectives of this study is to elucidate a possible quantification of coastal storm related morphological impacts as a first step and possible amplifications through changing boundary conditions following the hypothesis of non-linear interactions and amplifications.

North Sea morphology is sustained by sediment influx coming from the major estuaries as well as material from coastal cliff erosion during winter storm periods. The estimated sediment influx into the German Bight amounts to  $1.3 \times 10^6 \text{ tyr}^{-1}$ . Entrained sediments are sorted according to their density related settling characteristics, creating bed formed areas as well as flow formed regions, with medium sand characterizing the coastal zone of the focus region and fine materials being transported off-shore to calmer regions. Particulate matter (N, P and K) nourish ecosystem engineers and impacts soil generation and composition of the Wadden Sea. Environmental changes, e.g. increased ocean temperatures, impact biogeochemical processes, which regulate ecosystem services and impact coastal morphology, composition and surface roughness, directly impacting hydromechanics. Initial research indicates that numerical models can be used to predict potential impacts.

### ▪ **Hydraulic structures**

Coastal infrastructure, either hard or soft, is predominantly designed to defend against flooding and/or facilitate navigation and maritime trade. Structures are purposefully designed to influence natural currents and transport processes favorably. Hydraulic works are usually planned and designed for longer time scales spanning multiple decades given their size and investment volumes. Lower Saxony maintains 610 km of main dike line along the North Sea coast, Germany. Currently, sea dikes are being elevated to account for an additional 0.5 m SLR, linearly super positioned onto existing design water levels. Recent research findings indicate that a linear superposition is falling short to account for non-linear amplification effects potentially exceeding 0.5m added defense and increasing erosion volumes. Following this line of argument, the study at hand investigates potential impacts of port development as well as fairway incisions upon impeding European Windstorms under changing boundary conditions as outlined in chapter 3.2.6.



▪ **Hydraulic structures (continued)**

System wide oceanographic approaches or process based physical research usually omits off-shore and coastal infrastructure, as their research focus rests on in-depth process understanding and system responses to changing environmental conditions. Consequently, most climatologic studies investigating possible changes in physical process-based parameters, do not reflect or assess and incorporate infrastructure, which is purposefully designed to influence physical nearfield processes. On oceanic scales such as the Atlantic, infrastructure might be negligible, but within the shelf seas and coastal regions with their engineered character, it is not. The barrier islands and their back-barrier tidal flats of the southern North Sea exhibit a strongly engineered character, interrupting their natural eastward migration pathway, due to settlements on them and to maintain navigability of cut through estuaries. Climate impacts upon the regional morphology and resulting feed-back impacts are not yet at the attention of earth system sciences.

## 2.4 Research focus area

The study at hand aims to investigate potential storm surge impacts within the German Bight as described in chapter 1.2. The storm surges are induced by ETC events forming over the north Atlantic, travelling east towards Europe (see figure 2.11 a), where the majority of events passes over England and is deflected northwards at the shores of Scandinavia (see figure 2.11 b). As the events pass through the North Sea, they induce a surge along the south east coast with largest water level amplitudes within the German Bight, where the focus region of this study is located as can be seen in figure 2.11.

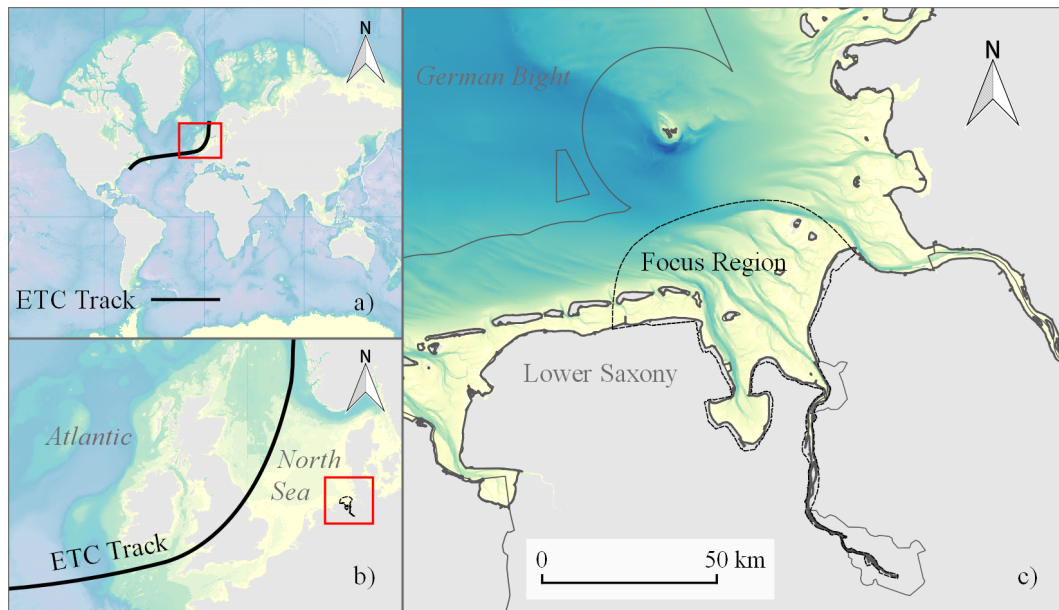


Figure 2.11: Research focus region a) global scale; b) continental scale; c) regional scale

Consequently, the focus region is located at the impact end of the ETCs, where the European Windstorms develop their full potential, equivalent to stages four and five defined by the conceptual IMLAST cyclone model presented in figure 2.2 in chapter 2.2.2. With this setup, impact magnitudes and potential amplifications through climate change can be ideally investigated.

### 2.4.1 Jade Weser Estuary

The Jade, created by storm surge impacts (see Section 2.4.2), is a tidal bay cutting deep into the mainland, which is named after the small non-navigable riverine entering the Jade Bight from the southern most point through the Wapeler Siel into a network of tidal creeks and gullies. The water body is segmented into the outer and the inner Jade as well

as the Jade Bight, with a large intertidal area denominated the *Hohe Weg* separating the Jade from the Weser estuary in the east. An overview of the region is given in figure 2.12.

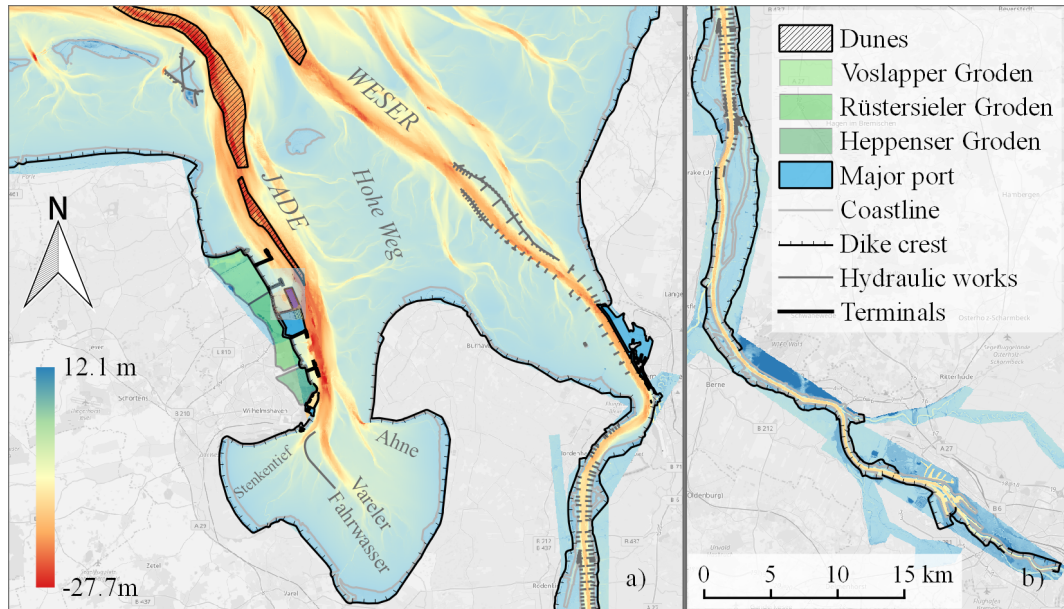


Figure 2.12: The Jade Weser Estuary a) with major ports, dike lines and terminals as well as the lower Weser b) comprising the focus region.

The negligible fresh water influx reduces the salinity to 2.9‰ to 3.2‰ compared to the open North Sea and does not support the formation of a brackish water zone (Götschenberg and Kahlfeld, 2008; Akkermann et al., 2015). The Jade Bight spans 190 km<sup>2</sup> and comprises subtidal, intertidal and supratidal flats (Akkermann et al., 2015). The Jade is mainly characterized by its deep navigational channel, in part lined by equally deep tidal channels. Inside the bight the navigational channel branches into numerous channels (Ahne, Vareler Fahrwasser and Stenkentief), in turn diminishing in depth and width upon entering the bay until they merge into tidal creeks. The sedimentological inventory is comprised of medium and fine sand forming the navigational as well as other tidal channels and their respective sandbanks, whilst the intertidal flat areas contain silt (Akkermann et al., 2015; Valerius et al., 2015). The morphological regime is governed by tides and waves, as well as anthropogenically induced changes through construction and dredging. A net sediment import is reported for the Jade, stemming from a seaward flood dominated tidal asymmetry and resulting residual flows over the *Hohe Weg* into the Weser estuary, as well as negligible landward fresh water discharge and last but not least the geometry of the Jade Bight (Götschenberg and Kahlfeld, 2008).

A total of eight tide gauges are operated within the Jade region by the Federal Shipping Office Wilhelmshaven. In Wilhelmshaven the average tidal range reaches 3.69 m inducing

a strong flood current, resulting in a tidal volume of  $400 \times 10^6 \text{ m}^3$  entering the Jade Bight (WSV, 2018b). Figure 2.13 a) gives an overview of the tidal water levels along the Jade fairway based on values gauged between 2000 to 2010.

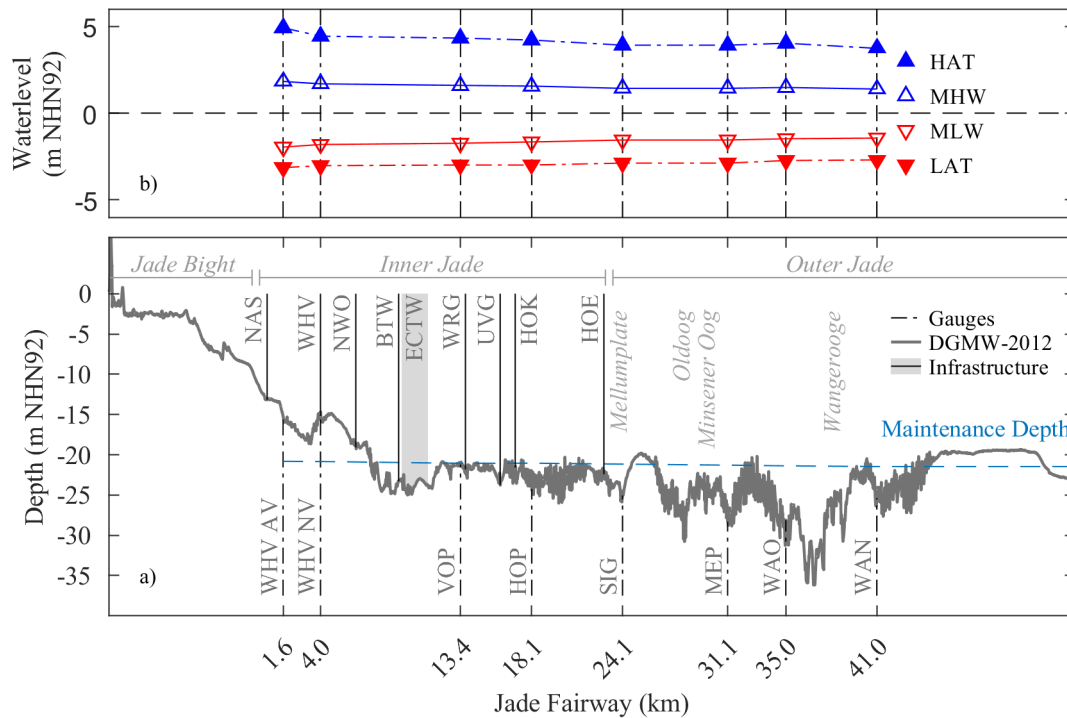


Figure 2.13: Inner and Outer Jade fairway with hydraulic works a) and associated tidal parameters b). Bulk-terminals, Ports and other critical infrastructure are marked below the fairway in a). Gauges are marked above the bed, with islands marked in *italic*. Depth is based on the Digital terrain model of the waterbody (DTMW) 2012. Tidal parameters in b) are derived from tide gauge data of the WSV (2018a).

The MHW increased by 0.43 m, whilst the mean low water (MLW) decreased by 0.56 m between Wangerooge North (WAN) and Wilhelmshaven Alter Vorhaven (WHV AV) coming from the North Sea increasing the tidal range by 0.98 m upon entering the Jade (WSV, 2018b).

No permanent wave data are collected within the Jade. The nearest wave measurements are taken at the Leuchtturm Alte Weser (LAW) located on a sandbank between the Jade and Weser marking their respective seaward boundaries. However, only amplitude and period are measured here and no information regarding direction is available. Furthermore, wind speed and direction are measured at the LAW.

Sediment transport measurements are not readily available, along the permanent measurement chain of six stations, local suspended sediment concentration (SSC) is measured and ranges from 50 NTU to 80 NTU (D5, D0). Elevated SSC-values in the Jade Bight are caused by resuspension of fine material located on tidal flats during flood/ebb cycles resulting in observed SSC of  $0.200 \text{ gL}^{-1}$  to  $2 \text{ gL}^{-1}$ . Nevertheless, the main sediment transport mass consists of medium and fine sand bed load, which forms large subaqueous dunes in some regions. Two dune fields can be found within the Jade, one in the inner Jade covering fairway kilometer (fkm) 14.8 to 33.9. The second area is located in the outer Jade from fkm 23.65 to 33.5 with dune patches reaching as far as fkm 41. Dunes range between 1.5 m to 9.4 m high and span 13.5 m to 450 m in length, while the primary dunes are superimposed by secondary small scale ripples following the definition of Ashley (1990). In the outer dune field, migration speeds vary between  $30 \text{ myr}^{-1}$  to  $100 \text{ myr}^{-1}$  (Kubicki and Bartholomä, 2011; WSV, 2018a). Analyzing fairway safety sounding charts between 2005 and 2010 revealed a morphological very active region in the outer Jade, due to long shore sediment transport and anthropogenic dredging and fairway maintenance activities. The Jade Bight shows a net sediment export downstream, whilst the inner Jade is characterized by a mostly stable sediment budget, resulting in a net depositional environment up to south west of Mellum island (Kubicki and Bartholomä, 2011). Dredging activities concentrate on the vicinity of the ECTW as well as the fairway north of Minsener Oog (Götschenberg and Schlüter, 2005), whilst the remaining fairway is mostly stable as no regular dredging is required or found in soundings. Dunes reaching 17.6 m chart datum (CD) reducing the navigational depth jeopardize the navigational safety of vessels bound for the Wilhelmshaven transshipment complex and are immediately dredged below a defined level.

Tidally induced currents are measured at six permanent locations distributed along the shipping channel in the inner Jade since 2006 between the Varel fairway and Horumer-siel. Figure 2.14 a) gives an exemplary tidal cycle measurement of the current velocities observed during average atmospheric conditions. Velocity magnitudes on average reach  $1.0 \text{ ms}^{-1}$  and easily exceed this value during storm conditions (Götschenberg and Kahlfeld, 2008).

#### 2.4.2 Brief hydraulic history

The Jade Bight, like other coastal land losses along the North Sea coast, can be traced back to storm surge impacts. Historians agree that the *Grote Mandrenke*, a major storm surge impacting the North Sea 1362, initiated many of the coastline changes leading up to the present day geography of the Wadden Sea (Liedtke, 2003; Behre, 2012; NLWKN, 2018; Akkermann et al., 2015; Waldemar, 1979).

Initial coastal engineering practices in Lower Saxony pertain to the construction of dwelling



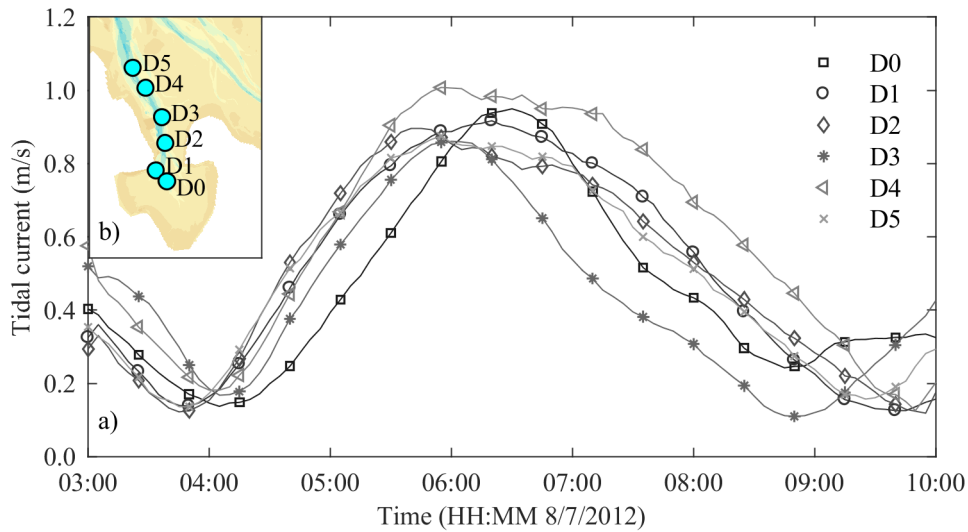


Figure 2.14: Current velocities observed in the Jade a) currents developing over a tidal cycle at the six stations along the measurement chain b) of six permanent observation points.

mounds within the coastal zone and date back to the 9<sup>th</sup> century before Christ (BC) (Kramer and Rohde 1992, p.20). Around the year zero, a short period of transgression allowed the construction of coastal defense structures along the coast, with the main purpose being to prevent storm surge induced flooding of settlements (see fig. 2.15 year 0). With an increase in winter storm surges during the 2<sup>nd</sup> century, an areal expansion of dwelling mounds was documented. During the 4<sup>th</sup> and 5<sup>th</sup> century, the coastal population experienced repeated flooding and destruction of their settlements, resulting in seaward migration of the Angles and Saxons towards Great Britain. During the dark ages (5 – 7<sup>th</sup> century), the coastal population remained relatively thin, with settlement areas being smaller due to extensive land loss and flooding (see fig. 2.15 year 800). With the migration of Frisian (Dutch) people in the 8 – 11<sup>th</sup> century, came know-how in dike building and drainage construction allowing for cultivation of areas along tidal channels and coastal lowlands (Kramer and Rohde, 1992; Waldemar, 1979). Constructed ring-dikes were inter-connected to form the so-called golden ring-dike by the 13<sup>th</sup> century. Throughout the middle ages dike system elevations were based on experienced events; neither relative sea level rise due to agricultural practices such as soil compaction from peat cutting and drainage, nor statistical extreme events were considered. Another important aspect is that frequent wars, the black plague as well malnourishment lead to depopulation and consequently, those anthropogenic influences and lack of maintenance rendered

the coast prone to storm surge impacts (see fig. 2.15 year 1300). The Grote Mandrenke (1362) led to large storm surge related land losses along the German coast creating the Ems-Dollart, the Leybight and the Jade-Bight, shattering Frisia and creating coastal barrier islands but also sinking former islands like the legendary Rungholt in North Frisia, fundamentally changing the coastline (see fig. 2.15 year 1362). The event also resulted in a breaching of the Jade into the Weser river bed in the East, creating an estuarine like Jade-Weser delta, which existed for around 130 years (Akkermann et al., 2015; Behre, 2012; Waldemar, 1979; Brahms, 1989; NLWKN, 2018). A series of three consecutive extreme storm surges from 1509 to 1511 devastated the Jade Bight region and resulted in its largest known expansion (see fig. 2.15 year 1510) nearly four times larger than today, with over 45 islands within the Jade Bight (Akkermann et al., 2015; Behre, 2012; Waldemar, 1979; Brahms, 1989; NLWKN, 2018).

Figure 2.15: Historic coastal evolution of the German North Sea coast between 0 and 2018 AD based on historic maps from Behre (2012).

Following vast land losses experienced, land reclamation encroached on the waterline of the Jade Bight, successively reducing its extend through impoldering (see fig. 2.15 year 1520). The Imperial Naval Port Act of 1883 prohibited further land reclamation along

the Jade Bight, in order to not reduce the tidal volume of the Bight, and thus its flushing capacity, to an extent where the naval port of Wilhelmshaven would experience accretion (Akkermann et al., 2015). Butjadingen, the area between Jade Bight and Weser, meanwhile experienced repeated heavy dike breaches throughout the 17<sup>th</sup> century, as hydraulic works were difficult to found in the swamp-like area (Waldemar, 1979; Kramer and Rohde, 1992). Systematic land reclamation and river training as well as port development mark the 19<sup>th</sup> century (see fig. 2.15 year 1888). The lower Weser between Bremen and the North Sea was transformed from a natural meandering braided shallow river to a modern water straight starting in 1888 by dredging the main stream, installing river training walls and groins and reducing the river islands (Franzius, 1888; Lange et al., 2008). The main goal was to guarantee safe navigation to trade ships bound for Bremen. In the Jade Bight Wilhelmshaven was founded in 1869 as a naval base and ensuing port development. During the 20<sup>th</sup> and 21<sup>st</sup> century, the Jade has experienced numerous hydraulic construction phases (see Fig. 2.15 year 2018), resulting in its present day coastline. A more detailed list of individual historic storm surges can be found at the Universität Siegen, Forschungsinstitut Wasser und Umwelt (2012).

### 2.4.3 Recent hydraulic development

Given the numerous anthropogenic alterations throughout the last centuries, the Jade-Weser region exhibits a heavily engineered character. Embedded within the estuary are the two fairways of the Jade and the Weser. As the focus of the study rests on the Jade, the Weser fairway is not described in detail here. A longitudinal section can be found in appendix A.6. The Inner Jade fairway starts at km0 near Wilhelmshaven (former first entrance) and ends at km25 at the imaginary line Schillig-Mellum. The outer Jade fairway continues for 29 km and enters the North Sea north of Spiekeroog at km54 at a continuous width of 300 m (Götschenberg and Kahlfeld, 2008; WSV, 2016).

Beginning with the construction of the island Minsener Oog (1909) and Jade-correction 1909-1931 including incision of the fairway to  $-10$  m CD, the tidal dynamics changed in reaction to the altered bathymetry. These changes are displayed in figure 2.16 as the development of the MHW gauged at Wilhelmshaven in conjunction with hydraulic constructions.

The industrialization of the Wangerland led to impoldering of the Heppenser Groden (1938), the Rüstersieler Groden (1965) and the Voslapper Groden (1975) for bulk terminal construction (Jade-Weser-Port, 2008). Along with the coastal development went a consecutive deepening to  $-18.5$  m CD in 1976. Subsequently, these reclaimed areas were developed and harbour Germany's largest oil, gas and coal bulk terminals today. Most recent the European Container Terminal Wilhelmshaven (ECTW) was constructed (2012) representing the only deep-water harbour in Germany (Götschenberg and Kahlfeld, 2008).

For the near future, an extension of the recently built ECTW is currently being investigated (ISL, 2016; NMW, 2016). As for the Lower and outer Weser an incision plan is being debated (WSV, 2006a,b).

From long term time series gauged at WHV AV a construction related impact on the MHW can be discerned and attributed to the Jade correction 1909 to 1931 as shown in figure 2.16 together with the nautical fairway development.

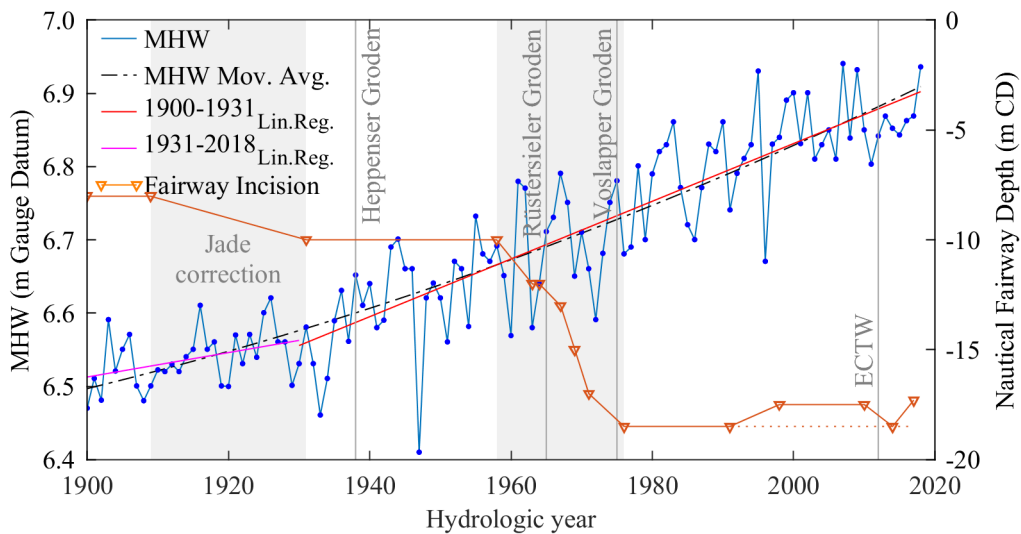


Figure 2.16: Development of the Mean Tidal highwater (MHW) between 1900 to 2017 in conjunction with hydraulic works and the development of the nautical fairway depth based on data given in WSV (2016); BFG (2018); Götschenberg and Kahlfeld (2008) and Bolle and Lehnert 1979, pp. 35 table 1).

In addition to the tidal amplification of the MHW, the tidal wave also propagates 20 min faster into the bay compared to 1950.

#### 2.4.4 Critical coastal infrastructure

Defined by the BMI, a working group of various federal institutions worked out a bill, which requests the identification and protection of critical infrastructure (BSI, 2017). Under the patronage of the Federal Office for Civil Protection and Disaster Assistance (*Ger.: Bundesamt für Bevölkerungsschutz und Katastrophenhilfe - BBK*) (BBK), thresholds were derived for identifying critical infrastructure (BSI, 2016). These thresholds are used to classify coastal infrastructure, listed subsequently, presented in the Jade accordingly in table 2.4.1.

Wilhelmshaven, founded 1869 as a naval port on the western bank of the transition into the Jade Bight, constitutes a major port and economic center in the region housing Germany's largest naval base as well as docks and numerous transshipment facilities (Akker-mann et al., 2015; Götschenberg and Kahlfeld, 2008). Along the western shoreline of the inner Jade, a transshipment complex comprised of four bulk terminals, as well as a large container terminal line the deep Jade fairway and form Germany's only deep water port. This outer port can be accessed by vessels with an unrestricted draught of 16.5 m or up to 20 m tide-dependant. Figure 2.17 a gives an overview of hydraulic works and coastal infrastructure located within the Jade, whilst infrastructure locations relative to the fkm are given in figure 2.13 a.

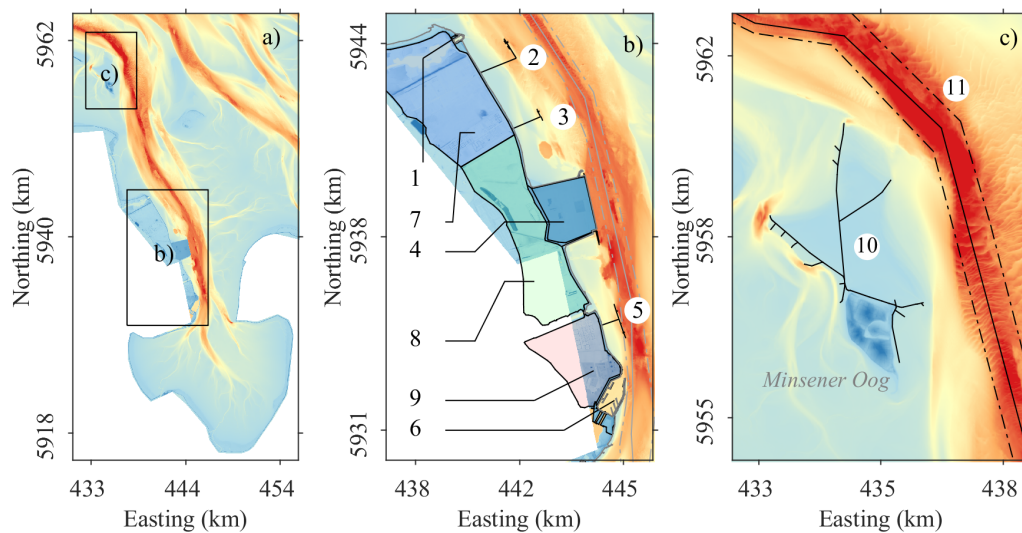


Figure 2.17: Hydraulic works along the Jade Fairway a) with the Wilhelmshaven transshipment complex b) as well as the artificial groyne system Minsener Oog c).

Considered a commercial hub, the transshipment complex Wilhelmshaven entails a wide variety of terminals, partly of national importance, which are interconnected by the Jade navigational and adjacent access channels and constitutes critical infrastructure, which is shortly described following the consecutive numbering in figure 2.17 b): (1) Hooksiel at the northern end of the 1970 impoldered Voslapper Groden constitutes a small harbor, berthing sea rescue vessels and functioning as shelter and service port for the ECTW upstream. The harbor access channel cuts diagonally across the tidal flat into the navigational channel, rendering it prone to sedimentation. (2) Voslapper Groden Terminal operated by Vynova is Europe's largest processing plant for suspension poly-vinyl-chloride - a widely used material (VYNOVA, 2018). (3) Wilhelmshaven Refinery Terminal was a

refinery, which is currently used as an oil depot with a capacity of  $1.3 \times 10^6 \text{ m}^3$  with plans to rebuild the refinery and extend the salt cavern network. A bridge pier extends into the navigational channel and slants in main flow direction, offering two berthing stations for liquid gas transfer (HES, 2018). (4) ECTW, constructed 2012 ranked sixth among Germany's seaports with a turnover of  $978 \times 10^3 \text{ t}$  (05/2018) at a 177% increase compared to 02/2016 (DeStatis 2017, pp. 419). With a capacity of  $2.7 \times 10^6 \text{ TEU}$  the ECTW is projected to grow, with a possible northward extension being currently investigated (ISL, 2016; NMW, 2016). The ECTW offers four container berthes along a 1.7 km long quay wall. At the southern end of the newly built port the Bulk Terminal Wilhelmshaven (BTW), a bridge pier extending into the navigational channel offering two bulk berthes is located. It was extended with the construction of the ECTW, handling  $8 \times 10^6 \text{ tyr}^{-1}$  to  $10 \times 10^6 \text{ tyr}^{-1}$  of coal, and natron it constitutes Germany's biggest coal bulk terminal representing nearly a third of Germany's maritime oil, gas and coal turnover (DeStatis, 2018). (5) Nord-West Oelleitung is a liquid terminal, extending into the navigational channel. In 2017 the bridge pier handled  $19 \times 10^6 \text{ t}$  of mineral oil imports (19.9% of Germany and 54.3% of Germany's maritime oil trade, NWO 2018). (6) Wilhelmshaven (WHV) port ranked third among Germany's seaports with  $1.844 \times 10^3 \text{ t}$  turnover (05/2018) (DeStatis, 2018). WHV houses Germany's largest naval base as well as various dry docks and infrastructure of the Water and Shipping Directive (WSV) for fairway maintenance. (7) Voslapper Groden was created 1973 is a  $11.96 \text{ km}^2$  large polder, stabilizing the formerly fluctuating western shore of the Crildummer Bight. (8) Rüstersieler Groden was diked in 1965 covering  $9.55 \text{ km}^2$  (9) Heppenser Groden was the first large land reclamation since the Imperial Naval Port Act of 1883 (Wilhelm, von Gottes Gnaden Deutscher Kaiser, König von Preußen, 1883). It was created 1938 and claimed  $5.07 \text{ km}^2$ . Together the three polders shifted the coastline eastwards, reducing the cross-sectional area of the Jade, in turn elevating the tidal current velocities and stabilizing the self-maintaining character of the tidal channel system. (10) Minsener Oog is a 10.5 km long groyne system, which was constructed 1909 to 1931. Migrating sandbanks and bars due to littoral sand-transport are deflected from the fairway, reducing maintenance. Together with the armoured west-point of Wangerooge, Minsener Oog contributes substantially to the stabilization of the tidal channel used as fairway. (11) The Jade Fairway is nearly 50 km long, 300 m wide and accomodates vessels with a draught of up to 16.5 m below CD. Littoral and lateral sediment transport, as well as storm induced bed changes requires annual maintenance culminating in dredging costs of 6 Mio. €.

Overall, the Jade area harbors 121 hydraulic works (WSV, 2018b) of which the major ones such as the fairway itself or the large transshipment complex of Wilhelmshaven are classified as critical due to their turnover volumes of goods and especially bulk energy carriers such as coal and oil (BMVI, 2015a). Scarcity of natural resources such as oil, gas and coal as well as long transport routes and logistics lead to a naval dependency regarding liquid

and dry bulk. The Wilhelmshaven terminal complex alone handles 30 % of Germany's crude oil imports. Coastal infrastructure depicted in figure 2.17 and explained above, is subsequently compared to threshold values defined by the BBK within the BSI-KritisV (BSI, 2016) in table 2.4.1 to identify critical systems. Thresholds are based on personal equivalent (PE) centered consumption values given in Appendix A.11.

Table 2.4.1: Critical infrastructure in the Jade classified according to the KRITIS-V thresholds (BSI, 2016).

No.	Abbrev.	Description	Volume	KRITIS Threshold	Classification
1	HOK	Hooksiel harbor			non-critical
2	VOS	Vynova PVC-plant	$1.2 \times 10^6 \text{ tyr}^{-1}$ (EU largest)	$1.8 \times 10^6 \text{ tyr}^{-1}$	non-critical
3	WRT	Wilhelmshaven Refinery Terminal	$1.3 \times 10^6 \text{ m}^3 \text{ yr}^{-1}$	$4.2 \times 10^5 \text{ tyr}^{-1}$	critical
4	ECTW	Container terminal	$9.8 \times 10^5 \text{ TEU}$ (2017) $2.7 \times 10^6 \text{ TEU}$ (planned)	$1.35 \times 10^5 \text{ TEU}$	(critical)
		BTW	Coal terminal	$8 \times 10^6 \text{ tyr}$	$4.4 \times 10^6 \text{ tyr}^{-1}$
5	NWO	oil terminal	$19 \times 10^6 \text{ tyr}^{-1}$	$4.4 \times 10^6 \text{ tyr}^{-1}$	critical
6	WHV	Wilhelmshaven	$1.85 \times 10^6 \text{ tyr}^{-1}$	$1.8 \times 10^6 \text{ tyr}^{-1}$	critical
7-9	VHR	Reclaimed areas; Voslapper Groden, Heppenser Groden, Rüstersieler Groden impoldered to stabilize the former existent Crildummer Bight			NA
10	MOG	Minsener Oog; 10.5 km groins and 8 km train tracks; constructed to stabilize the Jade fairway and prevent lateral shoal migration			NA
11	JFW	Jade fairway; 54 km long, 300 m wide and 18.5 m CD deep; facilitates navigation and trade			NA

With 252.377 Mio. € export surplus 2017, a plus of 3.3 % compared to the previous year (DeStatis, 2017), Germany heavily relies on international trade. The transshipment complex of Wilhelmshaven contributed roughly 3-4 % to Germany's 2017 gross domestic product. The maritime sector and related infrastructure is accordingly classified as critical (BMVI, 2015a; BMI, 2009). Against the background of changing environmental conditions brought about by climate change, potential impacts and possible mitigation strategies are (becoming) a focal point of coastal engineering and research in order to guarantee safe navigation and trade.

#### 2.4.5 Climate impact research

Initial climate impact research based around numerical modelling regarding the Jade Weser region was conducted through a series of consecutive national research projects.

*KLIMU* (1998 to 2000) was one of the early projects, employing a 1D model to simulate an 80 km stretch of the Weser (Franzius-Institute, 2000; Leichtweiß-Institute, 2000). The

project investigated various ecological parameters varying boundary conditions running time slice simulations. Storm surge polders were investigated, simulating a design storm of 28/01/1998. The follow-up project KRIM (2001 to 2004) used a structured area model to simulate hydrodynamics more accurately (Zimmermann and Mai, 2004). Again boundary conditions were varied, increasing tidal range and including MSLR as well as increased storminess. Three scenarios were simulated within time slice studies. Both KLIMU and KRIM used boundary conditions based on pre-defined scenarios provided by von Storch and Reichardt (1997). Furthermore, both studies entail rather large degrees of uncertainty given the limited model domains and resolutions.

**MUSE** (2002 to 2005) focused on constructing extreme storm surge scenarios, which are physically realistic but feature low probabilities. Simulating a range of events, the joint research project elucidated that external surges are more important in combination with Scandinavian type events, as these feature prolonged wind surge duration at the coast and make an additional external surge amplification more likely. Furthermore, findings show that higher wind speeds in conjunction with short duration Jutland type events cause more agitate sea states, which have larger impacts on coastal (defense) structures compared to prolonged wind surge duration with lower peak values. The project related ProMUSE method is based around a generalized extreme value statistic, which allowed for statistical extrapolation of water levels for events featuring probabilities as small as  $10^{-4}$  (once every ten-thousand years). The project concluded that observed extreme events range around a *RI* of  $10^{-2}$  and that events with an  $RI=10^{-4}$  feature around 0.6-1.1 m elevated water levels compared to those (Jensen, 2005; Jensen et al., 2006a).

**KLIFF** and **KLIWAS** (both 2009 to 2013) were launched by Lower Saxony (KLIFF, Beese and Aspelmeier 2014) and the Federal Republic of Germany (KLIWAS, BMVI 2015b) respectively sparked by the fourth IPCC Assessment Report (IPCC, 2007). In contrast to the previous studies, KLIFF entailed transient simulations spanning 1960 to 2100 as well as time-slice studies to investigate potential storm surge impacts upon hydrodynamics and salinity of the Weser estuary (Zorndt et al., 2011, 2012; Zorndt, 2014). Within the KLIWAS framework a sensitivity type impact study was conducted, elucidating system dependencies. Within KLIFF uncertainties were specifically addressed and an emphasis put on reduction of model inherent uncertainties (e.g. Zorndt 2014), while the KLIWAS framework did not specifically address experimental uncertainties.

**XtremeRisk** (2008 to 2012) focused on storm surge impact research for the Elbe and Northern Frisia and employed an empiric-deterministic approach discerning single storm surge components (tide, waves, surge, wind set-up) and their respective non-linear interactions. A stochastic storm surge generator was created, randomly superimposing physically plausible parameter values, considering gauge-specific non-linearities through parameter reduction. Furthermore, the project database showed that the random combi-



nation of the single extreme components has to date not coincided once (Oumeraci et al. 2012, p.22). Non-linear interactions of single components were considered and the physically plausible not-yet observed event accordingly reduced in magnitude. Major findings of the project was two-fold, (1) combined occurrence of extreme values for all three major components (spring tide, wind setup, external surge) is physically plausible and possible and (2) linear superposition of storm surge components results in over estimation of water levels (Oumeraci et al. 2012, p.22). External surge was shown to reduce by 30 % between Aberdeen and Cuxhaven and 40 % between Cuxhaven and Hörnum (Gönnert, 2003; Oumeraci et al., 2012). Extreme surge for Cuxhaven reached 0.77 m (Gönnert and Thumm, 2010).

**Risk Assessment Storm Surge** was commissioned by the German Bundestag to estimate potential consequences of an unprecedented extreme scenario through the federal civil protection (Deutscher Bundestag, 2014). Figure 2.18 shows the estimated flood prone areas for events with a return interval of 100 years (magenta) and 200 years (blue) based on federal data (BfG, 2016).

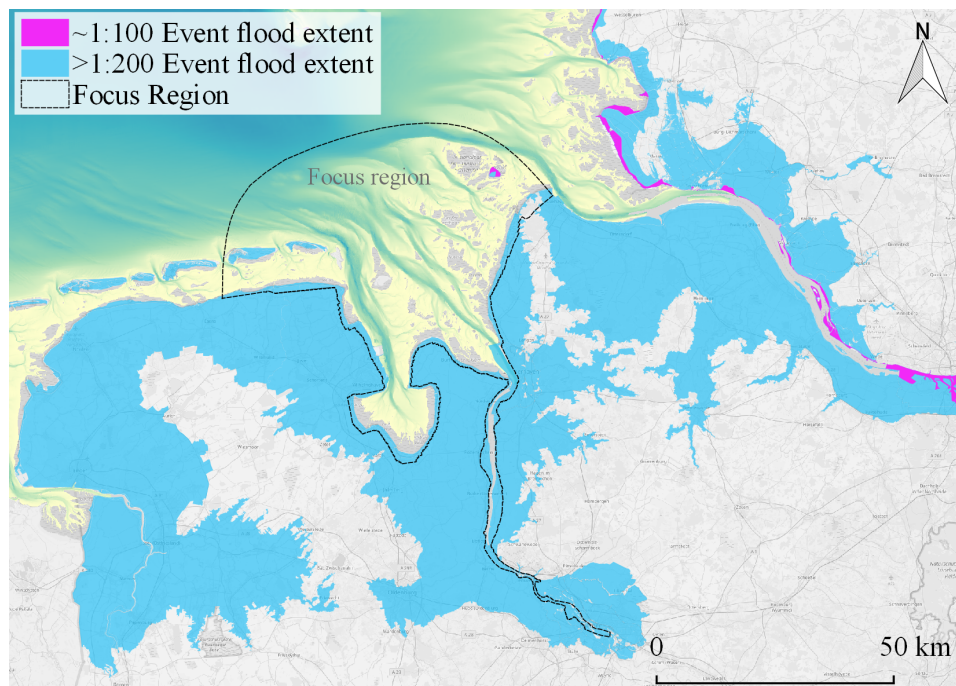


Figure 2.18: Potential flood extent for extreme surge event based on risk assessment for a possible scenario (Deutscher Bundestag, 2014).

The scenario assessment is based on a risk assessment scenario for a European Windstorm (Deutscher Bundestag, 2013) with wind speeds  $\geq 70$ kt from NW including 5 % add-on due to storm gusts, resulting in a wind surge of 5.56 m NHN16 at the coast. Coastal

defenses may experience failure due to extensive surge and agitated sea state causing over-topping and landward erosion of dikes (KFKI, 2002). Experienced events show that dike breaches give rise to a complex and challenging scenario caused by the destruction and inundation of critical infrastructure through wind and water. A special character arises due to the combination of European Windstorm force winds with a very heavy storm surge making landfall and causing widespread blackouts. Geographically around 9000 km<sup>2</sup> are prone to storm induced flooding, the area is shown in figure 2.18. An estimated 15% of the area are assumed to be flooded as consequence of additive water levels in excess of 9 m from surge and waves. Within the flooded 1350 km<sup>2</sup> approximately 150000 inhabitants are affected by the storm. Nation wide 6 Mio. people experience a blackout, which lasts over three weeks in flooded regions impacting  $\geq 300000$  people. A major aspect of the risk assessment scenario is the coincidence of the highest wind speeds and the maximum surge level, which in turn is a prerequisite for extreme surges. Storm related damage on flood defense structures is identified as a major problem; even if dikes are not breached successive storm events may destroy them and also extend already flooded areas. A quantitative estimate regarding the destruction of individual and critical infrastructure assessed rendered impossible due to the degree of complexity arising from the varying system state as well as the unique character of any storm surge. Therefore, qualitative descriptions based on impacted systems and rough estimates of affected population are made based on BBK formulated KRITIS-V thresholds and are presented in table 2.4.2 as given by the official study (Deutscher Bundestag, 2013).

Table 2.4.2: KRITIS-V storm surge impact classification (BSI, 2016).

Protected good	Damage parameter	Detriment level <sup>1</sup>				
		A	B	C	D	E
Human	M1 Casualties	> 1000-10000				
	M2 Injured and ill	> 10000				
	M3 Needy	> 1 Mio for > 1 week or > 100000 for > 1 month				
	M4 Missing	> 10-100				
Environment	U1 Protected areas	>0.5-5 % damaged				
	U2 Surface & ground water	0.1-1 % damaged				
	U3 Forests	>10 % damaged				
	U4 Agricultural area	1-10% damaged				
	U5 Livestock	>1.5 Mio wounded/dead				
Economy	V1 Public sector	Federal budget required; EU relief avb.				
	V2 Private sector	Supraregional impact				
	V3 Private households	> 40000-200000 impacted				
Non-material	I1 National security	endangered on supraregional and federal level				
	I2 Political impacts	very large impact on national scale				
	I3 Psychological impacts	> 1 Mio.-10 Mio. affected share				
	I4 Cultural goods	1% of heritage sites damaged				

<sup>1</sup> For a more detailed description and methodology for deriving these values the reader is referred to Deutscher Bundestag (2014) pp. 61 and/or the KRITIS-V (BSI, 2016)

***EXTREMENESS*** (2016 to 2019) is a research project in succession to XtremeRisk, utilizing transient simulations in combination with physically plausible but statistically unlikely extreme events to identify impact potentials along the German Bight. A major research aspect is the tide-independent event impact and related failure of any given coastal defense structure. No peer reviewed publications of results exist as the project is active. Nevertheless, neither morphodynamic aspects of storm surges nor process attribution are specifically addressed (BMBF, 2018; Tabea Brodhagen et al., 2017).

### **Summary of chapter 2:**

Coastal key drivers have been identified, investigated and major findings summarized for each driver at the end of section 2.3.

The chosen focus region is located at the impact end of the European Windstorm trajectories within the German Bight. The geographic nature of the coastline results in highest water levels along the German estuaries and bights. The Jade Weser estuary features barrier islands, extensive tidal flats as well as deep tidal channels and shoals, making it an ideal coastal research region for storm surge impacts. The origin of the Jade Bight is directly connected to extreme events, as the bight was created by consecutive storm surges over the last centuries. Embedded within are the two extensively developed navigational channels of the Jade and Weser (see fig. 2.11), both lined with terminals and harbors. Within the last century, the fairways have experienced consecutive incisions and widenings along with numerous hydraulic stabilization works such as the Minsener Oog in the Jade or the Franzius related Weser correction.

Today numerous (bulk) terminals line the Jade forming the transshipment complex of Wilhelmshaven (see fig. 2.12). Given their yearly turnover volumes, several of the Wilhelmshaven terminals are critical infrastructure according to national classification. Furthermore, several hydraulic structures are crucial for the stability of the fairways. Potential further incisions and port development projects are underway. Previous impact studies investigating changing environmental parameters and system states clearly show, that the region experiences changes and is of national importance given its critical infrastructure. Studies have investigated system changes related to tidal asymmetry, salt intrusion due to sea level rise, potential threats from extreme storm surges related to defense structure failure.

The study at hand incorporates previous findings, where possible, and seeks to advance the knowledge regarding potential impact amplifications and key driver attribution as outlined in section 1.2 through scenarios constructed around climate projections of coastal key drivers elucidated in section 2.3 using the methodology explained in the ensuing section 3.

## 3 Methodology

Short episodic extreme events comprise high internal dynamics and large parameter ranges, necessitating comparatively high spatial and temporal resolution of processes to capture non-linearities. Climate change in contrast describes statistically significant variations of physical quantities over extended periods of time, usually 30 years (United Nations 2015, §1; IPCC 2014, p. 1450).

Arriving at bed-forming characteristics and associated impact magnitudes of storm surges requires a representation of hydrodynamics as well as the sea bed sediment inventory and their interactions. Secondly, storm surges comprise a wind induced surge, which needs to be represented as well. Thirdly, wind-waves induced by wind gusts and sustained wind-fields both transfer atmospheric momentum onto the sea bed mobilizing surface sediments and need to be represented.

Classical climate change impact studies incorporate transient simulations spanning multiple decades (e.g. Dissanayake et al. 2012b,a; Gaslikova et al. 2012), which renders rather difficult given the vast range of major physical processes considered against the background of computational efficiency and run times. Sensitivity type climate change impact studies allow for investigating sensitivities of model-frameworks and climate systems towards single key parameters. Such studies most often employ idealized boundary conditions (e.g. Idier et al. 2017) and facilitate investigations of long term changes or processes with high lag-phases (system recovery). Consequently, a time slice type impact study (cmp. section 2.1.3) represents the tool that meets prerequisites established by the research focus, allowing for testing extreme hypotheses combining climate projections, augmenting boundary conditions and simulating impacts within defined short episodic periods.

Time slices allow for sufficiently long run times to accurately represent single storm events spanning several days, capturing the systems variability while maintaining a high degree of detail. Investigating storm surge impacts and especially morphodynamics within climate change projections is facilitated by the focus area, the Jade, comprising a sea bed dominated by fine and medium sand fractions (Valerius et al., 2015), which respond quickly to bed shear stresses exerted onto the bathymetry, eliminating the need for extended simulation periods.

### 3.1 Storm reference scenarios

Time slice studies come at the cost of uncertainties associated with the large natural system variability – elevating the importance of the representative character of scenarios for impact research. Clearly a predicament, individual storm events are unique (see section

2.2) making it difficult to choose representative events. In addition, it is essential that a sufficient data base is available for a given event to accurately simulate it. A decisive limitation is the availability of consistent bathymetric data, which forms the basis for coastal hydro- and morphodynamics to develop and act upon. Less critical data sets are observed wave conditions and atmospheric parameters such as wind speed and direction or mean sea level pressure, as those can be interpolated for regions using Kriging techniques or supplemented by re-analysis data. Conditionalized to these aspects, the predominant factor for simulating storm events is presented by the bathymetric requirements. With the DTMW-2012 being the most up to date, high resolution data set encompassing the navigational relevant areas as well as supra-tidal flats and dikes of the focus region, the time frame envelops the succeeding months to a few years (WSV, 2018a)<sup>5</sup>). Too large lags will inevitably result in deviations, given the morphological active character of the German Bight (Kösters and Winter, 2014) increasing uncertainties. Representative character of extreme storm events within this study is based upon different storm surge inducing types (see sections 2.2.2 and 2.3.3) segregating event data into westerly (Jutland-type) and northerly (Scandinavian-type) events. European Windstorms usually occur during the winter months (Sept.-Feb.), further reducing the events to choose from. The first ETC event chosen is Christian (03:00 25/10/2013-06:00 30/10/2013), which induced the highest water levels along the tide gauges located within the focus area. Extreme European Windstorm Christian classifies as a westerly event (Jutland-Type) according to the storm track shown in figure 2.2 (Roberts et al., 2014; XWS, 2015). Secondly, the ETC Xaver (06:00 04/12/2013 – 00:00 12/12/2013) is selected, given its unsurpassed magnitude in induced surge levels along the German coast and the focus area. The European Windstorm Xaver moved along a northern track shown in figure 2.2 across Europe (Scandinavian-Type). These two extreme windstorm events induced two major storm surge events that impacted the German coast in the winter of 2013 and represent the two major categories found in European Windstorm events (see section 2.2.2). These two events are selected based on the data for the focus region available within the temporal limitation imposed by the bathymetric boundary conditions. Table 3.1.1 gives an overview over the selected reference storm events.

Table 3.1.1: Reference Storm events chosen to represent the different major storm types.

Name	Description	Start (dd/mm/yyyy)	Simulation period (days)	Tides (n)	Type
1 ETC Christian	westerly event	24/10/2013	7	14	Scandinavian
2 ETC Xaver	northerly event	03/12/2013	10	20	Jutland

<sup>5</sup>Outer Weser North/East/West and Lower Weser - Resolution of 1x1m Raster xyz-ASCII-Data, Wasserstraßen- und Schifffahrtsverwaltung des Bundes, www.kuestendaten.de, 22.05.2018

### 3.1.1 European Windstorm Christian

The storm Christian (St. Jude Storm) was an ETC, which originated as peripheral low on October the 24<sup>th</sup>, 2013 over the western Atlantic. Illustrating the hydro-meteorological magnitude of ETC Christian, figure 3.1 presents exemplary measurements of wind speed and direction obtained at the Lighthouse Alte Weser (LAW) (a), as well as significant wave height (SWH) and mean wave period both observed at the LAW as well (b), together with the water level (c) gauged in Wilhelmshaven Alter Vorhafen (WHV AV).

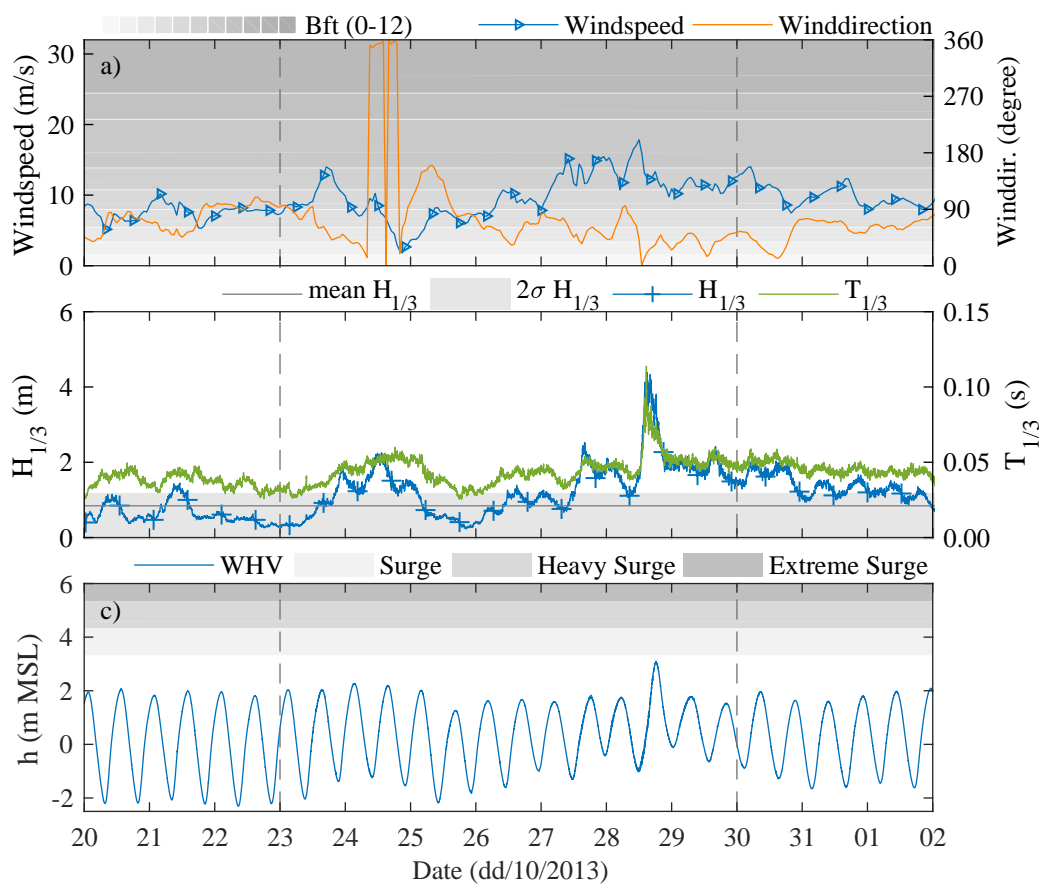


Figure 3.1: Hydro-meteorologic quantities & magnitudes of ETC Christian comprising wind speed and direction (a) including a wind speed classification according to Beaufort measured at Lighthouse Alte Weser (LAW); significant wave height (VHM0) and mean wave period (HM01), measured at LAW as well as the mean VHM0 for 2013 and a twofold standard deviation enveloped (b); water level gauged at Wilhelmshaven Alter Vorhafen (WHV AV).

Moving east, it took up energy of the diminishing former tropical storm Lorenzo, greatly decreasing pressure, forming an ETC. Heading towards Europe at migration speeds of  $1200 \text{ km h}^{-1}$ , Christian was a fast moving event (DWD, 2013a). On October 27<sup>th</sup> the storm eye made landfall at the southwest coast of the United Kingdom, with measured wind gust speeds of up to  $168 \text{ km h}^{-1}$  (Met Office, 2013).

The following Monday, October 28<sup>th</sup>, the storm reached the German coast and induced the first storm surge of 2013, with higher surge elevations along the North- compared to the East-Frisian coast. Along the German Bight Christian induced sustained wind-speeds of 10 Bft with gusts up to 12 Bft, causing 1.74 m 1.44 m of surge above MHW in Hamburg and Bremerhaven respectively. The storm proceeded towards Denmark and diminished, reaching phase seven of the ETC model presented in figure 2.2. Coastal storm impact was measured at various points throughout the Jade-Weser Region, employing tide gauges, wave buoys and anemographs. Storm Christian shows the clear short-duration high magnitude impact character of westerly (Jutland-Type) events (XWS, 2015; Sturmflutwarndienst, 2013a).

### 3.1.2 European Windstorm Xaver

Xaver originated from a diminutive warm frontal wave crossing a low-pressure zone over the North Atlantic, south of Greenland during the night from the 4.<sup>th</sup> to the 5.<sup>th</sup> December, 2013. On the 5.<sup>th</sup> of December the quickly intensifying storm reached Europe, causing power outages and widespread destruction. The south east coast of England (Norfolk cliffs) experienced massive cliff erosion, with residential areas built upon them falling into the North Sea. The backside of the cold front, the maritime arctic air was sucked into the storm, causing intense snow fall. The storm induced up to 8 m high waves in the German Bight at the buoy Elbe (DWD, 2013b; Sturmflutwarndienst, 2013b). Similar to the European Windstorm Christian, the coastal storm impact was recorded along the North Sea coast with figure 3.2 showcasing the same parameters observed at the same locations for ETC Xaver.

Wind speeds reached  $150 \text{ km h}^{-1}$  to  $160 \text{ km h}^{-1}$  (Bft 11) along the German coast. Compared to the Jutland-type ETC Christian with its short duration high intensity wind speeds, Xaver was a Scandinavian-type storm moving slower and exerting prolonged wind shear stress onto the North Sea, inducing surge heights of 3.30 m and 3.16 m above MHW in Wilhelmshaven and Bremerhaven respectively, classifying as extreme storm surge. In Hamburg the water level only fell short 0.06 m of the historic storm surge of 1962 closely resembling the skew-surge curve of the 1962 event (Sturmflutwarndienst, 2013b; XWS, 2015; LSBG, 2014).



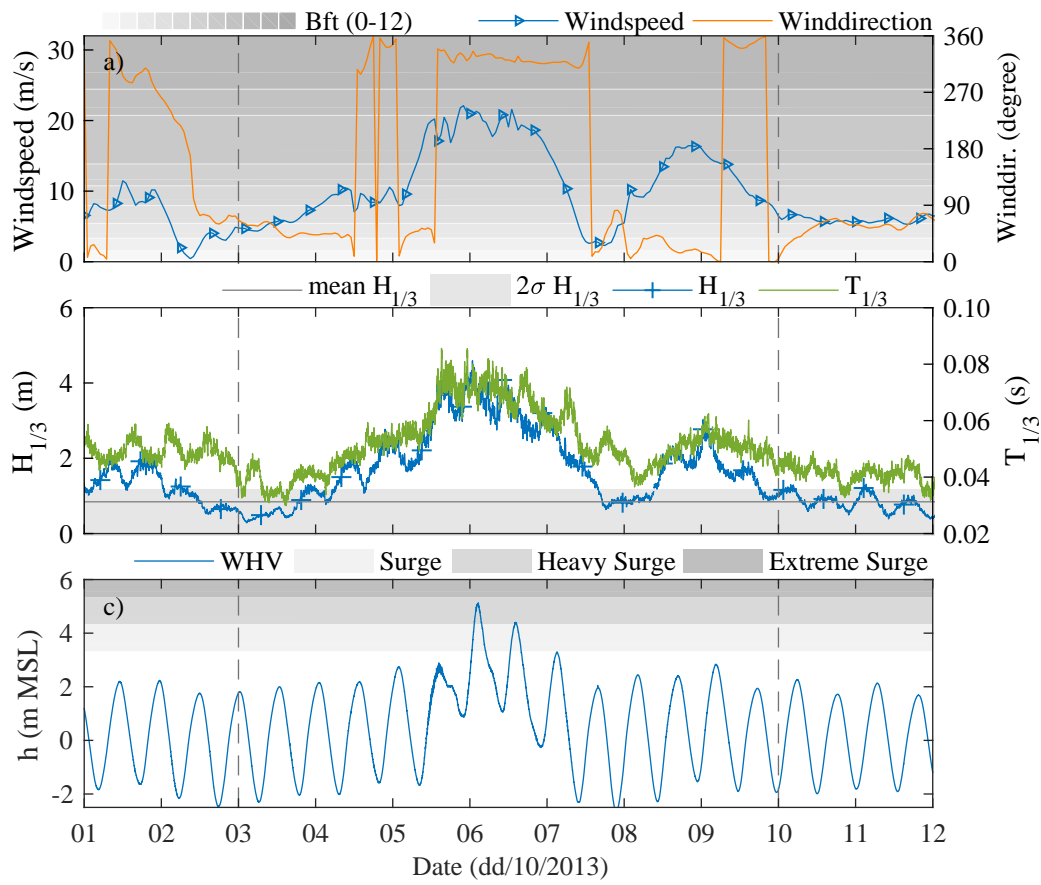


Figure 3.2: Hydro-meteorologic quantities & magnitudes of ETC Xaver comprising wind speed and direction (a) including a wind speed classification according to Beaufort measured at Lighthouse Alte Weser (LAW); significant wave height (VHM0) and mean wave period (HM01), measured at LAW as well as the mean VHM0 for 2013 and a twofold standard deviation enveloped (b); water level gauged at Wilhelmshaven Alter Vorhaven (WHV AV).

### 3.2 Storm research scenarios

Given the two different storm events laid out in section 3.1 these are used for designing research scenarios with changes in boundary conditions representing coastal key drivers (see table 2.1.1) oriented at future projections of climate change research presented in section 2.3.

Drawing on future projections of potential climate change impacts, figure 3.3 juxtaposes contrasting physical ranges of variations in key drivers, from which two sets of boundary parameters are extracted, representing the average and extreme values representing a likely future development as well as an alarming extreme scenario evolution.

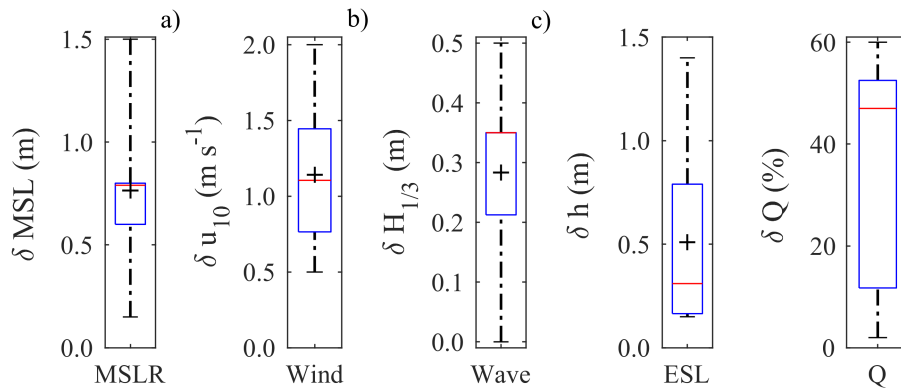


Figure 3.3: Literature based ranges of Coastal main drivers according to IPCC with research based projected levels in 2100. Boxes indicate 25 % to 75 %, whiskers 1 % to 99 %, mean (+) and median (-); a) is based on findings presented in section 2.3.1 pertaining to regional sea level rise (RSLR); b) summarizes literature findings presented in section 2.3.4; c) presents findings given in section 2.3.5; d) shows projected ranges for ESL stated in section 2.3.6, finally e) gives projected estimates of changes in discharge for winter months regarding the Weser compiled in section 2.3.7.

Given are parameter ranges for RSLR in  $\delta h$ , Windspeed in  $u_{10}$ , SWH, ESL and discharge values researched specifically for the focus area in the North Sea and the Weser river with a temporal horizon until 2100.

For MSLR a vast range of studies is available within literature giving a good estimate for future changes. Wind speed on the contrary is regarded as a very difficult parameter to predict, due to highly dynamic small scale processes involved, which are still not sufficiently resolved and represented in GCMs and partly still discussed by atmospheric research (see section 2.3.4). Current research predicts a slight increase of surface waves

within the German Bight across a variety of model studies. Research focused on discharge of the Weser projects an increase in winter time peak discharge volumes, which is considered here for constructing compound events.

Storm research scenarios considering boundary changes are defined and chosen individually parameters explained with a synopsis given in table 3.2.1. Values given and implemented reflect findings from the literature research (see section 2) and constitute the median for the **M** and extreme values for the **E** scenarios. The baseline scenario is denoted by **R** as reference and constitutes the current state system parameters, simulating the storm impacts under current conditions.

Furthermore, ESL projections for the southern North Sea also predict a slight increase in water levels due to climate change. However, these are investigated further in section 3.2.4 and excluded from simulations within this study, due to a lack of data, physical process understanding and inconclusive research studies on the subject.

Table 3.2.1: Storm research scenarios investigated within this study with projected future changes in coastal key drivers.

Storm Scenarios	Acronym	MSLR (m)	Wind uv(m/s)	Wave $H_{1/3}$ (m)	Q (%)	Bathymetry (m)
(1) Christian (2) Xaver	R <sup>1</sup>	-	-	-	-	DTMW
	RC <sup>4</sup>	-	-	-	-	DTMW <sup>i</sup>
	M <sup>2</sup>	0.74	1.14	0.28	34.8	DTMW
	MC	0.74	1.14	0.28	34.8	DTMW <sup>i</sup>
	E <sup>3</sup>	1.50	2.00	0.50	60.0	DTMW
	EC	1.50	2.00	0.50	60.0	DTMW <sup>i</sup>

R<sup>1</sup> Reference; M<sup>2</sup> Medium; E<sup>3</sup> Extreme; C<sup>4</sup> Construction

DTMW<sup>i</sup>: Digital terrain model of the water body, 2012 with planned incisions

Boundary amplification values presented in tab. 3.2.1 are derived from the literature research and are based solely on findings for the North Sea and the German Bight in order to reduce the unwanted effect of system bias due to consideration of findings for different geographical regions. Therefore, neither a dynamic downscaling nor a regionalization approach are required for implementing the derived values. Nevertheless, it should be noted that, most of these values stem from numerical model experiments, which inherently contain model-specific assumptions and simplifications (see also section 2.1.2).

### 3.2.1 Mean sea level change

Storm scenarios investigated within this study consider RMSL in order to investigate how elevated coastal water levels amplify possible storm surge impacts. On average reviewed research studies project an MSLR of 0.74 m by 2100. Formerly associated with a medium confidence by the IPCC (AR5), recent findings of accelerated MSLR (e.g. Nerem et al. 2018) show that this assessment is unlikely to hold true but instead should be assigned a higher likelihood. Extreme sea level rise values according to RCP8.5 simulations reach 1.5 m, with various studies projecting elevation changes within this range (see section 2.3.1). Associated with low confidence in the AR5, more recent research indicates a probable readjustment of confidence levels associated with the magnitude of change. However, within this study a RMSL of 1.5 m represents the extreme scenario conditions investigated for different storm events.

### 3.2.2 Wind speed change

Projections of wind speed are generally associated with large margins of uncertainty, given the transient nature of atmospheric processes. Research focusing on the North Sea projects an average increase of  $1.14 \text{ ms}^{-1}$  until 2100 (see section 2.3.4). An increase of up to  $2.0 \text{ ms}^{-1}$  is projected for the German Bight and constitutes the extreme wind scenario considered within this study. Nevertheless, it should be noted that atmospheric processes are very difficult to reproduce with state of the art GCM simulations. Therefore, currently available future projections of atmospheric changes used within this study are associated with low confidence levels. Similarly, the IPCC AR5 puts low confidence in observed trends and projected changes due to poor sampling density in observations and inefficiencies in GCMs. However, the AR5 was the first IPCC report to even address possible changes and investigate the possibility. One consequence was, that atmospheric model components received attention and it was shown that both, GCMs and reanalysis data used to force these, lacked resolution and processes (see section 2.2.2).

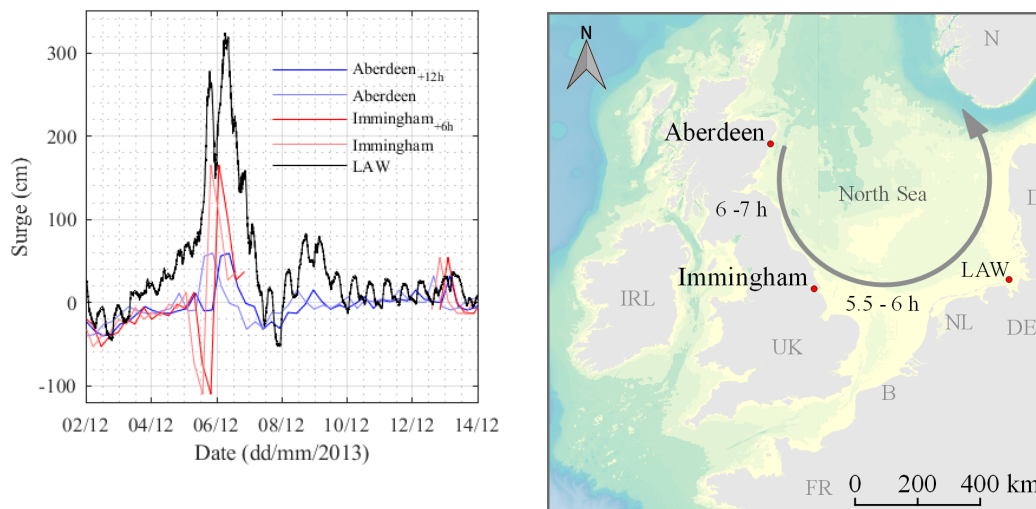
### 3.2.3 Wave changes

Future changes in surface waves within the southern North Sea constitute projected increases in SWH of 0.28 m on average as well as extreme values of up to 0.5 m. Both values constitute the average and extreme scenario boundary modifications investigated within this study. Observed trends of SWH are associated with medium confidence in the AR5, whilst future projections were generally paired with low confidence given a large increase in studies investigating surface waves since AR4. It should be pointed out that, surface wave simulations largely depend on atmospheric boundary conditions, which in turn are

linked to large margins of uncertainty (see section 3.2.2). Likewise, implemented changes and related impacts investigated within this study contain these uncertainties.

### 3.2.4 Extreme Sea Level changes (external surge)

Extreme Sea Levels are the result of non-linear interactions and superposition of various parameters, which are investigated individually (waves, wind, MSLR, external surge). External surges are the remaining parameter, they originate in the Atlantic as deep water surges due to sharp edged pressure gradients passing by (storm systems), which result in a pressure related disturbance of the water surface (Schmitz, 1965) and enter coastal shelf seas as non-stationary external surge (see figure 3.4(a)).



(a) Surge levels of tide gauges Aberdeen, Immingham and LAW for storm event Xaver (b) Map of surge wave progression in the North Sea and travel times between select gauges

Figure 3.4: Xaver related surge levels a) and their temporally shifted surge signals as well as gauge locations b) for three characteristic gauges Aberdeen, Immingham and Leuchtturm Alte Weser with estimated surge travel times.

External surges within the North Sea preferentially accompany Scandinavian type storm systems and propagate counter clockwise (see figure 3.4(b)) mimicking a tidal wave (Schmitz et al., 1988; Gönnert, 2003). The highest observed external surge occurred 1962 during the historic storm surge and exhibited a height of 1.08 m in Aberdeen and 0.75 m in Cuxhaven, resulting in a reduction of 30 %. Transferring the geo-spatial reduction coefficient for Aberdeen-Cuxhaven to Aberdeen-LAW yields a reduction of 28.125 % rounded to 28 %.

This results in a surge height of 0.77 m for LAW. Storm surge research revealed a reduction range of 8 % to 43 % between Aberdeen and Cuxhaven (Oumeraci et al. 2012, p.28), given the spatial proximity of Cuxhaven and LAW (38 km) with marginal bathymetric obstructions, the range is transferred to LAW using the rule of three narrowing the range to 7.5 % to 40 % (0.99 m to 0.65 m) remaining external surge height at LAW. Deep water surges depend on the atmospheric pressure differences developing over the north Atlantic (Gönnert, 2003; Gönnert and Thumm, 2010). Contrasting observed high and low pressure values over the United Kingdom are compiled in appendix A.4 from Burt (2007) and give a good indication of the resulting surge potential. Given as well is the recently observed low pressure value of Tayphoon Hayian in 2013 further increasing the theoretical surge potential, as the storm featured a low pressure system below 900 mbar with tendencies to classify it as a class 6 on the Hurrican scale. Figure 3.4(a) shows the surge development observed at tide gauges in Aberdeen (UK) and Immingham (UK) as well as LAW (DE). The UK data is time shifted in order to better compare the surge development across the North Sea. A clear increase is visible. Figure 3.5 shows the decomposition of the tide gauge signal observed during the storm Xaver at the tide gauge Leuchtturm Alte Weser following the approach described in Oumeraci et al. (2012) using the  $t\_tide$  toolbox (Pawlowicz et al., 2002) and wind speed related surge levels for the German Bight (Hansen, 1950).

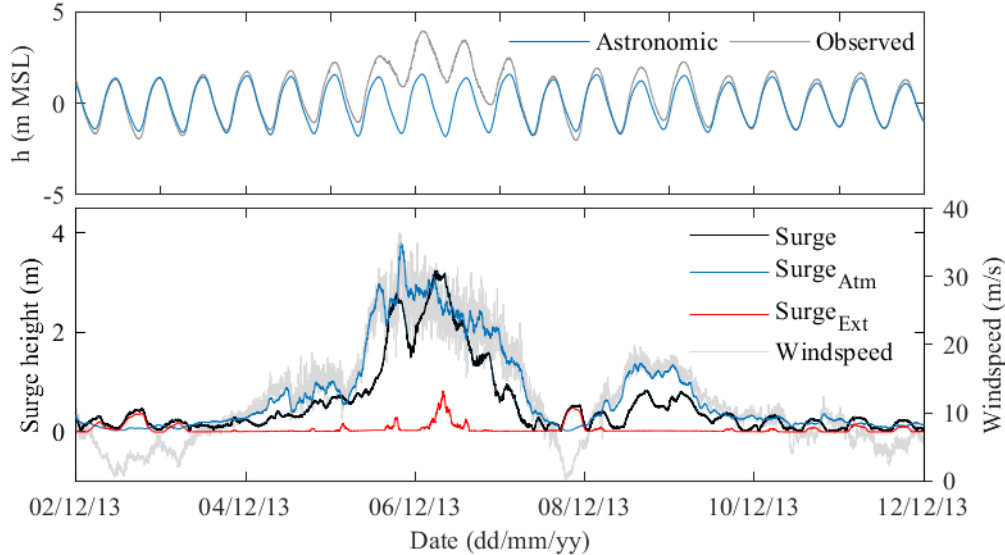


Figure 3.5: Tidal water level observation during Xaver at the tidal gauge station Leuchtturm Alte Weser (LAW) (upper panel) and single components (lower panel) comprising astronomic constituents, wind related surge, external surge and residual set up as well as wind speed.

Storm event Xaver clearly comprised no significant external surge component. Decompositions for the other select storm event as well as a chain event can be found in appendix A.2 & A.3 and show a small external surge for the chain event Elon in 2015, which is not further investigated within this study.

Barometric surge potentials given in appendix A.4 yield a physically observed mean potential of 1.12 m for the winter month October-March with a maximum pressure gradient of 128 hPa translating to 1.27 m of surge height. Applying previously discussed reduction coefficients, the extreme value of 1.27 m is reduced to 0.91 m reaching LAW and 1.08 m would reach the German Bight under a barometric gradient equal to 151.5 hPa observed during the Typhoon Haiyan, which is possible to occur over the Gulf Stream in the North Atlantic resulting in explosive cyclogenesis (Sanders and Gyakum, 1980).

The recently observed extreme low pressure during Typhoon Haiyan in 2013 of 895 hPa would result in theoretical surge potential of 1.5 m, giving a glimpse of future surge potentials under increasing storm intensity.

### 3.2.5 Discharge changes

Fresh water influx into the Weser estuary is projected to increase during winter periods on average by 34.8% and in extreme cases by up to 60.0%. The IPCC AR5 assigns a medium confidence level to observed trends towards an annual net decline in discharge volume (Stocker, 2014). What is more, the AR5 also associates a medium confidence with a general increase in volume for higher latitudes as well as wet tropical regions. The focus area of this study is located at 54.1° and research projects a winter time increase in peak discharge, which could substantially contribute to inbound storm events from the sea having a dam like effect, increasing water levels. The coincidence of a storm surge and an inland high discharge event is not a given yet physically possible and constitutes a compound event (Petroliagkis et al., 2016).

### 3.2.6 Constructive changes

Coastal engineering formed today's coastline through land reclamation measures successively reducing the former land losses due to heavy storm surges (see section 2.4.2). Impoldering of coastal marshes and erection of hydraulic works marked the recent development of the Jade-Weser estuary.

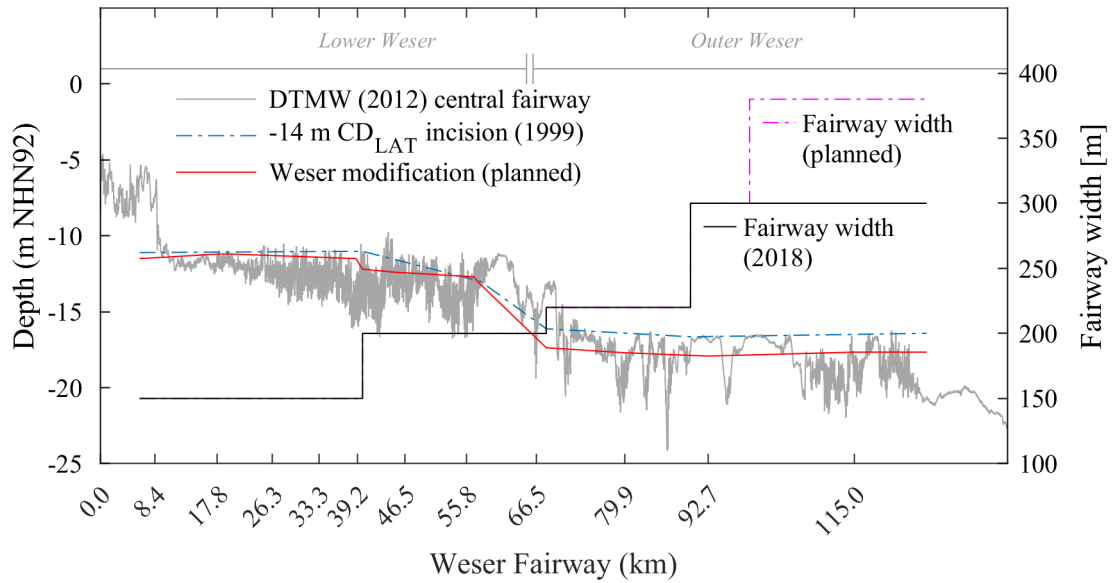


Figure 3.6: Planned hydraulic works and development of the Weser fairway showing the current approval depth of the fairway as well as projected incision plans in conjunction with widening of the fairway along the outer Weser from fkm 92.7 to 126. Reference depth is based on the DTMW of 2012.

Especially the construction of river training measures like the groyne-spider Minsener Oog and successive incisions of the fairways along the Jade and the Weser characterize the domain. Given the overarching anthropogenic influence, especially with the recent development of the ECTW and a projected northward extension, an increase of coastal infrastructure is associated with high confidence, not only locally but globally. Therefore, a constructive scenario (C) is designed, investigating potential impacts of storm surges upon a deepened fairway system along the Weser and Jade navigational channels. Projected nautical trade and container ship development show a clear increase in very large ships with a draught of 16 m carrying in excess of 19.000 TEU. Along the outer and lower Weser various adaptation measures are planned aiming to deepen and also widen the fairway (WSV, 2006a,b). Figure 3.6 shows the official planning approval depth along the lower and outer Weser according to the  $-14\text{ m CD}_{\text{LAT}}$  extension of 1999. Given as well are the currently planned incisions and fairway widening along the Weser together with the DTMW of 2012 as a reference.

Furthermore, the currently debated extension of the ECTW in the Jade is implemented and possible impacts investigated. Additionally, the official planning approval depth of  $-18.5\text{ m CD}$  is implemented, as the fairway is currently not maintained to this depth, due to a lack of deep draft vessels making port in the transshipment complex Wilhelmshaven.



Figure 3.7 gives the details of the Jade fairway depth and width as well as the projected ECTW extension (NMW, 2016; ISL, 2016).

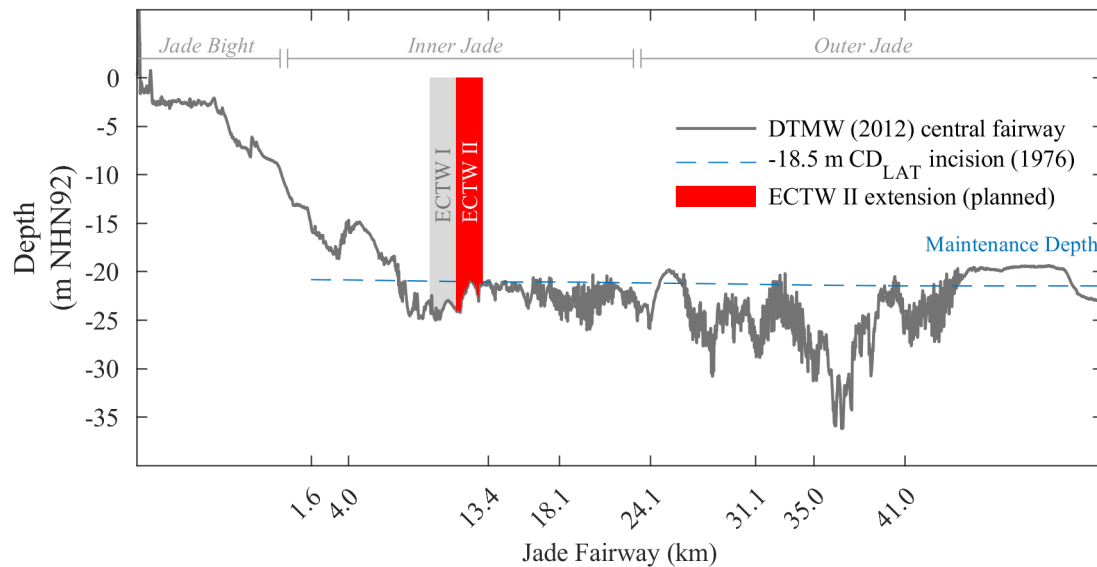


Figure 3.7: Planned hydraulic works and development of the Jade fairway showing the official planning approval depth up to which the fairway may be dredged and maintained as well as the projected position and extend of the ECTW extension downstream of the current position. Reference depth forms the DTMW of 2012.

In order to investigate possible impacts of these planned constructive alterations within the focus area, the model bathymetry is adapted accordingly to represent geometry changes denoted with a C and scenario combinations given in table 3.2.1.

### 3.3 Atmospheric Reanalysis Data

Numerical model simulations conducted within this study are forced with synoptic scale reanalysis data sets of various hydro-meteorologic quantities of Europe's atmosphere, provided by various European agencies (Marsigli et al., 2005; Dee et al., 2011; Weisse et al., 2014b; Geyer and Rockel, 2013). Figure 3.8 presents exemplary coastDat2 data for the European Windstorm Xaver.



Figure 3.8: CoastDat2 data for European Windstorm Xaver regarding geostrophic wind speed and mean sea level pressure. Coastal water level observed during the storm in Wilhelmshaven Neuer Vorhaven is given.

However, reanalysis data have been doubted to reproduce certain atmospheric phenomenon such as the sting jet (compare section 2.2.2) and have other known issues<sup>6</sup>. Given the degree of complexity and number of processes included in the reanalysis products as well as their temporal extent, the spatial resolution at which these are computed ranges between 50 km to 100 km (e.g. Stachnik and Schumacher 2011) given large extents but also high-resolution approaches with grid-spacings of  $0.22^\circ$  are being constructed in order to

<sup>6</sup><https://confluence.ecmwf.int//display/CKB/ERA-Interim+known+issues>

represent small scale atmospheric processes. Data sets covering Europe and especially the North Sea comprise the Era-Interim data set computed by the ECMWF, the COSMO-CLM data set computed by DWD and the coastDat data set currently in its second edition, with coastDat3 projected for 2019<sup>7</sup> created by the Helmholtz Zentrum Geesthacht (HZG). Given the special maritime focus of the coastDat2 reanalysis data set, as well as its comparatively high resolution of 0.22° and temporal coverage of the the storm events to be investigated within this study, geostrophic wind-fields and mean sea level pressure data is extracted at hourly intervals from the coastDat2 reanalysis data set for simulating coastal impacts of European windstorms.

### 3.4 Numerical modeling

Numerical analysis constitutes a subfield of mathematics tasked with the construction and analysis of algorithms used to describe continuous problems. Coastal and hydraulic engineering employ numeric methods to describe and simulate coastal processes. Compared to analytical methods, numerical analysis provides approximations instead of exact solutions. However, numerical analysis facilitates the computation of quantities at high speeds, which are typically incomputable from an analytical point of view but desirable from an engineering point of view. Any numerical method in question exhibits a certain quality, which is determined by three main characteristics:

- Consistency - describes how any numerical solution compares to its analytic counterpart under perfect conditions
- Condition - is the dependency of results obtained with any numerical method towards input data quality
- Stability - robustness of the numerical algorithm against poor quality input data

Apart from these any numerical algorithm chosen for a problem needs to verify for the task at hand and subsequently requires calibration and validation to converge and yield best possible results. Numerical software meeting the three main criteria listed above and hence suitable for modelling coastal waters and various processes is available in many forms from different developers (Delft3D, Telemac, Mike, SMS). Individual model quality is characterized by uncertainties stemming from stochastics of natural processes, parameters optimized for chosen sample sets and finally, from incomplete understanding or lack of representation of physical processes.

---

<sup>7</sup>An exemplary list of known issues of reanalysis products is available at: [https://cera-www.dkrz.de/WDC/ui/ceraresearch/entry?acronym=coastDat-3\\_COSMO-CLM\\_ERAi](https://cera-www.dkrz.de/WDC/ui/ceraresearch/entry?acronym=coastDat-3_COSMO-CLM_ERAi)

### 3.4.1 Processes and scales

Primary objective of this sensitivity study is to quantify potential storm surge impacts upon the coastal environment with a focus on sediment transport and bed forming characteristics of storm events (cmp. section 1.2). Therefore, a rather large number of processes must be reproduced and validated by the model of choice covering:

- Hydrodynamics (tidal characteristics and currents)
- Salt and temperature transport
- Morphodynamics (suspended and bed load, sea bed changes)
- Atmospheric forcing (wind and sea level pressure)
- Surface waves (evolution and re-mobilization of coastal sediments)

As well as their respective interactions and feedback on one another including morphodynamic bed changes. Furthermore, the numerical model is required to resolve the focus area spanning approximately 2000 km<sup>2</sup> on contrasting scales mapping tidal flats, navigational channels, as well as dikes and harbor basins. Figure 3.9 gives an overview of morphologic units in contrast to numerical models. Morphologic units cover small scale features such as ripples and beaches, large subaqueous dunes, tidal flats or whole estuaries (Bosboom and Stive, 2015; Cowell and Thom, 1997; Kraus et al., 1991). Temporal scales associated with the morphologic units span seconds to centuries, whilst episodic storm events range within the meso scale (Cowell and Thom, 1997; Coco and Ciavola, 2018). Kraus et al. (1991) defined four different temporal scales, with the engineering scale covering a wide range of both the temporal and spatial scale. Morphologic units considered within this study pertain mainly to tidal flats, (navigational) channels as well as beaches. Numerical models suitable to resolve certain morphologic units are classified by Winter (2011b). Episodic storm events lasting days affecting the extensive estuarine Jade-Weser region involve multiple physical processes and scales, which might be resolved by a two dimensional depth integrated (2DH) morphodynamic model (MDM) to research bed forming characteristics of storm events on the spatial macro scale considered here.

Tidal characteristics within the focus region are semi-diurnal (see section 2.3.2) and can be sufficiently resolved on 30 min time steps with a numerical method (e.g. Zorndt, 2014). Nevertheless, fast moving storm systems require time steps of 10 min to accurately capture quick ramp ups of wind setup and surge (Gönnert, 2003). Values below this value greatly increase the computational efforts and yield no additional information.

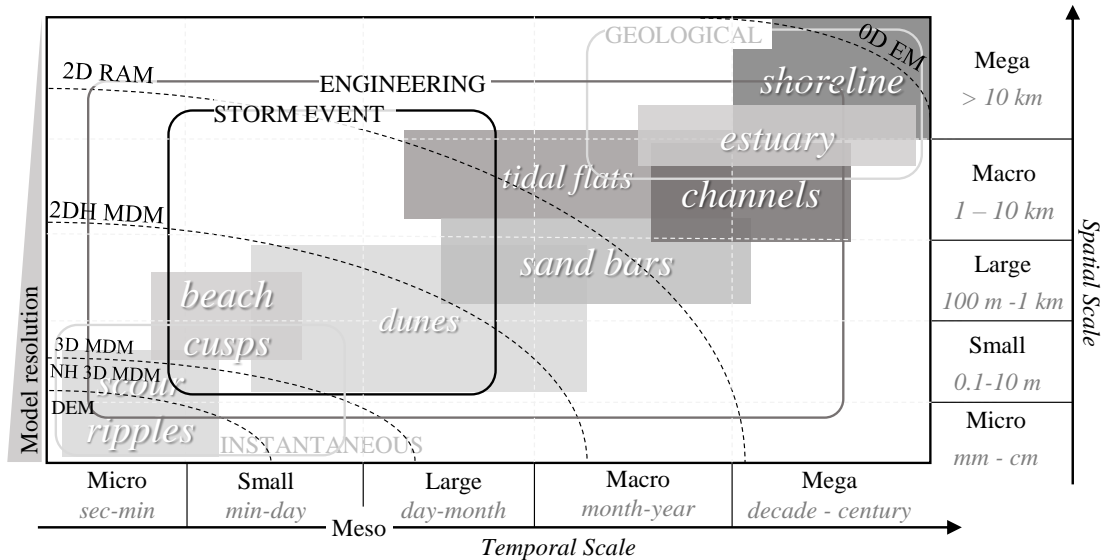


Figure 3.9: Morphologic units with associated temporal and spatial scales and typical ranges of discrete element models (DEM); non-hydrostatic 3D morphodynamic models (NH3D MDM); 3D coastal area morphodynamic model (3D MDM); 2DH coastal area morphodynamic model (2DH MDM); rapid assessment of morphodynamic models (2D RAM); 0D empirical models (0D EM). Combination of scales is based on classifications by Cowell and Thom (1997); Kraus et al. (1991) and Winter (2011a) as well as Bosboom and Stive (2015).

Current velocities and directions measured within the focus area are governed by the tidal characteristics. Consequently, a result time step of 10 min yields corresponding flow fields of sufficient resolution. Furthermore, the designated numerical model has to account for the extensive intertidal flats (bathymetry within tidal range) covering approximately 980 km<sup>2</sup> located within the eulittoral of the outer Weser and along the Jade, as well as extensive supralittoral areas, necessitating a robust solution for wetting and drying. Sediment transport processes encompassing the mobilization, transport and sedimentation of sediment as well as resulting bathymetric alterations (erosion/accretion) are required and facilitate researching the main objectives (see section 1.2).

Salinity and temperature gradients within estuaries may change significantly during storm impacts, as fresh water influx is dammed up inside the estuary by the incoming storm, influencing hydrodynamics as well as sediment dynamics. Consequently, the model has to account for these processes as well.

Surface waves constitute a major physical process within the model domain, as sea state and especially the coastal wave evolution during storm events transfers large amounts of atmospheric energy into the water body and subsequently onto the sea bed (see section

### 2.3.5).

Extreme atmospheric conditions, predominant during storm conditions, comprise rotating sustained high wind speeds as well as low pressure storm eyes, both affecting the coastal waters (see sections 2.3.4, 2.3.3 & 2.3.6). Surface winds exert wind shear forces onto the water surface and push the water landward, resulting in wind set up, substantially contributing to elevated coastal water levels. Furthermore, surface waves exhibit a wind growth, which translates a portion of the kinetic wind energy into sea state. Therefore, the model has to account for this transfer of atmospheric energy into the water body. Variations in mean sea level pressure (MSLP) may also contribute to the overall increase of coastal extreme sea levels and require representation.

Finally, an internal bi-directional coupling of various processes is required in turn allowing for feedback; for example if incoming waves break on the tidal flats and erode sediment, which is relocated to deeper waters, the eroded flat requires a bathymetric update with a coupled feedback onto the developing hydrodynamics and corresponding surface wave conditions.

## 3.4.2 Model

Confronted with multiple physical processes and their partially non-linear interactions, the numerical software suite Delft3D is chosen for this complex and demanding task comprising multiple model(s), which may be coupled to one another given the problem at hand. The manual of the model suite states various application areas with tide and wind-driven storm surges heading the list (Deltares 2014a, p. 31). Figure 3.10 shows a conceptual schematic of the three Delft3D sub-models used within this study.

The three models Delft3D-FLOW, Delft3D-MOR and Delft3D-WAVE are used. Delft3D-FLOW is a hydrodynamic model which may be operated in depth-integrated two dimensional as well as three dimensional mode. The model operates either on a regular or a curvilinear grid<sup>8</sup> and computes non-steady flow as well as salt and heat transport phenomena as a result from tidal and meteorological forcing. Main set of equations comprise the horizontal equation of motion, the continuity equation and the transport equations for conservative constituents (Deltares 2014a, pp. 188). At the sea floor a parametric bed roughness parameter is prescribed. Within FLOW hydrodynamic spatially and temporally varying boundary conditions may be implemented to force a simulation. Furthermore, spatiotemporal atmospheric boundary conditions can be implemented as well. Finally, parametric hydraulic structures may be implemented allowing for representing groynes, terminals and training walls.

Delft3D-MOR is a morphodynamic model, which is forced by flow fields computed by the

<sup>8</sup>A flexible irregular grid version is currently under development and not operational

FLOW model. Delft3D-MOR allows for implementing multiple non-cohesive (sand) as well as cohesive (mud) sediment fractions. MOR offers the possibility to represent a sediment inventory as one well mixed layer or as sequence stratigraphic representation of the sea floor subsurface. Sediment transport may be calculated according to various renowned semi-empirical transport formulae (Deltares 2014a, pp. 347). Coupled to the FLOW model, computed shear stresses are used to determine sediment transport magnitudes and directions. As a result of erosion and accretion MOR holds the option to dynamically update the bathymetry after each time step and forward it to the FLOW and WAVE models.

For further information on the FLOW and MOR models the interested reader is referred to the manual and validation literature of the model suite (Deltares, 2014a).

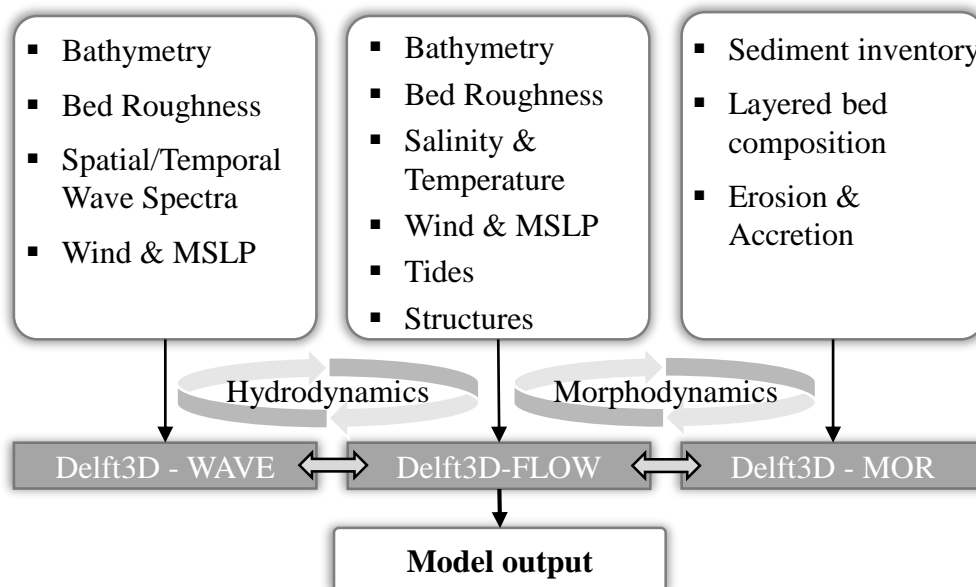


Figure 3.10: Conceptual flow chart of Delft3D-FLOW/WAVE/MOR with WAVE, SED/MOR, related inputs and interactions.

Delft3D-WAVE<sup>9</sup> is a phase-averaging surface wave model and can be forced either by parametric or spectral wave data, which may exhibit spatial and temporal evolution. The model solves the Wave Action Equation (WAE) on a rectilinear or curvilinear grid and represents all essential shallow water effects listed in table 2.3.4. The wave model may be coupled to the FLOW model (Deltares, 2014b), allowing for a bi-directional exchange of information. If coupled, the WAVE model receives instantaneous flow-field information for its computational grid from the FLOW model on a user-defined interval, incorporates

<sup>9</sup>The standalone version of the WAVE model is called Simulating WAVes Nearshore (SWAN)

wave and atmospheric forcing quantities and solves the WAE accordingly for the wave grid. Subsequently, WAVE forwards wave related energy and orbital velocity fields to the FLOW model, which in turn computes wave induced shear stresses and allows the MOR model to determine wave related sediment-mobilization and transport. The interested reader can find additional information regarding Delft3D-Wave in the corresponding manual (Deltares, 2014b) as well as on the standalone support website (TU Delft, 2018).

The software suite allows for a parallelized implementation of the source code using a message processing interface, facilitating the commitment of larger computational resources to a given problem.

### 3.5 Jade-Weser-Model

A model domain covering 2260 km<sup>2</sup> encompassing the Jade as well as the outer and lower Weser is delineated. Landward (closed) model boundaries are oriented along the main dike line (NLWKN, 2007a, 2011a). Consequently, retention areas are included in the model. Open boundaries are implemented at the Weser weir in Bremen (fkm 0) constituting a tidal boundary and the Hunte weir (fkm 37.5) facilitating freshwater influx into the model domain. Finally, an open sea boundary is implemented following tidal phase lines for the focus region and regarding tidal water sheds as lateral boundaries (Götschenberg and Kahlfeld, 2008; Lange et al., 2008). Furthermore, the northward extent of the domain is limited to 54° north by the complex hydrodynamic interactions stemming from the Elbe estuary in the East, which would interfere with local dynamics. The domain is discretized constructing a curvilinear grid with a horizontal resolution of 20 m to 100 m, resulting in over 1.2 mio. cells for the FLOW model on which the MOR module operates as well. Figure 3.11 shows the computational FLOW/MOR domain with details. The grid is designed according to model specific limitations and quality criteria featuring a Courant-Friedrichs-Lewy (CFL) number  $\leq 10$  (Deltares 2014a, pp. 38). Small tributaries of the Weser are the Lesum, Ochtum and the medium-sized Hunte. All three of them feature storm surge barriers, which are closed if a corresponding surge level is predicted<sup>10</sup>. Since the focus of this study rests on storm surge events, the small tributaries of the Weser are not covered by the model domain in detail since the barriers at their confluences are closed and prevent a mass exchange. This is a trade off, as in reality the weirs are closed during tidal phases, in turn influencing hydrodynamics. However, for investigating the bed forming characteristics of storm surges on the outer tidal flats and navigational channels the hydrodynamics of the lower Weser are of subordinate importance, though the model has the possibility to implement moving weirs.

<sup>10</sup>[https://www.nlwkn.niedersachsen.de/hochwasser\\_kuestenschutz/landeseigene\\_anlagen/sperrwerke/](https://www.nlwkn.niedersachsen.de/hochwasser_kuestenschutz/landeseigene_anlagen/sperrwerke/)



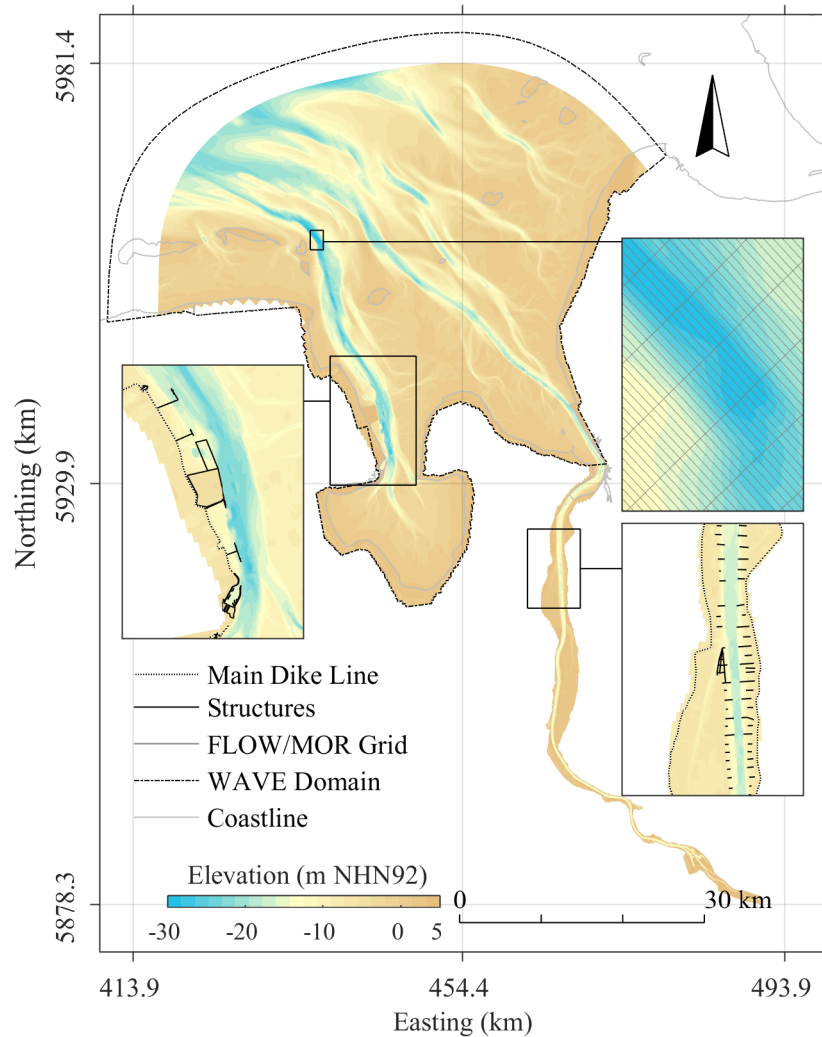


Figure 3.11: Delft3D FLOW/MOR and WAVE model domain with coastline, detailed model grid, dike line and exemplary infrastructure. Bathymetry is based on the DTMWs from 2012 for the Jade, the lower and outer Weser.

Modelling complex tidally and wind driven hydrodynamics and coupled sediment transport patterns in coastal waters requires a high resolution model bathymetry covering the area. For this study the state of the art federal DTMWs of the coastal zone are used. These are available for the Jade as well as the lower and outer Weser with a horizontal

resolution of 1x1m comprising 24 billion vertices covering the water bodies as well as the retention areas, dikes and adjacent infrastructure. It is noteworthy, that the survey year of 2012 for the DTMW includes the recently constructed ECTW within the Jade, absent from previous data sets. The DTMW of 2012 resembles the latest homogeneous bathymetric data set available, with a follow up data set being currently processed for 2019.

The northern model edge stretches slightly beyond the reach of the DTMWs necessitating additional bathymetric information, obtained from the BSH north sea data set with a horizontal resolution of 50x50m (BSH, 2013), surveyed between 2010 and 2016.

### 3.5.1 Active boundary conditions

Influx boundaries are located at the tidal weir in Bremen as well as the confluence of the Hunte with the lower Weser. Both model boundaries are designed as *total-discharge* types. At the tidal weir in Bremen mean daily discharge values are available for forcing the model. For the Hunte a long term mean discharge of 23.5 m is used as no daily values are measured near the confluence.

At the North Sea boundary, a *water-level* type boundary is implemented and forced with values observed at the tidal gauging station Leuchtturm Alte Weser. Given the predominant character of the M2 tide along the German bight, the layout of the boundary is oriented along its tidal phase line (Plüß, 2003; Gönnert et al., 2004; Malcherek, 2010). The station LAW is located centrally inside the outer Jade-Weser region 12 km from the open model boundary; consequently this approach represents a physical abstraction. A phase lag was added to the time series to account for the geographic shift. Furthermore, the lateral extent of the boundary shows a 15 min phase lag from the western to the eastern endpoint. This lateral phase lag was added to the endpoints, to account for the lateral tidal development. Delft3D offers the possibility to interpolate linearly between the endpoints of any given open boundary, which was done within this study to extrapolate the tidal measurements from LAW onto the open sea boundary. Measurements were used to account for external surges, possibly present during storm conditions, as well as astronomical tides. Alternatively, the model could be forced with partial tidal constituents. However, this approach would neglect potential external surge components of selected storm events. Furthermore, an astronomically forced model would also reduce the wind surge compared to measurements, since the model domain does not span the North Sea and consequently features a smaller wind fetch surface area required to reproduce observed coastal surge values.

Salinity & Temperature values are obtained at various point observations within the computational model domain and fitted as boundary conditions. Figure 3.12 shows exemplary observations of temperature and salinity at the LAW for 2012 used along the open North

Sea boundary. Further point observations from Elsfleth (Hunte) and Farge (lower Weser) are used to force the *total discharge* boundaries.

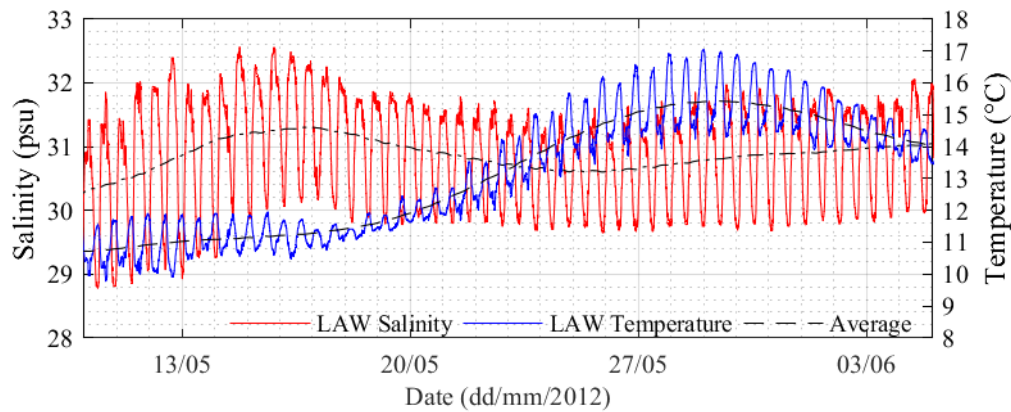


Figure 3.12: Salinity and Temperature boundary condition for the North Sea boundary obtained from measurements taken at the Leuchtturm Alte Weser at  $-5.5$  m above MSL (WSV, 2018a).

The diurnal influence of the tides is clearly visible, characterized by the regular fluctuations of the values. Furthermore, the salinity shows that the estuarine influence of the fresh water discharge is still present nearly 60 km from the estuary mouth. The computational domain of the WAVE model extends further into the North Sea (see figure 3.11) and ends inside the Weser estuary near Bremerhaven. This grid layout saves calculation resources, as the lower Weser is not incorporated, where wind waves would be comparatively small and are of lesser interest for the storm surge impact research conducted within this study. Furthermore, the extension of the seaward boundary allows for incorporating wave measurements of the wave buoy Elbe operated by the BSH at  $53^{\circ}59'25''\text{N}$   $08^{\circ}06'30''\text{E}$  at a water depth of 25 m. These observations are used to force the WAVE model with time series' of measured wave heights, periods and directions.

Atmospheric boundary conditions comprise near surface wind speed  $u_{10}$   $v_{10}$  (m/s) and mean sea level pressure MSLP (hPa). These physical quantities are applied to the free model surface using the maritime reanalysis dataset coastDat2 (see section 3.3), which are available for the North Sea at hourly intervals on a regular  $0.22^{\circ}$  spaced grid (Geyer and Rockel, 2013; Weisse et al., 2014b). Exemplary data for the European Windsorm Xaver from 2013 is given in figure 3.8.

### 3.5.2 Computational sediment inventory

Coastal morphology describes the physical shape and structural composition of the sea bed, tidal flats and foreshore (van Rijn, 1993; Bosboom and Stive, 2015). Morphological changes are defined as morphodynamics, themselves most often described as the *"mutual adjustment of fluid dynamics and topography involving sediment transport"* (Wright and Thom, 1977). However, this description omits the dominant role of the dynamic boundary conditions driving morphological changes and may lead to the false assumption of a homogeneous system striving towards a stable equilibrium. A more general definition defines morphodynamics as the *"dynamic behaviour of alluvial boundaries"* (de Vriend, 1991). Here the dynamic behaviour is the result of a bi-directional feedback between hydrodynamically driven sediment transport and resulting morphological changes of the bathymetry forced either by stationary or time-variant boundary conditions.

Morphodynamic simulations require a representation of sedimentological characteristics such as grain size distribution, available sediment mass and spatial distribution within the computational domain. On the one hand the climate change driven surge in coastal research (see section 2) spawns research projects investigating coastal seas and oceans alike amassing field data of ever increasing detail and resolution. On the other hand, numerical modelling of complex morphodynamic processes such as the initiation of motion, entrainment, transport and settling of sediment to name a few, is computationally costly and high degrees of detail rather obstruct efficient simulations as they tend to outpace computational capacities.

Input reduction is a consequence to assimilate as much data as possible into numerical investigations (van Rijn et al., 2013). However, depending on the application input reduction can significantly impact results. Walstra et al. (2013) for example show for long-term simulations that results are very sensitive to input reduction.

Given the transient nature of coastal storm events investigated within this study, significant input reduction of active boundary conditions (water levels, wind and pressure) is not necessary as simulated time spans are relatively short. Therefore the morphodynamic simulations are run in real-time and no additional morphological acceleration factor (MorFac) is used.

Two main types of morphodynamic simulations are discernible; (i) supply limited approaches, which prescribe observed sediment concentrations along the open numerical model boundaries and are operated on longer time scales to establish sediment distribution patterns within the domain and (ii) erosion limited approaches (this study), which implement sea floor sediments and require a detailed spatial database. The latter are ideal for short simulation spans and episodic impact research but require careful representation of the sea floor sediment inventory.

Sea bed surface sediment samples are available from a comprehensive survey recently conducted (Valerius et al., 2015). The project data base yields 520858 sample points within the computational FLOW/MOR domain and differentiates 12 different sediment fractions per point. Mean sea floor surface grain size distribution for the coastal zone is shown in figure 3.13.

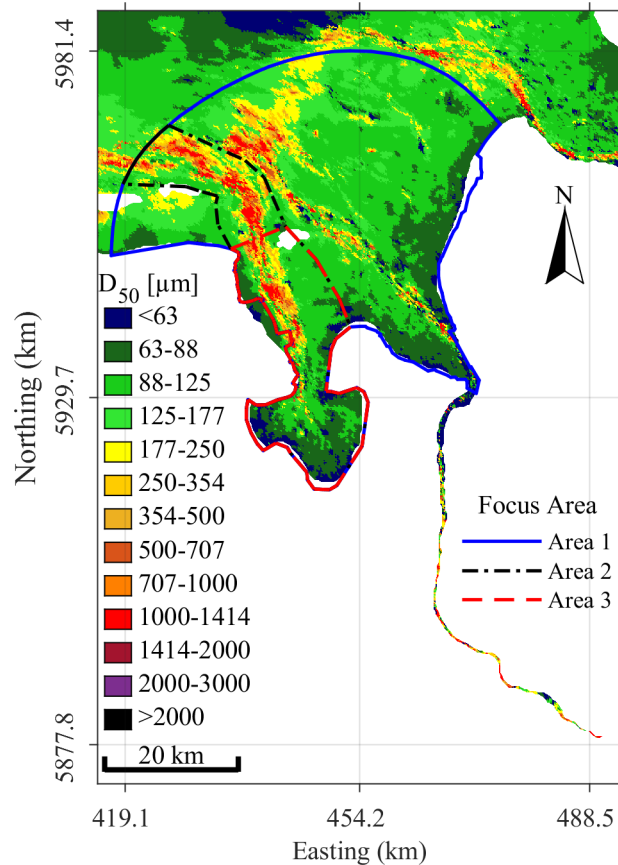


Figure 3.13: Sediment data for the Model domain based on AufMod data (Valerius et al., 2015) as well as different focus areas for subsequent sediment fraction re-classification schemes.

Implementing 12 individual sediment fractions would result in excessively large computational costs, therefore the available sediment data is reclassified into five representative fractions. Similar to the approach in (Herrling et al., 2017) weighted sample medians are used. Beyond that, different focus areas are defined for reclassifying sediments present within each polygon (see figure 3.13). Area 1 comprises the complete model domain, whilst area 2 encompasses mainly the Jade tidal system and area 3 concentrates on the Inner Jade and the Jade Bay. Resulting median grain size classes for the focus areas 1 - 3 are

given in table 3.5.1. This is done due to the different sedimentological characteristics present within Weser and (inner) Jade. The Weser is mainly characterized by fine and medium sand with (88 to 177 $\mu\text{m}$ ), while the Jade sea floor shows large areas dominated by medium sand (250 to 1414 $\mu\text{m}$ ). The sample distribution within the focus area one contains a less homogeneous sediment inventory (figure 3.14 lower panels) compared to the sample set for the whole German Bight (figure 3.14 upper panels) which accounts for the hydrodynamic grain size sorting.

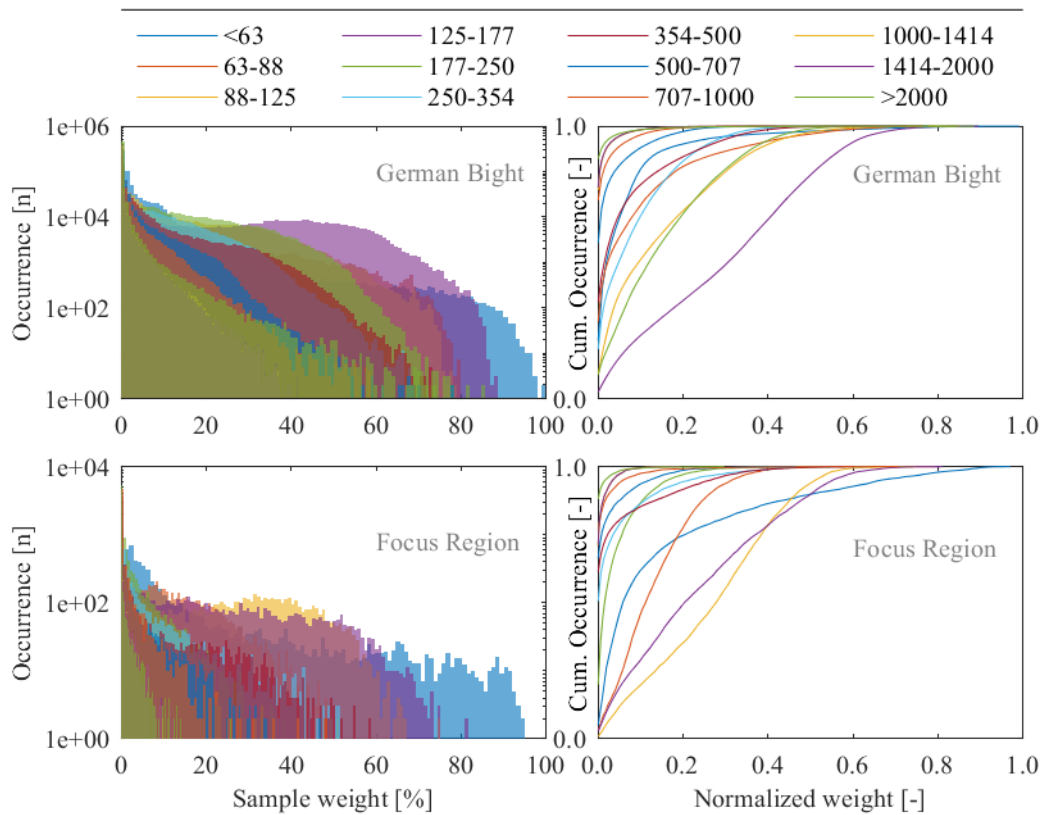


Figure 3.14: Sediment sample distributions in the German Bight (top panels) and focus area one (bottom panels).

Distributions for focus areas two and three are given in appendix A.3. The available 12 fractions are reclassified into four with the aim to preserve the representative distribution of medium and fine as well as coarse sand fractions throughout the Jade bathymetry. A fifth, cohesive fraction, is added in order to capture mud related processes dominant within the Jade Bight as well as the Hohe Weg between Jade and Weser (Götschenberg

and Kahlfeld, 2008). Reclassified fractions have weighted median grain sizes, which represent the dominant sedimentological character of the focus region. An overview of reclassified fraction diameters is given in table 3.5.1 .

Table 3.5.1: Reclassified sediment fractions for three defined focus area layouts as well as the whole data sample. Fraction grain size diameters are based on weighted medians of the summarized fractions.

Domain	Fraction I <sup>1,2</sup> D <sub>50</sub> ( $\mu\text{m}$ )	Fraction II <sup>1</sup> D <sub>50</sub> ( $\mu\text{m}$ )	Fraction III <sup>1</sup> D <sub>50</sub> ( $\mu\text{m}$ )	Fraction IV <sup>1</sup> D <sub>50</sub> ( $\mu\text{m}$ )	Fraction V <sup>3</sup> c <sub>dry</sub> (kg/m <sup>3</sup> )
German Bight	72.1	136	214	411	380
Focus Area 1	93.5	137	192	506	380
Focus Area 2	99.0	139	201	604	380
Focus Area 3	97.0	143	208	502	380

<sup>1</sup> non-cohesive fraction

<sup>2</sup> lower limit for coupled Delft3D FLOW/WAVE is 95 $\mu\text{m}$

<sup>3</sup> cohesive fraction ( $D_{50} \leq 63\mu\text{m}$ ) is represented by dry bulk density in Delft3D

Simulations conducted covering April 2012 using the three different reclassification patterns shown in figure 3.13 and described in table 3.5.1 yield sedimentation and erosion signals given in figure 3.15. These domain responses are obtained from combined wave-current forcing using the time step related volume changes per grid cell as well as the corresponding grid cell surface area. Mass is calculated using the specific density  $\rho_s$  of quartz sand 2650 kgm<sup>-3</sup> and a porosity of  $\Phi=0.3$ .

### 3.6 Base model configuration

A model setup is conceived using the aforementioned layout described in section 3.5 for conducting calibration and validation runs prior to investigating the storm research scenarios described in section 3.2. The research conducted within this study is based on the Delft3D open source version 6.01.12.4440 compiled on Ubuntu Linux 16.04 LTS using open source GNU Fortran and C++ compilers as well as Windows 10 using Microsoft Visual Studio 2015 in conjunction with Intel Fortran XE compilers . The source code operates on 64bit and was parallelized using MPICH2 libraries.

#### 3.6.1 Initial sediment distribution and transport

Given the extensive data base of sea floor surface samples for the German Bight, a reclassification scheme was derived yielding the Focus Area 1 as best suited for representing

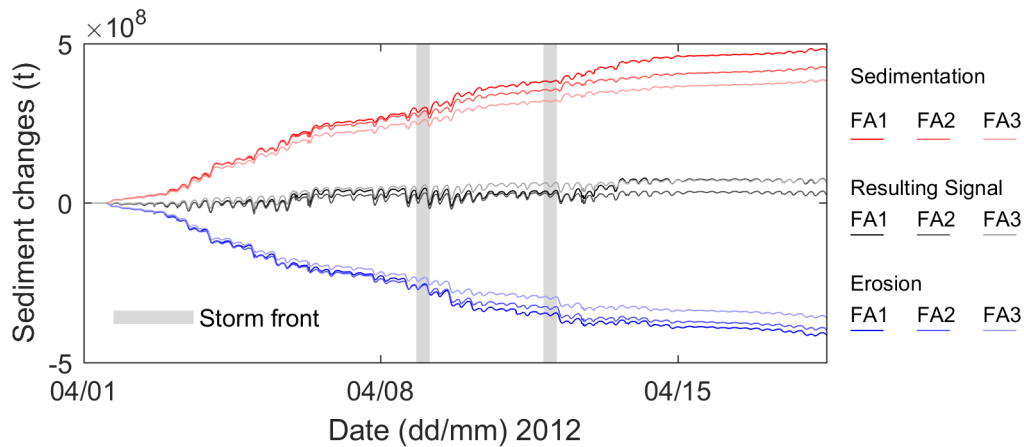


Figure 3.15: Morphologic domain response dependant on reclassification pattern for a simulation period of 21 days excluding the previous spin up period of 7 days, where the model converges towards realistic conditions, resulting in a total of 28 days runtime.

the sediment inventory of the Jade, while conserving the fine and medium sand fractions present on vast areas within the outer Weser.

Delft3D offers different options to prescribe sediments for morphodynamic simulations, sediments can be implemented as homogeneous single bed layer, which may consist of a single or multiple sediment fraction(s). As second option, a sequentially layered bed with different fractions, which may be mixed per layer, offers more flexibility in reproducing the spatially varying sediment distribution. Within this study the second option is chosen. The sea floor was vertically subdivided into 10 layers each one meter thick. Reclassified sediments are written to the topmost sea floor layer interacting with the hydrodynamic flow field using their respective mass fractions per sample point. The information is interpolated onto the computational FLOW/MOR grid. Following field data information (Valerius et al., 2015), the lower layers were filled with a homogeneous mixture of the four non-cohesive fractions to equal parts to serve as additional material source in case the covering toplayer is completely eroded in any scenario. This was done using MATLAB<sup>11</sup>, which was used for pre- and post-processing using routines written by the author, if not indicated differently.

Sediment transport in Delft3D is divided into bed-load (non-cohesive) and suspended load transport (non-cohesive & cohesive). Two dimensional suspended transport is calculated solving the depth averaged advection-diffusion equation (Deltares 2014a, pp. 323) using local flow velocities from the FLOW module. Feedback effects of suspended sediment

<sup>11</sup>R2017a (9.2.0.556344) 64-bit (win) Liscence: 40523081



concentration on fluid density are taken into account as well using an empirical formula (UNESCO, 1981). Dispersive transport is calculated using one of four available turbulence closure models. This study uses the  $k-\epsilon$  turbulence closure model. Non-cohesive sediment transport within this study is based on the empirical transport formulations by van Rijn (1993), with 11 other options available (see Deltares 2014a, table 11.1, p. 347). The used formulations allow for individual transport components (current induced bed-load, wave induced bed-load and suspended load) to be calibrated and incorporate transport induced by wave effects. Wave induced transport effects are accounted for following suggestions of Walstra et al. (2001).

Bedload transport is adjusted for bed-slope effects (Deltares 2014a, pp. 344), given the coastal estuarine like character of the bathymetry ranging from supra- via inter- to sub-tidal areas including deep (navigational) channels and bordering the open North Sea at a depth of  $-30$  m subaqueous slope effects are important to consider especially when researching storm surge impacts, which erode tidal flats and relocate material from shallow to deeper water regions.

Cohesive sediment flux between the bed and the water body is calculated using the Partheniades-Krone formulations (Partheniades, 1965), with erosion and settling related parameters allowing for individual calibration.

### 3.6.2 Bed roughness coefficient

Areal information on sea surface sediment composition is readily available for the research region (Valerius et al., 2015), showing a dominant fine and medium sand character of the Jade and outer Weser (see figure 3.13). Near the mouth of the Weser estuary (fkm 50 to 60) fluid mud was found (Schrottke et al., 2006). Extensive tidal flats are to be found within the Jade Bight (Götschenberg and Kahlfeld, 2008; Akkermann et al., 2015). Finally, the lower and outer Weser as well as the inner and outer Jade are characterized by subaqueous dune fields (Kubicki and Bartholomä, 2011; Kubicki et al., 2017; WSV, 2018a). Bed roughness coefficients ( $C_d$ ) influence local hydrodynamics and allow parametric calibration by varying values.

For this study, depth and sediment dependant roughness values are chosen and prescribed as Manning values shown in figure 3.16. The distribution shown in figure 3.16 is the final setup which resulted from preliminary testing of various parameter ranges and distributions. For this study a tidal flats are represented by a  $C_d$  of  $1.9 \times 10^{-3}$  sand dominated beaches and channels as well as deeper North Sea regions to the north are characterized by values between  $2.1 \times 10^{-3}$  to  $2.6 \times 10^{-3}$ . Delft3D offers the possibility to parametrize macro roughness elements such as subaqueous dunes using a dune/ripple predictor; nevertheless, for this study areas with dunes were accounted for by increased

sediment related bed roughness values, due to the increased degree of complexity and further increased computational cost by incorporating bed form predictors.

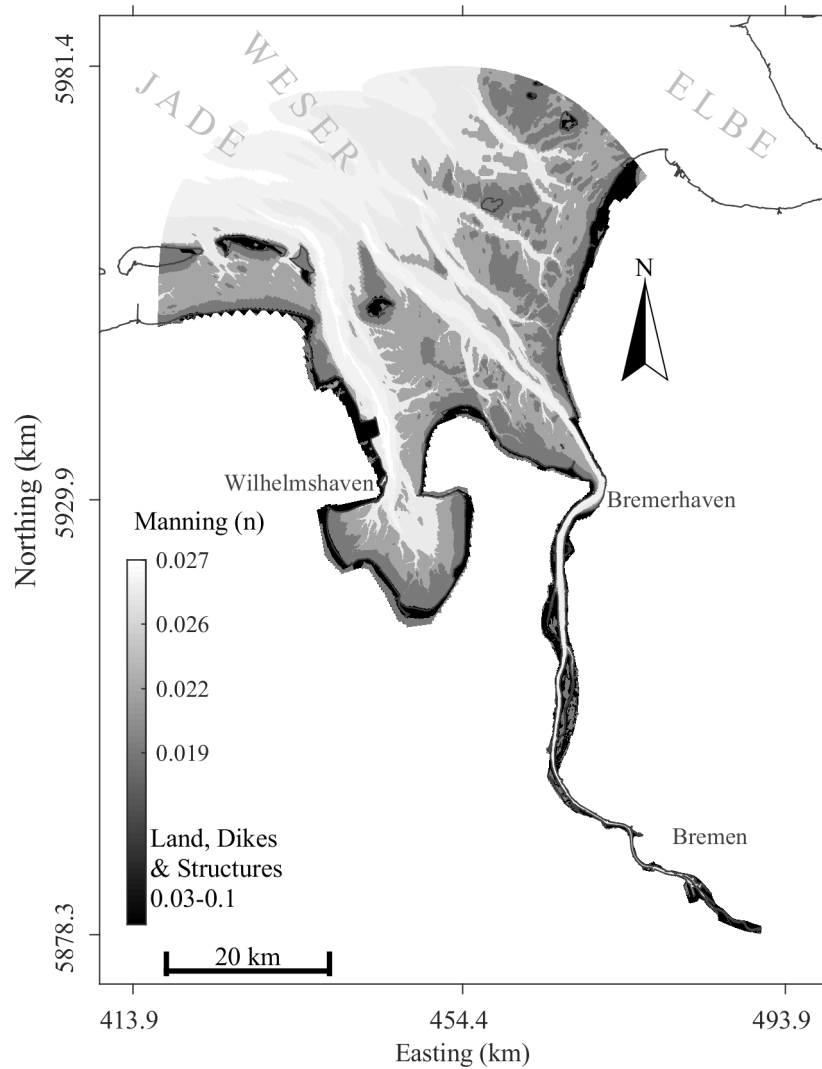


Figure 3.16: Bed roughness coefficients prescribed as Manning values with a spatial variance reflecting the naturally occurring sediment distribution patterns.

### 3.6.3 Chosen time steps

Delft3D FLOW is designed to allow for maximum freedom in terms of temporal discretization due to its high degree of stability, allowing for considering mainly accuracy arguments. Main accuracy argument to be regarded within this study is the spatial resolution (length scale) which depends on the CFL number:

$$CFL = \frac{\Delta t \sqrt{gH}}{\Delta x, \Delta y} \quad (3.6.1)$$

Here  $\delta t$  is the model time step in seconds,  $g$  is gravity,  $H$  resembles the water depth in meter and  $\Delta x$  &  $\Delta y$  are the characteristic (smallest) grid cell dimensions in meter (Deltares, 2014a). Delft3D allows for checking numerical grid layouts and interpolated bathymetries against selected time steps to test if the CFL criterion is met (Deltares, 2018). Furthermore, the time step has to be a multiple of the difference between the start and stop dates of any given simulation and is implemented in minutes. Different time steps, meeting the CFL specific criterion, were tested ranging from 0.01 min to 0.5 min. Finally, a time step of 0.03 min was identified as best suitable to resolve the physical processes. Delft3D MOR/SED operates on the numerical grid of the FLOW domain every half time step, solving source and sink terms (Deltares 2014a, p. 335) and on top of that allows for implementing a morphologic acceleration factor to speed up long term simulations spanning decades (Deltares 2014a, p.366).

Furthermore, the WAVE model is operated to incorporate wave related erosion and accretion effects on the tidal flats. The WAVE model may be coupled to Delft3D FLOW in offline (no feedback on hydrodynamics) or online (bi-directional time step-related feedback) mode (Deltares 2014a, p. 22). For this study, the FLOW and WAVE models are coupled online to account for effects of flow fields on waves (set-up, current refraction and enhanced bottom friction) as well as effects of coastal waves on hydrodynamics (enhanced turbulence and bed-shear stresses). The coupling is facilitated by a *communication-file*, containing simulation results of the last time step of the hydrodynamic and wave related computations. In parallel one communication file is created per computational domain.

A user defined update interval sets the time step at which computed WAVE related quantities are read by the FLOW model and vice versa. A value too large results in loss of valuable information and resolution regarding the temporal evolution of coastal processes and consequently impinges results. A time step too small produces a very large computational overhead, increasing computational costs and causing prolonged simulation times. For this study an update interval of 30 min was chosen based on the temporal evolution of tidal flow fields, while the WAVE model operates on 5 min time steps. Furthermore, atmospheric forcing variables (wind and pressure) are available at a 60 min resolution. Consequently, smaller coupling intervals would not use different atmospheric forcing but

solely be based on changes in hydrodynamics due to tidal forcing.

Temporal and spatial resolution of inputs and results as well time steps and coupling/update intervals are given in table A.2.1 in appendix A.2.

### 3.7 Calibration and Validation

The model calibration is performed for a period of 27 days, starts May 10<sup>th</sup> and ends on June 5<sup>th</sup>, 2012. The simulation is started seven days earlier (May 3<sup>rd</sup>) providing for sufficient spin up time. For this period observations of water levels, current velocities, wind and waves are available. Furthermore, consecutive navigational safety survey data for stretches with dunes of the Jade fairway are available from the 10<sup>th</sup> of May and June 5<sup>th</sup> for morphological assessments.

The model validation period is set from April 4<sup>th</sup> to May 10<sup>th</sup>. The time period is oriented at consecutive available fairway soundings to allow for sediment transport assessment and contains a medium frontal storm, allowing for testing if the calibrated model can sufficiently reproduce energetic system states with high dynamics.

Performance quality of the numerical models is assessed using observation data from various stations throughout the model domain. Measurements comprise tide gauge data, wind wave observations, current velocity measurements as well as bathymetric survey data. Figure 3.17 gives an overview over the available observation locations.

Performance quality of the hydrodynamic numerical model is assessed analyzing tidal water levels comparing them to observations of tide gauges throughout the domain. Performance is assessed based on root mean square error (RMSE) and absolute error in water level, as well as temporal peak shift and water levels for the calibration and validation periods. Finally, partial tidal constituents are investigated employing the `t_tide` toolbox (Pawlowicz et al., 2002). Current velocities observed at six permanent stations along the inner Jade fairway are used to compare simulated velocities for flood and ebb stream respectively as well as average duration. Wind speed and direction based on CoastDat2 data are compared to observational data collected at three stations within the domain located at Leuchtturm Alte Weser (LAW), Bremerhaven (BHV) and the Bulk Terminal Wilhelmshaven (BTW). Sea-state development is observed and compared at the station Leuchtturm Alte Weser, which features a wave gauge. Significant wave height and corresponding periods can be readily compared after extraction from the WAVE results. The morphodynamic performance of the model is assessed using navigational safety soundings of the Jade fairway along dune covered stretches. Based on survey data of consecutive dates, erosion and deposition volumes are calculated within evaluation polygons and compared to simulated bathymetric changes within the polygons. The calibration and validation periods were chosen based on absence of maintenance works, which could

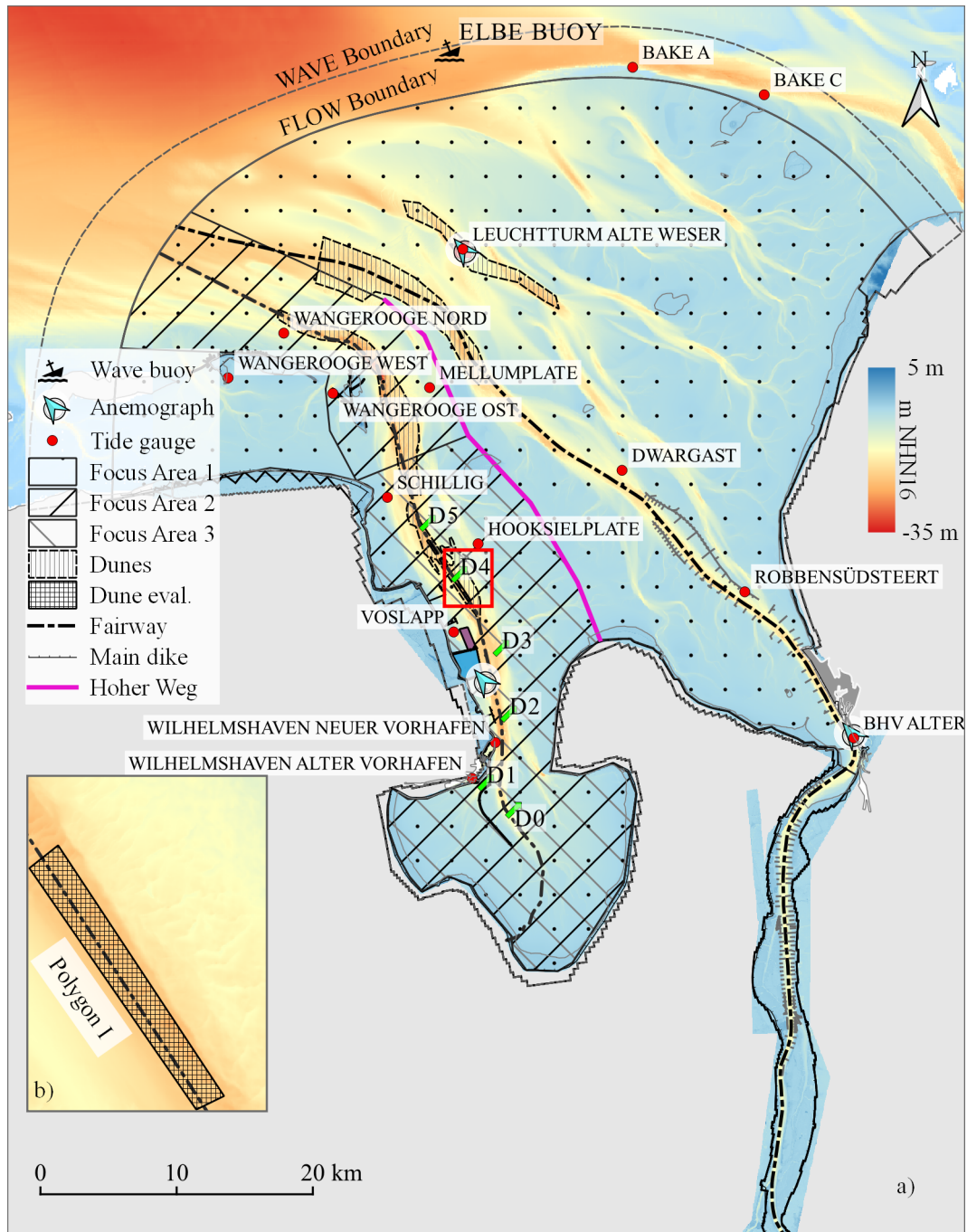


Figure 3.17: Observation data network for the Jade and outer Weser estuary comprising tidal gauges, wave measurements and anemographs. Areas covered with subaqueous dunes are indicated as well as hydraulic structures and the main dike line.

influence sediment budgets and make a morphodynamic calibration unfeasible without incorporating detailed information on local dredging and dumping processes.

### 3.7.1 Water Levels

Tidal water level comparisons for the validation period are given in figure 3.18 at tide gauge stations LAW near the seaward boundary and Wilhelmshaven at the landward side of the Jade Bight. Observations feature a temporal resolution of 1 min, while model results are stored every 30 min. For a subsequent tidal analysis, the observation data is processed using a moving average filter with a sliding window of 10 min to smooth instrument noise. The simulation results are interpolated onto a 10 min interval as well, using a spline function for a subsequent analysis. The processed time series' are then compared filtering high and low water events for both time series calculating temporal shifts and amplitude deviations.

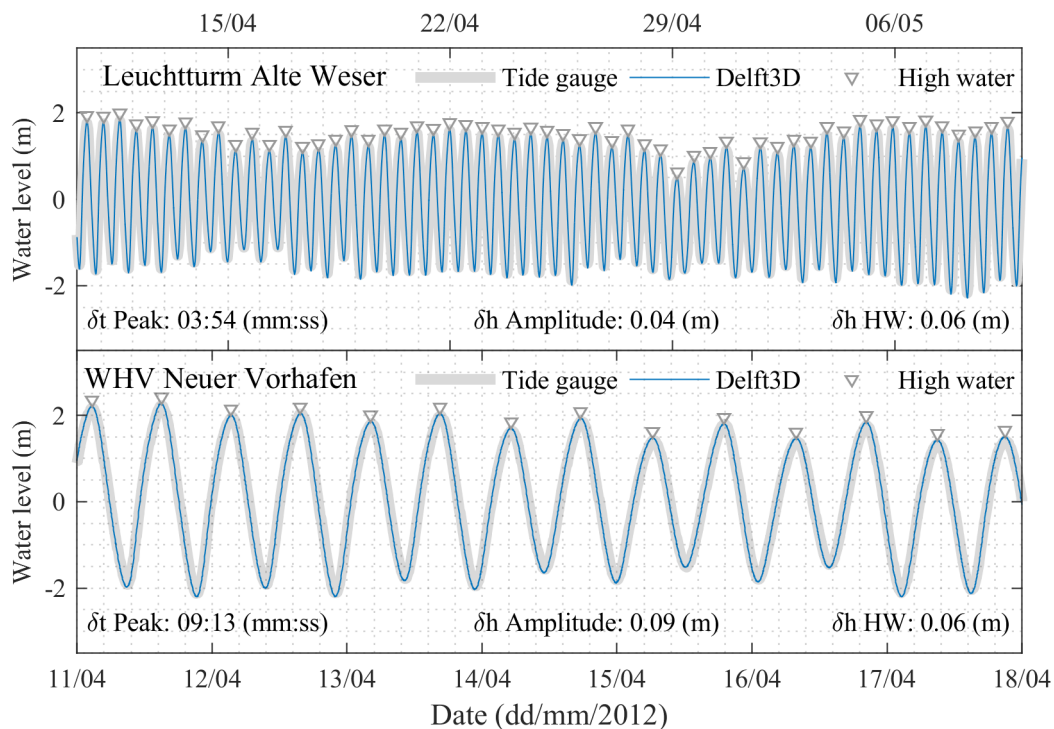


Figure 3.18: Observation and Simulation values for water levels at the gauges Leuchtturm Alte Weser (LAW) and Wilhelmshaven Neuer Vorhafen (WHV NV).

Overall model results are well in agreement with observed water levels as well as the tidal signal. Running a stretch of 41 km between the two stations the tidal wave experiences a

phase lag addition of 5:26 (mm:ss) within the model. Mean water level deviation at both stations is  $\leq 0.1$  m with max peak differences of 0.06 m at both stations. Values for the calibration and validation period for all available tide gauges are compiled in table 3.7.1. Values for the Jade show an average temporal peak shift of 06:53 (mm:ss) for calibration period and 06:52 (mm:ss) for the validation. The tide gauge Wangerooge West (WAW) shows irregular deviations, this can be attributed to the location of the tide gauge within a marina on the western side of the island of Wangerooge, which is not sufficiently resolved within the storm surge model.

Table 3.7.1: Delft3D Hydrodynamic calibration & validation coefficients for tide gauges along the Jade and outer Weser fairways.

	Tide gauge		Calibration				Validation				
	No.	Station	fkm (km)	$\delta t_{\text{peak}}$ (mm:ss)	$\delta h$ (m)	$\delta P$ (m)	RMSE (m)	$\delta t_{\text{peak}}$ (mm:ss)	$\delta h$ (m)	$\delta P$ (m)	RMSE (m)
Jade	1	WAN	41.0	05:14	0.07	0.13	0.091	05:57	0.07	0.12	0.088
	2	WAW	43.2	08:01	0.52	0.02	0.785	08:48	0.56	0.03	0.823
	3	WAO	35.0	04:10	0.06	0.06	0.083	05:41	0.05	0.05	0.089
	4	MEP	31.1	06:18	0.06	0.11	0.088	07:00	0.06	0.09	0.098
	5	SIG	24.1	05:35	0.07	0.06	0.099	05:08	0.07	0.07	0.114
	6	HOP	18.1	05:55	0.08	0.09	0.119	05:20	0.09	0.11	0.137
	7	VOP	13.4	06:10	0.07	0.04	0.115	05:32	0.08	0.05	0.137
	8	WHV AV	4.0	09:30	0.07	0.08	0.131	09:39	0.08	0.06	0.156
	9	WHV NV	1.6	09:12	0.08	0.09	0.128	09:13	0.09	0.06	0.156
Weser	10	LAW	115.0	03:51	0.03	0.05	0.065	04:07	0.04	0.05	0.069
	11	DWA	92.7	24:31	0.10	0.10	0.142	24:18	0.09	0.08	0.138
	12	RSS	79.9	24:40	0.10	0.90	0.131	24:31	0.08	0.06	0.141
	13	BHV	66.5	25:42	0.10	0.03	0.166	23:08	0.08	0.02	0.161

Values within the Outer Weser estuary show larger temporal deviations, ranging around 24:57 (mm:ss), with water level deviations of the same magnitude as for the Jade Bight. The increased temporal lag of the tidal wave arises due to the location of the seaward boundary, which is oriented along M2 phase lines and calibrated for the focus region of the Jade Bight. Mean amplitude deviations for the Jade amount to 0.07 m if the tide gauge of WAW is omitted and 0.09 m for the Outer Weser. The model reproduces the water levels with comparable accuracy for both the calibration and validation phase.

### 3.7.2 Tidal characteristics

Harmonic analysis of simulated and observed time series at tide gauge stations is obtained using the MatLab t-tide toolbox developed by Pawlowicz et al. (2002). Any simulated or observed tidal water level time series  $\eta$  can be approximated by means of super-

positioning harmonic constituents:

$$\eta(t) = \sum_{c=1}^{n_c} c_{amp} \cdot \cos(\omega_c t + \phi_c) \quad (3.7.1)$$

where  $t$  denotes the time step,  $c$  the tidal constituent,  $n_c$  the number of constituents used,  $c_{amp}$  (m) and  $\omega_c$  (min) the amplitude and frequency respectively and the constituents phase  $\phi_c$  (deg). For the present study, constituents with an amplitude  $\geq 0.05$  m within the domain are selected and compared between tidal gauge stations and simulated time series for the calibration and validation period. Exemplary results for the tide gauge station Wilhelmshaven Neuer Vorhafen are presented in figure 3.19 and show that the model reproduces the main tidal constituents with sufficient accuracy.

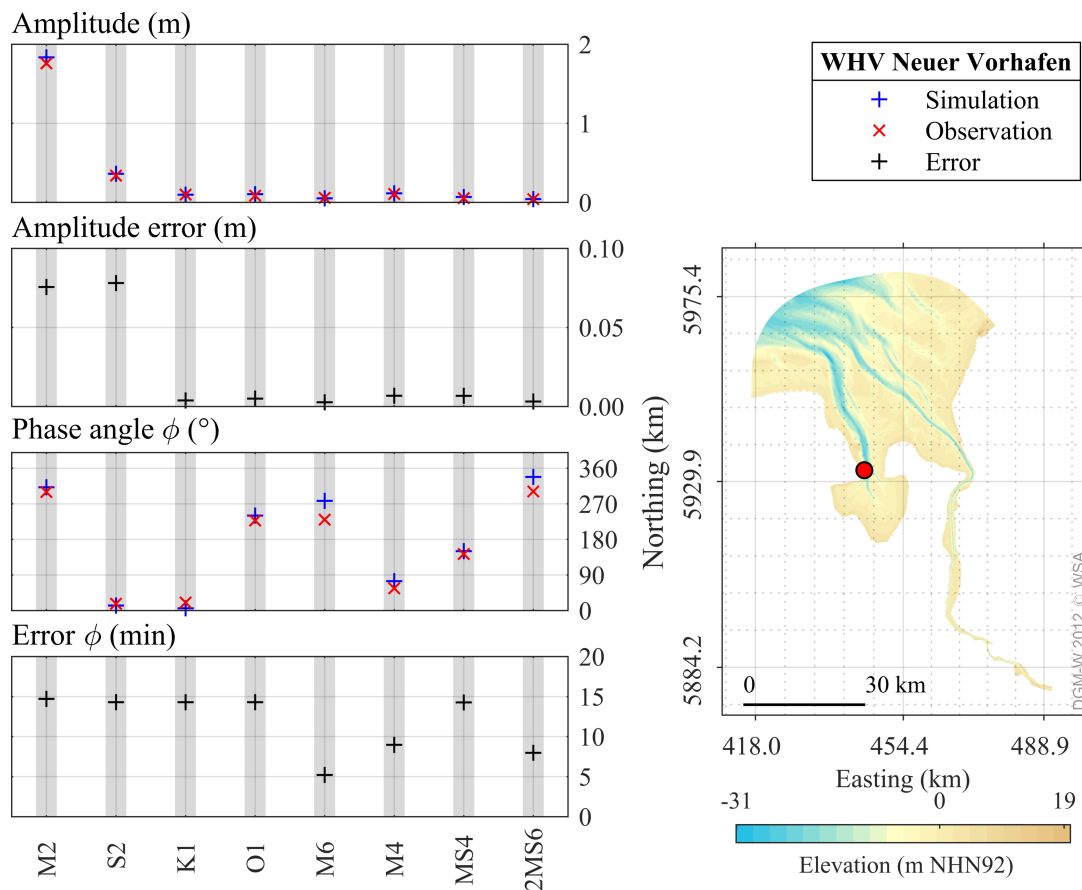


Figure 3.19: Simulated partial tidal constituents and model quality parameters compared to observed water levels using t-tide.

Due to the experimental setup with simulated real-time periods of 7 to 14 days, a har-



monic analysis renders unfeasible due to insufficient time series length. Therefore, the harmonic analysis is carried out for the calibration and validation phases only in order to verify that the model reproduces the tidal characteristics of the Jade-Weser estuary. Especially the tidal asymmetry, which arises from non-linear interactions of the tidal wave with the estuarine geometry (Friedrichs and Aubrey, 1988), is of interest for sediment transport (Postma, 1967; Friedrichs and Aubrey, 1994) and can be identified by tidal analysis calculating the relative sea surface distortion  $\gamma_{amp}$  for the dominant tidal constituent  $M_2$  and its higher harmonic the  $M_4$ . The relative sea surface distortion is calculated according to:

$$\gamma_{amp} = \frac{M_{4,amp}}{M_{2,amp}} \quad (3.7.2)$$

with,  $M_{N,amp}(m)$  the constituents amplitude. Furthermore, their relative surface phase  $\phi_{asy}(^\circ)$  is calculated according to:

$$\phi_{asy} = 2 \cdot \phi M_4 - \phi M_2 \quad (3.7.3)$$

where  $\phi M_N$  is the constituents respective phase. When  $\gamma_{amp}$  of  $\geq 0$  and the constituents corresponding  $\phi_{asy} \leq 180^\circ$ , the flood duration is shorter than the ebb duration, signaling a flood dominated domain (Friedrichs and Aubrey, 1988).

Table 3.7.2: Delft3D Hydrodynamic calibration & validation coefficients for tide gauges along the Jade and outer Weser fairways.

	Tide gauge			Calibration				Validation			
	No.	Station	fkm (km)	$\gamma_{amp}$ (m)	$\phi_{asy}$ ( $^\circ$ )	sim (f/e)	obs (f/e)	$\gamma_{amp}$ (m)	$\phi_{asy}$ ( $^\circ$ )	sim (f/e)	obs (f/e)
Jade	1	WAN	41.0	0.04	112	f	f	111	0.05	f	f
	2	WAW	43.2	0.36	181	e	f	184	0.35	e	f
	3	WAO	35.0	0.04	62	f	f	62	0.03	f	f
	4	MEP	31.1	0.05	105	f	f	120	0.06	f	f
	5	SIG	24.1	0.05	132	f	f	133	0.06	f	f
	6	HOP	18.1	0.06	145	f	f	146	0.06	f	f
	7	VOP	13.4	0.06	147	f	f	148	0.06	f	f
	8	WHV AV	4.0	0.06	187	e	f	198	0.06	e	f
	9	WHV NV	1.6	0.07	164	f	f	163	0.06	f	f
Weser	10	LAW	115.0	0.05	105	f	f	105	0.05	f	f
	11	DWA	92.7	0.06	88	f	f	88	0.05	f	f
	12	RSS	79.9	0.07	72	f	f	64	0.03	f	f
	13	BHV	66.5	0.08	56	f	f	56	0.09	f	f

Simulated values indicate a flood dominated Jade as well as a flood dominated Outer Weser, which are both in accordance with observations, as listed in table 3.7.2 or outlined in (Akkermann et al., 2015; Göttschenberg and Kahlfeld, 2008). However, the tide gauge

station of Wilhelmshaven Alter Vorhafen indicates an ebb-dominated tide regime in the model, which is inconsistent with observations. This can be explained by the fact, that the tidal gauge is located within the inner harbor of Wilhelmshaven, separated from the tidal regime of the Jade. Therefore, the model reproduces the main tidal constituent as well as the tidal asymmetry with its higher harmonic, which is important for accurately representing tidal currents and induced sediment transport.

### 3.7.3 Current velocities

Current velocities are measured within the Jade Bight at six permanent locations lining the navigational channel around the ECTW as part of proceedings for the preservation of evidence for the hydraulic impact of the constructed port. Figure 3.20 a illustrates the tidal water level measured at the tide gauge Schillig, 2.45 km downstream the tidal channel from D5.

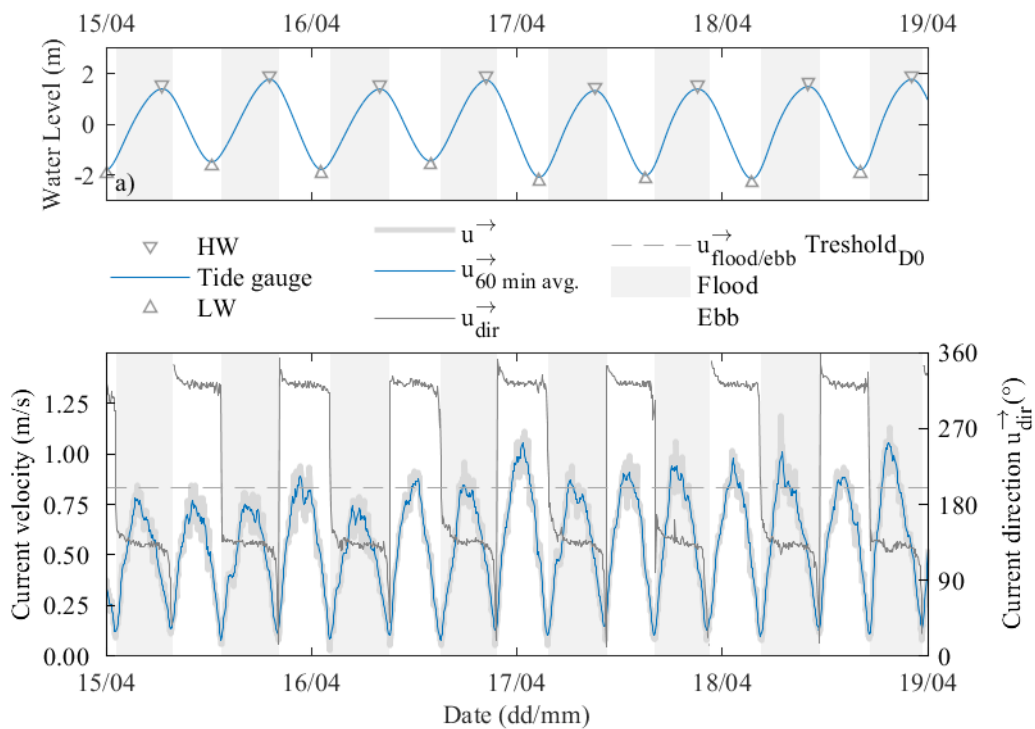


Figure 3.20: Tidal water levels and current velocities & directions observed at Schillig and D5 respectively within the Jade in 2012.

High and low waters are filtered and flood and ebb streams shaded gray and white respectively. Figure 3.20 b shows an exemplary excerpt of the tidally induced current velocities measured at the northernmost location D5 and corresponding current direction filtered

for ebb and flood, also shaded gray and white analogue to the corresponding tidal water level. Flood and ebb direction are identified based on histograms of directions and their respective bi-modal distributions in combination with slack water phases featuring  $\vec{u} \leq 0.01 \text{ m s}^{-1}$ . Corresponding simulated depth averaged current velocities at the position D5 and directions are given in figure 3.21.

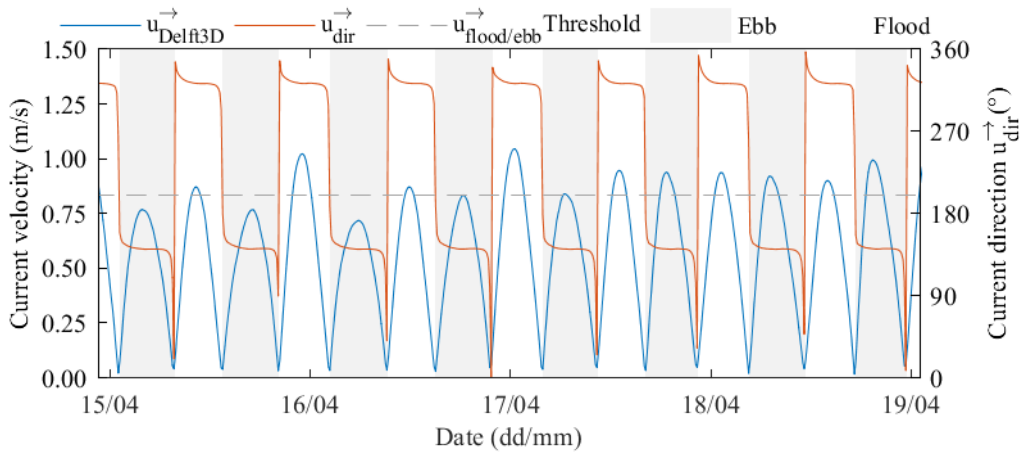


Figure 3.21: Tidal current velocities and directions simulated at D5.

Mean and max flood and ebb current velocities observed and simulated at all six measurement stations are shown in figure 3.22 a for the validation phase. Colored bars indicate the observed values, whilst the gray shaded bars represent the simulated values. The model reproduces the tidal mean and max current magnitudes well for flood, whilst the ebb stream magnitude is slightly under-predicted. Average flood and ebb duration at the six stations are visualized in figure 3.22 b for the validation phase.

Table 3.7.3 contains deviations in mean flood and ebb velocities, RMSE for the complete phase, respective standard deviation and mean durations for the calibration and validation phase. The model reproduces the flood and ebb current magnitudes with comparable accuracy for both calibration and validation phases. The flood magnitude on average is underestimated by  $0.09 \text{ m s}^{-1}$  and  $0.13 \text{ m s}^{-1}$  during calibration and validation respectively. The ebb current is underestimated on average by  $0.08 \text{ m s}^{-1}$  for the calibration and  $0.08 \text{ m s}^{-1}$  during the validation phase. Flood and ebb duration show largest deviations at the stations D1 and D2. Values for standard deviation and RMSE show a rather good reproduction of observed values by the numerical model for the two phases.

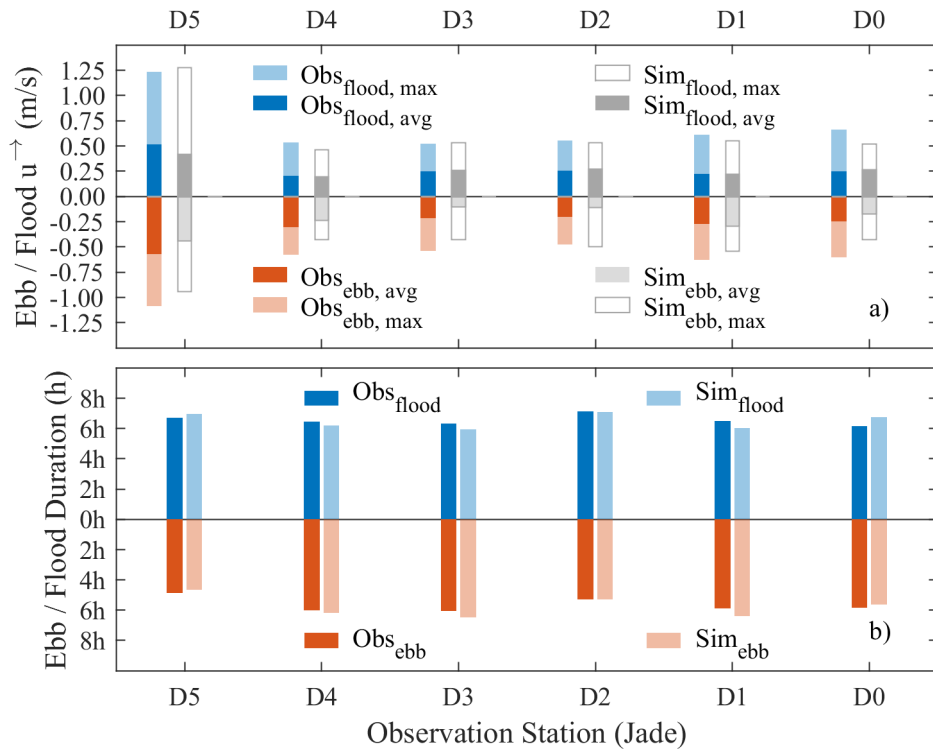


Figure 3.22: Simulated and observed ebb and flood current magnitudes and duration at the six observation stations, indicated on the map in figure 3.17, for the model validation period.

Table 3.7.3: Delft3D Hydrodynamic calibration & validation coefficients for tide gauges along the Jade and outer Weser fairways.

D	fkm (km)	Calibration						Validation					
		$\overline{\delta u_f}$ (m/s)	$\overline{\delta u_e}$ (m/s)	RMSE (m/s)	STDV (m/s)	$\delta D_f$ (min)	$\delta D_e$ (min)	$\overline{\delta u_f}$ (m/s)	$\overline{\delta u_e}$ (m/s)	RMSE (m/s)	STDV (m/s)	$\delta D_f$ (min)	$\delta D_e$ (min)
0	0.0	-0.06	0.10	0.13	0.25	+5	+5	-0.10	-0.13	0.12	0.25	+15	+12
1	2.5	0.03	-0.03	0.12	0.23	+18	+19	-0.07	-0.15	0.12	0.22	+15	+12
2	7.5	-0.28	-0.20	0.12	0.20	+24	+19	-0.29	-0.25	0.11	0.18	+25	+25
3	12.4	-0.12	-0.19	0.12	0.12	+6	+6	-0.15	-0.19	0.12	0.11	+3	+2
4	18.3	-0.07	-0.09	0.01	0.19	+16	+14	-0.06	-0.09	0.09	0.19	+7	+6
5	22.7	-0.09	-0.18	0.13	0.17	+22	+14	-0.11	-0.18	0.12	0.18	+23	+12

### 3.7.4 Atmospheric parameters

Wind speed and direction are implemented based on CoastDat2 data for the German Bight. Both parameters are measured at three locations in the domain, the LAW near the seaward boundary, the BTW in the Jade Bight and BHV in the Outer Weser. Figure 3.23 shows an exemplary excerpt of the validation phase for the location LAW.

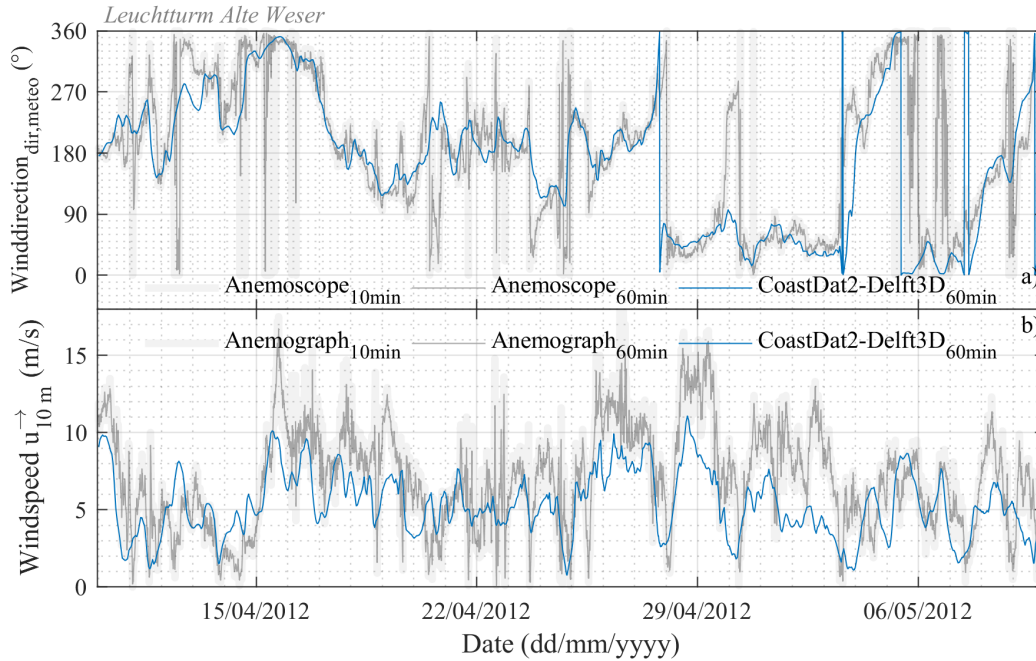


Figure 3.23: Observed and simulated wind direction (a) and speed (b) at LAW for the validation period.

Observed and simulated wind direction are given in figure 3.23 a and corresponding wind speed in Figure 3.23 b. Observations have a temporal resolution of 5 min, while the Coast-Dat2 data has a resolution of 60 min. For comparing the observations with simulated results and computing deviations the observations are processed with a moving average filter with a time window of 60 min. Computed values for RMSE, correlation and standard deviation are compiled in Table 3.7.4 for calibration and validation.

Furthermore, the *MSS* a dimensionless skill score based on the formulation by Murphy (1988); Murphy and Epstein (1989) is calculated according to:

$$MSS = 1 - \frac{\sum_{i=1}^n (qty_{sim} - qty_{obs})^2}{\sum_{i=1}^n (qty_{obs} - \overline{qty_{obs}})^2} \quad (3.7.4)$$

where  $n$  denotes the total number of time series values,  $i$  the respective value and  $qty_{obs/sim}$  the respective observed or simulated quantity. A  $MSS=1$  denotes perfect prediction of the observed values by the model, an  $MSS \geq 0$  indicates a good prediction of the mean of observed values by the model and a  $MSS \leq 0$  indicates an insufficient reproduction of observed quantities by any model.

Table 3.7.4: Delft3D wind calibration & validation parameters for three observation stations within the coastal zone.

parameter	unit	Calib.			Valid.		
		BTW	BHV	LAW	BTW	BHV	LAW
$\sigma_{dir}$	m/s	55.91	65.61	61.10	55.91	86.39	66.36
$\sigma_{u^-}$	degree	2.08	2.39	2.45	1.27	1.75	2.32
$RMSE_{dir}$	degree	73.13	65.66	61.18	56.27	87.22	68.11
$RMSE_{u^-}$	m/s	2.40	2.39	3.31	1.57	1.86	2.83
$R_{dir}^2$	degree	0.60	0.68	0.71	0.60	0.36	0.55
$R_{u^-}^2$	m/s	0.42	0.45	0.56	0.67	0.43	0.46
$MSS_{dir}$	–	0.74	0.69	0.60	0.76	0.70	0.46
$MSS_{u^-}$	–	0.58	0.63	0.67	0.73	0.19	0.64

Synoptic correlation of wind speed and direction show a quantitatively good correlation (see figure 3.23). Nevertheless, computed RMSE and  $R^2$  values compiled in table 3.7.4, show rather large deviations for the averaged observation values vs. the simulated parameters. The comparatively large deviations are traced back to the different temporal and spatial resolutions of the two data sets. Figure 3.23 a shows abrupt and large fluctuations in observed wind direction, while the CoastDat2 data shows a more continuous signal due to the discrete reanalysis model they are calculated with (Geyer and Rockel, 2013). Similarly the wind speed exhibits sudden wind speed changes due to observed wind gusts, which are not reproduced by the reanalysis data due to a grid resolution of  $0.22^\circ$  and a temporal output of 60 min. Consequently, these boundary conditions do not provide a wide range of optimization in terms of wind speed and directions, due to their origin. This will impact the coupled surface wave simulation results, which are directly affected by the overlaying wind and pressure fields.

### 3.7.5 Wave

Surface waves are measured at an offshore buoy called *Elbe* and near shore at the Leuchtturm Alte Weser. Consequently, wave parameters are obtained for both stations and the wave model forced at the sea boundary with the buoy data, whilst the near shore observations are used for model calibration and validation. Figure 3.24 shows the observed and

simulated significant wave height  $H_{1/3}$  and figure 3.25 corresponding peak wave periods  $T_p$ . Observation data features a temporal resolution of 1 min, whilst the numerical model results are available every 30 min. Data is processed with a moving average filter to obtain regular 60 min intervals for both time series and subsequently calculate quantitative performance parameters, which are listed in table 3.7.5.

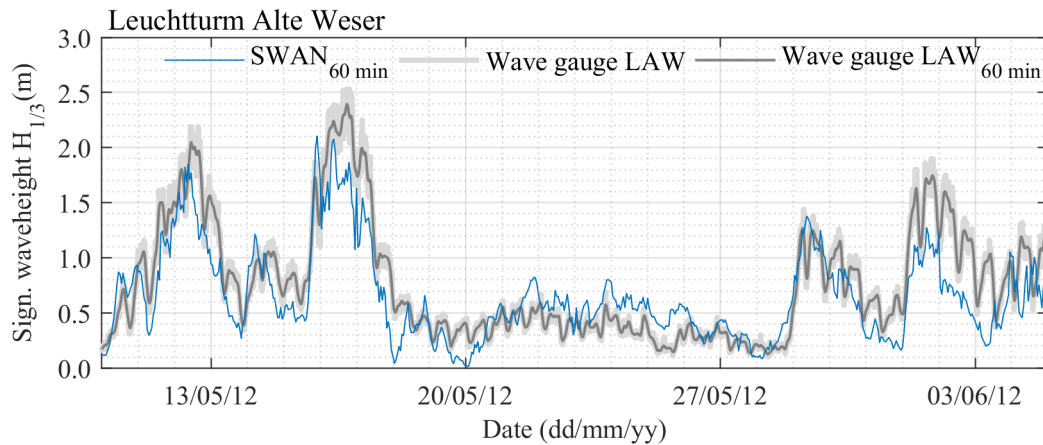


Figure 3.24: Observed and simulated significant wave height  $H_{1/3}$  at the station LAW.

Similar to the wind speed and direction results given in figure 3.23, observed wave characteristics also exhibit strong fluctuations, which are not captured due to the resolution of the applied atmospheric forcing data (Geyer and Rockel, 2013) as described in section 3.7.4.

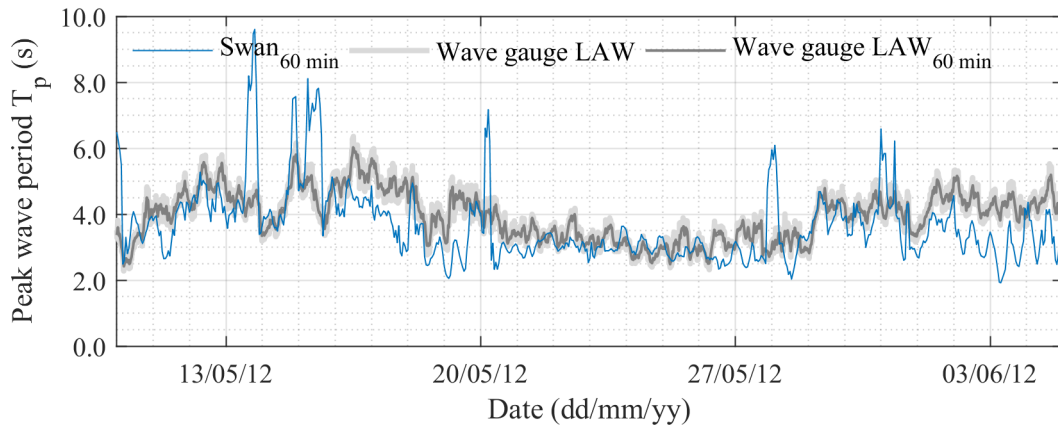


Figure 3.25: Observed and simulated peak wave period  $T_p$  at the station LAW.

Nevertheless, the qualitative wave height matches the observed values well, which is also

indicated by the obtained quantitative performance parameters in table 3.7.5. However, simulated peak wave periods given in figure 3.25 exhibits spontaneous fluctuations, which result in decreased performance scores compiled in table 3.7.5.

Table 3.7.5: Delft3D SWAN wave calibration & validation parameters for the observation station Leuchtturm Alte Weser.

quantity	Significant wave height			quantity	Peak wave period		
	unit	Calibration	Validation		unit	Calibration	Validation
$\bar{\delta}H_{1/3}$	(m)	0.11	0.20	$\bar{\delta}T_P$	(s)	0.31	1.20
$\sigma H_{1/3}$	(m)	0.29	0.19	$\sigma T_P$	(s)	1.02	1.51
RMSE $H_{1/3}$	(m)	0.31	0.28	RMSE $T_P$	(s)	1.06	1.93
MSSH $_{1/3}$	(-)	0.79	0.48	MSST $_P$	(-)	0.91	0.96

Possible influences arising from wave process related parameter settings, wave grid resolution, time step and coupling interval have been investigated extensively (not shown here) but no cause has been identified, leaving the bathymetry and the sea boundary orientation as last possibilities. The off-shore bathymetry is based on survey data from multiple years provided by the BSH (see section 3.5) and could therefore not be representative enough for the wave model to reproduce observed surface waves as they migrate from the deep water into the coastal zone and experience sea floor interaction. The sea boundary orientation could also result in wave-wave related interaction and redistribution of energy through Quadruplets and Triads (see table 2.3.4) in the domain and influence peak wave period. This was investigated reducing the directional spread of the wave boundary condition to  $1^\circ$  without significantly altering the simulated  $T_p$  at LAW.

### 3.7.6 Sediments

Morphologic calibration and validation of the numerical model renders rather difficult, as no consecutive survey exists for the whole domain since 2012, which forms the basis for the numerical model. Therefore, navigational safety survey data of the fairway are obtained from the local authorities from Wilhelmshaven for this purpose. These surveys exhibit a temporal resolution of about one month and a spatial resolution of  $2\text{ m} \times 2\text{ m}$  (Heinemann and Janßen, 2013). Volumetric changes between consecutive surveys are most pronounced along stretches covered by subaqueous dunes between fkm 30.0 to 34.5 and 16.3 to 21.0, the latter region is shown in figure 3.26.

Consequently, evaluation polygons are defined encompassing the dune areas and bathymetric changes computed between surveys. Figure 3.26 a shows the Jade area between fkm 16.3 to 21.0 with three defined evaluation polygons. Adjacent figures 3.26 b and c show the dune stretch in polygon I on the 10/04/2012 and 10/05/2012 respectively, mark-



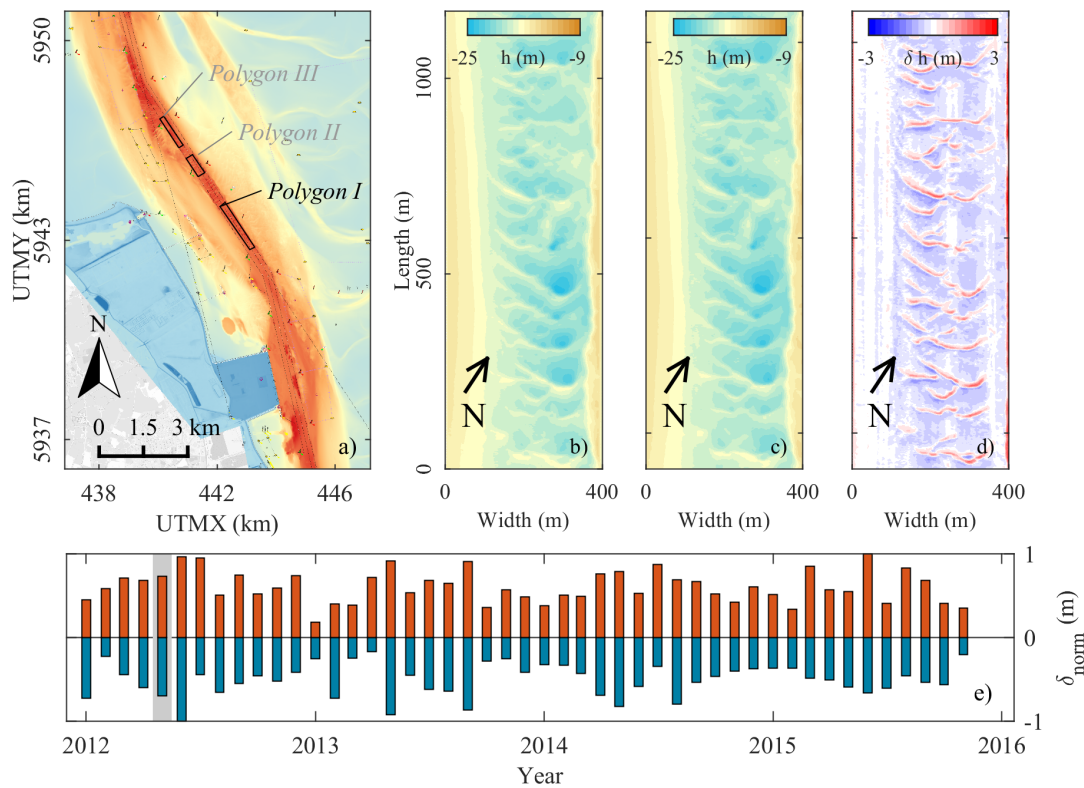


Figure 3.26: Morphodynamic signal analysis polygon I based on navigational safety surveys of dune covered stretches.

ing the beginning and end of the validation phase. Figures 3.26 d shows computed elevation differences, which are translated into normalized volume changes and displayed in figure 3.26 e for erosion and accretion with the validation period shaded gray. Analogue analysis were performed for the two other polygons in the area and another two polygons located in the Outer Jade. Normalized volume changes for the outermost polygon V are visualized in figure 3.27 and notably show that the European Windstorms Christian and Xaver in late 2013 induced the largest bed volume changes in a four year period closely followed by the winter period 2014/2015. Computed accretion and erosion volumes, for the survey data and the numerical model are compiled in table 3.7.6 together with absolute and relative volume differences per polygon.

Performance of the coupled morphodynamic model for the validation period shows an average volume deviation of 15 % for accretion and 16 % for erosion, with the largest differences occurring inside polygon I for accretion with  $-36\%$ , which can be attributed to the under-predicted tidal currents within this area (compare table 3.7.3 values for D2 and

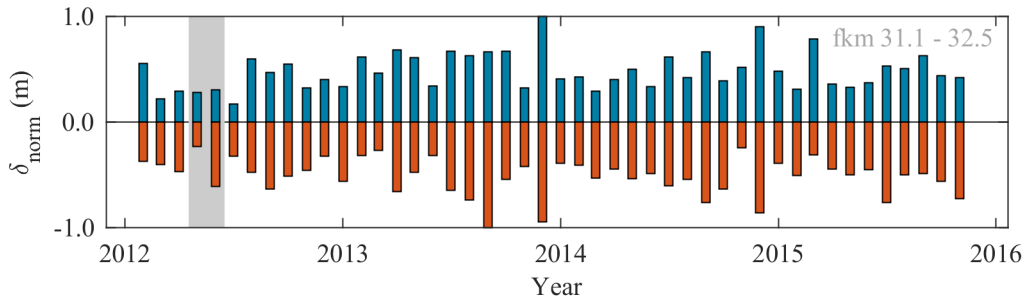


Figure 3.27: Morphodynamic signal analysis polygon V based on navigational safety surveys of dune covered stretches.

Table 3.7.6: Delft3D morphodynamic calibration & validation parameters for bed volume changes in five evaluation polygons.

			Inner Jade						Outer Jade			
			Polygon I		Polygon II		Polygon III		Polygon IV		Polygon V	
	qty.	unit	Calib.	Valid.	Calib.	Valid.	Calib.	Valid.	Calib.	Valid.	Calib.	Valid.
Accretion	obs.	m <sup>3</sup>	55700	74000	8300	23300	5100	22600	53500	127800	52200	15800
	sim.	m <sup>3</sup>	54400	47200	7500	24300	5000	18800	54500	151000	47700	15700
	$\delta_{m^3}$	m <sup>3</sup>	1350	-26800	800	1000	100	-3800	-1000	23700	4500	100
	$\delta_{\%}$	%	2	-36	10	4	2	-17	-2	18	9	1
Erosion	obs.	m <sup>3</sup>	65900	94200	15700	11000	16300	2700	34800	33800	34800	35000
	sim.	m <sup>3</sup>	30000	106600	18100	9700	-13500	2700	35300	22300	36400	27000
	$\delta_{L^3}$	m <sup>3</sup>	-35900	12400	400	-1300	-2800	0	500	-11500	1600	8000
	$\delta_{\%}$	%	-54	13	3	-12	-17	0	1	-34	5	-23

Note: Volumes are rounded to 100 m<sup>3</sup> precision for presentation

D3), which transport insufficient sediment volumes into the Jade Bight. The morphodynamic component of the numerical model represents the observed volume changes within the most active regions of the Jade Bight to a satisfactory degree of accuracy, comparable to values achieved in other morphodynamic studies (Dissanayake et al., 2012b,a; Herrling and Winter, 2015, 2017).

Geographic approaches such as the Brier Skill Score (BSS) (Sutherland et al., 2004; Murphy and Epstein, 1989) require a higher spatial resolution for analyzing the dune fields, which is not feasible for simulating such a large domain without compromising run times or a domain wide consecutive survey data set, which is not yet available. Furthermore, it is cautioned that the BSS was not developed for morphological applications specifically and does not capture detailed characteristics such as lateral displacements of morphologic features and is therefore not applicable within this approach (Dissanayake et al., 2012b; Roelvink et al., 2009).

**Summary chapter 3:**

Water Levels show small deviations in the range of  $\leq 0.1$  m for mean and RMSE and reach 0.06 m for high water levels for both calibration and validation. For the Outer Weser, model results exhibit a larger phase lag compared to the focus region of the Jade, which shows a mean phase lag of  $\leq 6$  min and reproduces dynamic states such as the frontal storm entailed in the validation period equally well.

Tidal Characteristics are analyzed, showing that the model reproduces the tidal characteristics of the flood dominated Jade Bight and the Outer Weser and captures the tidal asymmetry between M2 and M4, which is a main constituent for sediment transport.

Current velocities compared at the six permanent measurement locations show, that the incoming flood magnitude on average is underestimated by 0.1 m/s, whilst the ebb current at the positions is underestimated by 0.08 m/s. Maximum flood velocities are well reproduced, whilst maximum ebb currents are underestimated by 0.12 m/s on average. Flood and ebb durations compare well to observed values and show the largest deviations within the Inner Jade area, upstream of the transshipment complex with its critical infrastructure.

Atmospheric boundary conditions are given by the CoastDat2 data sets, which show differences compared to observations as a consequence of the spatial and temporal resolution, which cannot capture small scale wind gusts and frontal patterns. Synoptically, simulated wind speed and direction are in agreement with observed values. This is confirmed by the positive MSS values. Non covered small scale fluctuations impact the coupled wind wave simulations forced by the atmospheric conditions.

Waves values exhibit a degree of agreement comparable to the atmospheric conditions. Small scale and short term fluctuations are not reproduced by the model, as a consequence of the forcing conditions. MSS values computed show positive values and indicate a good prediction capability of the numerical model.

Morphodynamic simulation results compared for evaluation polygons along the Jade fairway show mean volume differences of 15% and 16% for erosion and sedimentation, respectively. Deviations are largest, within the area of the Inner Bight, in consequence of underestimated current magnitudes. Nevertheless, the Inner Bight is of secondary importance as the primary focus rests on the transshipment complex as well as the tidal flats and the deep navigational channel. Given these values, the numerical model is considered calibrated and validated for investigating the research questions within this study.



## 4 Results

Simulation results are evaluated at observation stations, a longitudinal section of the Jade fairway and along the tidal flats *Hoher Weg*, as well as areal depending on the individual coastal key driver. Impacts are classified into hydrodynamic impacts (sec. 4.1), wave related impacts (sec. 4.2) and morphological impacts considered with bed forming characteristics (sec. 4.3). Hydrodynamic impacts pertain to water levels, tidal current velocities as well as overall storm surge volume within the domain. Wave impacts are evaluated as changes in wave height and steepness under storm surge conditions at the position LAW and are inspected regarding changes in reach. Morphological impacts are evaluated for the whole domain regarding net changes and along the transshipment complex with its critical infrastructure for local impacts. Storm research scenarios are evaluated for the three impact classes - influences of coastal key drivers are unraveled permuting physical processes and their respective magnitudes according to the storm research scenarios defined in table 3.2.1.

### 4.1 Hydrodynamic impact

In a first step, mean tidal high and low water are extracted from the validation simulation for the Jade and Outer Weser (fig. 4.1a), revealing a total area of 2049.5 km<sup>2</sup> tidally

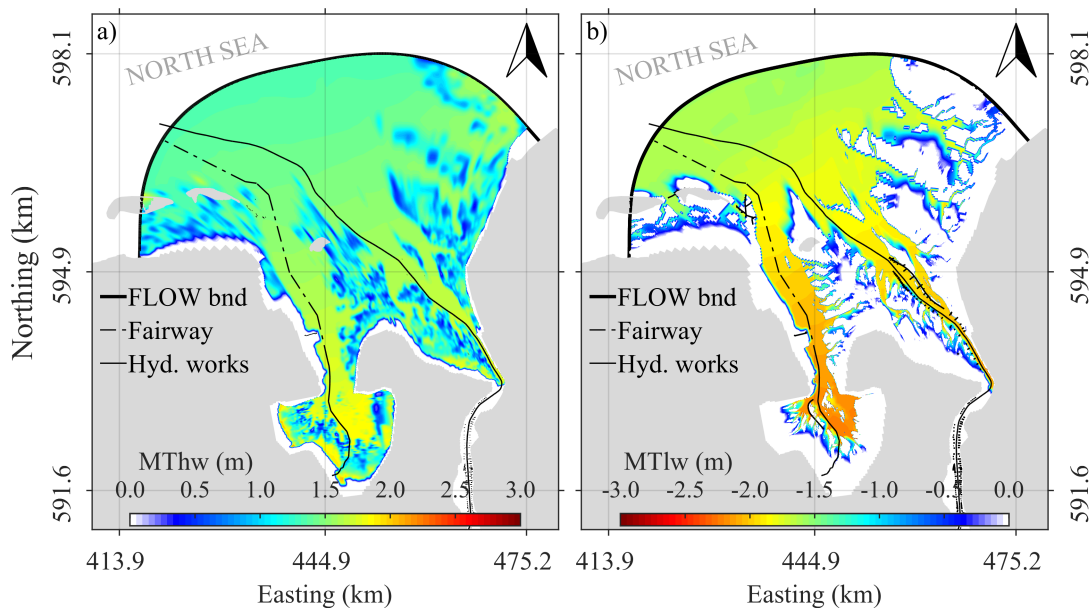


Figure 4.1: a) Mean tidal high and low water b) for the numeric domain of the Jade and the Outer Weser based on simulation results of a spring neap tide cycle.

inundated during high tide, which floods the domain to the toe of the delineating coastal dike. Mean tidal low water exposes 903.5 km<sup>2</sup> of inter-tidal area and inundates a sub-tidal area of 1146 km<sup>2</sup> (fig. 4.1b).

#### 4.1.1 Water levels

Introductory results constitute storm surge induced water levels, which are evaluated at the tidal gauging station Wilhelmshaven Neuer Vorhafen inside the Jade constituting a representative position within the focus region.

##### ▪ European Windstorm Christian

Model results for scenarios forced only with hydrodynamic/tidal boundary conditions across the three different RMSL levels derived in section 3.2 and given in table 3.2.1 are depicted in figure 4.2 a for European Windstorm Christian. Supplementary, the water level of the reference scenario is visualized with added RMSL values of 0.74 m (figure 4.2 b) and 1.5 m (figure 4.2 c) respectively.

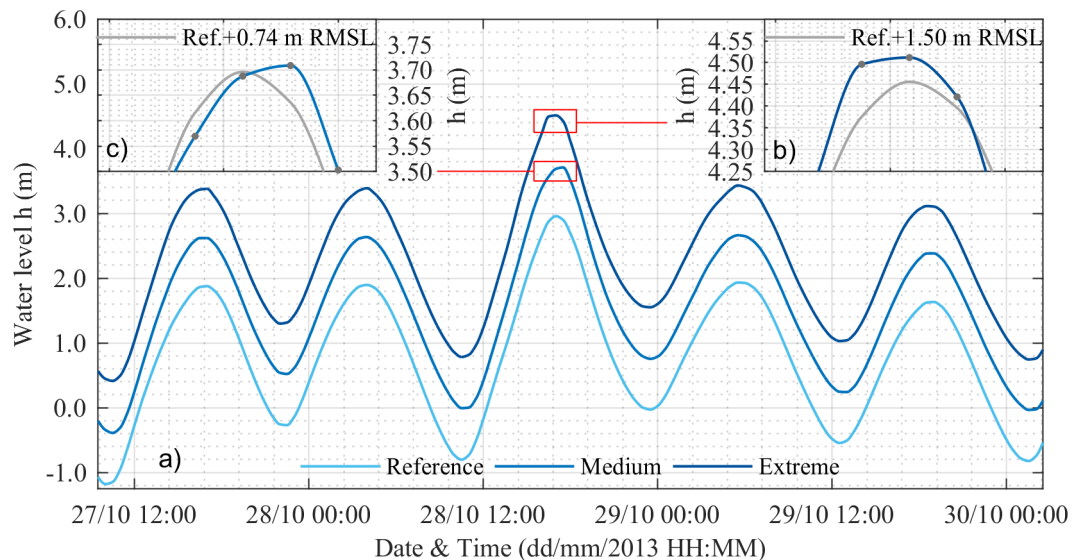


Figure 4.2: Evolution of storm surge water levels for Windstorm Christian at the tidal gauge station Wilhelmshaven Neuer Vorhafen for the three different RMSL scenario runs (a) reference (b) medium and (c) extreme scenario forcings with parameter settings given in table 3.2.1 under hydrodynamic/tidal forcing only.

Simulation results reveal an additionally elevated peak water level for the medium scenario of 2 cm due to 0.74 m RMSL alone (see figure 4.2 b). Furthermore, the extreme

scenario reveals a peak water level elevation of 6.0 cm (see figure 4.2 c). Referenced to the respective scenario RMSL, these represent an additional increase of 2.7 % and 4 %. However, under combined forcing of sea level pressure, wind and waves as well as discharge, the reference scenario shows an underestimation of the observed water level by 7 cm, whereas the medium scenario shows a reduced peak level of 3.59 m compared to 3.71 m under hydrodynamic forcing only, revealing a damping effect. The extreme scenario shows an increase for both, the hydrodynamic case as well as the compound event of 4 % and 2 % respectively. Computed values are compiled in table 4.1.1.

▪ European Windstorm Xaver

Similar to the results for Windstorm Christian, hydrodynamic forced simulations for the three RMSL levels as well as their compound simulations are investigated regarding their storm peak water levels observed at the tide gauge station Wilhelmshaven Neuer Vorhafen. Results are depicted in figure 4.3 and show, that the hydrodynamically forced simulations, as well as the compound simulation underestimate the observed peak water levels. Nevertheless, the simulations entail additional water level increases exceeding the linearly added RMSL values comparing the reference and medium runs as well as the medium and extreme runs.

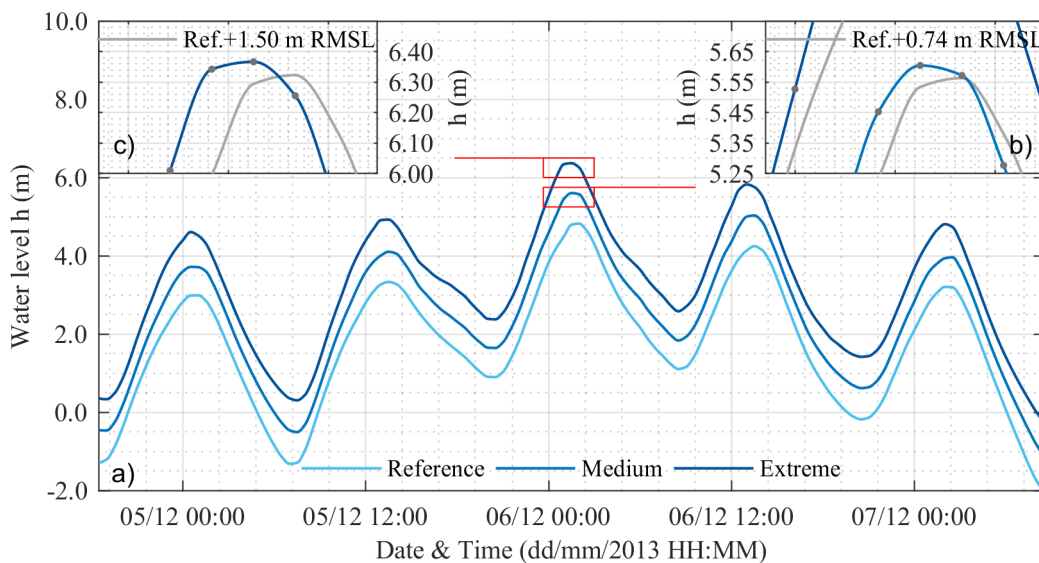


Figure 4.3: Evolution of storm surge water levels for Windstorm Xaver at the tidal gauge station Wilhelmshaven Neuer Vorhafen for the three different RMSL scenario runs (a) reference (b) medium and (c) extreme scenario forcings with parameter settings given in table 3.2.1 under hydrodynamic/tidal forcing only.

The hydrodynamic medium scenario reveals an additional 4 % increase (see figure 4.3 b), while the medium compound event shows an increase of 10.8 % with 8 cm water level increase due to metocean forcing. The extreme case simulations show added water levels of 3 cm and 9 cm (see figure 4.3 c). Values are compiled in table 4.1.1

Table 4.1.1: Surge levels for the New Outer Harbor Wilhelmshaven tide gauge for the three scenario levels of Christian and Xavier with tide forced simulations only and compound simulations.

Scenario	Christian		Xaver		
	Tide	Compound Event	Tide	Compound Event	
Observed	(m)	-	2.97	-	5.03
Reference	(m)	2.95	2.90	4.82	4.86
Medium	(m)	3.71	3.59	5.6	5.68
$\delta h_{R+RMSL}$	(cm)	+2	-5	+4	+8
$\delta h$	(%)	+2.7	-6.8	+5.4	+5.3
Extreme	(m)	4.51	4.43	6.35	6.45
$\delta h_{M+RMSL}$	(cm)	+6	+3	+3	+9
$\delta h$	(%)	+4	+2	+2	+6

Water level changes obtained for the two storm events under tide only forcing exhibit larger increases across the three scenario amplification levels for the westerly storm event compared to the northerly one. Furthermore, the westerly event shows a reduction in point water levels under combined metocean forcing, indicating non-linear internal friction and turbulences reducing the surge height. This stems from the low pressure system rotation, forcing water into the North Sea, drawing it out from the Jade Bight. For the northerly event however, the compound event with metocean forcing follows a north-south route, directly drawing a dome of surge water under the storm into the German Bight, elevating the tidal water levels. The resulting water levels given in table 4.1.1 reflect these two different storm mechanisms well between the tide only runs and the compound events. Furthermore, the surge water levels show a distinct phase shift (cf. figures 4.2b & 4.3b), induced through elevated water levels reducing the influence of bed roughness on the resulting current velocities, enabling the surge to travel into the Bight faster.

#### 4.1.2 Storm surge volume

Storm surge volume within the Jade and Outer Weser are investigated, calculating the simulated volume per grid cell per time step and summarizing these for every time step to arrive at surge volumes.



▪ European Windstorm Christian

Surge volumes computed are shown in figure 4.4 for the reference scenario of European Windstorm Christian. The signal shows a distinct storm response, with increasing surge volume peaking in the night of the October 28<sup>th</sup> with 3.12 km<sup>3</sup> until the storm system passes through the North Sea on the 28<sup>th</sup> of October, 2013, after which the overall volume begins to drop again. European Windstorm Christian features a cumulative surge volume of 297.85 km<sup>3</sup> between the evening high tide on the 27<sup>th</sup> and the evening high tide on the 29<sup>th</sup> based on tidal hydrodynamics only. The influence of metocean processes on the storm surge volume for the reference storm scenario of Christian is shown in figure 4.5 and amounts to a total of 36.5 km<sup>3</sup>. Influence of individual processes is given in table 4.1.2 in absolute volume and relative change related to the respective tidal reference run.

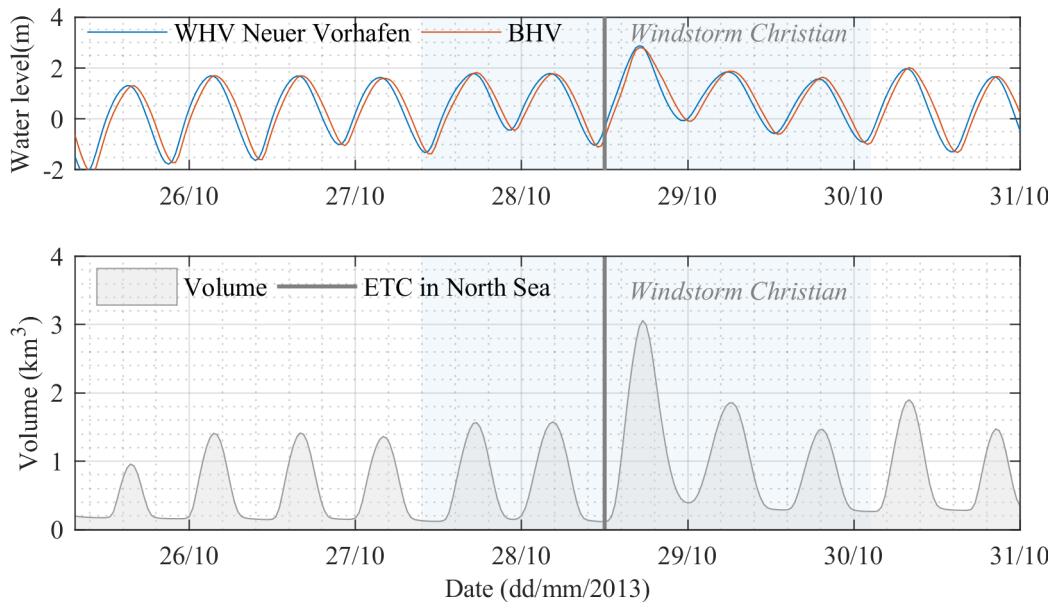


Figure 4.4: Simulated storm surge volume under European Windstorm Christian. Inter- and subtidal areas according to mean tidal high water and low water levels given in figure 4.1 includes metocean processes.

Simulation results show, that the surge volume varies, depending on simulated processes, by as much as  $-8.85\%$  compared to tidal forcing only. Atmospheric conditions reveal an additional reduction of the surge volume by  $-4.81\%$  due to southerly winds, whilst a tidal and wave forced simulation increases the overall surge volume by as much as  $3.72\%$  for the base case but shows diminishing influence with every scenario increase. The reduced wave effect can be explained by the increased water depth in the medium and extreme scenarios, where the overall SLR is larger and reduces the overall impact

of waves.. The Weser related inland discharge contributes an additional 1.43 % to the surge volume which scales through the scenarios and stays near constant compared to the overall surge volume. A coupled surface wave simulation with atmospheric forcing and inland discharge (compound event) reduces the surge volume by  $-8.85\%$  as a result of combined processes. The combination and interaction of atmospheric forcing and surface waves induces friction into the water body, resulting in internal turbulences reducing the landdirected surge input. A constructively altered bathymetry results in an additional surge volume of 1.95 % due to incisions along the Outer Weser, facilitating slightly higher current velocities due to increased depth. The tidally forced simulations show an increase of 87 % and 194.5 % compared to the reference case, revealing a large sensitivity towards RMSL for this event.

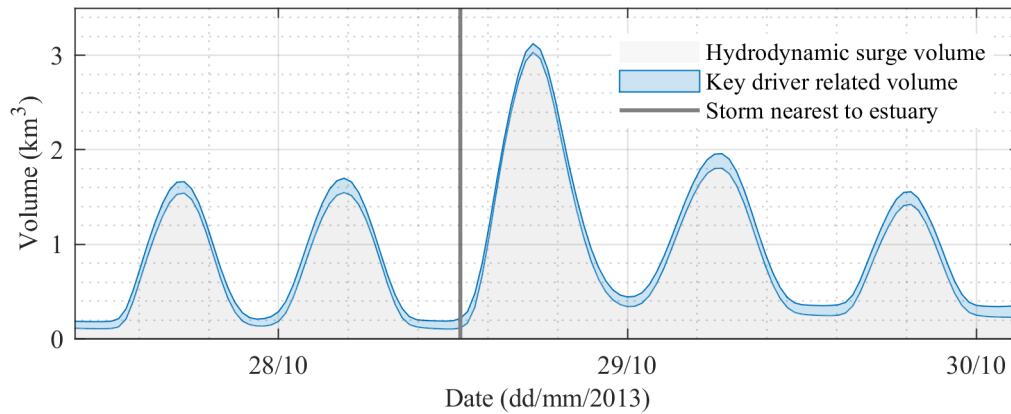


Figure 4.5: Envelope of simulated storm surge volume changes under European Windstorm Christian for the reference scenario.

Table 4.1.2: Process related surge volumes for reference European Windstorm Christian

Process	unit	Tide (T)	Atmosphere (A)	Waves (W)	Discharge (D)	T+A+W+D	Incision
Reference scenario							
Volume	(km <sup>3</sup> )	121.4	115.56	125.92	123.13	110.65	121.77
Rel. change	(%)	-	-4.81	+3.72	+1.43	-8.85	+1.95
Medium scenario							
Volume	(km <sup>3</sup> )	228.1	211.46	231.5	230.65	218.07	228.07
Rel. change	(%)	-	-7.29	+1.5	+1.12	-4.4	-0.1
Extreme scenario							
Volume	(km <sup>3</sup> )	358.07	359.86	359.33	362.37	345.67	358.10
Rel. change	(%)	-	+0.5	+0.35	+1.2	-3.46	+0.009

In contrast to the reference storm scenario, the medium research scenario yields a tidally induced surge volume of  $228.1 \text{ km}^3$  due to an implemented RMSL of 0.74 m, which equals an increase of almost 90 % compared to the tidally forced reference scenario. Compared to the westerly event, the Jutland type windstorm Xaver reveals a much smaller sensitivity towards added RMSL. Potential reasons could be the overall larger magnitude of the storm itself, rendering the impact of an increased water level smaller. Furthermore, the Jutland character of the storm brings with it a prolonged surge effect, filling the estuarine model domain previous to the storm peak, reducing the storm related impact smaller.

The scenario under combined metocean forcing for the medium scenario shows an overall reduction of  $-4.4 \%$ , which is approximately half that of the unaltered reference scenario. A constructively altered river bed shows a negligible influence of  $\leq 1 \%$  on the surge volume, as a result of the overall increased volume.

The tidally forced extreme case for windstorm Christian with an RMSL of 1.5 m, results in a tidal surge volume of  $358.07 \text{ km}^3$ , which represents an increase of 195 % and 57 % compared to the reference and medium scenarios respectively. In contrast to the reference and medium scenario, the atmospheric forcing results in a slight additional surge volume of 0.5 %. However, the wave related changes are reduced to a similar magnitude in comparison to the medium and reference wave scenarios. The combined forcing for the extreme scenario shows a further reduction of the metocean related influence with  $-3.46 \%$  compared to  $-8.85 \%$  for the reference case. Similarly to the other two scenarios, the constructive changes of the river bed result in marginally small changes of the overall volume.

Across all three scenarios, the single largest influence is exerted by the atmospheric boundary conditions, with nearly 5 % in the reference case. With increasing metocean conditions and RMSL, the influence of the individual and combined processes is reduced compared to the reference case, by  $-4.4 \%$  within the medium scenario and  $-3.46 \%$  within the extreme scenario.

▪ European Windstorm Xaver

Analogue to the European Windstorm Christian, the permutation is repeated for Xaver and obtained volumes compiled in table 4.1.3.

Table 4.1.3: Process related surge volumes for reference European Windstorm Xaver

Process	unit	Tide (T)	Atmosphere (A)	Waves (W)	Discharge (D)	T+A+W+D	Incision
Reference scenario							
Volume	(km <sup>3</sup> )	244.86	250.73	246.14	245.13	256.13	244.69
Rel. change	(%)	-	+2.8	+0.9	+0.5	+5.0	+0.3
Medium scenario							
Volume	(km <sup>3</sup> )	355.83	366.36	359.02	356.41	372.39	355.19
Rel. change	(%)	-	+3.0	+0.9	+0.2	+4.7	-0.2
Extreme scenario							
Volume	(km <sup>3</sup> )	484.44	492.31	485.13	485.11	500.84	484.76
Rel. change	(%)	-	+1.6	+0.1	+0.1	+3.4	+0.1

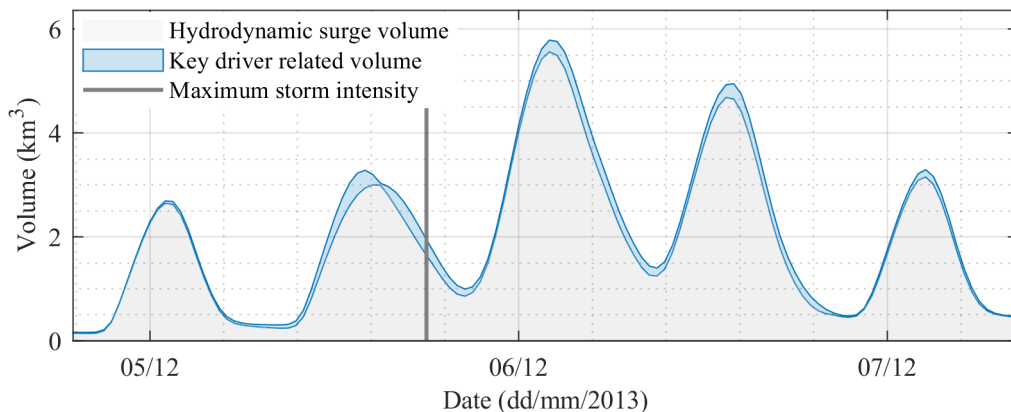


Figure 4.6: Envelope of simulated storm surge volume changes under European Windstorm Xaver for the reference scenario.

With increasing RMSL, tidal surge volume increases by 45 % for an added RMSL of 0.74 m and 97.8 % for 1.5 m. Identical to the westerly Skargarak type storm, the largest single impact on the overall tidal surge volume under Windstorm Xaver are the atmospheric boundary conditions with up to 3.0 % volume addition. Values for wind wave simulations are given, and show additional volume values of less than one percent. It is cautioned, that the simulations forced by wave conditions alone fell short of reproducing observed significant wave heights (see fig. 4.15). Therefore, added tidal storm surge volume due to waves is likely to differ from these values. Discharge related impacts upon the tidal surge volume are reduced with increasing RMSL and overall volume, as

the discharge volume is not increased by the magnitude, which is applied to the tidal boundary. In comparison to the simulations of the Skargarak type event, values are an order of magnitude smaller, which correlates well with the inversely proportional increase of the Tide driven surge volume due to RMSL. The compound event simulations (T+A+W+D) show an increase of 45 % and 34 % for the medium and extreme scenarios compared to the reference simulation. Compared to the tidally forced simulations, the compound simulations reveal added surge volume. The added volume percentage declines with increasing boundary conditions, similar to the simulations for Windstorm Christian, where the impact is reduced as well with increasing boundary conditions. Windstorm Xaver exhibits a much more pronounced surge character, due to the storm-track following along a north-south route. This draws a large dome of water under the low pressure center into the German Bight. Consequently, increasing the atmospheric conditions results in an increase in overall surge volume. The impact of surface waves diminishes with increased scenario intensity, similar to the westerly event. This effect is attributed to the overall increased water depth, resulting in a reduced sensitivity towards surface waves for the domain. Contrary to the windstorm Christian, the Weser discharge does not scale with the surge volume but increases less than the combined metocean surge effect from the sea. Given the relatively large increase in absolute surge volume compared to windstorm Christian, the incision scenario with constructive bathymetry changes shows a negligible impact on the overall volume.

#### 4.1.3 Current velocities along the Jade

Depth averaged current velocities induced by the different storm scenarios and the permutation of their respective metocean processes constitute a representative quantity for investigating storm related hydrodynamic impacts along the Jade with its transshipment complex bearing critical coastal infrastructure. The course of the Jade fairway is shown in figure 3.17. For investigating the key driver influence on the depth averaged current velocities under storm conditions, simulated quantities are extracted along the Jade fairway.

- European Windstorm Christian

Depth averaged velocities along the Jade fairway for European Windstorm Christian are extracted and filtered for flood and ebb phases depending on current direction of individual grid cell values. The amplitude range is computed for the reference scenario and given in figure 4.7, elucidating the potential influence of the different processes and system reactions.

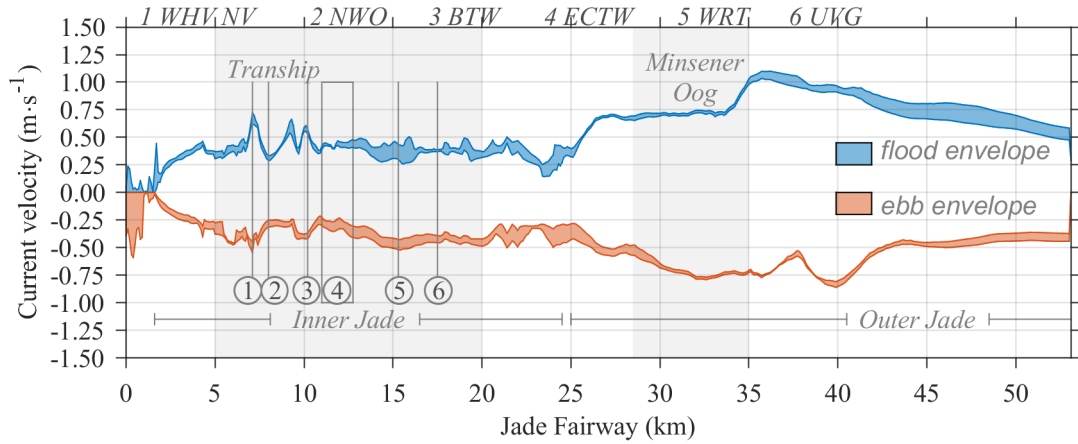


Figure 4.7: Simulated tidal velocities under European Windstorm Christian along the Jade fairway for the reference scenario with the bandwidth for flood (blue) and ebb (red) shows the envelope for the permuted metocean processes.

Largest tidal currents are induced by the combined forcing of tides, winds, waves and discharge and mark the outer limits. Smallest values are obtained under tidal forcing alone and mark the inner bounds. Different processes do not linearly cause larger current velocities but impact local flow patterns along the Jade and affect different sections of the Jade. The constructive scenario ranges between the outer and inner bounds and shows no significant alteration along the planned extension of the ECTW. The large span for the maximum ebb currents within the Jade Bight is traced back to the influence of the metocean processes, which result in increased surge volumes within the Bight and consequently increase ebb currents. Flood and ebb currents related to the different scenario permutations are given in table 4.1.4 for mean and max currents. Current velocities are converted into hydrodynamic kinetic energy density  $e_{kin}$  for assessing the cumulative storm impact along the fairway bed:

$$e_{kin,storm} = \sum_{i=t}^n \int_{JKM=0}^{JKM=54} \frac{1}{2} \cdot \rho \cdot \overline{uv}_i^2 \quad (4.1.1)$$

where  $\int$  denotes the line integral of the kinetic energy along the Jade fairway bed between kilometers 0 and 54,  $\rho$  is the sea water density and  $\overline{uv}^2$  is the depth integrated current velocity along the fairway at time step  $i$  and  $n$  is the number of time steps for the storm simulation. The cumulative storm energy  $e_{kin,storm}$  is computed and presented in table 4.1.4 in mega Watt (MW). All six reference simulations for Christian show, that no metocean process alters the flood dominance along the Jade, as the flood related current velocities and cumulative energies are larger for flood compared to ebb situations.

Table 4.1.4: Process related hydrodynamic impacts for European Windstorm Christian extracted and computed along the Jade fairway for individual key drivers

	Process	unit	Tide (T)	Atmosphere (A)	Waves (W)	Discharge (D)	T+A+W+D	Incision
Reference Scenario								
Flood	Max <sup>1</sup>	(ms <sup>-1</sup> )	1.04	1.09	1.07	1.03	1.09	1.04
	Mean	(ms <sup>-1</sup> )	0.13	0.14	0.12	0.13	0.14	0.13
	$\Sigma E_{kin}$	(MW)	41.19	48.04	39.56	38.46	45.73	41.13
Ebb	Max	(ms <sup>-1</sup> )	0.83	0.81	0.86	0.82	0.82	0.83
	Mean	(ms <sup>-1</sup> )	0.10	0.12	0.11	0.11	0.12	0.11
	$\Sigma E_{kin}$	(MW)	27.17	33.87	27.80	27.68	34.62	26.93
Medium Scenario								
Flood	Max	(ms <sup>-1</sup> )	1.05	1.71	1.07	1.04	1.12	1.04
	Mean	(ms <sup>-1</sup> )	0.13	0.15	0.12	0.13	0.14	0.13
	$\Sigma E_{kin}$	(MW)	43.29	56.66	39.39	39.64	49.49	43.11
Ebb	Max	(ms <sup>-1</sup> )	0.79	0.78	0.86	0.83	0.77	0.78
	Mean	(ms <sup>-1</sup> )	0.12	0.11	0.11	0.11	0.14	0.12
	$\Sigma E_{kin}$	(MW)	34.35	44.85	27.77	27.67	45.24	34.02
Extreme Scenario								
Flood	Max	(ms <sup>-1</sup> )	1.03	1.03	1.04	1.03	1.18	1.03
	Mean	(ms <sup>-1</sup> )	0.14	0.14	0.13	0.15	0.16	0.14
	$\Sigma E_{kin}$	(MW)	45.94	46.08	44.02	42.73	61.59	45.05
Ebb	Max	(ms <sup>-1</sup> )	0.73	0.73	0.77	0.73	0.87	0.73
	Mean	(ms <sup>-1</sup> )	0.13	0.13	0.13	0.12	0.15	0.13
	$\Sigma E_{kin}$	(MW)	38.79	40.87	42.11	27.97	54.30	40.87

<sup>1</sup> Maximum values are computed based on depth averaged current velocities, which are maintained for a minimum of 30 min.

Overall, current velocities along the Jade fairway show comparatively small variation in terms of maximum and mean values over the permuted metocean processes. Therefore, cumulative flood and ebb related kinetic energies are investigated. Within the reference scenario the largest quantitative effect on flood situations show the atmospheric boundary conditions with 16 % compared to the tidally forced scenario, whilst waves or discharge both reduce the incoming flood energy by -4 % and -7 %, as they redistribute the forces. Equally, the ebb situations are amplified the strongest by additional atmospheric forcing with 25 % due to the prevalent southerly wind direction during the storm, whereas the other processes appear to have negligible impacts (Waves 2 %; Discharge 1.8 %; Incision -1 %) within the reference case. The combined forcing within the reference scenario shows an increase for the flood energy along the Jade fairway by 10 % and an increase of 27.4 % for the ebb situation. Under wave forcing, the medium scenario reveals a reduction of the flood energy by 10 % compared to its tidally forced

base case, more than double the value obtained for the wave related reduction for the reference scenario. Medium discharge forcing results in a reduction of incoming flood energy of  $-8.5\%$ , similar to the reference scenario with  $-7\%$ . Combined metocean forcing for the medium scenario reveals a flood energy increase of  $14\%$  and an ebb related amplification of  $31.7\%$ . The development of the ECTW within the Jade incision scenario shows a flood energy reduction of  $0.5\%$  for flood and an ebb related reduction of  $1\%$  for the Jade. The extreme scenario reveals a negligible influence by atmospheric forcing on flood energy by  $\leq 1\%$  and an increase of  $5\%$  for ebb situations. Wave forcing in the extreme scenario shows a flood related decrease by waves of  $-4.1\%$  and an increase of  $9.6\%$  for ebb. For the constructive river bed changes the extreme scenario yields a flood related reduction of  $-2\%$  along the fairway due to the constructive layout of the ECTW extension. For ebb the extended port has a constrictive impact amplifying the ebb currents increasing the ebb related energy by  $5\%$ . However, for combined metocean forcing the extreme scenario reveals a flood situation impact of  $34\%$  and  $39.8\%$  ebb current energy amplification.

Similar to the tidal surge volumes presented in figure 4.5 and compiled in table 4.1.2, current velocities show a non-linear response to the different metocean processes and combined forcing does not result in the largest energies or highest current velocities along the fairway. An increased RMSL alone does not significantly increase the energies compared to the reference simulation. Neither do single key drivers account for the large energy increases along the fairway, but a combination of metocean processes. The largest individual contribution is attributed to the atmospheric forcing cases.

▪ European Windstorm Xaver

Complimentary to the Skargarak type storm compound event, the kinetic forces induced by the Jutland type windstorm Xaver are extracted along the Jade fairway and characteristic quantities computed. Figure 4.8 shows the results obtained for the reference simulations. Computed parameters are compiled in table 4.1.5.

Depth averaged current magnitudes for maximum ebb and flood currents across the different simulations presented in figure 4.8 generally show larger values for both, flood and ebb situations under European Windstorm Xaver compared to the westerly storm event Christian. Especially the Inner Jade lined by critical coastal infrastructure experiences  $0.25 \text{ ms}^{-1}$  higher current velocities, due to the northerly storm path and the complimentary effective direction impacting the focus region from due north. The transshipment complex Wilhelmshaven experiences larger flood than ebb peak velocities, with highest values found at the entrance of the New Outer Harbour of Wilhelmshaven (see 1 in fig. 4.8). What is more, the groyne spider Minsener Oog does not have such a reducing effect on the incoming flood current magnitudes, as for the westerly storm event.



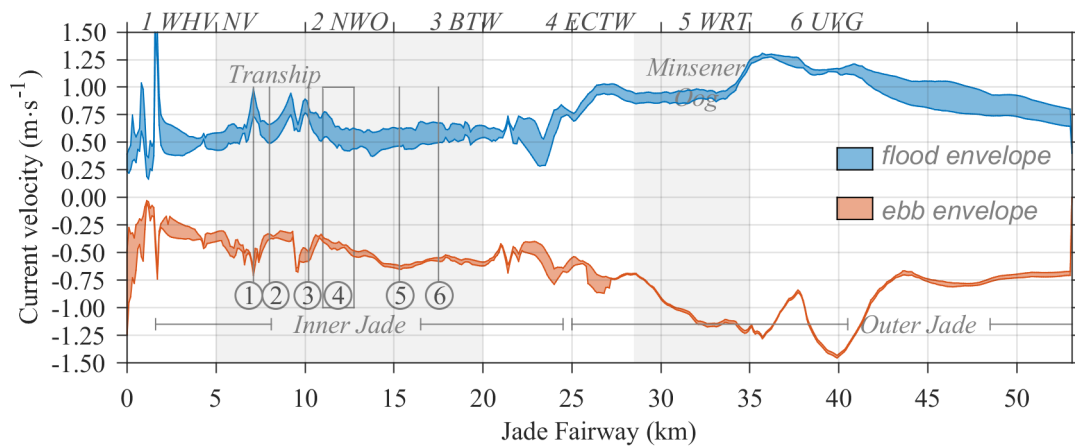


Figure 4.8: Simulated tidal velocities under European Windstorm Xaver along the Jade fairway for the reference scenario with permuted metocean processes

Largest single impact across the three scenario levels is attributed to RMSL, contributing the largest changes in depth averaged current velocities for both flood and ebb. Closely followed by the atmospheric conditions, which show an equally large impact on the hydrodynamic quantities.

Atmospheric boundary conditions show increasing effects for the flood phases and a reducing effect on the ebb phases, which is explained by the northerly trajectory of the storm inducing a pronounced surge. The magnitudes of the atmospheric impact upon the Jutland event are distinctly larger than the ones found for the Scandinavian type event.

Wave conditions show a reducing impact on both flood and ebb, with slightly larger reduction of the ebb phase related currents and energies. Compared to the westerly event, where waves have a strong impact on the hydrodynamics, the large surge extent of the northerly event reduces the wave related impacts. This is also observed in the diminishing reduction with increasing boundary conditions in table 4.1.5.

Discharge reveals the smallest of all scenario impacts upon hydrodynamic magnitudes along the Jade fairway, due to the comparatively small volume added through the Weser discharge compared to the large surge volume forced into the estuary by the storm system (cmp. sec. 4.1.2).

Compound simulations reveal a non-linear increase in kinetic energies and shifts in current velocity magnitudes, with increasing effects for the flood phase and a reducing impact upon the ebb phases. Overall, added kinetic energies appear small compared to the values found for the westerly event. Resembling a saturation function, this effect is attributed to the surge volume of the northerly event in conjunction with the

limited available volume within the model domain, which confines the surge due to an impervious coastal dike line.

Table 4.1.5: Process related hydrodynamic impacts for European Windstorm Xaver extracted and computed along the Jade fairway for individual key drivers

	Process	unit	Tide (T)	Atmosphere (A)	Waves (W)	Discharge (D)	T+A+W+D	Incision
<b>Reference Scenario</b>								
Flood	Max <sup>1</sup>	(ms <sup>-1</sup> )	1.88	2.19	1.67	1.87	1.49	1.89
	Mean	(ms <sup>-1</sup> )	0.18	0.25	0.18	0.18	0.25	0.19
	$\Sigma E_{kin}$	(MJ)	74.38	140.24	71.02	73.56	141.90	76.97
Ebb	Max	(ms <sup>-1</sup> )	2.18	1.44	1.73	2.16	1.46	1.43
	Mean	(ms <sup>-1</sup> )	0.18	0.15	0.16	0.18	0.15	0.18
	$\Sigma E_{kin}$	(MW)	72.30	50.58	71.9	72.34	50.53	71.40
<b>Medium Scenario</b>								
Flood	Max	(ms <sup>-1</sup> )	1.37	1.61	1.36	1.36	1.68	1.36
	Mean	(ms <sup>-1</sup> )	0.19	0.25	0.18	0.19	0.26	0.19
	$\Sigma E_{kin}$	(MW)	77.39	139.0	74.62	76.93	143.58	76.96
Ebb	Max	(ms <sup>-1</sup> )	1.39	1.42	1.37	1.38	1.43	1.40
	Mean	(ms <sup>-1</sup> )	0.20	0.17	0.21	0.2	0.16	0.20
	$\Sigma E_{kin}$	(MW)	86.14	60.0	84.24	86.18	57.84	86.30
<b>Extreme Scenario</b>								
Flood	Max	(ms <sup>-1</sup> )	1.37	1.65	1.36	1.36	1.36	1.35
	Mean	(ms <sup>-1</sup> )	0.2	0.26	0.19	0.2	0.26	0.19
	$\Sigma E_{kin}$	(MW)	80.54	158.21	77.86	80.1	147.84	79.43
Ebb	Max	(ms <sup>-1</sup> )	1.33	1.44	1.32	1.32	1.35	1.34
	Mean	(ms <sup>-1</sup> )	0.21	0.19	0.21	0.21	0.17	0.2
	$\Sigma E_{kin}$	(MW)	97.75	54.11	97.46	97.8	64.33	97.81

<sup>1</sup> Maximum values are computed based on depth averaged current velocities, which are maintained for a minimum of 30 min.

#### 4.1.4 Residual current velocities

- European Windstorm Christian related scenario dependant depth averaged residual current velocities for the whole storm duration are shown in figure 4.9.

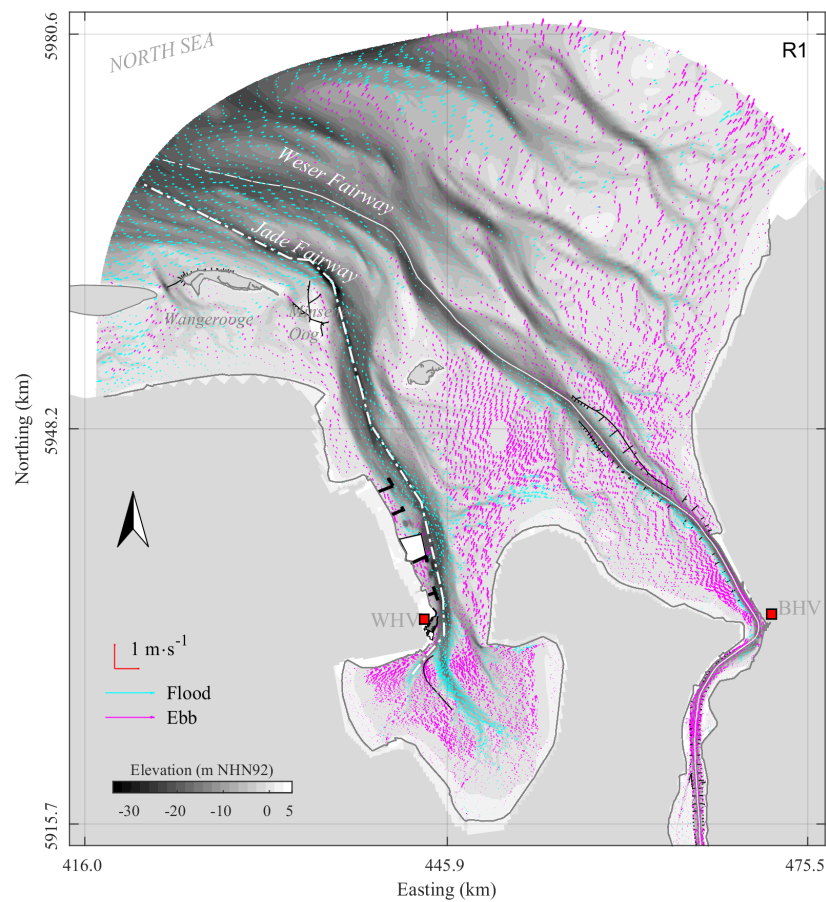


Figure 4.9: Simulated residual depth averaged currents for European Windstorm Christian with all metocean processes for the reference scenario.

Residual currents for the complete domain are visualized in figure 4.9 for the reference scenario (R1). Residual velocities are filtered for flood and ebb respectively in every grid cell based on their direction. Detailed depictions of focus Regions for the Outer Jade and

the transshipment complex lining the Inner Jade for the reference (R), medium (M) and extreme (E) scenarios are given in Appendix A.12.

▪ **R1 / M1 / E1**

Results for the reference scenario (R1) clearly show a flood dominated reach along the deep Jade channel all the way up into the Jade Bight (see figure 4.9). Similar for the Outer Weser until the port of Bremerhaven. Tidal flats adjacent to the two tidal channels show ebb dominated residuals. The back barrier island tidal area shows ebb dominated regions behind the islands and flood impacted areas within the tidal gat between the islands of Spiekeroog and Wangerooge.

The medium scenario (M1) in contrast shows slightly extended areas for the flood dominated residuals within the outer Jade and Weser region (cf. figure A.12). Especially the back barrier island Wadden area exhibits a distinct change from ebb dominated to flood dominated for the storm period.

For the extreme scenario (E1), the flood dominated residual area is further extended along the outer Weser tidal flats, completely inverting large ebb dominated tidal areas into flood dominated regions (cf. figure A.15). Furthermore, the Outer Weser and adjacent Fedderwarder tideway reveal a pronounced flood dominance compared to the reference and medium scenarios. Finally, the Jade channel experiences an extension of flood dominated areas as well. Overall, the extreme scenario shows an extended affected model area reaching to the dike line, whereas within the reference scenario the extent is less due to the implemented RMSL and other amplified processes.

▪ **R2 / M2 / E2**

The hydraulic structure of *Minsener Oog* at the northwest tip of the Jade fairway exhibits a clear influence on residuals of the westerly storm event, as the south-east directed flood currents are largely deflected by the structure and exhibit decreased magnitudes in the wake of the structure. Within the reference scenario (R2) the tidal area between the coast and the structure is ebb dominated, while the seaward side shows flood dominance (see figure A.10).

The deflection of the incoming flood by the structure results in locally enhanced velocities. On the eastern side of *Minsener Oog*, the flood travels inland upstream the Jade channel, which shows a distinct flood dominance. The sand spit to the north of *Minsener Oog*, lining the Jade channel to the east, is ebb dominated.

Within the medium scenario (M) for storm Christian, the local velocities at the structure are amplified (cf. figure A.13). Furthermore, the back barrier tidal flat shows an extension of flood dominated area towards the coast as well as in eastward direction. Ebb and flood residuals show larger residuals along the tidal channel as well as the adjacent shoals.

Within the extreme scenario (E2), the sand spit to the north of Minsener Oog emerges as flood dominated, in contrast to it previously being ebb dominated in the other two scenarios (cf. figure A.16). In addition, the back barrier tidal flat shows a further extension of the flood dominated area towards the Jade channel, which is ebb dominated during the storm within the reference scenario.

▪ **R3 / M3 / E3**

Analogue to the Outer Jade, residual currents for the storm surge along the transshipment complex of the Jade with its critical coastal infrastructure are computed and given in figure A.11 and show a mixed result. The deeper parts of the Jade channel with the tips of the structures and terminals are mainly flood dominated, whilst the shallower western bank is characterized by ebb directed residuals. The reference scenario (R3, see figure A.11) reveals overall smaller residual current velocities compared to the Outer Jade (R2, cf. figure A.10).

Nevertheless, the deep Jade channel remains flood dominated up to Wilhelmshaven and along the tidal channels of the *Stenkertief* and the *Vareler fairway* leading into the Jade Bight. The *Ahne fairway* leading to the southeast of the Bight shows a mixed flood and ebb dominated character. The tidal area around the *Hohe Weg* shows a pronounced ebb dominated character with strong residual currents directed north east to east into the Outer Weser estuary.

The liquid bulk terminal Voslapper Groden (UVG) shows a flood dominated area around the tip of the structure protruding into the deeper Jade channel and an ebb dominated regime near the coastline. The situation repeats for the Wilhelmshaven Refinery Terminal (WRT). The ECTW is an exception, where ebb directed residual currents occur along the pier. The currents between the bulk terminal Wilhelmshaven, the western bank and the ECTW are constricted and show elevated residual magnitudes flowing through the small gap between the structures during ebb.

The northern side of the ECTW induces a vortex during flood, with an ebb dominated region east of it, in part explaining the wedge in the bathymetry reaching into the fairway, since this resembles an area prone to sedimentation. Further upstream, the oil pier (NWO) resembles the situation observed at UVG/WRT with no particularities. Wilhelmshaven at the end of the transshipment complex shows marginal residual currents within the port basin but exhibits a shear flow in front of the harbor entrance with flood dominance.

- European Windstorm Xaver related scenario dependant depth averaged residual current velocities are shown in figure 4.10.

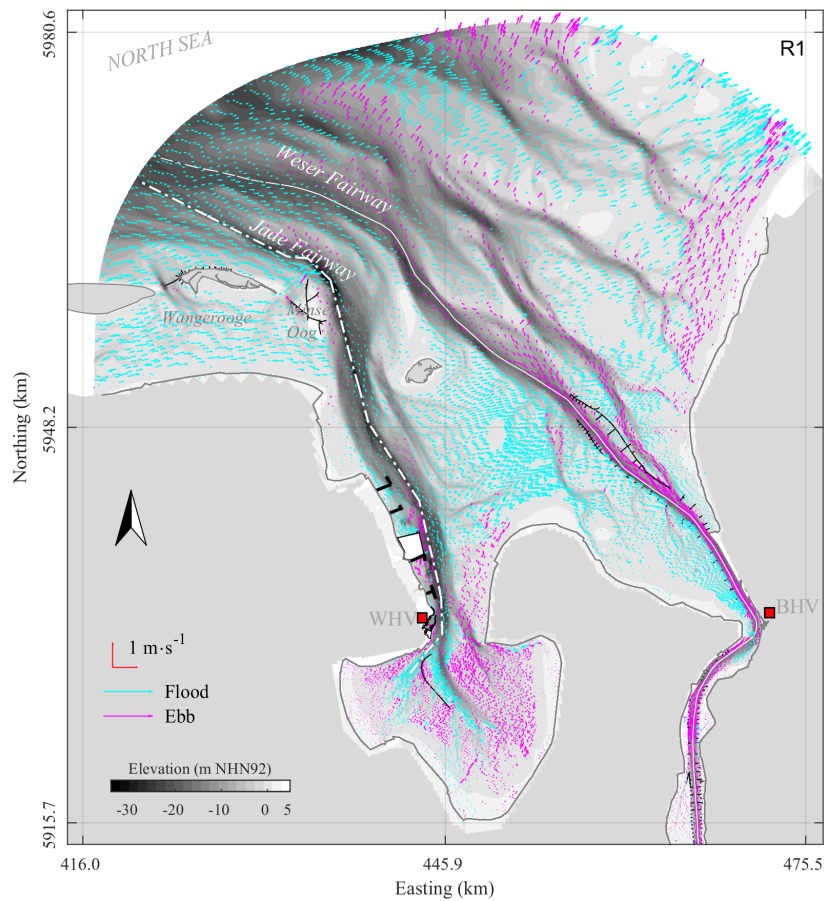


Figure 4.10: Simulated residual depth averaged currents for European Windstorm Xaver with all metocean processes.

- **R1 / M1 / E1**

Residual current velocities obtained for the reference scenario are visualized for the complete model domain (see fig. 4.10 R1) and show flood characterized areas for the Outer Jade and Weser, as well as for the Hohe Weg tidal ridge. The back barrier tidal flat of Wangerooge also exhibits flood dominated residuals during the storm in stark

contrast to the reference compound event simulation of European Windstorm Christian (cmp. fig. 4.9 R1). For the medium (M1, see figure A.21) and extreme (E1, see figure A.24) compound scenarios, the areal extent of regions characterized by flood residuals is increased, while the ebb directed residuals are reduced, with the largest shift observed in the extreme case (see fig. A.24 E1). Furthermore, the extreme scenario also reveals the largest inundation extent, reaching all the way to the dike line around the Jade Bight and along the Lower Weser.

■ **R2 / M2 / E2**

For the area around Minsener Oog the reference scenario shows larger extents for flood dominated areas, compared to ebb residuals. On the eastern flank of Minsener Oog in the deeper Jade Channel as well as north of the island along a sand spit lining the north-eastern side of the Jade fairway, ebb directed residuals are found (see figure A.19). In line with these findings, the medium compound event results (M2, see figure A.22) overall show larger residual current magnitudes along the Outer Jade. What is more, the ebb characterized area along the sand spit extends south into the Jade channel across the large dune field situated here (cmp. fig. 3.17). Results for the extreme (E2) compound simulation are shown in figure A.25 and show an areal reduction of the previously extended regions characterized by ebb residuals. Amplitudes are slightly elevated compared to the medium compound scenario. In contrast to the westerly compound event simulation, the northerly event exerts a strong flood dominance onto the tidal flats.

■ **R3 / M3 / E3**

Along the transshipment complex, residual current velocities are given in the bottom row for the three different compound scenarios. For the reference case (R3, see fig. A.20) the western bank of the Jade north of the ECTW shows flood directed residuals, whilst the bank south of the terminal is characterized by ebb directed residuals. Along the pier of the ECTW ebb directed residuals are found, forming a large ebb driven vortex at the northern end of the ECTW adjacent to the service port located at the corner. The remaining area of deep Jade channel is characterized by flood directed residuals, which are smaller compared to the Outer Jade region. Areas of elevated current residuals are found at the north-west of the entrance into the Inner Jade, at the tips of the ECTW and in the deep channels leading into the Jade Bight. The Hohe Weg tidal flat area exhibits large parts of flood directed residuals, which is in stark contrast to the westerly event, where this area is mainly ebb dominated and experiences high north-east directed current stresses. Along the pier of the ECTW a large elongated residual vortex is formed. The extreme compound scenario results show a matching image, with overall larger residual current magnitudes. Through the medium (M3, see figure A.23) and extreme (E3, see A.26) cases, the flood directed residuals extend further onto the Hohe Weg tidal ridge.

▪ **Hydraulic development scenario**

Residual current vectors for European Windstorm Christian is shown in figure 4.11 for the hydraulic construction scenario under extreme (E) forcing. The focus area shows the Jade fairway with reinstated maximum depth of  $-17.6$  m below CD as well as the planned extension of the ECTW.

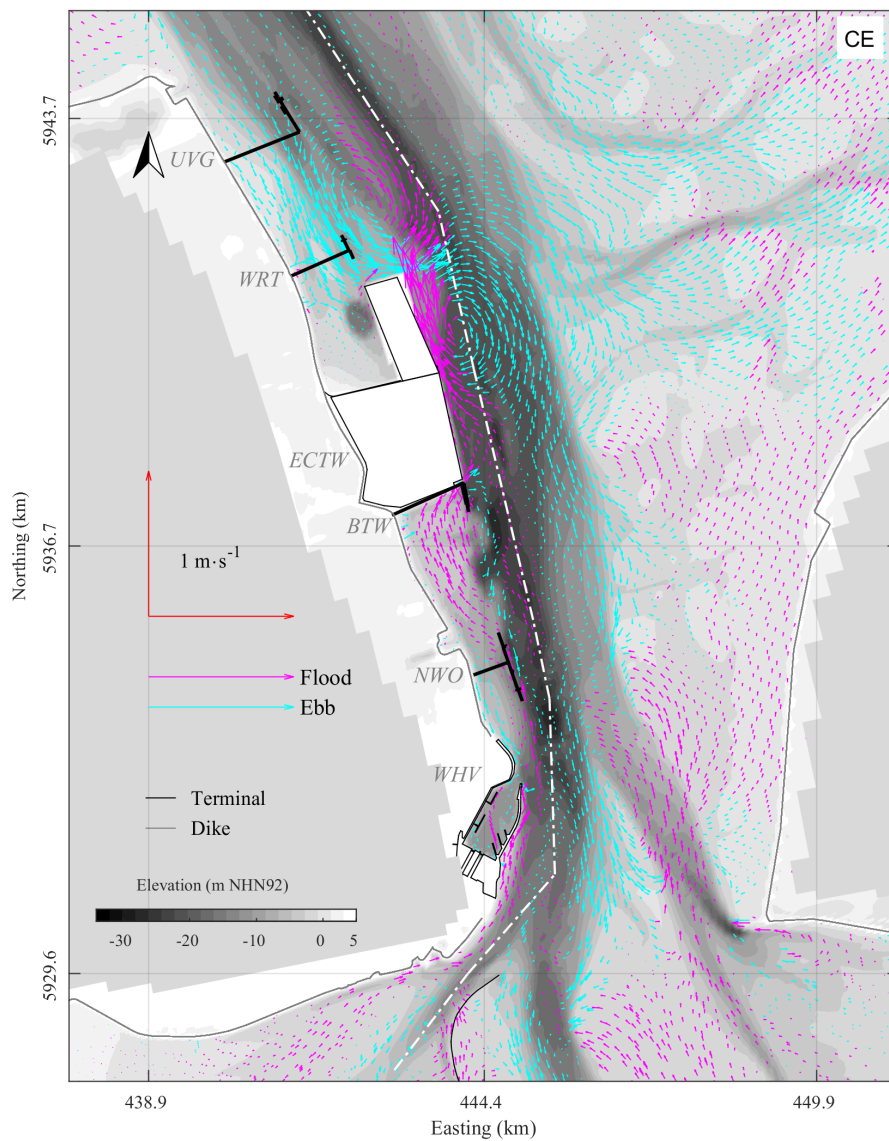


Figure 4.11: Residual currents in the hydraulic intervention scenario for European Windstorm Christian for the extreme scenario.



Results obtained for the windstorm Xaver for the hydraulic construction scenario under extreme boundary conditions are depicted in figure 4.12.

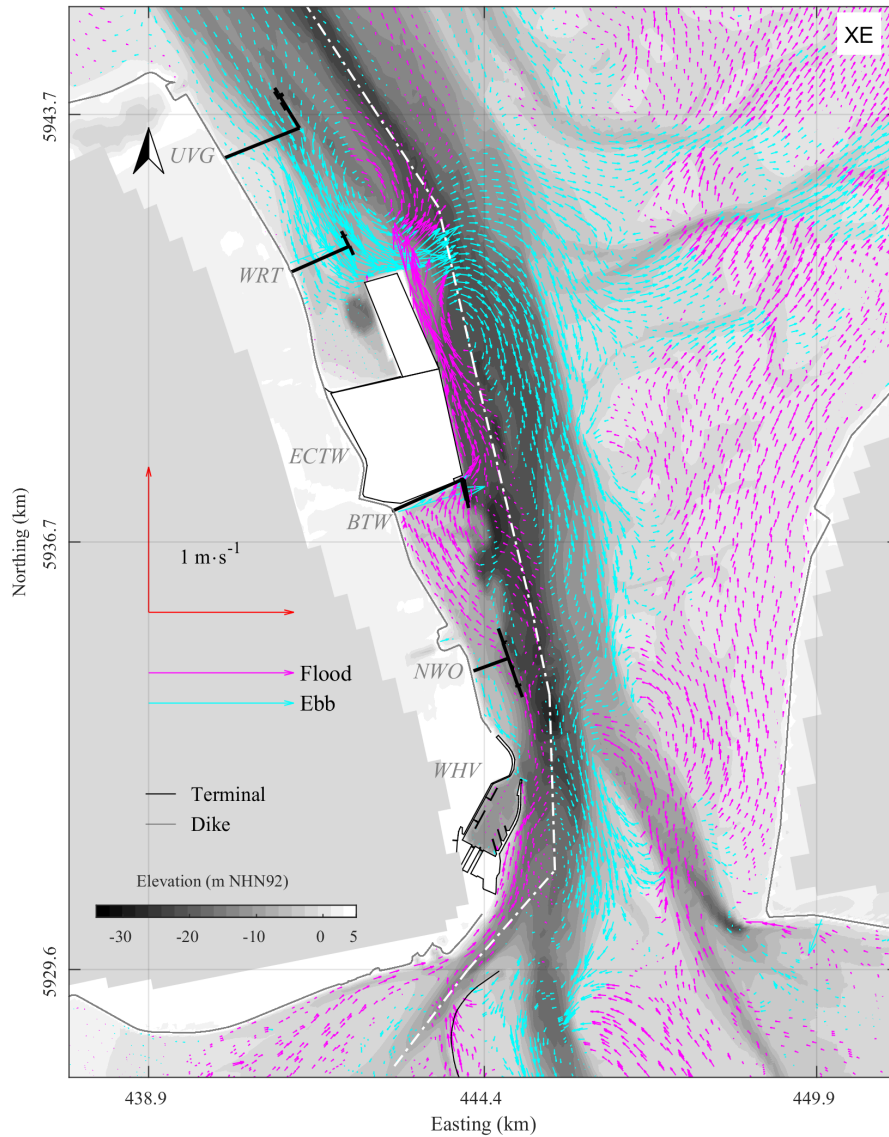


Figure 4.12: Residual currents in the hydraulic intervention scenario for European Windstorm Xaver for the extreme scenario.

Both storm events show a pronounced stream like concentration of ebb residuals along the extended ECTW jetty, which expand at the northern end of the terminal. The bank north-west of the ECTW is characterized by flood directed residuals across all simula-

tions, which exhibit a backlog behind the protruding ECTW jetty and a jet like residual flow pattern crossing the ebb directed stream at the north-eastern corner of the extended jetty, inducing large hydrodynamic forces at this position.

Results obtained for the hydraulic construction scenarios under reference and medium forcing for the two storm events are given in appendix A.13

Furthermore, the altered geometry induces a shift from ebb towards flood dominated residuals along the bank area between the NWO terminal and the New Outer Harbour of Wilhelmshaven. Unaltered simulations reveal ebb directed residuals within this area (cmp. fig. A.17 E3).

## 4.2 Wave impact

Surface waves are simulated on a second grid, covering the Jade and Outer Weser, allowing for coastal wave impact research. Simulation results for the reference scenario of European Windstorm Christian are visualized in 4.13a for the whole domain and corresponding time series of observed and simulated significant wave height at the station LAW are given in figure 4.13b and c.

Figure 4.13: Simulated significant wave height for the reference compound scenario of European Windstorm Christian

The surface waves reach the Jade Bight as well as the tidal flats and back barrier island areas with atmospheric forcing, compared to wave forcing alone, clearly showing the need for including surface wind waves for simulating storm conditions. The simulation results show, that the model reproduces the overall characteristics of the storm induced  $H_{1/3}$  development.

### 4.2.1 Significant wave height impact

▪ Windstorm Christian

Simulated significant wave height evolution at the position LAW for the three different scenarios and their respective atmospheric signals of ETC Christian are compiled in figure 4.14 a-c. Complimentary, the observed significant wave height at LAW is given as well as a reference.

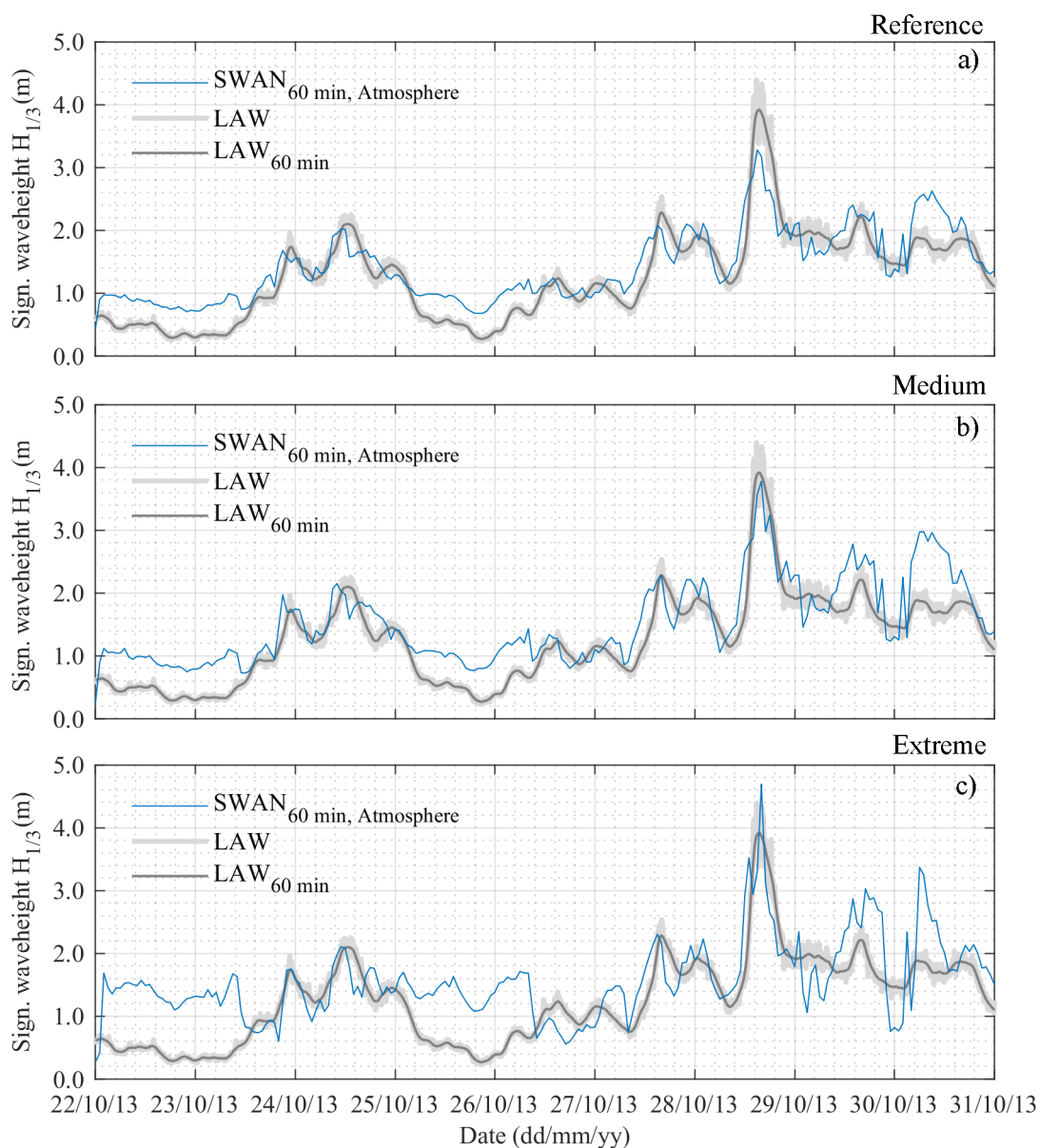


Figure 4.14: Simulation results for sig. wave height for ETC Christian for the reference and compound storm research scenarios.

The reference simulation (see figure 4.14 a) including metocean processes (—) shows a good agreement with the observed signal. Observed mean peak values of 3.8 m are underestimated by the model at 3.2 m as a result of the meteorologic forcing by the reanalysis data and inherent problems (see section 2.2.2). Nevertheless, *MSS* values indicate a satisfactory agreement at 0.74. Without atmospheric boundary conditions the model underestimates the significant wave height, especially the periods where the frontal systems of the ETC reach the region and a peak value of 1.65 m. This exemplifies the essential character of atmospheric conditions, when simulating surface waves. The ensuing figure 4.14 b shows the simulated significant wave height at the same location for the medium storm research scenario, with metocean processes. Synoptically, the results show a similar pattern obtained within the reference research scenario for ETC Christian, in that the atmospherically forced scenario run develops more pronounced peaks at 3.78 m. Furthermore, the elevated water level within this scenario results in deeper water at the location, allowing for the development of overall higher waves (cmp. section 2.3.5). This situation prevails for the more quite situations on the 22<sup>nd</sup> and through the period from the 25<sup>th</sup> to the 27<sup>th</sup>. The combined forcing within the medium scenario reaches the observed storm peak values, in contrast to the unchanged reference scenario. The extreme scenario, displayed in figure 4.14 c, shows wind wave heights simulated without metocean processes, that almost reach the observed  $H_{1/3}$  values that peak at 2.6 m, as a result of the enhanced water level in combination with increased off shore wave conditions. Under combined metocean forcing however, the simulated significant wave height values exceed 2 m for most of the simulation period. The simulated storm peak value reaches 4.62 m while observed peak values reach 4.4 m.

Given the amplification of the wave boundary conditions by 0.28 m for the medium and 0.5 m for the extreme scenario, the underlying RMSL of 0.74 m and 1.5 m show a nonlinear impact on the wind waves generated. Without atmospheric forcing, the medium scenario value shows a peak value of 2.1 m, while the reference scenario without atmospheric forcing peaks at 1.65 m, yielding a difference of 0.45 m of which 0.28 m are attributed to the enhanced wave conditions. However, the enhanced water depth exhibits a non-linear impact on the waves. For the extreme scenario runs the peak values without atmospheric forcing reach 2.6 m, compared to 1.65 m reached within the reference scenario. Here the difference of 1.05 m can partially be attributed to the amplified wave conditions of 0.5 m but the remaining height difference is induced by the implemented RMSL of 1.5 m. Differences between the medium and extreme compound simulations compared to the reference case are non-linear and exhibit an increment of 5%, which has been reported for compound simulations (Vousdoukas et al., 2017; Grabemann et al., 2015; Groll et al., 2014)

▪ Windstorm Xaver

Complimentary to the compound simulations of European Windstorm Christian, these are conducted for the European Windstorm Xaver. Results for the reference, medium and extreme scenarios are extracted at the observation station LAW as well and compared to observed values. Obtained results are depicted in figure 4.15.

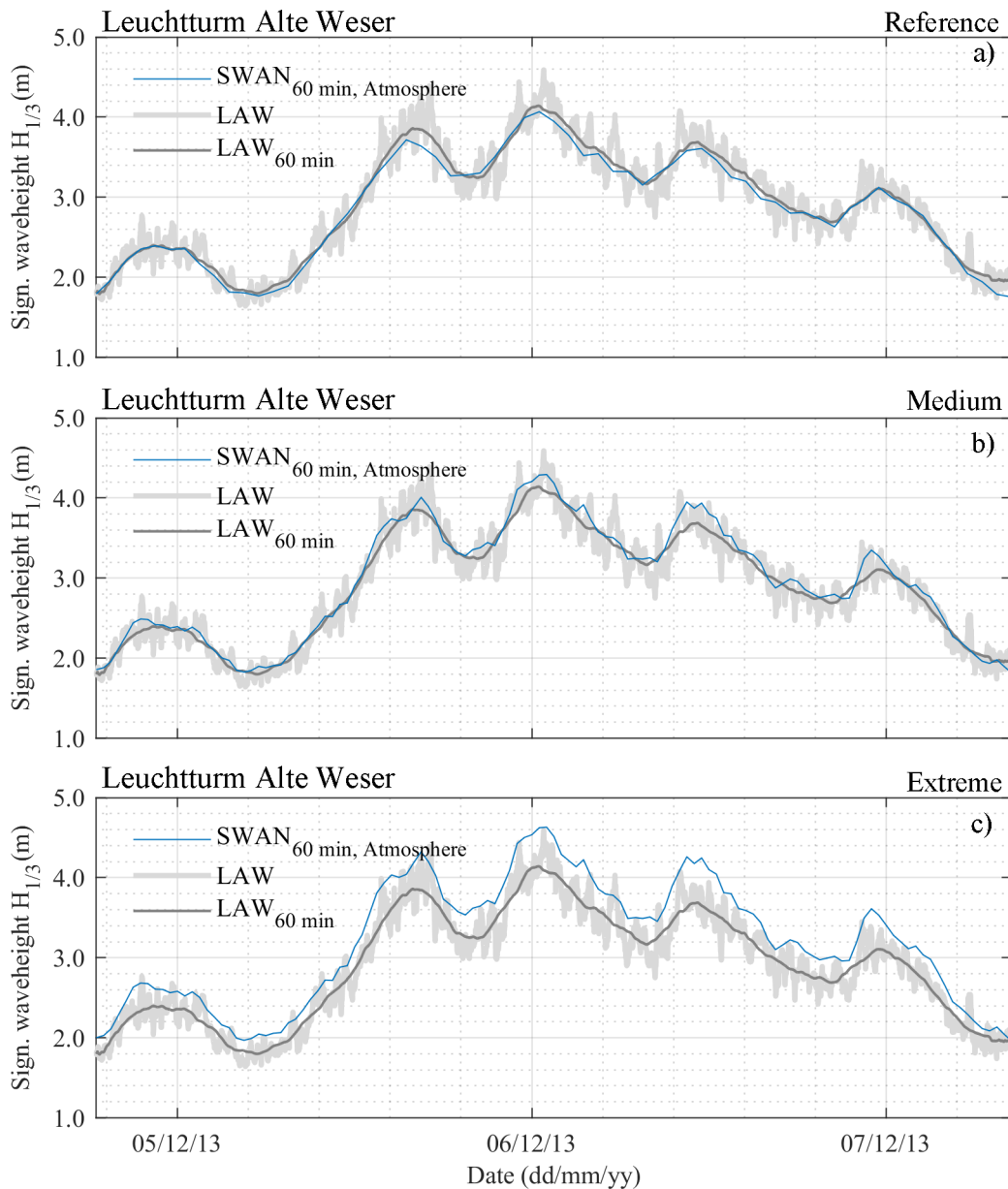


Figure 4.15: Simulation results for sig. wave height for ETC Xaver for the reference and storm research scenarios.

Significant wave heights are underestimated by the model within the reference scenario (see fig. 4.15 a) similar to Windstorm Christian (see fig. 4.14 a). With an observed significant wave height peak value of 5.01 m and a moving average maximum of 4.13 m, the model under predicts the peak values with 4.1 m due to spatial and temporal resolution. Nevertheless, the skill score for the reference simulation amounts to 0.87, indicating a good reproduction of the significant wave height. In contrast, the simulations without atmospheric boundary conditions create a very different signal, which does not reproduce the storm characteristics. Due to this reason, a further analysis of the wind wave simulation scenarios without atmospheric boundary conditions is not included, as the signal shows that without wind shear, the wave model does not correctly simulate the storm wave conditions. The medium compound event (see fig. 4.15 b), shows elevated wind wave conditions throughout the storm period, with a mean  $H_{1/3}$  of 3.1 m and a peak value of 4.4 m. These values correlate well with the increased wave amplitude of 0.28 m, while an additional increase of  $\leq 0.1$  m is identified due to RMSL and increased atmospheric forcing. Compared to the Skargarak type storm event, this Jutland type reveals a non-linear amplification as well, which is smaller than the one for the westerly storm. The extreme compound event scenario shows a significant wave height peak value of 4.6 m and a mean of 3.2 m for the storm event. These values reflect the boundary amplifications of wind and wave as well as underlying RMSL. Nevertheless, the increase is non-linear and much smaller in comparison to the results for the westerly extreme compound event (see fig. 4.14 c). This can be explained by the different storm type, coming from a northerly direction, European Windstorm Xaver develops a longer lasting surge component, which allows the surface waves to develop more evenly, as most of the inter tidal areas in the outer Jade-Weser is already inundated. In contrast, the westerly compound event reveals a higher sensitivity to the underlying RMSL in respect to surface wave development, as the fetch length increases with RMSL, due to the less developed surge character of the event. The mean wave length for the three scenarios increase from 131 m in the reference case, to 138 m and 145 m in the medium and extreme scenarios. In conjunction with the coastline geometry and its geographic orientation, the different compound events react differently to amplified boundary conditions, revealing (1) non-linear increases for both events of different storm types, (2) a stronger impact for the westerly event due to underlying RMSL. Finally, the wave steepness reaches higher overall values during the compound simulations for Windstorm Xaver. Relative changes amount to 6 % for the medium compared to the reference and 5 % for the extreme compared to the medium scenario.

#### 4.2.2 Wave steepness impact

The impact of amplified environmental key drivers on wave steepness over the storm period is evaluated for potential changes.

Results shown in figure 4.14 are used to derive the respective wave length for each scenario according to:

$$L_{wave} = \frac{g \cdot T_{wave}^2}{2\pi} \cdot \tanh\left(\frac{2\pi h}{L_{wave}}\right) \quad (4.2.1)$$

where  $L_{wave}$  is the wave length in m,  $g$  is the gravitational force in  $\text{ms}^{-2}$  and  $T_{wave}$  is the wave period in s (Holthuijsen, 2007). Yielding the wave steepness  $s_{wave}$  as quotient, which is depicted in figure 4.16 for storm Christian for all three scenarios including all metocean processes. The wave steepness for the three scenarios of European Windstorm Christian shows an increasing trend towards the storms peak water level and a diminishing trend afterwards. What is more, the three scenarios show not a linear increase in steepness but form a regional response signal based on the local water depth, incoming wave parameters and atmospheric forcing.

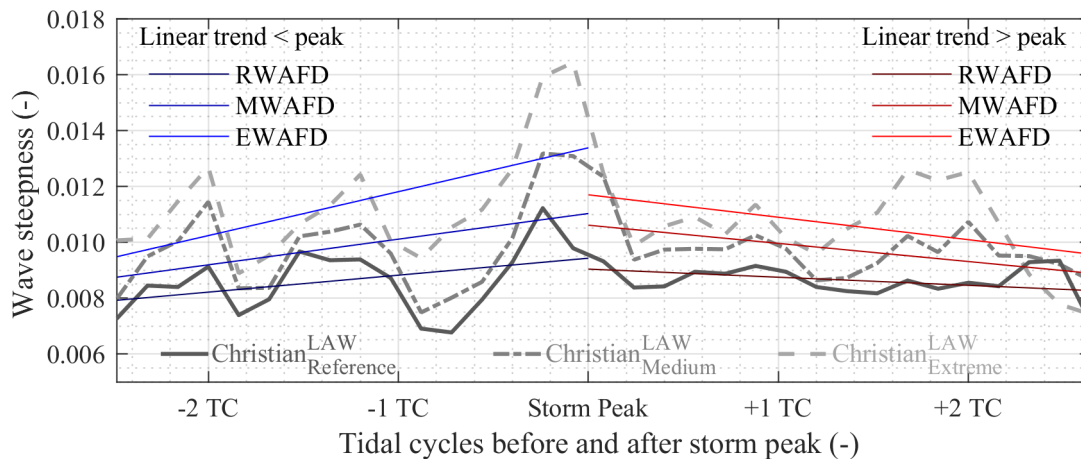


Figure 4.16: Wave steepness development for the three compound event simulations of European Windstorm Christian at the wave gauge station Leuchtturm Alte Weser (LAW).

Linear regression functions are calculated for the three scenarios for the wave steepness for two and a half tidal cycles before and after the peak water level. Results are compiled in table 4.2.1, where  $m1$  describes the slopes of the pre-storm-peak functions and  $m2$  the ensuing functions.

Table 4.2.1: Wave steepness during Windstorm Christian referenced to storm peak water level.

	period f(s <sub>wave</sub> )	Storm Research Scenario			Relative increase		
		Reference	Medium	Extreme	M/R	E/R	E/M
slope	m1	+12e-4	+18e-4	+30e-4	1.5	2.59	1.71
	m2	-6e-4	-12e-4	-15e-4	2.2	2.77	1.24

Fitted linear functions for wave steepness generally show steeper increase before peak water compared to decline post peak water. The reference scenario shows the smallest values, while the extreme scenario resembles the top most functions. Obtained values indicate, that the medium scenario bears an increase factor of 1.5 for wave steepness before peak water compared to the medium scenario and 2.2 after. Analogue, the extreme scenario shows factors of 2.59 before and 2.77 after peak water compared to the reference scenario. Wave steepness under storm conditions does not respond linearly to scenario related amplification of coastal key drivers for European Windstorm Christian.

Complimentary to the westerly compound event, this analysis is performed for the northerly compound event. Obtained results are visualized in figure 4.17 for the three scenarios. Computed linear regression functions are given and corresponding slope parameters compiled in table 4.2.2.

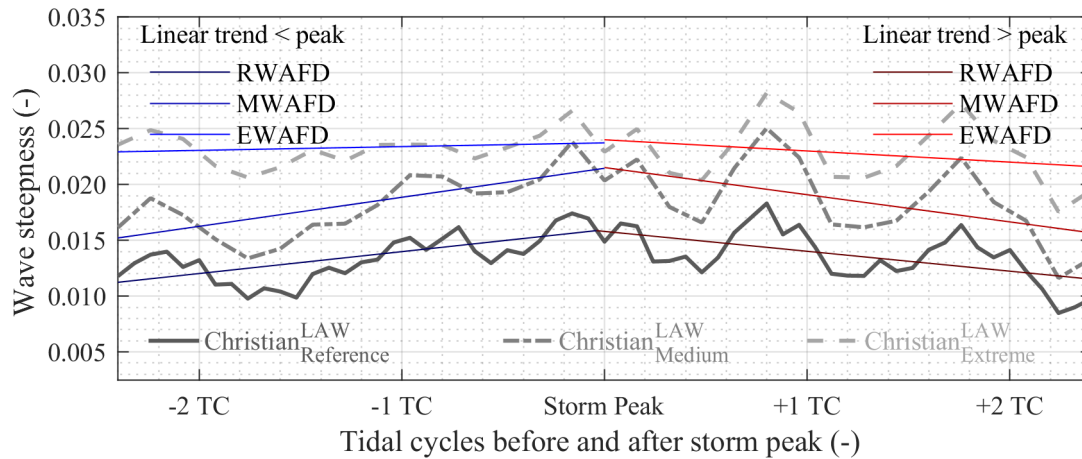


Figure 4.17: Wave steepness development for the three compound event simulations of European Windstorm Xaver at the wave gauge station Leuchtturm Alte Weser (LAW).

Similar to the westerly compound event, the simulations around Windstorm Xaver show an increasing wave steepness towards the storm peak water level for the reference case



and an ensuing decline in wave steepness. The steepness signal follows the characteristics of the tidal water level, with peaks and troughs. Within the medium compound event, the slopes show an increase in steepness, which is smaller than that obtained for the westerly event (cmp. table 4.2.1 *Relative increase*). The extreme scenario shows a very similar signal with overall increased amplitude. However, the fitted linear functions reveal, that the ramp up towards the storm peak exhibit a strongly reduced slope almost leveling out, as the wave steepness has developed early on due to elevated water levels and the storm trajectory coming from the North, resulting in a prolonged surge at the German North Sea coast. The post peak signal also shows a much smaller negative slope, having a longer wave related impact on the coastal region.

Table 4.2.2: Wave steepness during Windstorm Xaver referenced to storm peak water level.

	period $f(S_{wave})$	Storm Research Scenario			Relative increase		
		Reference	Medium	Extreme	M/R	E/R	E/M
slope	m1	+38 - 4	+5 - 3	+6e - 4	1.32	0.16	0.12
	m2	-34 - 4	-47e - 4	-19e - 4	1.38	0.56	0.56

### 4.2.3 Wave reach impact

Finally, significant wave heights are extracted from the simulation runs along a transect running the length of the wadden divide *Hoher Weg* (see figure 3.17), to evaluate wave development along the tidal flats dividing Jade and Weser under storm conditions. The transect starts landward of the coastal dike line and ends 30 km north at the tip of a sand pit merging into the North Sea.

#### ▪ Windstorm Christian

Figure 4.18 shows results for the European Windstorm Christian for the three scenario levels forced with the coastal key driver wind waves only, excluding atmospheric conditions. The upper panel (a) shows the maximum significant wave height values developing during the simulations along the transect. Within the reference scenarios parts of the tidal flats are not impacted by wind waves. Without atmospheric forcing, the medium and extreme scenario both show diminishing significant wave heights of 0.5 m 15 km from the dike. Similar, panel b shows the mean significant wave height over the storm period along the transect. Analogue to the maxima, wind waves do not affect parts of the tidal flats in the reference scenario without atmospheric forcing. For the ensuing scenario runs, mean wave heights develop on the northern parts, on the seaward side of the island Mellumplate, whilst the area behind the island shows negligible wave development for all three scenarios.

In comparison, results obtained with added atmospheric forcing are shown in figure 4.19 allows wind waves to reach the dike line with 0.5 m given the medium and extreme scenario conditions. Similar to the maximum, the medium and extreme compound scenario with atmospheric forcing, both reveal mean significant wave heights close to 0.5 m south of Mellumplate, which diminish to 0.25 m at the dike. Overall, mean (a) and maximum (b) significant wave heights for European Windstorm Christian show a direct response to increased water depth as well as atmospheric forcing, which allows the waves to travel further towards the coast before breaking as postulated by Niemeyer et al. (2016) reaching and impacting coastal defenses. With increasing water depth and atmospheric forcing in the medium and extreme scenario, the tidal area sheltered by the island of Mellumplate experiences enhanced wave stresses re-mobilizing surface sediments.

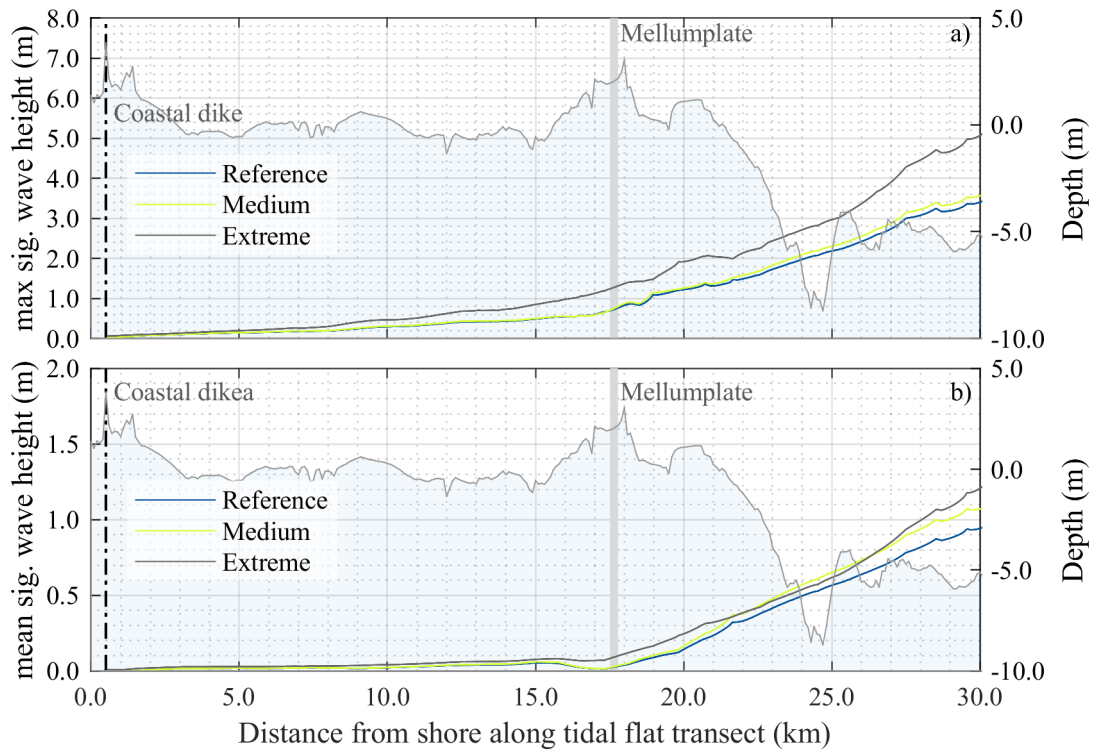


Figure 4.18: Simulation results for sig. max (a) and mean (b) wave heights for ETC Christian for the wind wave scenarios along a transect running along the tidal wadden divide *Hoher Weg*.

▪ Windstorm Xaver

Correspondingly, the transect is evaluated for the compound simulations of European Windstorm Xaver and obtained results displayed in figure 4.20. The wave only forced

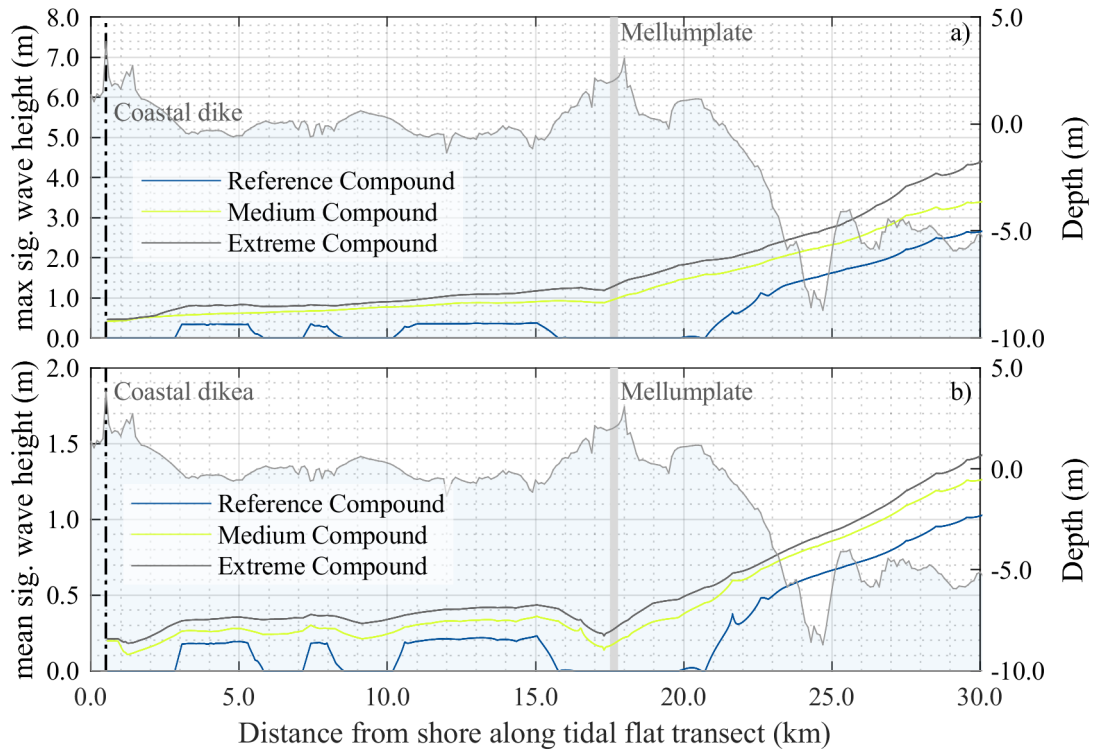


Figure 4.19: Simulation results for sig. max (a) and mean (b) wave heights for ETC Christian for the compound scenarios along a transect running along the tidal wadden divide *Hoher Weg*.

simulations did not yield consistent data, as previously described (see fig.4.15) and are therefore excluded from this evaluation.

The maximum significant wave height values along the transect in fig.4.20 a show a similar signal as the values obtained for the westerly storm event simulations (cmp. fig. 4.18 a) with a distinct kink in the signal, where the small island of Mellumplate is situated. With increasing RMSL in the different cases, the maximum  $H_{1/3}$  increases, while the increase is non linear between the scenarios. In contrast to the westerly storm event, the Jutland type scenario shows larger values along the tidal ridge of the Hohe Weg. The incident signal is reduced transitioning from the deeper North Sea onto the shelf with its sand bars and tidal channels 25 km to 20 km off the coast. The island of Mellumplate exhibits a wave reducing impact on the signal. Directly south of Mellumplate (17.5 km) the reference scenario shows values of up to 1.0 m, which are maintained almost all the way to the dike, crossing the dike foreshore the signal is slightly reduced impacting the coastal defense structure with 0.65 m. The medium and extreme compound events (X MWAFD & X EWAFD) show a similar signals with larger magnitudes. In the medium scenario max-

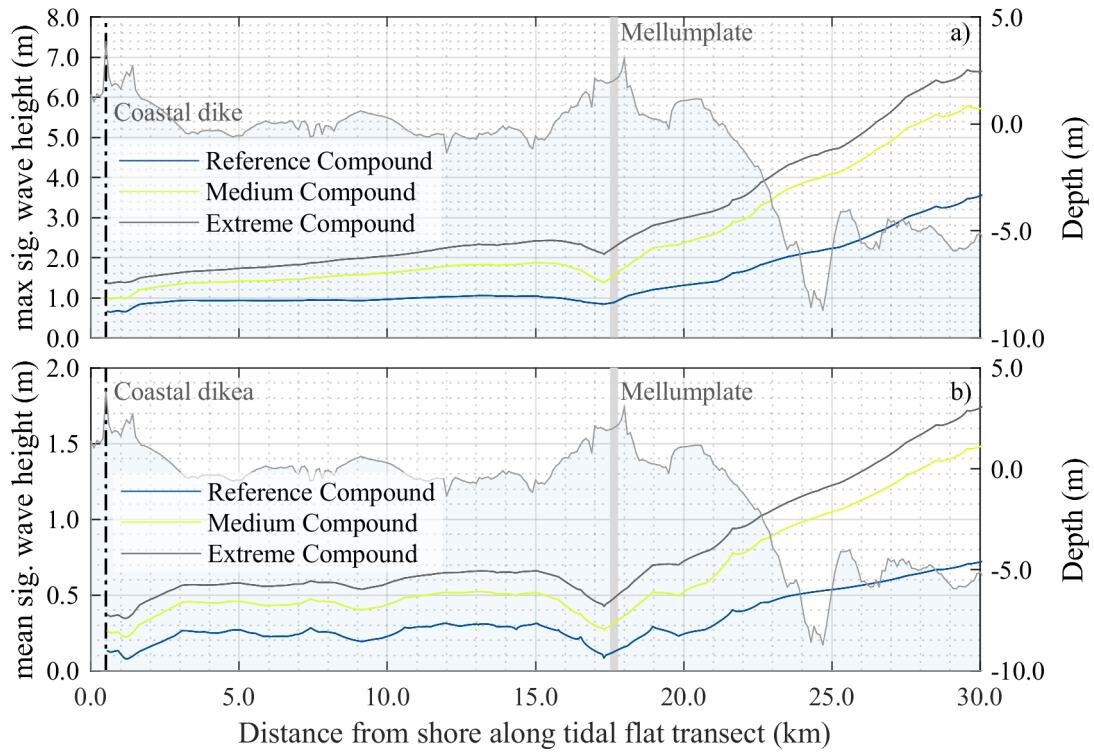


Figure 4.20: Simulation results for sig. max (a) and mean (b) wave heights for ETC Xaver for the compound scenarios along a transect running along the tidal wadden divide *Hoher Weg*.

imum significant wave heights of up to 1.0 m impact the coastal dike, while the extreme scenario shows values of up to 1.5 m.

Corresponding mean sig. wave height values are given in figure 4.20 b and exhibit very similar characteristics, with smaller magnitudes. Mean sig. wave height values reach 0.25 m to 0.55 m along the Hohe Weg. The dike foreshore here is characterized by the *Langwarder Groden*, which extends close to a kilometer onto the tidal flat in front of the coastal dike and is enclosed by a summer dike, dissipating incoming wave energy.

### 4.3 Morphologic impact

Storm induced sea bed changes for the different scenario simulations are computed using the cell related depth changes and surface area per time step for the coastal region entailing the Jade as well as the Outer Weser. Changes are summarized, yielding the net volume change under the storm simulations. Results are presented in section 4.3.1. Furthermore, morphological bed evolution is evaluated for the compound event simulations over the storm periods visualizing sea bed changes in conjunction with residual transport directions and magnitudes. Results are compiled in section 4.3.2 for areas of the focus region to assess potential impacts upon critical coastal infrastructure.

#### 4.3.1 Net sediment volume changes

##### ▪ European Windstorm Christian

Obtained signals for the different coastal key driver simulations for European Windstorm Christian, with different impacts attributed to individual key drivers for the reference scenarios (figure 4.21), analogue results for the medium scenarios (figure 4.22) and finally the extreme conditions (figure 4.23).

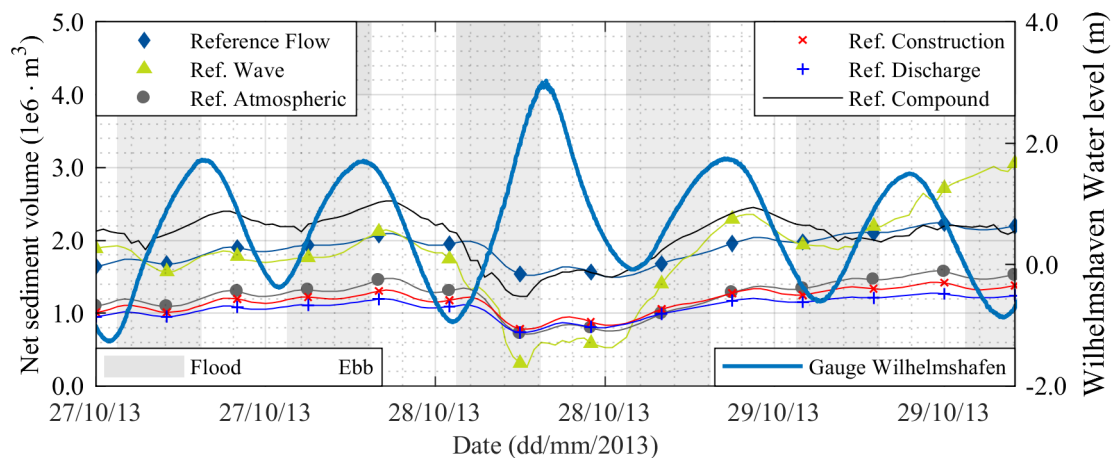


Figure 4.21: Net sediment changes for European Windstorm Christian for the reference scenario for individual coastal key drivers and combined metocean forcing.

Impact magnitudes of individual coastal key drivers show no linear superposition for any of the three scenarios. Throughout the storm simulations the focus region remains a net depositional environment, despite the large erosive impact of European Windstorm Christian. Largest individual impact show the wave forced scenarios from  $-1.88 \times 10^6 \text{ m}^3$  and  $-1.96 \times 10^6 \text{ m}^3$  in the reference (Ref. Wave, see figure 4.21) and

medium (Medium Wave, see figure 4.22) scenario and up to  $-2.4 \times 10^6 \text{ m}^3$  in the extreme scenario (Extreme Wave, see figure 4.23).

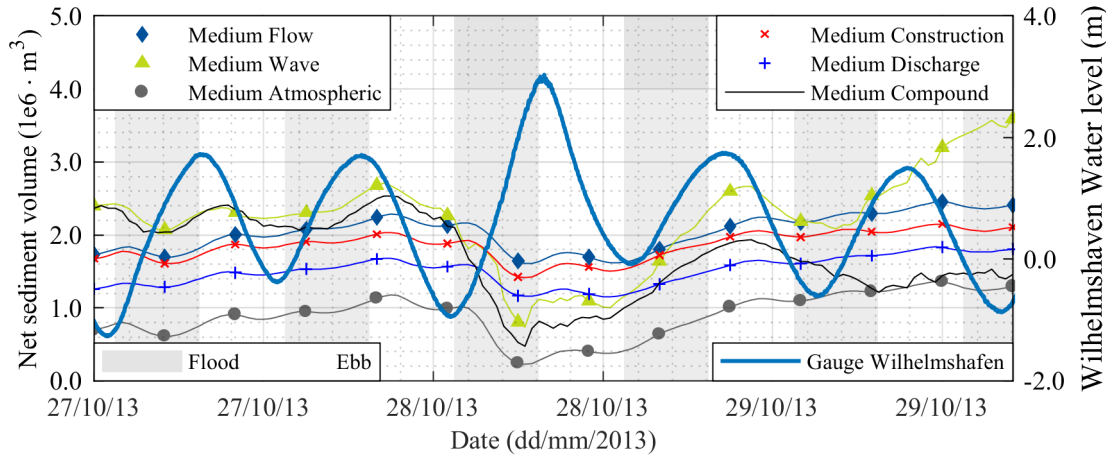


Figure 4.22: Net sediment changes for European Windstorm Christian for the medium scenario for individual coastal key drivers and combined metocean forcing.

Secondary impact magnitudes are revealed by the scenarios entailing atmospheric forcing. Here the reference scenario bears a  $-7.6 \times 10^5 \text{ m}^3$  impact (Ref. Atmospheric, cf. figure 4.21), while the medium scenario shows an enhanced impact of  $-9.3 \times 10^5 \text{ m}^3$  (Medium Atmospheric, cf. figure 4.22), the extreme case reveals a reduced impact of  $-6.5 \times 10^5 \text{ m}^3$  (Extreme Atmospheric, cf. figure 4.23).

The increased water depth due to RMSL of 1.5 m in extreme atmospheric scenario reduces surge related effects, as the model domain is inundated to an extent, where atmospheric processes do not result in added sediment transport due to episodic overflowing of tidal shoals anymore. Generally, the impact attributed to atmospheric forcing is one order of magnitude smaller than the wave impacts. Impacts related to discharge and constructional changes show comparable signals and magnitudes with  $-4.5 \times 10^5 \text{ m}^3$  to  $-5.8 \times 10^5 \text{ m}^3$  for the discharge related impacts and  $-5.4 \times 10^5 \text{ m}^3$  to  $-6.5 \times 10^5 \text{ m}^3$  for the constructively altered model geometries (Ref. Discharge, cf. figure 4.21; Medium Discharge, cf. figure 4.22; Extreme Discharge, cf. figure 4.23).

The scenarios resembling the compound events, entail all coastal key drivers. The reference scenario for Windstorm Christian reveals an impact of  $-1.3 \times 10^6 \text{ m}^3$ , with a net change signal following the tidal storm characteristics for two tidal cycles, before the Windstorm impacts the model domain and exerts bed shear stresses mobilizing surface sediments and transporting them out of the model domain, into the North Sea (see figure 4.21). During the two tidal cycles following the storm peak, the net volume signal recovers almost to its previous level once more developing its net depositional (positive)

trend, but without pronounced tidal influence. Only one tidally influenced peak can be observed after the storm, which constitutes the systems readjustment to the increasing atmospheric pressure after the storm system passes through the area and the surge recedes.

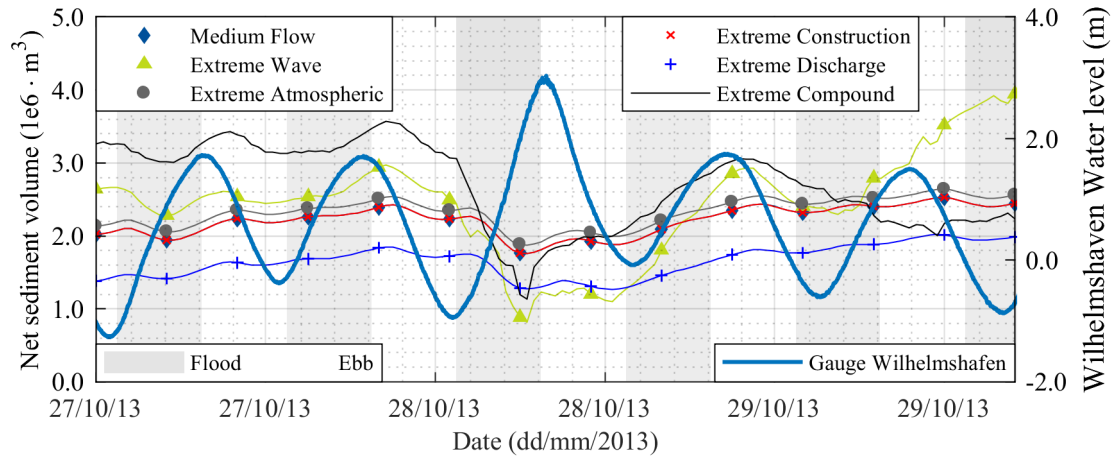


Figure 4.23: Net sediment changes for European Windstorm Christian for the extreme scenario for individual coastal key drivers and combined metocean forcing.

The medium compound event scenario (Medium compound) results in a storm related impact of  $-2.1 \times 10^6 \text{ m}^3$  (see figure 4.22). Similar to the reference scenario, the signal follows the tidal water level prior to the storm peak but shows a less depositional trend compared to the reference scenario. In contrast to the reference scenario, the post storm peak signal does not recover to the same level as before the storm but remains approximately  $1 \times 10^6 \text{ m}^3$  below the entrance level. Like the reference scenario, the post storm peak signal shows one peak as the system readjusts to the receding surge but afterwards the signal does not directly retain its positive trend but levels out and requires a couple of days until it regains its positive trend. The unlikely Extreme compound event induces a morphological impact of  $-2.4 \times 10^6 \text{ m}^3$  and shows an ensuing recovery of the signal (see figure 4.23). Similar to the medium compound scenario, the signal exhibits a post-storm peak of  $1 \times 10^6 \text{ m}^3$ , as the system readjusts to the falling surge level, which drops again resulting in a signal level  $1.5 \times 10^6 \text{ m}^3$  below the entrance level. What is more, the signal does not regain a positive trend shortly after the storm as the impact is too large.

### ■ European Windstorm Xaver

Cumulative morphodynamic signals corresponding to individual coastal key drivers under European Windstorm Xaver are computed and shown in figure 4.24 for the reference case, the medium scenario in figure 4.25 and the extreme compound event results are shown in figure 4.26.

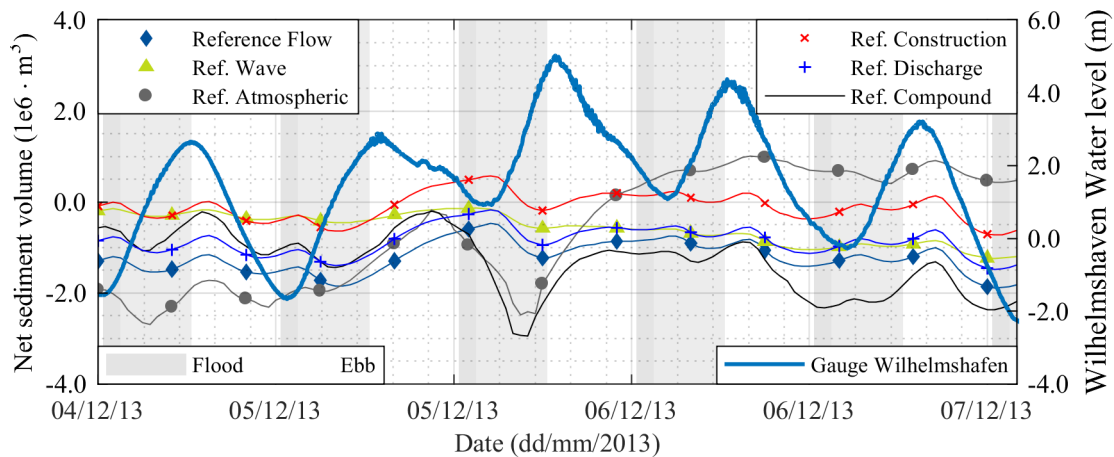


Figure 4.24: Net sediment changes for European Windstorm Xaver for the reference scenario for individual coastal key drivers and combined metocean forcing.

Similar to the simulations for the Skargarak type event, this Jutland type storm exhibits the largest single driver impact signal under wave forcing alone. The reference scenario shows a fluctuating signal, which exhibits a signal spike of  $1.3 \times 10^6 \text{ m}^3$  from  $-0.5 \times 10^6 \text{ m}^3$  to  $0.7 \times 10^6 \text{ m}^3$  during the storm's maximum intensity. Followed by a sudden drop of  $-1.7 \times 10^6 \text{ m}^3$  as the storm eye passes over Scandinavia, it ramps up again once the rear frontal system of the European Windstorm leaves the focus area reaching values of  $1.2 \times 10^6 \text{ m}^3$ , depositing large quantities of material, resulting in a net depositional impact (see figure 4.24). For the medium and extreme compound simulations, this characteristic signal is observed as well (cmp. figures 4.25 & 4.26), with the difference that the medium scenario shows values of  $3 \times 10^6 \text{ m}^3$  for the signal spike, a  $-3.5 \times 10^6 \text{ m}^3$  drop to  $2.0 \times 10^6 \text{ m}^3$  and finally a ramp up to  $7.5 \times 10^6 \text{ m}^3$ , once the storm passes over Scandinavia. The extreme case reveals values of  $3.75 \times 10^6 \text{ m}^3$  for the spike,  $-3.75 \times 10^6 \text{ m}^3$  for the drop and a ramp up to  $13.5 \times 10^6 \text{ m}^3$  as the storm diminishes.

Second largest signal response is found in wind and pressure forced simulations, which also exhibit a signal spike under the maximum storm intensity reaching  $-0.4 \times 10^6 \text{ m}^3$  within the reference scenario (see figure 4.24). However, unlike the wave forced simulations, the atmospheric boundary conditions result in a step wise drop of the cumulative signal, following the tidal water level, entraining material with every tidal high water



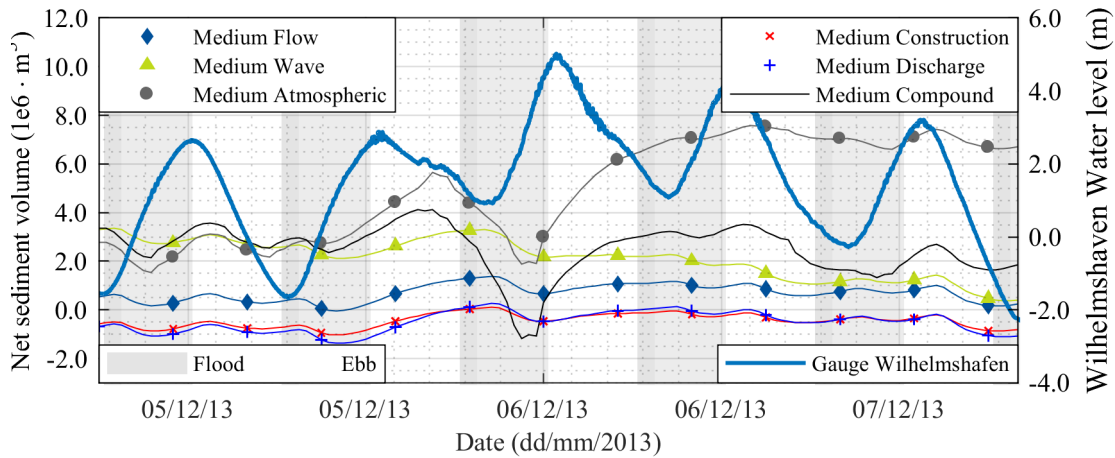


Figure 4.25: Net sediment changes for European Windstorm Xaver for the medium scenario for individual coastal key drivers and combined metocean forcing.

and eroding it into the North Sea during ebb. This process leads to a consecutive signal decline reaching  $-2.95 \times 10^6 \text{ m}^3$  by the end of the storm, resulting in a net export of sediment. Tidally forced simulations (Ref. Flow / Medium Flow / Extreme Flow) show a characteristic behaviour, with a 5 h delayed signal spike of  $1.2 \times 10^6 \text{ m}^3$  to  $1.8 \times 10^6 \text{ m}^3$  across the three different RMSL scenarios (cmp. figures 4.24, 4.25, 4.26). Nevertheless, the hydrodynamically forced simulations all show a declining signal, which ranges within the net erosion zone for the reference case and changes to positive values for the medium and extreme cases, as the overall moved volumes increase but maintains its negative trend resembling a net export due to tidal currents. Other key drivers such as the inland discharge or the constructively altered bathymetry reveal impacts inferior to the other two, as they mainly impact overall water volume fluxes and act as auxiliary processes for transporting material already entrained by the wind waves. Consequently, these processes show marginal influences with a signal peak of  $1 \times 10^6 \text{ m}^3$  to  $1.5 \times 10^6 \text{ m}^3$  for the discharge scenario across the three cases, with an overall net export of material. The constructive changes result in comparatively small impacts as well with  $0.9 \times 10^6 \text{ m}^3$  to  $1.7 \times 10^6 \text{ m}^3$  spikes and ensuing net export trends, closely resembling the tidally forced simulation signal.

The extreme compound simulations show the largest amplitude variations, as the simulated waves mobilize surface sediments from the tidal flats, from where these are transported by the different physical processes. The reference scenario shows a peak of  $0.8 \times 10^6 \text{ m}^3$  under the storm peak during slack tide, with an adjacent steep drop of  $-2.8 \times 10^6 \text{ m}^3$ , as the out-flowing ebb tide transports entrained material out of the estuary. With the ensuing high tide, the entrained material is re-imported and settles during slack tide, causing a large depositional signal of  $1.9 \times 10^6 \text{ m}^3$ . Despite the slack

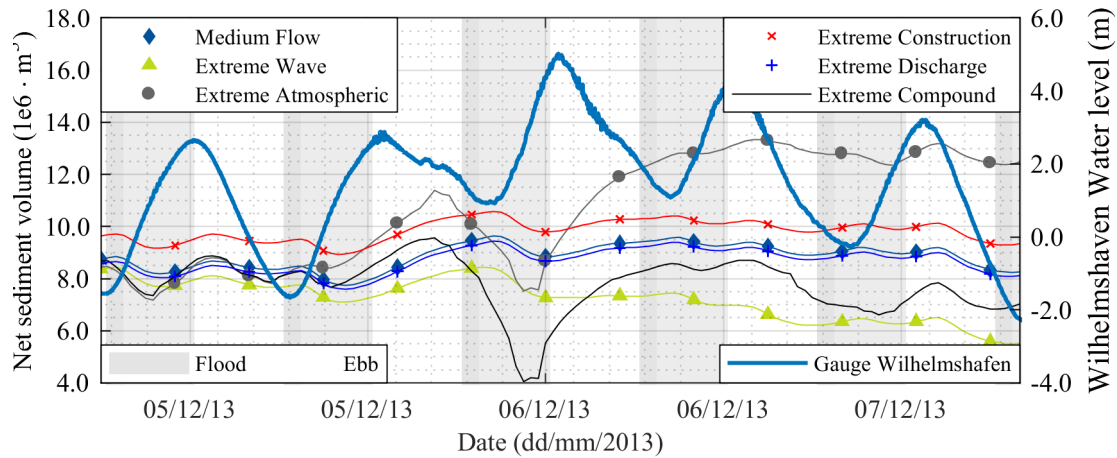


Figure 4.26: Net sediment changes for European Windstorm Xaver for the extreme scenario for individual coastal key drivers and combined metocean forcing.

tide effects, the combined metocean forcing results in a step-wise decline following the sequential pattern of the tidal high and low waters under storm surge conditions. Very similar signals are found for the medium and extreme compound event simulations, which exhibit larger overall volumes but a net export of material.

### 4.3.2 Morphologic bed evolution

Utilizing the numerically approximated bed evolution, difference maps are generated based on the pre- and post-storm model bathymetry. Changes are depicted as  $\delta z$  in  $m$ . Additionally, the total transport, resultant of the five sediment fractions transported in suspension as well as bed load, for every grid cell and time step during the storm period is extracted for the numerical grid and averaged, readily yielding residual transport vectors of direction and magnitude. Individual transport directions and magnitudes for the different fractions and transport modes (suspended/bed) have been investigated but no directional mode was identified for the coastal region of interest as both suspended and bed load transport residuals reveal nearly identical directions with largest differences amounting to  $5^\circ$ .

#### ▪ European Windstorm Christian

Results obtained for the reference compound simulation of European Windstorm Christian are given in figure 4.27 for the Outer Jade and the transshipment complex in a) and b) respectively. Main transport pathways are accentuated with gray arrows for better visibility and due to scaling only every  $28^{th}$  value is shown.

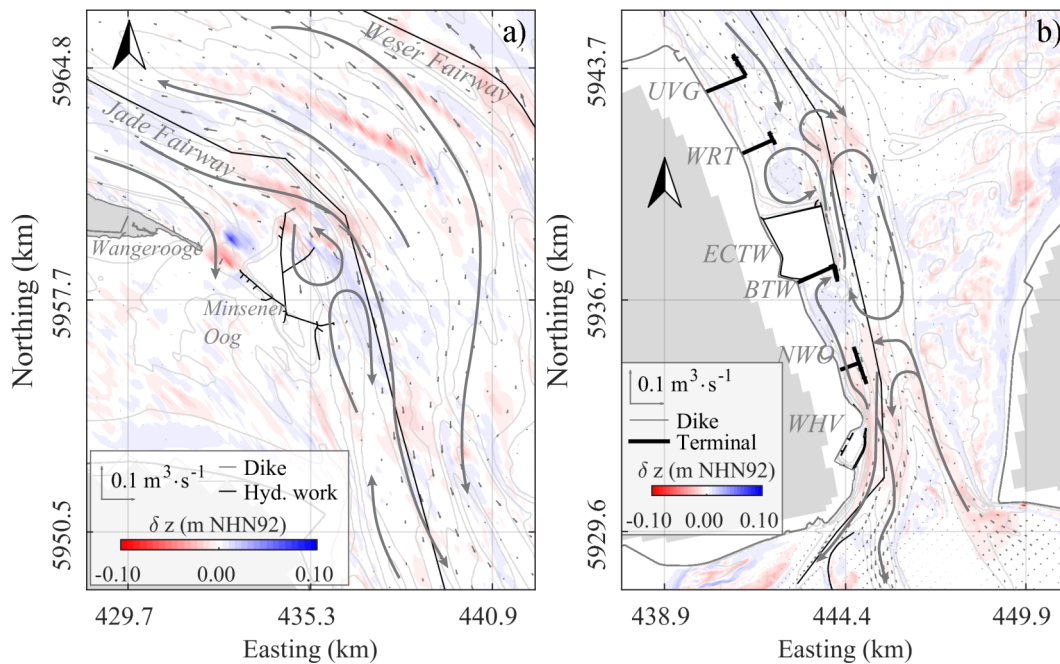


Figure 4.27: Morphological impact reference scenario Christian with a) the outer Jade and b) the transshipment complex Wilhelmshaven.

The Outer Jade (see 4.27a) shows depositional areas in the deeper area north of Wangerooge, as well as east of the island Minsener Oog and near the coastal dike on the back barrier tidal flats south of Wangerooge and Minsener Oog. Erosive tendencies are identified due north of Minsener Oog within the Jade fairway, as well as south east of Minsener Oog within the Jade fairway. Furthermore, the sand spit lining the Jade fairway to the north east shows erosion along its crest as does the Outer Weser fairway. The imminent back barrier tidal flats show predominantly erosive tendencies due to wave stresses. The sea gat between Wangerooge and Minsener Oog shows erosion on the southern end and deposition on the northern, forming an ebb tidal delta (Herrling and Winter, 2015). Transport residuals are directed north west along the outermost part of the Jade fairway and subtended in the Jade fairway east and south of Minsener Oog, directed inland. Similar, the southern bank of the Weser fairway shows south east directed transport, whilst the northern side is characterized by north west directed residuals. Along the east side of Minsener Oog two large elongated re-circulation zones are identified, which have been defined before in literature (Kubicki et al., 2017). Along the east side of the bend of the Jade fairway, another elongated re-circulation is identified, covering an extensive dune field (Kubicki et al., 2017; Kubicki and Bartholomä, 2011). The northern shoreline of Wangerooge exhibits littoral shore transport.

The transshipment complex (see 4.27b) shows a depositional tendency along the north-

ern part of the Jade fairway lining the terminals *UVG & WRT* with flood directed residual transport. The north and south flanks of the ECTW are also depositional environments, with 0.04 m to 0.07 m increased bed height. However, the fairway north of the ECTW shows erosive tendencies, while the immediate jetty front of the ECTW exhibits accretion of 0.06 m. The area around the *NWO* as well as the deep tidal channels entering the Jade Bight show erosion. Wilhelmshaven shows a depositional region at the harbor entrance, which has been detected before (see appendix A.7). Transport residuals are smaller compared to the Outer Jade region (cmp. 4.27a) and predominantly show transport directions along the deeper Jade channel, with the northern and eastern/southeastern part of the fairway showing inland directed vectors, while the ECTW is framed by a residual transport vortex to the north of the terminal, which rotates counterclockwise and is mainly ebb driven, while the southern side of the terminal shows a constriction of the ebb stream between the western bank, the BTW to the east and the ECTW to the north, greatly reducing the flow velocity (cmp. figure 4.9 R3) resulting in a settling of ebb entrained sediment. Furthermore, the jet-like current between the structures induces a local scour, which has been observed in nature (see appendix A.8). The jetty of the ECTW is lined by ebb driven residuals, while further into the fairway the residuals are directed into the Bight, creating a shear zone, with a corresponding depositional area. The area around the *NWO* shows ebb directed residuals, while similar to the ECTW the deeper fairway exhibits inland directed transport residuals. Along Wilhelmshaven and through the neck of the Jade into the Bight, transport residuals are largest with southern direction following the channels of the Stenkentief to the south west and the Vareler fairway to the south. The Ahne to the south east shows ebb directed transport residuals, which continue northward and form a zone of confluence at the height of the BTW, resulting in a counterclockwise residual transport circulation.

For the medium scenario, the main residual transport ways are identical to those identified within the reference scenario, thus a renewed accentuation is not needed (for pathways see figure 4.27). Results are depicted in figure 4.28.

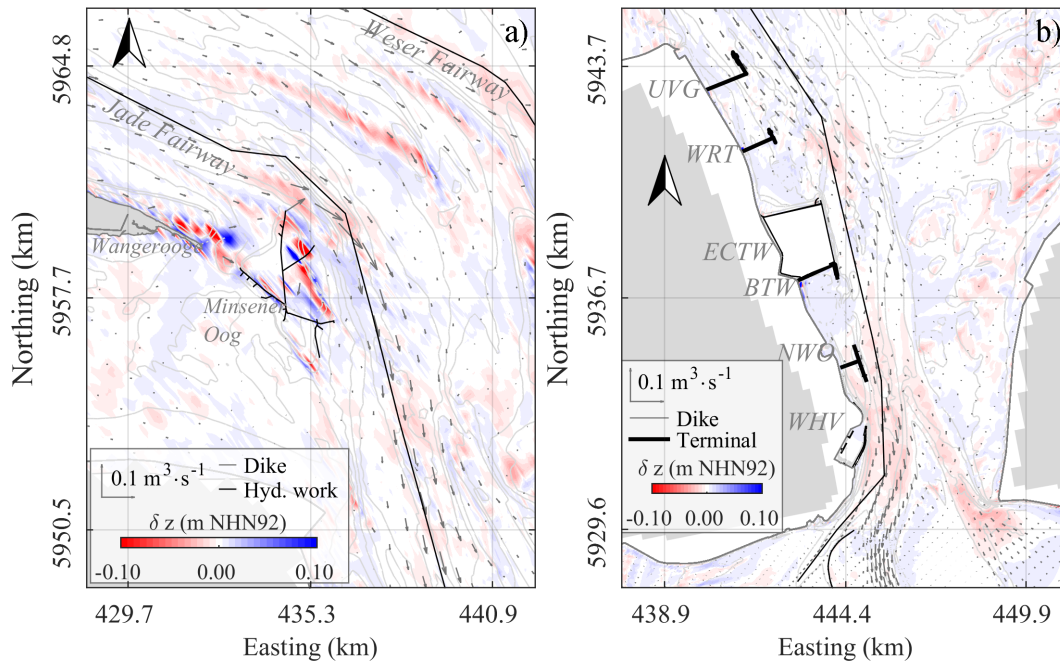


Figure 4.28: Morphological impact medium scenario Christian with a) the outer Jade and b) the transshipment complex Wilhelmshaven.

Overall transport magnitudes increases as do the bed elevation changes. For the Outer Jade (see figure 4.28a) the eastern beach head of Wangerooge shows erosion, with a depositional band leading through the sea gat onto the back barrier island tidal flats. The hydraulic structure Minsener Oog shows pronounced areas of erosion and deposition within its groyne field system, while the northern head of the artificial island as well as the Jade tide channel north of it show erosion, with transport residuals indicating a transport into the dune field east of Minsener Oog, reducing the navigational depth. At the southern tip of Minsener Oog a local scoure occurs due to prolonged inundation and elevation current velocities flowing over the tidal flats around the structure (cmp. figure 4.9 M2). The transshipment complex (see figure 4.28b) reveals an extension of the eroding areas north of the ECTW as well as along the neck leading into the Bight by 2.1 km, reaching almost midway between NWO and BTW. Furthermore, the depositional areas along the eastern bank of the Jade tide channel are extended and previous erosion areas reduced, due to the increased water level of 0.74 m. The depositional extent inside the Wilhelmshavener port entrance is extended further into the port basin.

Results for the extreme scenario are given in figure 4.29. A changes in main residual transport pathways has been identified for the Outer Jade area. The ridge of the sand spit lining the north eastern side of the Jade fairway shows erosion similar to the previous simulations but the residual transport pathways have redirected from previously

north-west to south-east into the Jade, disrupting the previously established recirculation area along the northern end of the dune field. Overall bed elevation changes increase in magnitude compared to the reference and medium scenarios. The back barrier tidal flats south of Wangerooge (see figure 4.27a) reveal erosion, where the other two simulations predominantly show accretion. This is attributed to the wave stresses and increased water levels during the storm, inundating the tidal flats. Similar to the medium scenario, the north of Minsener Oog and the Jade fairway show erosion, with adjacent accretion areas east of Minsener Oog inside the dune field. Furthermore, the previously ebb directed transport path along the western bank of the Jade fairway south of Minsener Oog is inverted within the extreme scenario and shows flood directed vectors and erosive tendencies compared to depositional before.

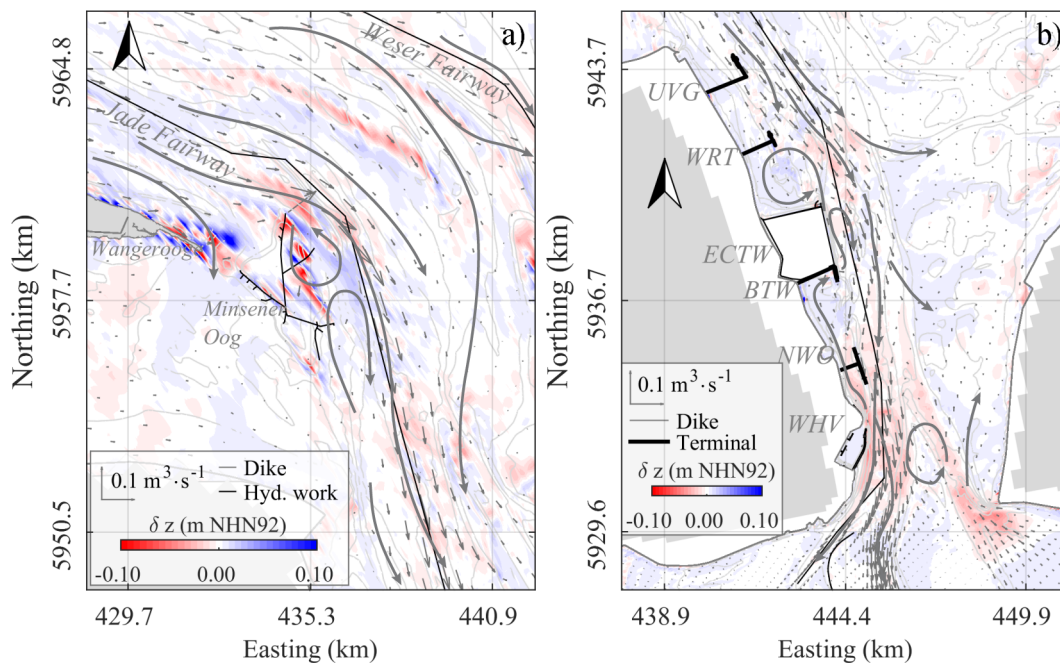


Figure 4.29: Morphological impact extreme scenario Christian with a) the outer Jade and b) the transshipment complex Wilhelmshaven.

Analogue to the Outer Jade, main residual transport pathways have changed along the transshipment complex as well (see figure 4.29b). The previously existend complex pattern of re-circulation cells along the fairway is disrupted due to elevated current velocities. The vortex at the northern flank of the ECTW prevails but the re-circulation to the east inside the fairway is tided over by the amplified environmental conditions and shows flood dominated inland directed transport residuals. Similar, the large elongated re-circulation zone stretching along the fairway in front of the ECTW has been dimin-

ished and is confined to the proximity of the ECTW jetty. The NWO terminal is engulfed by flood directed residuals, compared to ebb directed ones during the previous simulations but the area remains erosive. Wilhelmshaven shows accretion within the whole port basin of 0.05m, while the fairway along the Jade neck shows accentuated erosion. What is more, the erosion perviously reaching midway between the BTW and NWO, reaches the southern tip of the ECTW within the extreme scenario. The Ahne channel shows flood directed residuals inside the Jade Bight and ebb directed vectors north of the neck of the Bight. Additionally, a small re-circulation area has established at the confluence of the Vareler and Ahne channels, rotating counter clockwise, indicating ebb related forcing. Finally, along the east bank of the Jade channel, accretion can be seen to extend onto the Hohe Weg tidal flat area in comparison to the previous simulations. A comparison between the simulations shows, that with increasing RMSL the peripheral affected by erosion lining the accretion dominated area extends further onto the tidal flat area, affecting more highly situated regions. Analogue to this pattern, the shift is also observed within the Jade Bight, where the affected areas extent with the medium scenario and are relocated directly onto the dike toe lining the Bight and the Hohe Weg tidal area.

▪ **European Windstorm Xaver**

Complimentary to the Scandinavian type storm, European Windstorm Xaver, constituting a Jutland type event, is simulated and morphodynamic changes visualized in figure 4.30 for the Outer Jade as well as the transshipment complex. For better visibility every 26<sup>th</sup> value is shown in a) and every 12<sup>th</sup> in b).

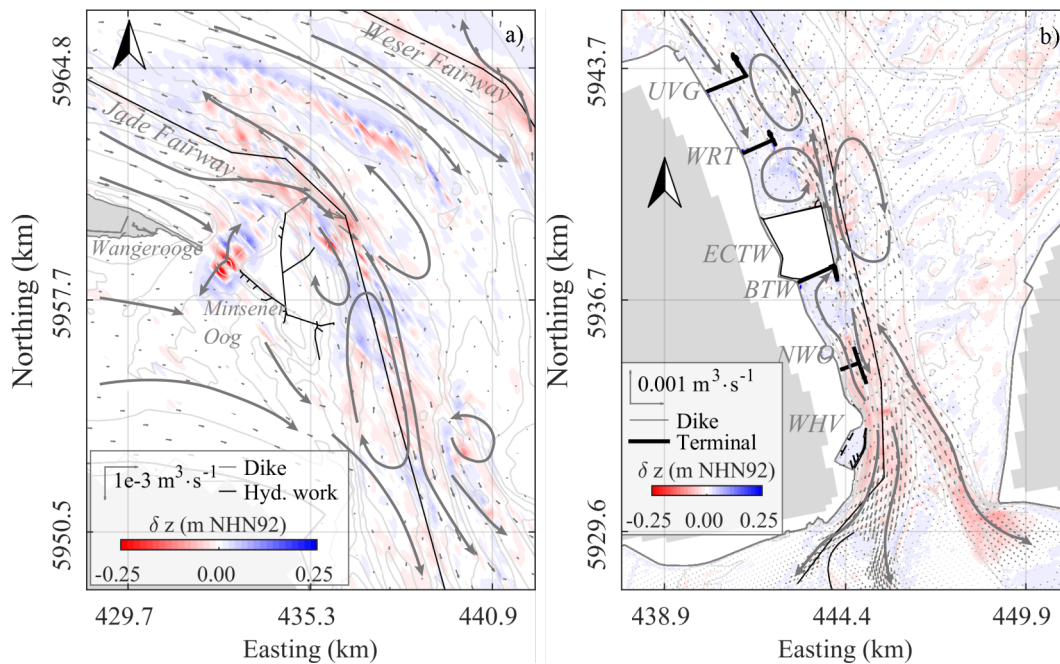


Figure 4.30: Morphological impact reference scenario Xaver with a) the outer Jade and b) the transshipment complex Wilhelmshaven.

The simulation of European Windstorm Xaver induces transport residual pathways similar to those found for the reference simulation of European Windstorm Christian, with elongated re-circulation zones found along the Jade fairway. The back barrier tidal area south of Wangerooge and Minsener Oog (see fig. 4.30 a) shows depositional tendencies, with a distinct eastward alongshore transport band entering the Jade fairway. Overall, the transport magnitudes along the Outer Jade are an order of magnitude larger than those induced by Windstorm Christian. Along the transshipment complex lining the Inner Jade, three large ebb driven re-circulation zones are identified occurring at the terminals UVG, WRT and the ECTW (see fig. 4.30 b). North of the ECTW the western bank of the Jade shows flood directed transport residuals, with accretion areas around the terminals. Confined by the western bank, the ECTW to the north and the BTW to the east, entrained material settles at the southern flank of the ECTW. Around the NWO terminal, erosive tendencies due to elevated current velocities are identified, with



ebb directed transport residuals between the coast and the terminal jetty, and flood directed residuals on the eastern jetty side. The foundations of the terminals show local accretion of up to 0.17 m. During the storm, the New Outer Harbor of Wilhelmshaven shows an areal mean accretion of 0.11 m. Meanwhile, the deeper Jade tidal channel lining the neck of the Bight shows erosion along its tidal channel system, with magnitudes of  $-0.12$  m to  $-0.18$  m eroding material with residual transport vectors pointing into the Jade Bight for the western side of the main channel, splitting into the Stenkentief and the Vareler fairway. The Ahne channel to the east however shows net export north of the narrowest point at the Prussian corner and net import south of it. The Hohe Weg tidal flat shows accretion taking place inside the tidal channel system intervening the space between the shoals which are eroded. Compared to the reference scenario of the Skargarak type storm, Windstorm Xaver induces larger sea floor changes

Morphologic results for the medium compound event for European Windstorm Xaver are depicted in figure 4.31. The main residual transport pathways are identical to those identified in the reference scenario and thus are not accentuated (for pathways see fig. 4.30).

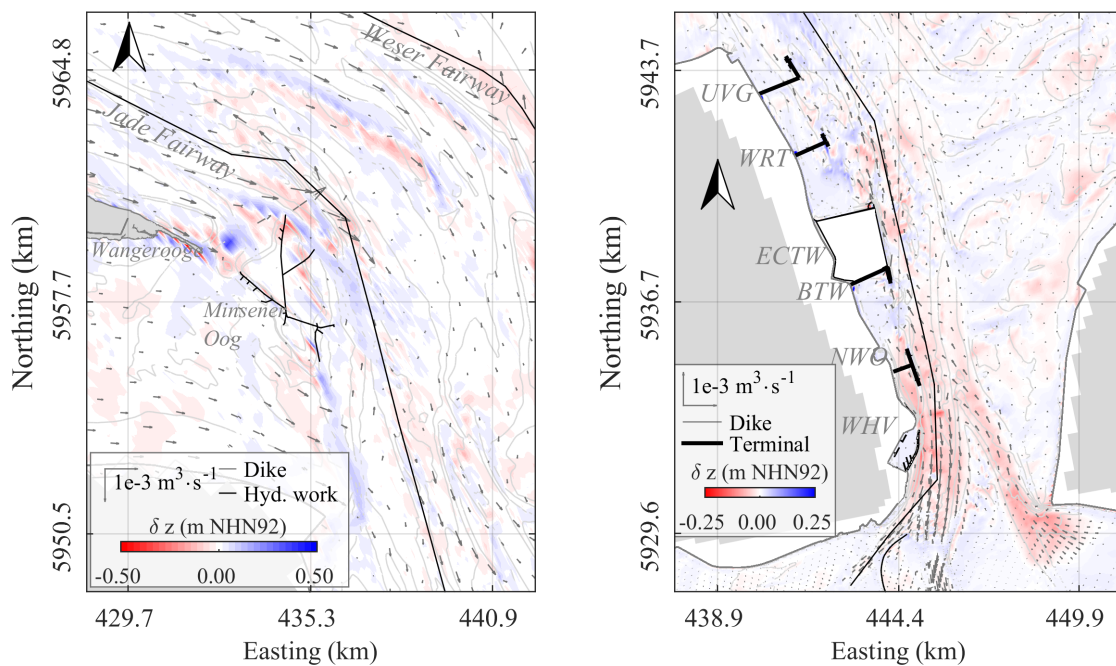


Figure 4.31: Morphological impact medium scenario Xaver with a) the outer Jade and b) the transshipment complex Wilhelmshaven.

However, the resulting sea bed changes differ from those obtained for the reference scenario, in that the back barrier tidal area of Wangerooge is predominantly eroded

by the increased storm surge currents, transporting material eastward into the Jade channel system (see fig. 4.31 a). The transition zone between the estuary with its sand spits and tidal channels and the deeper North Sea reveals extensive accretion in the deeper water zone, while the sand bars and ridges lining the tidal channels of Jade and Weser are eroded, revealing an off shore transport of mobilized material. Results along the transshipment complex (see fig. 4.31 b) reveal a pattern of accretion and erosion similar to that found in the reference scenario. Noteworthy are the elevated magnitudes of sea bed elevation changes, which reach up to 0.5 m differences along the Outer Jade and up to 0.28 m along the transshipment complex.

The extreme compound event simulation results in figure 4.32 show a change in residual main transport pathways, which was identified and accentuated by renewed main transport pathways. In the wake of Minsener Oog the circulation zone is pushed into the Jade channel south and elongated by the exerted storm forces. Overall transport residuals are up to three times larger compared to the Reference scenario (cmp. fig. 4.30 a). The minor circulation zone on the eastern bank of the tide channel at the entrance to the Inner Jade is suppressed by the amplified boundary conditions.

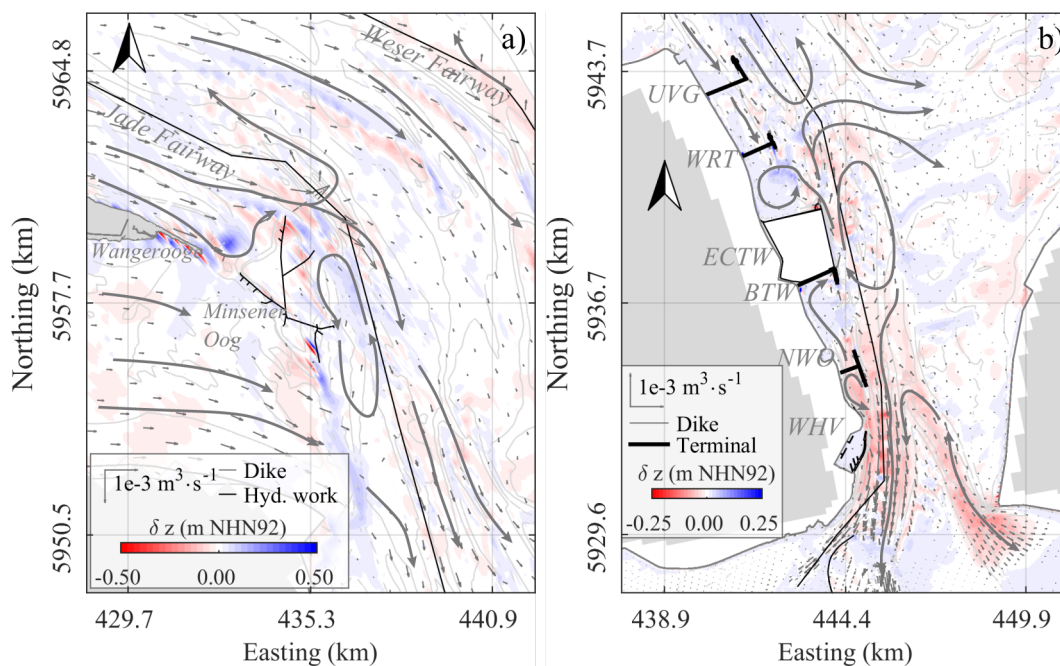


Figure 4.32: Morphological impact extreme scenario Xavier with a) the outer Jade and b) the transshipment complex Wilhelmshaven.

The back barrier tidal zone of Wangerooge shows erosion similar to the other cases, with an adjacent band of accretion lining the western bank of the Jade tide channel, where

the water depth increases and entrained material is settling due to reduced alongshore transport current (cmp. fig. 4.10 E2).

The Inner Jade shows changes in residual transport pathways in the extreme storm scenario as well (see fig. 4.32b). Between the terminals UVG and WRT at the northern end, the residual transport vectors form a U-shaped trajectory leaving the Inner Jade northward. The ECTW jetty is lined by a rotary residual transport pattern following a clockwise rotation, with large residual vectors branching off at the northern corner of the ECTW pointing east and west, as the vectors from the north describe a U-shape. Here the residual transport pathways seem to collide and are redirected, resulting erosion. To the west a rotary pattern forms an accretion zone on the northern flank of the terminal, similar to the previous simulations. To the east the residuals fan out onto the Hohe Weg tidal flat, where accretion zones are formed along the deeper channel systems, while the elevated shoals are eroded. South of the ECTW, transport residuals point into the Jade Bight, following the deep main channel, branching into the Varerler fairway and the Stenkentief to the west. To the east, the Ahne channel shows a bi-directional transport pattern in combination with an erosion zone. To the north of this zone, the vectors describe a turnaround to the south-west into the two other tidal channels. South of the Perussian corner, the vectors fan out onto the extensive tidal flats of the Jade Bight. What is more, behind the NWO terminal a rotary pattern is found, indicating a counter-clockwise directed re-circulation zone in front of the WHV. The WHV finally, shows mean areal accretion of 0.15 m with an elevated bar of 0.2 m forming in the entrance (see fig. A.8), which is also found in nature (cmp. fig. A.7). This phenomenon is observed within the previous two simulations for the medium and the reference scenario of Windstorm Xaver as well with smaller magnitudes.

### 4.3.3 Hydraulic development scenario

Finally, simulations with an altered bathymetry resembling a northward extension of the ECTW for both storms are carried out for the three different RMSL levels under hydrodynamic forcing only. Results for the reference scenarios with no altered water levels are shown in figure 4.33.

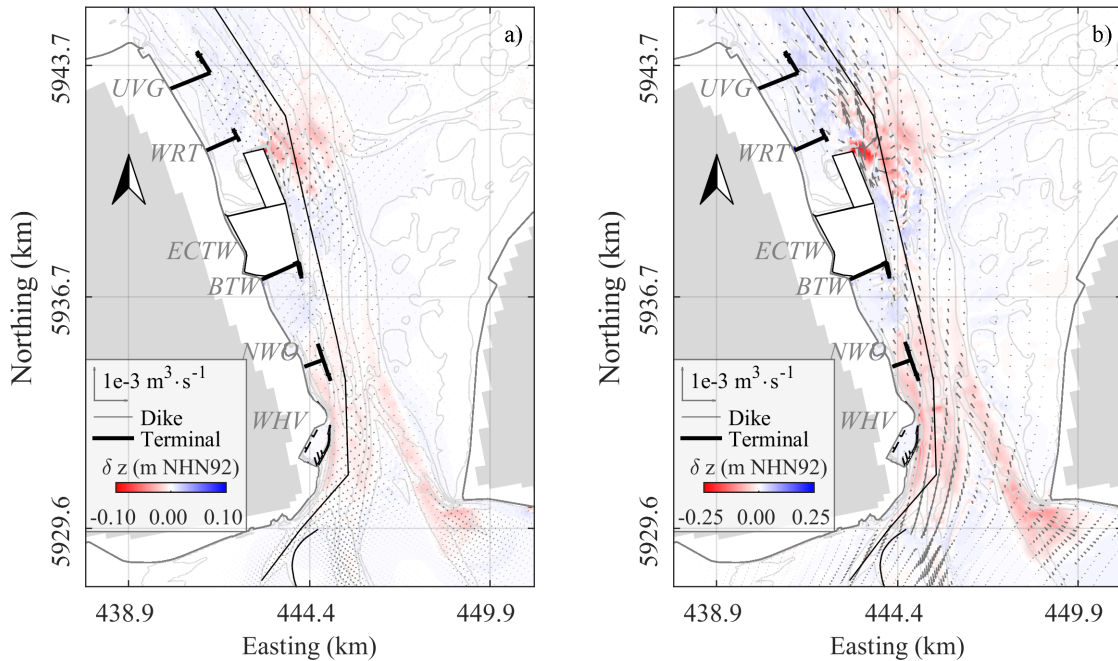


Figure 4.33: Morphological impact under hydraulic development of the northward extension of the ECTW for the reference scenario of Windstorms Christian a) and Xavier b).

Both storm scenarios induce erosion at the north-east corner of the jetty head of the ECTW extension, inducing bed level changes of 0.1 m directly at the toe of the structure under storm Christian and up to 0.34 m under storm Xavier. Both simulations affect a large area showing erosion due to the altered residual current patterns (cmp. fig. 4.11). The spatial extent of the eroded area reaches 500 m to 750 m along the Jade fairway. With increasing RMSL local scouring intensifies to 0.14 m and 0.16 m for Windstorm Christian and 0.38 m and 0.47 m for Windstorm Xavier under medium and extreme RMSL conditions respectively. These simulations reveal, that a further constructive alteration of the Jade tide channel through a planned northward extension of the ECTW may potentially result in local scouring under storm conditions due to changes in current patterns as a consequence of cross profile reduction creating a backwater zone west of the protruding terminal jetty.

### 4.4 Coastal key driver impacts

Emergence from the numerous investigations of hydrodynamic, atmospheric and morphological quantities are the clear non-linear interactions of the permuted coastal key drivers. A visualization for hydrodynamic (blue), wave (green) and morphological (gray) quantities is given in figures 4.34 and 4.35 for European windstorms Christian and Xaver respectively. Given are various scenarios around coastal key drivers indicated with capital letters (T = Tide, W = Wave, A = Atmosphere, Q = Discharge, I = Incision, C = Compound), where C always denotes the compound event with combined forcing under tides, wind, waves and discharge for the reference scenario, medium amplification scenarios and the extreme, unlikely high end, scenarios. Within the reference/medium/extreme boundaries, the influence of individual coastal key drivers, listed on the abscissa, on the respective quantity is referenced to the tidal base case in % on the ordinate, while the size of the spheres is normalized to the individual quantity and again referenced to the tidal base scenario value.

▪ **European Windstorm Christian**

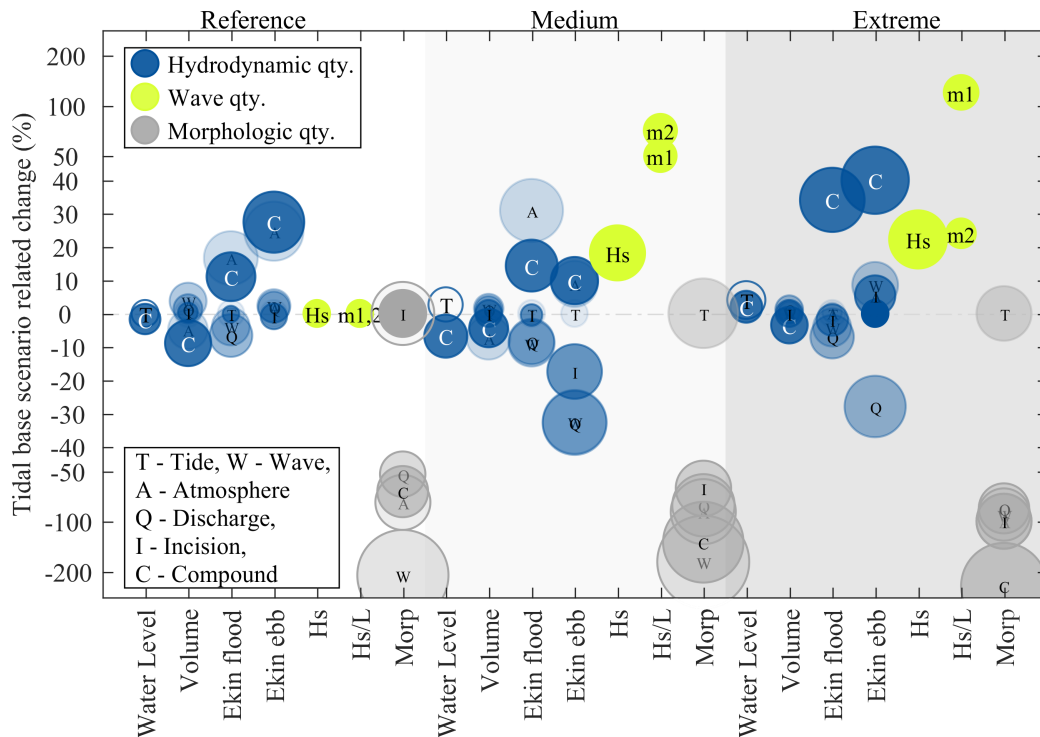


Figure 4.34: Impacts and non-linearity of coastal key drivers on estuarine system quantities for storm Christian.

Hydrodynamic quantities obtained for European Windstorm Christian, presented in figure 4.34 show that the compound events forced by all coastal key drivers dynamically develop an equivocal pattern. Tidal water levels are evaluated areal for the whole model domain and exhibit a reduction across all three scenario levels compared to tidally forced simulations. Surge volumes obtained for individual coastal key drivers vary across a range of  $-8\%$  to  $7\%$ , while the compound simulations unanimously reveal a reducing effect, which decreases with increasing scenario conditions from  $-10\%$  to  $-5\%$  and  $-3\%$ , clearly showing a reduced impact due to geometric constraints of the domain. Cumulative kinetic ebb and flood energy is examined along the line integral of the Jade fairway and shows a mixed pattern with increases of up to  $47\%$  compared to the plain tide scenarios. While the reference and extreme compound scenarios both show larger increases for the ebb related energy, the medium compound scenario shows an inverted situation, with larger cumulative flood than ebb energy. Interestingly the medium scenarios forced with combined tide+wave and tide+atmosphere show strong reduction of kinetic ebb energy due to depth related bed roughness influence, showcasing the effect of increased water depth and larger flood extends upon the complex coastal geometry, which is not as prevalent in the extreme scenarios due to further increased water depth.

Significant wave heights observed at the station Leuchtturm Alte Weser (LAW) show an expected increase across the three scenario levels. Wave steepness is referenced to its respective previous scenario (Medium/Reference and Extreme/Medium) and reveals a strong non-linear increase from the reference to the medium scenarios and again from the medium to the extreme scenarios reaching up to  $187\%$ . This marks a distinct sensitivity of the observation point (LAW) within the focus region towards westerly wind wave events in combination with RMSL and amplified atmospheric conditions, which are projected for this region (cmp. sec. 2.3.5).

Morphological impacts of the compound simulations are erosive and increase from the reference towards the extreme scenario. Individual key driver related sediment transport shows the various levels of erosion tendencies under single driver forcing, whilst the combined simulations do not automatically result in the largest volumes, which are achieved under wave forcing alone for the reference and medium scenario, again showcasing the sensitivity towards westerly wind waves of the model domain. The compound scenarios show an increase in eroded sediment volume, which corresponds roughly to the increase in forcing.

Windstorm Christian shows a non-linear behaviour towards increased compound forcing, with a high sensitivity for westerly wind wave impacts. The reference and extreme cases clearly show the compound scenarios with the largest impacts on nearly all processes. However, for the medium forcing, the compound scenarios are surpassed by single coastal key processes, which show more dominant effects upon an increased water level.

▪ **European Windstorm Xaver**

Results obtained for the European Windstorm Xaver are depicted in figure 4.35. In contrast to the westerly storm event, simulations of this event consistently yield the largest quantities for the compound events emphasizing the northerly surge character of the storm as well as the susceptibility of the focus region towards northerly events. Unlike for windstorm Christian, this event reveals an amplifying effect on surge water levels compared to tidally forced simulations, whilst the westerly event reveals a damping effect due to geographic orientation. The surge volume reveals an increase of 5 % for the reference scenario, which is reduced to 4.7 % and finally 3.4 % in the extreme compound scenario, as the domain reaches a saturation plateau, where further water volume is difficult to add under dynamic atmospheric conditions as was pointed out earlier (Gönnert et al., 2004).

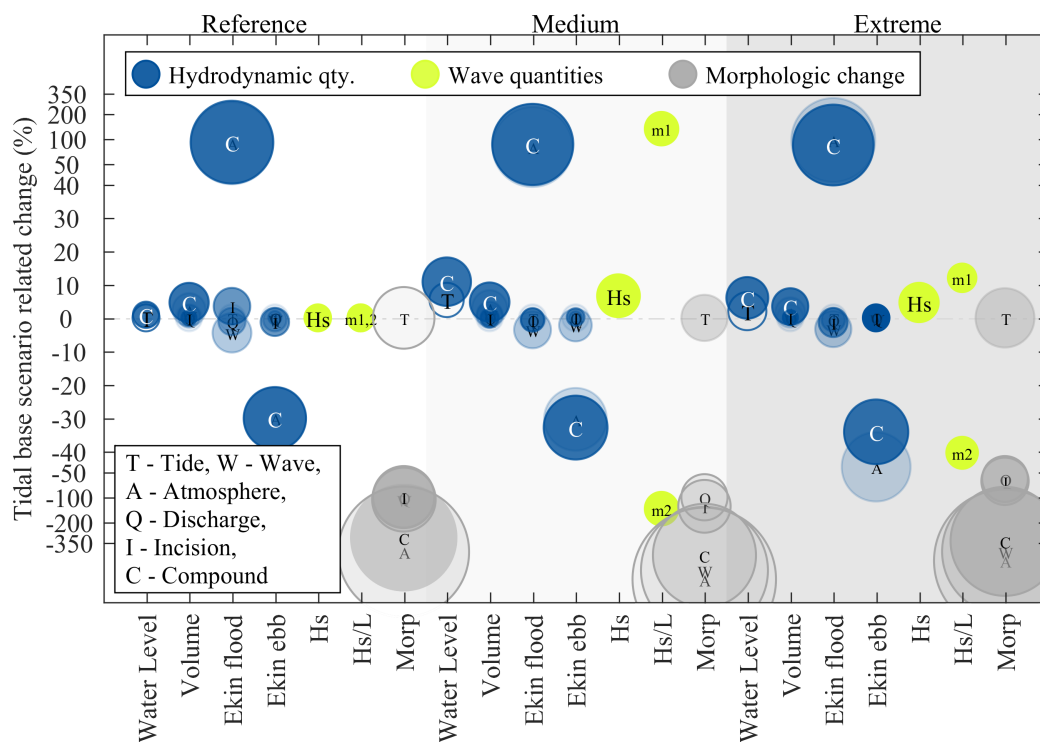


Figure 4.35: Impacts and non-linearity of coastal key drivers on estuarine system quantities for storm Xaver.

Cumulative kinetic ebb and flood energies show a strong increase for flood related values under compound forcing, and a slightly smaller reduction of cumulative ebb energy; corroborating the surge character of the storm. Significant wave heights show a stronger increase from the reference to the medium scenario compared to the medium vs. the extreme scenario, due to the fully developed sea state under the given atmospheric con-



ditions. This assumption is also supported by the obtained wave steepness values, which show a pronounced increase from the reference to the medium scenario but much smaller increase from the medium towards the extreme scenario, as the sea state appears to reach a developmental plateau, which is not further increased in the extreme case (cmp. sec. 4.2.2). Morphodynamic quantities show comparably small impacts through tide (T), discharge (Q) and incision (I) simulations but large effects due to atmospheric conditions (A), wave simulations (W) and compound scenarios (C), this is in line with results reported (Herrling and Winter, 2015, 2017; Dissanayake et al., 2012b; Herrling et al., 2017; Huang et al., 2018; Kösters and Winter, 2014).



## 5 Summary and Conclusion

Recapitulating the motivating and leading questions (sec. 1.2) of this study, potential impacts of (extreme) storm surge events under current and changing environmental boundary conditions regarding hydro and morphodynamics are investigated for the Jade-Weser Estuary taking into consideration local critical coastal infrastructure (e.g. ECTW, Bulk terminals, Minsener Oog, Jade fairway).

A systematic literature research reveals a bandwidth in projected changes for coastal key drivers. Processes relevant for the focus region are identified and storm research scenarios developed around them.

### 5.1 Summary

#### ▪ **Extreme event: European Windstorm**

No universal definition of an extreme event exists (sec. 2.2), due to the unique character of individual events, regional and/or local conditions. Therefore, a recently developed conceptual cyclone model (sec. 2.2.2) is used to define general aspects of European Windstorms and identify main storm categories. Finally, storm surge impacts recorded for the German Bight are presented (sec. 2.2.3) giving an overview of previous as well as historic events shaping the coastline (sec. 2.4.2).

#### ▪ **Critical coastal infrastructure**

Coastal engineering is tasked with developing, constructing and maintaining hydraulic works within the coastal zone. Consequently, coastal infrastructure located within the focus Region is briefly depicted (sec. 2.3.9) and the critical character of individual structures according to national classification established (sec. 2.4.4).

#### ▪ **Coastal Key Drivers**

System defining processes are identified for the focus region adopting definitions outlined by the AR5 (sec. 2.1.2). Projected changes are elucidated for individual coastal key drivers (sec. 2.3) and compiled for the North Sea region as well as the focus region, if applicable.

#### ▪ **Experimental design**

In line with global climate change related impact research (sec. 2.1), types of impact studies are compared (sec. 2.1.3) and a Time Slice impact study identified as suitable research framework for investigating storm related impacts under climate change projections. Two main types of European Windstorms are chosen, representing a western or Scandinavian type storm and a northern or Jutland type (sec. 3.1).

#### ▪ **Numerical model**

A suitable numerical tool is characterized and selected (sec. 3.4) and a model of the focus

region developed (sec. 3.5), calibrated and validated (sec. 3.7) reproducing observed values to a satisfactory degree while incorporating all main coastal key drivers as well as critical coastal infrastructure.

## 5.2 Coastal key driver impacts

### ▪ Sea level

A systematic literature research reveals, that (1) GMSLR currently experiences a phase of rise due to changing environmental conditions. Furthermore, recent altimeter measurements show that (2) the rate of rise is accelerating and is very likely to surpass values observed in the recent past. An international reference framework, the AR5 by the IPCC projects a GMSLR of 0.74 m as likely mean scenario based on RCP simulations. Given the recapitulatory character of the AR5, this value has also been identified and chosen as mean storm research scenario. An unlikely extreme sea level increase scenario has been developed around a GMSLR of 1.5 m, representing the upper limit of projected changes. However, regional mean sea level rise RMSL entails associated uncertainties, due to local non-linear effects impacting tidal dynamics.

### ▪ Tidal dynamics

Recent studies reveal that (1) engineered coastlines and waterways exert a distinct impact upon local tidal dynamics. (2) Due to non-linear interactions with the shallow coastal bathymetry and intricate coastline, additional tidal water level increases of up to 0.1 m are projected, revealing a regional sensitivity of coastlines to GMSLR of up to 8% (Arns et al., 2015). Numerous studies have investigated the impact of GMSLR upon North Sea tidal dynamics and show multiple possible impacts ranging from a decrease to an increase in tidal range. (3) These results have been shown to exhibit a sensitivity towards underlying bathymetry data, as well as floodable model extent of tidal flats (Idier et al., 2017). Consequently, a consistent bathymetric data set is used within this model and contemporary compound events simulated to minimize temporal discrepancies due to the unique character of extreme storm events.

### ▪ Storms

Storm research projects a (1) likely increase in the extreme events in conjunction with (2) a systematic shift towards a majority of westerly events. Furthermore, (3) an alarming eastward extension of the storm tracks of European Windstorms across Europe is projected by a number of studies Feser et al. (2015); Romero and Emanuel (2017); Michaelis et al. (2017). Finally, (4) a pole-ward shift of the Atlantic storm track is very likely, resulting in the projected intensification of storms. On average 10 storm surge events occur every season in the German Bight, resulting in large monetary losses and annual restoration of beaches and repairs of coastal defenses. Despite a systematic literature research on storm research, projected changes are associated with rather large

levels of uncertainty due to large signal to noise ratios regarding changes.

#### ▪ **Wind**

An integral part of storm impact research, surface near winds show two prevalent directions inducing storm surges within the German Bight coming from West-South-West to North-North-West from  $247.5^\circ$  to  $337.5^\circ$  (Jensen et al., 2006a). Historic observations show that windspeed and duration under storm conditions has increased since 1900 (Gönnert, 2003). Areal re-analysis data is used for forcing the numerical model provided by the Helmholtz Centre Geesthacht for Materials and Coastal Research (Weisse et al., 2014a), which represent the current state of science. Nevertheless, atmospheric re-analysis data has been shown to not necessarily capture detailed small scale processes such as the *Sting-Jets*, which can contribute significant impact energies on a regional scale (Browning, 2004; Schultz and Browning, 2017). Projected changes in extreme wind speeds are identified and amount to an increase of  $1.14 \text{ m s}^{-1}$  for storms with extreme values of up to  $2.0 \text{ m s}^{-1}$ . Both values are derived from a range of studies and represent the mean and extreme amplification levels for the research scenarios. Finally, a clear anthropogenic liability can be identified with enhanced SST, as well as a northward shift of the storm track and a regime shift to more westerly winds (see sections 2.3.3 & 2.3.4).

#### ▪ **Waves**

Changes in wave heights and periods investigated are based solely on numerical GCMs or RCMs simulations, which in turn are forced with atmospheric re-analysis data including the previously identified shortcomings of these data sets. Projected changes for extreme conditions in the German Bight show mean amplitude increases in  $H_{1/3}$  of 0.28 m with extreme values reaching 0.5 m (Vousdoukas et al., 2017; Weisse et al., 2012). Accordingly, these values are identified as mean and extreme scenario for amplifying the wave boundary conditions within the storm research scenarios, acknowledging potential limitations due to missing processes in the re-analysis data.

#### ▪ **Extreme Sea Levels**

Storm surge water levels are shown to exhibit a high range of natural variability, rendering the identification of climate change related trends virtually impossible (Weisse et al., 2014b). Nevertheless, several studies show that single surge components interact non-linearly with one another (Arns et al., 2015; Vousdoukas et al., 2017). By the use of dynamic modelling, several studies show that non-linear interactions of storm surge components potentially result in additional water level increases, with up to 0.1 m (Arns et al., 2015; Gaslikova et al., 2012; Debernard and Roed, 2008; Schrum et al., 2016; Vousdoukas et al., 2017). Consequently, different storm components and their respective impacts investigated within this study, reveal non-linear augmentations of ESL levels.

### ▪ **Discharge**

Discharge related changes for the Jade-Weser estuary are investigated and reveal (1) a likely shift of the annual discharge volume towards a more pronounced winter peak discharge and (2) reduced summer low flows (Hattermann et al., 2017; Lobanova et al., 2018). Projected volume changes for the Weser amount to 40 % to 60 % (Hattermann et al., 2014b, 2017; Hölscher et al., 2012), which are applied to long term winter mean discharge values for the Weser. Changes in the discharge regime depend on changes in atmospheric processes and precipitation volumes due to climatic changes. Thus these values are associated with large degrees of uncertainty, as atmospheric processes exhibit a large natural range with large fluctuations, rendering their correct reproduction through re-analysis data in GCM simulations rather difficult and attribute projections a rather experimental character.

### ▪ **Sediment delivery**

Estimates of sediment volumes entering the North Sea are researched and a sensitivity towards European Windstorm impacts identified. The North Sea sediment is supplied by 12 main rivers in conjunction with the East Anglian plume and transported by a littoral transport band into the German Bight, which constitutes a net accretion zone (Quante and Colijn, 2016; Winter, 2011a; Kösters and Winter, 2014). A sediment inventory is developed for the focus region based on extensive surface sediment samples gathered for the German North Sea coast (Valerius et al., 2015), applying a reclassification scheme (Herrling and Winter, 2017). Domain sensitivity towards different reclassification schemes is investigated and shows identical response signals varying only in magnitude (see sec. 3.5.2). Large scale processes such as the NAO correlate with North Sea characteristics and coupled sediment budgets but are not considered within the numerical research conducted within this study, due to the limited model extent as well as insufficient data for deriving representative boundary conditions resulting in an erosion limited model.

### ▪ **Hydraulic works**

Sculpting coastlines, constructing adapting and maintaining coastal and maritime infrastructure, coastal engineering is a system defining element of the worlds coastal zone. Depending on type and structural layout of hydraulic works, coastlines and morphological elements react to and are formed by hydraulic structures (Bosboom and Stive, 2015; Quante and Colijn, 2016; Luijendijk et al., 2018). The German North Sea coastline exhibits extensive dike lines, groynes, breakwaters as well as river training walls and elevated terminals (NLWKN, 2011b). Furthermore, the focus region is lined with a number of elevated terminals and ports, which form the transshipment complex Wilhelmshaven. Five of these terminals are classified as critical according to national law (BSI, 2016, 2017). Terminals, groynes, training walls and harbours are implemented in the model accordingly.

### 5.3 Concluding remarks

Impact research results of key drivers evaluated through a systematic literature research reveal that, extreme events such as European Windstorms and changes in their individual compounds present a range of projected changes and associated levels of confidence and likelihood. Due to the large signal-to-noise ratio of changes in extreme events, earth system science is faced with difficulties discerning robust trends in underlying changes, giving rise to the development of various attribution schemes (cmp. sec.2.2.5). As a consequence, projected ranges of changes in key drivers are compiled from recent climate change studies and an arithmetic mean as well as an extreme value extracted and applied to two European Windstorm simulations. Individual driver contributions are discerned simulating single components as well as compound events revealing non-linear interactions of external drivers.

Investigated parameters comprise hydrodynamic quantities, wave parameters and morphologic changes (see sec.4). It can be concluded that, independent of uncertainties in projected changes of individual coastal key drivers, storm scenarios have a large episodic impact on estuarine hydrodynamics as well as associated wave conditions and resulting morphodynamic system reactions (Quante and Colijn, 2016). Changes for the two main storm categories differ with the largest single driver being the underlying RMSL. Atmospheric boundary conditions are crucial for sea state development and wind surge and show the largest effects on water levels and hydrodynamics as has been theorized previously (de Vet et al., 2018; Herrling and Winter, 2017). Increased wave reach has been shown to prevail with increasing water depth following a literature hypothesis (Niemeyer et al., 2016). Discharge related changes shows small impacts on system variables of the Jade which is in accordance with previous findings Hattermann et al. (2017). Hydraulic development of coastal infrastructure shows a pronounced impact, revealing the system forming character of coastal engineering for estuarine morphodynamics recently affirmed in literature (Luijendijk et al., 2018).

#### ▪ **Scandinavian type European Windstorm**

Peak surge levels exhibit non-linear water level additions, which are larger for hydrodynamic forcing alone compared to compound simulation results, which is in line with results reported elsewhere (Jensen, 2005). Compound simulations of mean scenario conditions for the Scandinavian type storm event reveal a reduction of peak water levels by  $-6\%$ , while extreme conditions result in an increase of  $2\%$ .

Resulting maximum and minimum depth averaged current velocities reveal small flood increases for the compound events, which are non linear due to reduced hydraulic friction impacts with increasing water depth. Mean conditions show amplifications of reference values, while extreme conditions invert previous damping effects of wave conditions on ebb phases slightly increasing instead of reducing ebb induced kinetic energies

along the Jade fairway. Similar the constructive scenario shows an amplification of ebb directed energies for the extreme case in contrast to reductions under reference and medium conditions.

Computed residuals for the compound scenarios reveal an increase in areas characterized by flood directed residuals among the Outer Jade and Weser and the back barrier tidal flat of Wangerooge and Minsener Oog. Along the transshipment complex of the Inner Jade, the storm surge induces a complex pattern of flood directed residuals along the deeper Jade channel, framed by ebb directed residuals along the western bank harbouring the (bulk) terminals. The ECTW induces a vortex like pattern driven by flood and ebb alike at its northern end as well as a flow constriction and ebb directed jet-like outflow at its southern end. Simulated significant wave impacts reveal, that the westerly Scandinavian type storm exhibits a stronger influence on the overall obtained significant wave heights due to the storm track and underlying RMSL, with waves from a westerly direction traversing the intertwining estuarine channel shoal network. This results in additional wave height amplifications of 5%, which has been reported previously (Vousdoukas et al., 2017; Groll et al., 2014; Grabemann et al., 2015). Wave steepness is investigated as a parameter indicating intensification of wave conditions. With increasing boundary conditions, the wave steepness increases in slope towards the storm peak and shows steeper post peak decline. Relative intensification is non-linear with an increase of 1.5 to 1.71 for the ramp up and 2.2 to 1.24 for the diminishing conditions, clearly showing a reduced dissipation due to increased water levels causing for a steeper incline and a slower decline with increasing boundary conditions. Furthermore, the wave reach is investigated along a transect running the length of the *Hohe Weg*. Results reveal an increase in maximum and mean significant wave heights with increasing scenario conditions, impacting the coastal foreland and dike line with up to 0.5 m. A clear influence of the underlying RMSL is discerned, which reduces the high-pass filter function of the tidal flats (Niemeyer et al., 2016).

The morphological signals simulated for Windstorm Christian show tidally influenced fluctuations, with a distinct erosive signal trough under the maximum storm intensity, which is most pronounced under wave forcing alone. Overall a net depositional environment is preserved despite the large eroded sediment volume. Compound event simulations increase the overall transported sediment volume, with increasing boundary conditions. What is more, while the reference scenario shows a positive (depositional) trend shortly after the storm, the medium and extreme scenarios show a declining signal post storm - as the recovery period for the coastal environment is extended resulting in possible system changes. Residual transport pathways remain identical within the medium scenario, but change under extreme conditions with overall small depth changes for the focus region. The WHV transshipment complex reveals accretion along the western bank and a mix of erosion and deposition zones lining the Jade channel.

### ▪ Jutland type European Windstorm

Peak water levels of the Jutland type event show an increase for all drivers marginally increasing with elevated boundary conditions resulting in up to 0.09 m added water level, which was reported previously (Arns et al., 2015; Vousdoukas et al., 2017). Overall, largest contribution to changes in peak water levels are attributed to underlying RMSL changes impacting the focus region.

Depth averaged flood and ebb current velocities and energies under the European Windstorm Xaver reveal a flood enhancing and ebb reducing effect of atmospheric boundary conditions for the simulations. Wave conditions unanimously exhibit a reducing or damping effect on both, flood and ebb conditions. Discharge related impacts show an unaltered reduction of incoming flood phases. For medium and extreme conditions, Weser discharge enhances ebb phase related values within the focus region of the Jade. Hydraulic development shows an inverted marginal impact, with flood reducing and ebb enhancing effects under medium and extreme conditions compared to flood enhancing and ebb reducing effects under reference conditions. Compound event simulations consistently show flood amplification and ebb reduction.

Residual current patterns for the European Windstorm Xaver reveal a different picture. In contrast to the Scandinavian storm event, extensive tidal flat areas of the *Hohe Weg*, and Outer Weser as well as the back barrier tidal flat of Wangerooge are characterized by flood directed current residuals. Ebb residuals are mainly found along the Lower Weser and the Outer Weser thalweg and inside the Jade Bight and their extent decreased with increasing boundary conditions. The transshipment complex of Wilhelmshaven is characterized by the emergence of a residual current pattern contrasting that induced by the Scandinavian storm type. The shallower western bank is characterized by flood directed residuals north of the ECTW and forms a vortex like pattern at its northern flank. The eastern main jetty of the ECTW shows an elongated re-circulation pattern, with ebb directed residuals along the jetty and flood directed ones along the center of the Jade channel extending to the eastern bank. Finally, the neck leading into the Jade Bight reveals ebb directed residuals coming from the Ahne channel which are in redirected south-westerly direction pointing towards the New Outer Harbour of Wilhelmshaven and the adjacent Vareler and Stenkentief channels.

The Jutland type storm event has a pronounced northerly surge character, which results in overall larger significant wave heights. Due to the relative orientation of the observational source for the wave boundary conditions situated north of the wave gauge LAW, the northerly storm event reveals a more smooth and overall better reproduction of the observed wave parameters. Changes in significant wave height amount to 6% and 5% within the medium and extreme scenario respectively. The wave steepness for Xaver shows a similar pattern observed for the westerly event, with increasing steepness towards the storm peak and declining signals post peak. However, due to the surge

character of the Jutland type, the wave conditions reach a saturation plateau with the extreme conditions, reducing the relative increase from 1.32 for the medium to 0.12 in the extreme case. Investigated wave reach along the *Hohe Weg* tidal flat reveals, that the increased water levels result in elevated significant wave heights impacting the area. Values for the reference scenario show values reported for the European Windstorm Xaver (Vuik et al., 2016; Dreier and Fröhle, 2017). The medium and extreme cases impact the coastal foreland with maximum values of 1.0 m to 1.45 m, revealing the reduced wave dissipation with increasing water depth.

Cumulative morphological signals for Windstorm Xaver show a similar pattern, with tidal signal characteristics and a pronounced erosive signal trough under the peak storm intensity. Largest single impact reveals the wave conditions. Overall, the storm mobilizes less sediment volume within the compound reference simulation than the westerly event. This is attributed to overall larger water depth and incident angle, reducing wave stresses on tidal flats sheltered by barrier islands. However, with increasing boundary conditions sediment fluxes increase non-linearly, showing a threefold increase in overall volume for the medium scenario and another twofold increase for the extreme conditions. This is traced back to the inundation of the island Mellumplate as well as erosion along the coastal dike line due to wave impacts. The net trend of the compound signal shows a declining trend with  $-1 \times 10^6 \text{ m}^3$ , which increases in the medium and extreme events by a net export of  $1.4 \times 10^6 \text{ m}^3$  and  $2 \times 10^6 \text{ m}^3$ . Residual transport pathways under varying boundary conditions change with increasing amplitude. The reference scenario reveals larger bed level changes of up to 0.5 m compared to the westerly event due to incident angle. Back barrier tidal areas as well as narrow deep channel sections of the Jade reveal erosion, while vortex like patterns line the Jade fairway, creating accretion zones in their centres and erosion at their edges. The medium and extreme case scenarios amplify the areal extent of bed level changes reaching 0.3 m to 0.5 m in the focus region.

#### ▪ Hydraulic development scenario

The hydraulic development of the ECTW has been investigated for different RMSL levels under hydrodynamic forcing only. Residual current patterns show that the northward extension of the terminal induces a backlog and constriction of the incoming flood stream, elevating current velocities at the northern tip of the structure for both storm scenarios. Analogue the ebb directed residuals are concentrated along the jetty of the ECTW, crossing the flood directed jet like flow at the northern corner of the structural extension, exerting large hydrodynamic forces at this location. Residual transport vectors and resulting bed level changes show that the constructive alteration of the model geometry results in the formation of a large erosion area engulfing the northern tip. A local scour forms east on the jetty corner, potentially requiring scour protection in order to ensure structural safety.



## 5.4 Outlook

Based upon the literature research and findings within this study, the following aspects constitute further topics to be investigated in future research:

- Model related aspects

Given the large impacts of hydraulic construction measures upon the system, further anthropogenic interventions should be investigated covering local maintenance operations such as dredging and dumping of sediments, as the numeric model used within this study can reproduce such processes. Furthermore, the numerical model has the potential to refine hydraulic roughness representation through the parametric representation of subaquatic dunes as well as their migration through advection (Deltares, 2014a), facilitating a more detailed research of morphological macro elements and their response to extreme hydrodynamic conditions under future projections. Given the large impacts of the constructive layout changes, a depth resolving 3D approach could shed a more detailed light on local processes forming around the structure. An important future field of coastal research entails the impact research of invasive species, resulting in altered sediment compositions, erosion behaviour and changes in hydraulic roughness, which can be predicted with numerical models (Borsje et al., 2013) and are major components defining coastal environments (Krämer and Winter, 2016). Complimentary, the impact of endemic sea grass meadows on local sedimentation patterns on back barrier tidal flats could be investigated as a more ecologic measure to counteract scouring and erosion. The numerical model entails approaches for implementing parametric vegetation influences on local hydrodynamics and coupled sediment dynamics (Deltares, 2018). Another aspect of coastal zones is the development of wind power, with the wind park *Nordergründe* under development in the Outer Weser estuary, potential storm impacts could be simulated for these structures as well.

As a major aspect, storm surge chain events should be investigated regarding a potential amplification of sea state and related coastal impacts (see section 2.3.5) in turn mobilizing sediments (Holthuijsen, 2007; Bell et al., 2017; Cavaleri et al., 2016).

Another crucial future impact research topic constitutes storm induced flooding due to dike breaching, which has been shown to be reproducible with the numerical tool utilized within this study (Kerin et al., 2018).

Finally, the atmospheric boundary conditions used for this study exhibit a lack of detailed high impact processes and show deviations from locally observed values (cmp. sec. 3.7.4). Correspondingly, coastDat3, a new iteration of the coastDat data sets is currently being developed and could mitigate these shortcomings as the temporal and spatial scale of the reanalysis data is increased (HZG, 2017).

- Large scale processes

Given the spatial limitation of the model domain within this study, a larger scale nu-



merical model would be required to trace potential storm impacts onto annual sediment budgets entering the German Bight through littoral transport from the Rhine delta and the East Anglian plume (cmp. sec. 2.3.8). Such a large scale model would also provide the possibility to investigate the future development of external surges under climate projections and their respective impacts on coastal water levels under storm conditions (see sec. 3.2.4). Furthermore climate change induced warming of winter periods in central Europe could reduce atmospheric friction and amplify impact magnitudes of European Windstorms due to unstable low level air masses.

## References

- Akkermann, R., H. Brunken, W. Michaelson, V. Moritz, and L.-M. von Essen  
2015. *Die Jade: Flusslandschaft am Jadebusen : landes- und naturkundliche Beiträge zu einem Fluss zwischen Moor, Marsch und Meer : mit 438 Abbildungen, 25 Tabellen und 72 Übersichtskarten*. Oldenburg: Isensee Verlag.
- Allen, M.  
2003. Liability for climate change. *Nature*, 421(6926):891–892.
- Andersen, U. J., E. Kaas, and W. May  
2001. *Changes in the storm climate in the North Atlantic/European region as simulated by GCM time-slice experiments at high resolution*, volume 01-1 of Report / Danish Climate Centre. Copenhagen: Danish Climate Centre, DMI, Ministry of Transport.
- Androulidakis, Y. S., K. D. Kombiadou, C. V. Makris, V. N. Baltikas, and Y. N. Krestenitis  
2015. Storm surges in the mediterranean sea: Variability and trends under future climatic conditions. *Dynamics of Atmospheres and Oceans*, 71:56–82.
- Arns, A., S. Dangendorf, J. Jensen, S. Talke, J. Bender, and C. Pattiaratchi  
2017. Sea-level rise induced amplification of coastal protection design heights. *Scientific reports*, 7:40171.
- Arns, A., T. Wahl, S. Dangendorf, and J. Jensen  
2015. The impact of sea level rise on storm surge water levels in the northern part of the german bight. *Coastal Engineering*, 96:118–131.
- Ashley, G. M.  
1990. Classification of large-scale subaqueous bedforms; a new look at an old problem. *Journal of Sedimentary Research*, 60(1):160–172.
- Avila, L. A.  
28/11/2017. Tropical cyclone report: Hurricane katia.
- Bakker, M. M., G. Govers, A. van Doorn, F. Quetier, D. Chouvardas, and M. Rounsevell  
2008. The response of soil erosion and sediment export to land-use change in four areas of europe: The importance of landscape pattern. *Geomorphology*, 98(3-4):213–226.
- Bamber, J. L., M. Oppenheimer, A. W. P. Kopp, R. E., and R. M. Cooke  
2019. Ice sheet contributions to future sea-level rise from structured expert judgement. *Proceedings of the National Academy of Sciences of the United States of America*, 116(23):11195–11200.
- Basson, G.  
2008. Reservoir sedimentation—an overview of global sedimentation rates and predicted sediment deposition: Oral contribution to the international chr workshop-expert consultation: Erosion, transport and deposition of sediments, berne. *CHR Workshop*, 2008:74–79.
- Beersma, J. J., K. M. Rider, G. J. Komen, E. Kaas, and V. V. Kharin  
2016. An analysis of extra-tropical storms in the north atlantic region as simulated in a control and 2 × co 2 time-slice experiment with a high-resolution atmospheric model. *Tellus A: Dynamic Meteorology and Oceanography*, 49(3):347–361.

- Beese, F. and S. Aspelmeier  
2014. Kliff - klimafolgenforschung in niedersachsen: Abschlussbericht: 2009 bis 2013.
- Befort, D. J., M. Fischer, G. C. Leckebusch, U. Ulbrich, A. Ganske, G. Rosenhagen, and H. Heinrich  
2015. Identification of storm surge events over the german bight from atmospheric reanalysis and climate model data. *Natural Hazards and Earth System Sciences*, 15(6):1437–1447.
- Behre, K.-E.  
2012. Sea-level changes in the southern north sea region: A response to bungenstock and weerts (2010). *International Journal of Earth Sciences*, 101(4):1077–1082.
- Bell, R. J., S. L. Gray, and O. P. Jones  
2017. North atlantic storm driving of extreme wave heights in the north sea. *Journal of Geophysical Research: Oceans*, 122(4):3253–3268.
- Bengtsson, L., K. I. Hodges, and E. Roeckner  
2006. Storm tracks and climate change. *Journal of Climate*, 19(15):3518–3543.
- Beniston, M., D. B. Stephenson, O. B. Christensen, C. A. T. Ferro, C. Frei, S. Goyette, K. Halsnaes, T. Holt, K. Jylhä, B. Koffi, J. Palutikof, R. Schöll, T. Semmler, and K. Woth  
2007. Future extreme events in european climate: An exploration of regional climate model projections. *Climatic Change*, 81(S1):71–95.
- Berg, R.  
20/02/2018. Tropical cyclone report: Hurricane jose.
- Beusen, A. H. W., A. L. M. Dekkers, A. F. Bouwman, W. Ludwig, and J. Harrison  
2005. Estimation of global river transport of sediments and associated particulate c, n, and p. *Global Biogeochemical Cycles*, 19(4):n/a–n/a.
- BFG  
2018. Tide gauge data for the lower and outer weser.
- BfG, F. W. A.  
2016. Überflutungsszenarien der hwrml-de, fachportal wasserblick.
- Blake, E. S., T. B. Kimberlain, R. J. Berg, J. P. Cangialosi, and J. L. Beven II.  
2013. Northern oceanic atmospheric administration - tropical cyclone report: Hurricane sandy: (al182012). *Hurricane Reports of the National Hurricane Center (NHC)*, 2013:1–157.
- Blake, E. S. and D. A. Zelinsky  
17/08/2018. Tropical cyclone report: Hurricane harvey.
- BMBF  
2018. Extremeness: Extreme nordseesturmfluten und mögliche auswirkungen.
- BMI  
2009. Bmi-broschüre kritis-strategie: Nationale strategie zum schutz kritischer infrastrukturen (kritis-strategie) national strategy for the protection of critical infrastructures. *Bundesministerium des Innern, für Bau und Heimat*, 2009(1):1–20.
- BMJV  
10/2008. Bekanntmachung des handbuchs der rechtsförmlichkeit.
- BMVI

2015a. 2015 - bmvi - sicherheitsstrategie für die güterverkehrs- und logistikwirtschaft: Schutz kritischer infrastrukturen und verkehrsträgerübergreifende gefahrenabwehr. *Sicherheitsstrategie für die Güterverkehrs- und Logistikwirtschaft*, 2018:1–28.

## BMVI

2015b. Kliwas: Auswirkungen des klimawandels auf wasserstraßen und schifffahrt in deutschland: Abschlussbericht des bmvi - fachliche schlussfolgerungen aus den ergebnissen des forschungsprogramms kliwas.

## Bolle and Lehnert

1977/1978/1979. *Jahrbuch der Hafenbautechnischen Gesellschaft: Sechsendreißigster Band*, volume 36. Berlin, Heidelberg, (GE), New York (U.S.A.): Springer-Verlag Berlin Heidelberg and Springer Berlin Heidelberg.

## Bormann, H.

2010. Runoff regime changes in german rivers due to climate change. *ERDKUNDE*, 64(3):257–279.

## Bormann, H., N. Pinter, and S. Elfert

2011. Hydrological signatures of flood trends on german rivers: Flood frequencies, flood heights and specific stages. *Journal of Hydrology*, 404(1-2):50–66.

## Borsje, B. W., P. C. Roos, W. M. Kranenburg, and S. Hulscher

2013. Modeling tidal sand wave formation in a numerical shallow water model: The role of turbulence formulation. *Continental Shelf Research*, 60:17–27.

## Bosboom, J. and M. J. Stive

2015. *Coastal Dynamics I lecture notes CIE4305*. Delft: Delft University of Technology Press.

## Brahms, A.

1989. *Anfangs-Gründe der Deich- und Wasser-Baukunst: Teil 1 und 2*, unveränd. nachdr. der ausg. aurich, 1767 u. 1773 edition. Leer: Schuster.

## Brasseur, G. P., D. Jacob, and S. Schuck-Zöller

2017. *Klimawandel in Deutschland*. Berlin, Heidelberg: Springer Berlin Heidelberg.

## Bray, R. N., A. D. Bates, and J. M. Land

1997. *Dredging: A handbook for engineers: A handbook for engineers*, 2. ed. edition. London: Arnold.

## Brohan, P., J. J. Kennedy, I. Harris, S. F. B. Tett, and P. D. Jones

2006. Uncertainty estimates in regional and global observed temperature changes: A new data set from 1850. *Journal of Geophysical Research*, 111(D12):15525.

## Brönnimann, S.

2015. *Climatic Changes Since 1700*, volume 55. Cham: Springer International Publishing.

## Brooks, S. M., T. Spencer, A. McIvor, and I. Möller

2016. Reconstructing and understanding the impacts of storms and surges, southern north sea. *Earth Surface Processes and Landforms*, 41(6):855–864.

## Brown, J. M., A. J. Souza, and J. Wolf

2010. Surge modelling in the eastern irish sea: Present and future storm impact. *Ocean Dy-*

- namics*, 60(2):227–236.
- Brown, J. M., J. Wolf, and A. J. Souza  
2012. Past to future extreme events in liverpool bay: Model projections from 1960–2100. *Climatic Change*, 111(2):365–391.
- Browning, K. A.  
2004. The sting at the end of the tail: Damaging winds associated with extratropical cyclones. *Quarterly Journal of the Royal Meteorological Society*, 130(597):375–399.
- BSH  
2013. Meeresboden-dgm.
- BSH  
2018a. Sturmfluten: Berichte zu sturmfluten und extremen wasserständen: Zahlen und fakten.
- BSH  
2018b. Sturmflutwarndienst: Seeaufgabengesetz § 1 abs. 9: Din en iso 9001 certified.
- BSI  
2017. Gesetz über das bundesamt für sicherheit in der informationstechnik (bsi-gesetz - bsig): Bsi.
- BSI  
22/04/2016. Verordnung zur bestimmung kritischer infrastrukturen nach dem bsi-gesetz (bsi-kritisverordnung - bsi-kritisv): Bsi-kritisv.
- Burt, S.  
2007. The highest of the highs ... extremes of barometric pressure in the british isles, part 2 – the most intense anticyclones. *Weather*, 62(2):31–41.
- Callies, U., L. Gaslikova, H. Kapitza, and M. Scharfe  
2017. German bight residual current variability on a daily basis: Principal components of multi-decadal barotropic simulations. *Geo-Marine Letters*, 37(2):151–162.
- Captain Evans, A. D. and R. J. Director Falvey  
2013. Annual tropical cyclone report.
- Carter, D. J. T. and L. Draper  
1988. Has the north-east atlantic become rougher? *Nature*, 332:494 EP –.
- Cavaleri, L., F. Barbariol, A. Benetazzo, L. Bertotti, J.-R. Bidlot, P. Janssen, and N. Wedi  
2016. The draupner wave: A fresh look and the emerging view. *Journal of Geophysical Research: Oceans*, 121(8):6061–6075.
- Church, A. J., P. U. Clark, A. Cazenave, J. M. Gregory, S. Jevrejeva, A. Levermann, M. A. Merrifield, G. A. Milnes, R. S. Nerem, P. D. Nunn, A. J. Payne, W. T. Pfeffer, D. Stammer, and A. S. Unnikrishnan  
2014. Sea level change: Chapter 13. In *Climate change 2013*, T. Stocker, ed. Cambridge: Cambridge University Press.
- Church, J. A. and N. J. White  
2011. Sea-level rise from the late 19th to the early 21st century. *Surveys in Geophysics*, 32(4-5):585–602.

- Church, J. A., P. L. Woodworth, T. Aarup, and W. S. Wilson  
2010. *Understanding Sea-Level Rise and Variability*. Oxford, UK: Wiley-Blackwell.
- Ciavola, P., O. Ferreira, P. Haerens, M. van Koningsveld, and C. Armaroli  
2011. Storm impacts along european coastlines. part 2: Lessons learned from the micore project. *Environmental Science & Policy*, 14(7):924–933.
- Coco, G. and P. Ciavola, eds.  
2018. *Coastal storms: Processes and impacts*, Hydrometeorological extreme events. Chichester, West Sussex: John Wiley & Sons Inc.
- Cole, S.  
2001. *An Introduction to Statistical Modeling of Extreme Values*. New York: Springer-Verlag London.
- Conte, D. and P. Lionello  
2013. Characteristics of large positive and negative surges in the mediterranean sea and their attenuation in future climate scenarios. *Global and Planetary Change*, 111:159–173.
- Cornes, R. C.  
2014. Historic storms of the northeast atlantic since circa 1700: A brief review of recent research. *Weather*, 69(5):121–125.
- Cornes, R. C. and P. D. Jones  
2011. An examination of storm activity in the northeast atlantic region over the 1851–2003 period using the emulate gridded mslp data series. *Journal of Geophysical Research*, 116(D16):97.
- Cowell, P. J. and B. G. Thom  
1997. Morphodynamics of coastal evolution. In *Coastal Evolution*, R. W. G. Carter, C. D. Woodroffe, and O. van de Plassche, eds., Pp. 33–86. Cambridge: Cambridge University Press.
- Croll, J.  
2009. Xiii. on the physical cause of the change of climate during geological epochs. *The London, Edinburgh, and Dublin Philosophical Magazine and Journal of Science*, 28(187):121–137.
- Cusack, S.  
2013. A 101 year record of windstorms in the netherlands. *Climatic Change*, 116(3-4):693–704.
- Dangendorf, S. abd Marcos, M., C. C. P. F. T. Wöppelmann, G., and R. Riva  
2017. Reassessment of 20th century global mean sea level rise. *Proceedings of the National Academy of Sciences of the United States of America*, 114:5946–5951.
- Dangendorf, S., M. Marcos, A. Müller, E. Zorita, R. Riva, K. Berk, and J. Jensen  
2015. Detecting anthropogenic footprints in sea level rise. *Nature communications*, 6:7849.
- Dangendorf, S., S. Müller-Navarra, J. Jensen, F. Schenk, T. Wahl, and R. Weisse  
2014. North sea storminess from a novel storm surge record since ad 1843\*. *Journal of Climate*, 27(10):3582–3595.
- Davies, G. L.  
1964. Robert hooke and his conception of earth-history. *Proceedings of the Geologists' Association*, 75(4):493–498.
- de Kraker, A.

1999. A method to assess the impact of high tides, storms and storm surges as vital elements in climatic history the case of stormy weather and dikes in the northern part of flanders, 1488 to 1609. *Climatic Change*, 43(1):287–302.
- de Vet, P. L. M., B. C. van Prooijen, R. A. Schrijvershof, J. J. van der Werf, T. Ysebaert, M. C. Schrijver, and Z. B. Wang  
2018. The importance of combined tidal and meteorological forces for the flow and sediment transport on intertidal shoals. *Journal of Geophysical Research: Earth Surface*, 123(10):2464–2480.
- de Vriend, H. J.  
1991. Mathematical modelling and large-scale coastal behaviour. *Journal of Hydraulic Research*, 29(6):727–740.
- de Winter, R. C., A. Sterl, and B. G. Ruessink  
2013. Wind extremes in the north sea basin under climate change: An ensemble study of 12 cmip5 gcms. *Journal of Geophysical Research: Atmospheres*, 118(4):1601–1612.
- Debernard, J. B. and L. P. Roed  
2008. Future wind, wave and storm surge climate in the northern seas: A revisit. *Tellus A*, 60(3):427–438.
- Dee, D. P., S. M. Uppala, A. J. Simmons, P. Berrisford, P. Poli, S. Kobayashi, U. Andrae, M. A. Balmaseda, G. Balsamo, P. Bauer, P. Bechtold, A. C. M. Beljaars, L. van de Berg, J. Bidlot, N. Bormann, C. Delsol, R. Dragani, M. Fuentes, A. J. Geer, L. Haimberger, S. B. Healy, H. Hersbach, E. V. Hólm, L. Isaksen, P. Kállberg, M. Köhler, M. Matricardi, A. P. McNally, B. M. Monge-Sanz, J.-J. Morcrette, B.-K. Park, C. Peubey, P. de Rosnay, C. Tavolato, J.-N. Thépaut, and F. Vitart  
2011. The era-interim reanalysis: Configuration and performance of the data assimilation system. *Quarterly Journal of the Royal Meteorological Society*, 137(656):553–597.
- Della-Marta, P. M., H. Mathis, C. Frei, M. A. Liniger, J. Kleinn, and C. Appenzeller  
2009. The return period of wind storms over europe. *International Journal of Climatology*, 29(3):437–459.
- Deltares  
2014a. : *Hydro-Morphodynamics: 3D/2D modelling suite for integral water solutions*, volume Version: 3.15.34158 of *Delft3D User Manual*. Delft, Netherlands: Deltares, Boussinesqweg 1, The Netherlands.
- Deltares  
2014b. *Wave: Simulation of short-crested waves with SWAN: 3D/2D modelling suite for integral water solutions*, volume Version: 3.05.34160 of *Delft3D User Manual*. Delft, Netherlands: Deltares, Boussinesqweg 1, The Netherlands.
- Deltares  
2018. *Quickin: 3D/2D modelling suite for integral water solutions: Hydro-Morphodynamics & Water Quality*, volume SVN Revision: 57594, version: 4.00 edition. Delft, Netherlands: Deltares, Boussinesqweg 1, The Netherlands.
- Deltawerken  
2004. Deltaplan.



## DeStatis

2017. *Statistisches Jahrbuch Deutschland 2017*, 1., auflage edition. Wiesbaden: Statistisches Bundesamt.

## DeStatis

2018. *Verkehr: Seeschifffahrt: Mai 2018*, volume 5 of *Fachserie 8*. GE: Bundesdruckerei.

## Deutscher Bundestag

2013. *Risikoanalyse Bevölkerungsschutz Bund: Wintersturm*, volume 18 of *Drucksache 18/208*. Berlin, GE: Bundesdruckerei.

## Deutscher Bundestag

2014. *Risikoanalyse Bevölkerungsschutz Bund: Sturmflut*, volume 18 of *Drucksache 18/3682*. Berlin, GE: Bundesdruckerei.

## DIN

4049-1, 1992. Hydrology; basic terms.

## Dissanayake, D., A. Wurpts, M. Miani, H. Knaack, H. D. Niemeyer, and J. A. Roelvink

2012a. Modelling morphodynamic response of a tidal basin to an anthropogenic effect: Ley bay, east frisian wadden sea – applying tidal forcing only and different sediment fractions. *Coastal Engineering*, 67:14–28.

## Dissanayake, D. M. P. K., R. Ranasinghe, and J. A. Roelvink

2012b. The morphological response of large tidal inlet/basin systems to relative sea level rise. *Climatic Change*, 113(2):253–276.

## Dole, R., M. Hoerling, J. Perlwitz, J. Eischeid, P. Pegion, T. Zhang, X.-W. Quan, T. Xu, and D. Murray

2011. Was there a basis for anticipating the 2010 russian heat wave? *Geophysical Research Letters*, 38(6):n/a–n/a.

## Donat, M. G.

2010. *European wind storms, related loss potentials and changes in multi-model climate simulations*. Doctoral thesis, Freie Universität Berlin, Berlin, GE.

## Donat, M. G., G. C. Leckebusch, J. G. Pinto, and U. Ulbrich

2009. Examination of wind storms over central europe with respect to circulation weather types and nao phases. *International Journal of Climatology*, 31:n/a–n/a.

## Donat, M. G., G. C. Leckebusch, S. Wild, and U. Ulbrich

2011. Future changes in european winter storm losses and extreme wind speeds inferred from gcm and rcm multi-model simulations. *Natural Hazards and Earth System Sciences*, 11(5):1351–1370.

## Donnelly, C., W. Greuell, J. Andersson, D. Gerten, G. Pisacane, P. Roudier, and F. Ludwig

2017. Impacts of climate change on european hydrology at 1.5, 2 and 3 degrees mean global warming above preindustrial level. *Climatic Change*, 143(1-2):13–26.

## Doodson, A. T.

1924. Perturbations of harmonic tidal constants. *Proceedings of the Royal Society A: Mathematical, Physical and Engineering Sciences*, 106(739):513–526.

- Dreier, N. and P. Fröhle  
2017. Operational wave now- and forecast in the german bight as a basis for the assessment of wave-induced hydrodynamic loads on coastal dikes. *Journal of Ocean University of China*, 16(6):991–997.
- DWD  
2013a. Orkantief christian am 28. oktober 2013.
- DWD  
2013b. Orkantief xaver über nordeuropa vom 5. bis 7. dezember 2013.
- DWD  
2018a. Seevorhersagen nordsee 3 tage.
- DWD  
2018b. Wetterlexikon: Sturmzyklone.
- Eady, E. T.  
1949. Long waves and cyclone waves. *Tellus*, 1(3):33–52.
- Easterling, D. R., K. E. Kunkel, M. F. Wehner, and L. Sun  
2016. Detection and attribution of climate extremes in the observed record. *Weather and Climate Extremes*, 11:17–27.
- Elsner, J. B., J. P. Kossin, and T. H. Jagger  
2008. The increasing intensity of the strongest tropical cyclones. *Nature*, 455:92 EP –.
- Enfield, D. B., A. M. Mestas-Nuñez, and P. J. Trimble  
2001. The atlantic multidecadal oscillation and its relation to rainfall and river flows in the continental u.s. *Geophysical Research Letters*, 28(10):2077–2080.
- EU  
2004a. Living with coastal erosion in europe - sediment and space for sustainability: Part 1 - major findings and policy recommendations of the euroseion project.
- EU  
2004b. Living with coastal erosion in europe - sediment and space for sustainability: Part 2 - maps and statistics.
- Eyring, V., S. Bony, G. A. Meehl, C. A. Senior, B. Stevens, R. J. Stouffer, and K. E. Taylor  
2016. Overview of the coupled model intercomparison project phase 6 (cmip6) experimental design and organization. *Geoscientific Model Development*, 9(5):1937–1958.
- Fangmann, A., A. Belli, and U. Haberlandt  
2013. Trends in streamflow observation series in lower saxony. *Hydrologie und Wasserbewirtschaftung*, 57(5):196–205.
- Feser, F., M. Barcikowska, O. Krueger, F. Schenk, R. Weisse, and L. Xia  
2015. Storminess over the north atlantic and northwestern europe-a review. *Quarterly Journal of the Royal Meteorological Society*, 141(687):350–382.
- Field, C. B., V. R. Barros, D. J. Dokken, K. J. Mach, and M. D. Mastrandrea, eds.  
2014. *Climate Change 2014 Impacts, Adaptation, and Vulnerability*. Cambridge: Cambridge University Press.

Fournier, F.

1960. Climat et erosion. *Presses Universitaires de France, Paris*, 1960(1).

Franke, R.

2009. Die nordatlantischen orkantiefs seit 1956: The north atlantic storms since 1956. *Naturwissenschaftliche Rundschau*, 2009(7):349–356.

Franzius, L.

1888. *Die Korrektion der Unterweser: Auf Veranlassung der Bremischen Deputation für die Unterweserkorrektion: mit 2 Tafeln*. Bremen, GE: A. Guthe.

Franzius-Institute

2000. *Teilprojekt "Technik des Küstenschutzes" im Projekt "Klimaänderung und Unterweserre-gion" (KLIMU) - "Fallstudie Weserästuar" des Bund-Länderprogramms "Klimaänderung und Küste" : Abschlussbericht: Teilprojekt "Technik des Küstenschutzes" im Projekt "Klimaänderung und Unterweserre-gion" (KLIMU) - "Fallstudie Weserästuar" des Bund-Länderprogramms "Kli-maänderung und Küste" : Abschlussbericht*. Hannover, GE: Deutsches Zentrum für Luft- und Raumfahrt (DLR) - Umweltsystemforschung (USF).

Friedrichs, C. T. and D. G. Aubrey

1988. Non-linear tidal distortion in shallow well-mixed estuaries: a synthesis. *Estuarine, Coastal Shelf Science*, 1988(27):521–545.

Friedrichs, C. T. and D. G. Aubrey

1994. Tidal propagation in strongly convergent channels. *Journal of Geophysical Research*, 1994(99):3321–3336.

Gaslikova, L., I. Grabemann, and N. Groll

2012. Changes in north sea storm surge conditions for four transient future climate realizations. *Natural Hazards*, 66(3):1501–1518.

GDV

2014. *Naturgefahrenreport 2014: Die Schaden-Chronik der deutschen Versicherer in Zahlen, Stimmen und Ereignissen: Tabellen, Grafiken und Karten*, Naturgefahrenreport. Berlin: Ruk-saldruck, Berlin.

GDV

2015. *Naturgefahrenreport 2015: Die Schaden-Chronik der deutschen Versicherer in Zahlen, Stimmen und Ereignissen: Tabellen, Grafiken und Karten*, Naturgefahrenreport. Berlin: Ruk-saldruck, Berlin.

GDV

2016. *Naturgefahrenreport 2016: Die Schaden-Chronik der deutschen Versicherer in Zahlen, Stimmen und Ereignissen: Tabellen, Grafiken und Karten*, Naturgefahrenreport. Berlin: Ruk-saldruck, Berlin.

GDV

2017. *Naturgefahrenreport 2017: Serviceteil zum Naturgefahrenreport 2017: Tabellen, Grafiken und Karten*, Naturgefahrenreport. Berlin: Ruksaldruck, Berlin.

Geyer, B. and B. Rockel

2013. *coastDat-2 COSMO-CLM Atmospheric Reconstruction: This is an atmospheric hourly*

*hindcast for Western Europe and the North Atlantic using COSMO-CLM version 4.8\_clm\_11 with spectral nudging from 1948-2012. The model uses a rotated grid with 254 x 248 grid points and a grid point distance of 0.22 degrees, the rotated North pole is located at 170 W, 35 N. In rotated coordinates the model area extends from 30.44 W to 25.22 E, 25.72 S to 28.62 N, in geographical coordinates this corresponds to about 68 W to 82 E, 25.6 N to 81.4 N. GE: HZG.*

Gierloff-Emden and G. Hans

1954. *Die morphologischen Wirkungen der Sturmflut vom 1. Februar 1953 in den Westniederlanden*, volume 4 of *Hamburger geographische Studien*. Hamburg, GE: Selbstverlag des Instituts für Geographie und Wirtschaftsgeographie der Universität Hamburg.

GISTEMP Team

2018. Giss surface temperature analysis (gistemp). nasa goddard institute for space studies.

Gönnert, G.

2003. Sturmfluten und windstau in der deutschen bucht charakter, veränderungen und maximalwerte im 20. jahrhundert. In *Die Küste*, KFKI, ed., volume 67, Pp. 185–365. Karlsruhe: Bundesanst. für Wasserbau (BAW).

Gönnert, G., K. Isert, H. Giese, and A. Plüß

2004. Charakterisierung der tidekurve. In *Die Küste*, volume 68, Pp. 99–141. Karlsruhe: Bundesanst. für Wasserbau (BAW).

Gönnert, G. and S. Thumm

2010. Das risiko von extremsturmfluten in ästuaren angesichts globalen klimawandels: LsbG (hamburg, ge). In *Forschung für ein Integriertes Küstenzonenmanagement*, A. Kannen, ed., volume 16 of *Coastline reports*, Pp. 77–86. Hannover and Rostock: Technische Informationsbibliothek u. Universitätsbibliothek and EUCC Die Küsten Union Deutschland.

Götschenberg, A. and A. Kahlfeld

2008. The jade. In *Die Küste*, KFKI, ed., volume 74, Pp. 263–274. Karlsruhe: Bundesanst. für Wasserbau (BAW).

Götschenberg, A. and V. Schlüter

2005. Monitoring von baggergut-verklappungen auf der klappstelle "vareler fahrwasser" im jadebusen: Zwischen wesen und ems verklappungen: Monitoring von baggergut. *Schriftenreihe der DVW e.V. – Gesellschaft für Geodäsie, Geoinformation und Landmanagement*, 2005(47):43–55.

Grabemann, H.-J., I. Grabemann, and D. P. Eppel

2004. Climate change and hydrodynamic impact in the jade-weser area - a case study. In *Coastline Reports: Proceedings of the 22nd annual conference*, G. Schernewski and T. Dolch, eds., volume 1, Pp. 83–91. Warnemünde: EUCC - The Coastal Union.

Grabemann, I., N. Groll, J. Möller, and R. Weisse

2015. Climate change impact on north sea wave conditions: A consistent analysis of ten projections. *Ocean Dynamics*, 65(2):255–267.

Grabemann, I. and R. Weisse

2008. Climate change impact on extreme wave conditions in the north sea: An ensemble study. *Ocean Dynamics*, 58(3-4):199–212.

- Gräwe, U. and H. Burchard  
2012. Storm surges in the western baltic sea: The present and a possible future. *Climate Dynamics*, 39(1-2):165–183.
- Groll, N., I. Grabemann, and L. Gaslikova  
2014. North sea wave conditions: An analysis of four transient future climate realizations. *Ocean Dynamics*, 64(1):1–12.
- Groll N., Weisse R., B. A. G. H. M. J.  
2014. *Berechnung von Seegangsszenarien für die Nordsee*. Koblenz, Germany: Bundesanstalt für Gewässerkunde.
- Haberlandt, U., A. Belli, and J. Hölscher  
2010. Trends in beobachteten zeitreihen von temperatur und niederschlag in niedersachsen: Trends in observed time series of temperature and precipitation lower saxony. *Hydrologie und Wasserbewirtschaftung*, 54(1):28–36.
- Hadley, D.  
2009. Land use and the coastal zone. *Land Use Policy*, 26:S198–S203.
- Hanna, E., P. Huybrechts, K. Steffen, J. Cappelen, R. Huff, C. Shuman, T. Irvine-Fynn, S. Wise, and M. Griffiths  
2008. Increased runoff from melt from the greenland ice sheet: A response to global warming. *Journal of Climate*, 21(2):331–341.
- Hansen, J., R. Ruedy, M. Sato, and K. Lo  
2010. Global surface temperature change. *Reviews of Geophysics*, 48(4):644.
- Hansen, W.  
1950. Triftstrom und windstau. *Deutsche Hydrographische Zeitschrift*, 3(5-6):303–313.
- Harley, M. D., I. L. Turner, M. A. Kinsela, J. H. Middleton, P. J. Mumford, K. D. Splinter, M. S. Phillips, J. A. Simmons, D. J. Hanslow, and A. D. Short  
2017. Extreme coastal erosion enhanced by anomalous extratropical storm wave direction. *Scientific reports*, 7(1):6033.
- Harvey, B. J., L. C. Shaffrey, and T. J. Woollings  
2014. Equator-to-pole temperature differences and the extra-tropical storm track responses of the cmi5 climate models. *Climate Dynamics*, 43(5-6):1171–1182.
- Harvey, B. J., L. C. Shaffrey, and T. J. Woollings  
2015. Deconstructing the climate change response of the northern hemisphere wintertime storm tracks. *Climate Dynamics*, 45(9-10):2847–2860.
- Harvey, B. J., L. C. Shaffrey, T. J. Woollings, G. Zappa, and K. I. Hodges  
2012. How large are projected 21st century storm track changes? *Geophysical Research Letters*, 39(18):97.
- Hattermann, F. F., S. Huang, O. Burghoff, W. Willems, H. Österle, M. Büchner, and Z. Kundzewicz  
2014a. Modelling flood damages under climate change conditions – a case study for germany. *Natural Hazards and Earth System Sciences*, 14(12):3151–3168.
- Hattermann, F. F., S. Huang, and H. Koch

- 2014b. Climate change impacts on hydrology and water resources in Germany. *Meteorologische Zeitschrift*, 2014:1–11.
- Hattermann, F. F., V. Krysanova, S. N. Gosling, R. Dankers, P. Daggupati, C. Donnelly, M. Flörke, S. Huang, Y. Motovilov, S. Buda, T. Yang, C. Müller, G. Leng, Q. Tang, F. T. Portmann, S. Hagemann, D. Gerten, Y. Wada, Y. Masaki, T. Alemayehu, Y. Satoh, and L. Samaniego  
2017. Cross-scale intercomparison of climate change impacts simulated by regional and global hydrological models in eleven large river basins. *Climatic Change*, 141(3):561–576.
- Haunschild, R., L. Bornmann, and W. Marx  
2016. Climate change research in view of bibliometrics. *PloS one*, 11(7):e0160393.
- Hay, C. C., E. Morrow, R. E. Kopp, and J. X. Mitrovica  
2015. Probabilistic reanalysis of twentieth-century sea-level rise. *Nature*, 517(7535):481–484.
- Heinemann, F. and H. Janßen  
2013. Navigational safety surveys of the Jade fairway 2012 - 2015: Verkehrssicherungspeilungen des Jade Fahrwassers 2012 - 2015.
- Hensen, W.  
1959. *Modellversuche für die Unterweser und ihre Nebenflüsse: Textteil*, volume 15a of *Mitteilungen der Hannoverschen Versuchsanstalt für Grundbau und Wasserbau Franzius-Institut der Technischen Hochschule Hannover*, 200 edition. Hannover, GE: Eigenverlage der Hannoverschen Versuchsanstalt für Grundbau und Wasserbau Franzius-Institut der Technischen Universität Hannover.
- Herrling, G., M. Benninghoff, A. C. Zorndt, and C. Winter  
2017. Drivers of channel-shoal morphodynamics at the outer Weser estuary: Proc. *Coastal Dynamics*, 2017(261):333–345.
- Herrling, G. and C. Winter  
2015. Tidally- and wind-driven residual circulation at the multiple-inlet system East Frisian Wadden Sea. *Continental Shelf Research*, 106:45–59.
- Herrling, G. and C. Winter  
2017. Spatiotemporal variability of sedimentology and morphology in the East Frisian barrier island system. *Geo-Marine Letters*, 37(2):137–149.
- HES  
2018. HES Wilhelmshaven tank terminal: Facts & features: Hestya Energy BV.
- Hewson, T. D. and U. Neu  
2015. Cyclones, windstorms and the Imilast project. *Tellus A: Dynamic Meteorology and Oceanography*, 67(1):1–33.
- Hoerling, M., J. Hurrell, J. Eischeid, and A. Phillips  
2006. Detection and attribution of twentieth-century northern and southern African rainfall change. *Journal of Climate*, 19(16):3989–4008.
- Hölscher, J., U. Petry, M. Bertram, M. Anhalt, S. Schmidtke, U. Haberlandt, H. Müller, S. van der Heijden, S. Berndt, A. Verworn, M. Wallner, A. Belli, J. Dietrich, G. Meon, K. Förster, M. Gelleszun, G. Rieder, A. Lange, and F. Eggelsmann  
2012. Globaler Klimawandel - wasserwirtschaftliche Folgenabschätzung für das Binnenland

- biw: Abschlussbericht phase 1+2: Nlwkn.
- Holthuijsen, L. H.  
2007. *Waves in oceanic and coastal waters*. Cambridge: Cambridge University Press.
- Hoskins, B. J. and K. I. Hodges  
2002. New perspectives on the northern hemisphere winter storm tracks. *Journal of the Atmospheric Sciences*, 59(6):1041–1061.
- Howard, T., J. Lowe, and K. Horsburgh  
2010. Interpreting century-scale changes in southern north sea storm surge climate derived from coupled model simulations. *Journal of Climate*, 23(23):6234–6247.
- Howard, T., A. K. Pardaens, J. L. Bamber, J. Ridley, G. Spada, R. T. W. L. Hurkmans, J. A. Lowe, and D. Vaughan  
2014. Sources of 21st century regional sea-level rise along the coast of northwest europe. *Ocean Science*, 10(3):473–483.
- Huang, B., P. W. Thorne, V. F. Banzon, T. Boyer, G. Chepurin, J. H. Lawrimore, M. J. Menne, T. M. Smith, R. S. Vose, and H.-M. Zhang  
2018. Noaa extended reconstructed sea surface temperature (ersst), version 5.global land and ocean temperature anomalies january-december 1901-2018: Noaa national centers for environmental information. NOAA.
- Huang, S., V. Krysanova, and F. F. Hattermann  
2013. Projection of low flow conditions in germany under climate change by combining three rcms and a regional hydrological model. *Acta Geophysica*, 61(1):151–193.
- Huler, S.  
2004. *Defining the wind: The Beaufort Scale, and how a nineteenth-century admiral turned science into poetry*. New York, NY: Crown Publishers.
- Huthnance, J., R. Weisse, T. Wahl, H. Thomas, J. Pietrzak, A. J. Souza, S. van Heteren, N. Schmelzer, J. van Beusekom, F. Colijn, I. Haigh, S. Hjøllø, J. Holfort, E. C. Kent, W. Kühn, P. Loewe, I. Lorkowski, K. A. Mork, J. Pätsch, M. Quante, L. Salt, J. Siddorn, T. Smyth, A. Sterl, and P. Woodworth  
2016. Recent change—north sea. In *North Sea Region Climate Change Assessment*, M. Quante and F. Colijn, eds., Regional Climate Studies, Pp. 85–136. Cham: Springer International Publishing.
- HZG  
2017. coastdat-3\_cosmo-clm\_erai.
- Idier, D., F. Paris, G. Le Cozannet, F. Boulahya, and F. Dumas  
2017. Sea-level rise impacts on the tides of the european shelf. *Continental Shelf Research*, 137:56–71.
- IPCC  
2007. *Climate Change 2007: Synthesis report: Contribution of Working Groups I, II and III to the Fourth Assessment Report of the Intergovernmental Panel on Climate Change [Core Writing Team, Pachauri, R.K and Reisinger, A. (eds.)]*. IPCC, Geneva, Switzerland, 104 pp. *Climate Change*: [a report of the Intergovernmental Panel on. Geneva: IPCC.

IPCC

2014. Annex iii: Glossary [planton, s. (ed.)]. In *Climate change 2013*, T. Stocker, ed., Pp. 1447–1466. Cambridge: Cambridge University Press.

IRFC

2016. *World disasters report 2016: Resilience : saving lives today, investing for tomorrow*. Geneva: International Federation of Red Cross and Red Crescent Societies.

ISL

01/2016. Machbarkeitsstudie jadeweserport 2: Los 1: bedarfsanalyse, planungsgründung, nutzen-kosten-analyse, betriebliches terminaldesign: Endbericht zur bedarfsanalyse und zur kosten-nutzen-analyse.

Jade-Weser-Port

2008. The construction of jadeweserport: A deepwater container terminal in wilhelmshaven. In *Die Küste*, KFKI, ed., volume 74, Pp. 411–417. Karlsruhe: Bundesanst. für Wasserbau (BAW).

Jensen, J.

2005. Muse: Modellgestützte untersuchungen zu sturmfluten mit sehr geringen eintrittswahrscheinlichkeiten an der deutschen nordseeküste : Abschlussbericht des kfki-forschungsvorhabens ; laufzeit: 2002 - 2005.

Jensen, J., A. Arns, and M. Ulm

2017. Untersuchungen zu möglichen auswirkungen extremer sturmfluten am beispiel der region emden/krummhörn: 22. kfki-seminar, 22.11.2017, dsm bremerhaven abstract: Conference paper. *KFKI-Seminar*, 2017:1–2.

Jensen, J., C. Mudersbach, S. H. Müller-Navarra, I. Bork, C. Koziar, and V. Renner

2006a. Modellgestützte untersuchungen zu sturmfluten mit modellgestützte untersuchungen zu sturmfluten mit sehr geringen eintrittswahrscheinlichkeiten an der deutschen nordseeküste deutschen nordseeküste. In *Die Küste*, KFKI, ed., volume 71, Pp. 123–167. Karlsruhe: Bundesanst. für Wasserbau (BAW).

Jensen, J., C. Mudersbach, S. H. Navarra-Müller, I. Bork, C. Koziar, and V. Renner

2006b. Modellgestützte untersuchungen zu sturmfluten mit sehr geringen eintrittswahrscheinlichkeiten an der deutschen nordseeküste. In *Die Küste*, KFKI, ed., volume 71, Pp. 123–167. Karlsruhe: Bundesanst. für Wasserbau (BAW).

Jensen, J. and S. Müller-Navarra

2008. Storm surges on the german coast. In *Die Küste*, KFKI, ed., volume 74, Pp. 92–124. Karlsruhe: Bundesanst. für Wasserbau (BAW).

Jevrejeva, S., J. C. Moore, M. A. P. Grinsted, A., and G. Spada

2017. Trends and acceleration in global and regional sea levels since 1807. *Global and Planetary Change*, 2014:11–22.

John Tyndall

1873. Further researches on the absorption and radiation of heat by gaseous matter. In *Contributions to Molecular Physics in the domain of radiant heat*, Royal Institution, ed., Pp. 117–121. New York: D. Appleton and Company.

Jordà, G., D. Gomis, E. Álvarez-Fanjul, and S. Somot



2012. Atmospheric contribution to mediterranean and nearby atlantic sea level variability under different climate change scenarios. *Global and Planetary Change*, 80-81:198–214.
- Judson, S. and D. F. Ritter  
1964. Rates of regional denudation in the united states. *Journal of Geophysical Research*, 69(16):3395–3401.
- Kaufmann, S., C. Qing, N. Levenson, and M. Hanson  
11/2012. Transportation transportation during and after hurricane sandy.
- Kay, J. E., M. M. Holland, and A. Jahn  
2011. Inter-annual to multi-decadal arctic sea ice extent trends in a warming world. *Geophysical Research Letters*, 38(15):n/a–n/a.
- Keller, D. P., A. Lenton, V. Scott, N. E. Vaughan, N. Bauer, D. Ji, C. D. Jones, B. Kravitz, H. Muri, and K. Zickfeld  
2017. The carbon dioxide removal model intercomparison project (cdr-mip): Rationale and experimental design. *Geoscientific Model Development Discussions*, Pp. 1–72.
- Kelletat, D.  
1992. Coastal erosion and protection measures at the german north sea coast. *JOURNAL OF COASTAL RESEARCH*, 8(3):699–711.
- Kennedy, M. and A. O'Hagan  
2001. Bayesian calibration of computer models. *Journal of the Royal Statistical Society*, 63(3):425–464.
- Kerin, I., S. Giri, and D. Bekić  
2018. Simulation of levee breach using delft models: A case study of the drava river flood event. In *Advances in Hydroinformatics*, P. Gourbesville, J. Cunge, and G. Caignaert, eds., Springer Water, Pp. 1117–1131. Singapore: Springer Singapore.
- KFKI  
2002. *EAK 2002: Empfehlungen für die Ausführung von Küstenschutzwerken*, volume 65.2002 of *Die Küste*. Heide: Westholsteinische Verl.-Anst. Boyens.
- Knippertz, P., U. Ulbrich, and P. Speth  
2000. Changing cyclones and surface wind speeds over the north atlantic and europe in a transient ghg experiment. *Climate Research*, 15:109–122.
- Kopp, R. E., A. C. Kemp, K. Bittermann, B. P. Horton, J. P. Donnelly, W. R. Gehrels, C. C. Hay, J. X. Mitrovica, E. D. Morrow, and S. Rahmstorf  
2016. Temperature-driven global sea-level variability in the common era. *Proceedings of the National Academy of Sciences of the United States of America*, 113(11):E1434–41.
- Kossin, J. P. and D. J. Vimont  
2007. A more general framework for understanding atlantic hurricane variability and trends. *Bulletin of the American Meteorological Society*, 88(11):1767–1782.
- Kösters, F. and C. Winter  
2014. Exploring german bight coastal morphodynamics based on modelled bed shear stress. *Geo-Marine Letters*, 34(1):21–36.

- Kramer, J. and H. Rohde, eds.  
1992. *Historischer Küstenschutz: Deichbau, Inselschutz u. Binnenentwässerung an Nord- u. Ostsee*. Stuttgart: Wittwer.
- Krämer, K. and C. Winter  
2016. Predicted ripple dimensions in relation to the precision of in situ measurements in the southern north sea. *Ocean Science*, 12(6):1221–1235.
- Kraus, N. C., M. Larson, and D. L. Kriebel  
1991. Evaluation of beach erosion and accretion predictorspp.527-587. *Proc. Co. Sediments'91*, 1991(91):527–587.
- Kreye, P., M. Gocht, and K. Förster  
2010. Development of process descriptions of infiltration and near-surface runoff in water-balance modelling. *Hydrologie und Wasserbewirtschaftung*, 54(5):268–278.
- Kroese, D., T. Taimre, and Z. Botev  
2011. *Handbook of Monte Carlo Methods, Wiley Series in Probability and Statistics, John Wiley and Sons, New York*. New York: Wiley Series in Probability and Statistics. John Wiley and Sons.
- Kubicki, A. and A. Bartholomä  
2011. Sediment dynamics in the jade tidal channel prior to port construction, southeastern north sea: Ics2011. *JOURNAL OF COASTAL RESEARCH*, 2011(64).
- Kubicki, A., F. Kösters, and A. Bartholomä  
2017. Dune convergence/divergence controlled by residual current vortices in the jade tidal channel, south-eastern north sea. *Geo-Marine Letters*, 37(1):47–58.
- Lange, D., H. Müller, and F. Piechota  
2008. The weser estuary. In *Die Küste*, KFKI, ed., volume 74, Pp. 275–285. Karlsruhe: Bundesanst. für Wasserbau (BAW).
- Leckebusch, G. C., B. Koffi, U. Ulbrich, J. G. Pinto, T. Spangehl, and S. Zacharias  
2006. Analysis of frequency and intensity of european winter storm events from a multi-model perspective, at synoptic and regional scales. *Climate Research*, 31:59–74.
- Leckebusch, G. C., A. Weimer, J. G. Pinto, M. Reyers, and P. Speth  
2008. Extreme wind storms over europe in present and future climate: A cluster analysis approach. *Meteorologische Zeitschrift*, 17(1):67–82.
- Legeais, J., Z. L. Ablain M., S. M. F.-M. L. F. M. A. O. R. S. C. P. Q. G. P. M. C. A. Zuo H., Johannessen J.A., and B. J.  
2018. An improved and homogeneous altimeter sea level record from the esa climate change initiative. *Earth System Science*, 10(1):281–301.
- Leibniz, G. W., C. L. Scheidt, W. v. Engelhardt, and F.-W. Wellmer, eds.  
2014. *Protogaea: Sive de prima facie telluris et antiquissimae historiae vestigiis in ipsis naturae monumentis dissertatio*, Historia Scientiarum Fachgebiet Philosophie. Hildesheim: Olms-Weidmann.
- Leichtweiß-Institute  
2000. *Flussgebietsmodell für den Wasser- und Stoffhaushalt im Einzugsgebiet des Weserästuars: Teilprojekt: Wasserwirtschaft: Endbericht*. GE: Deutsches Zentrum für Luft- und Raumfahrt

- (DLR) - Umweltsystemforschung (USF).
- Leuliette, E. W.  
2015. The balancing of the sea-level budget. *Current Climate Change Reports*, 1(3):185–191.
- Liedtke, H.  
2003. *Relief, Boden und Wasser*, volume 2 of *Nationalatlas Bundesrepublik Deutschland*. Heidelberg, Berlin: Spektrum Akad. Verl.
- Lin, I.-I., I.-F. Pun, and C.-C. Lien  
2014. “category-6” supertyphoon haiyan in global warming hiatus: Contribution from subsurface ocean warming. *Geophysical Research Letters*, 41(23):8547–8553.
- Lindenberg, J., H.-T. Mengelkamp, and G. Rosenhagen  
2012. Representativity of near surface wind measurements from coastal stations at the german bight. *Meteorologische Zeitschrift*, 21(1):99–106.
- Lionello, P., I. F. Trigo, V. Gil, M. L. R. Liberato, K. M. Nissen, J. G. Pinto, C. C. Raible, M. Reale, A. Tanzarella, R. M. Trigo, S. Ulbrich, and U. Ulbrich  
2016. Objective climatology of cyclones in the mediterranean region: A consensus view among methods with different system identification and tracking criteria. *Tellus A: Dynamic Meteorology and Oceanography*, 68(1):29391.
- LKNSH  
2013. Generalplan küstenschutz des landes schleswig-holstein: Fortschreibung 2012.
- Lobanova, A., S. Liersch, J. P. Nunes, I. Didovets, J. Stagl, S. Huang, H. Koch, M. d. R. Rivas López, C. F. Maule, F. Hattermann, and V. Krysanova  
2018. Hydrological impacts of moderate and high-end climate change across european river basins. *Journal of Hydrology: Regional Studies*, 18:15–30.
- Loewe, P.  
2009. System nordsee: Zustand 2005 im kontext langzeitlicher entwicklungen.
- Losada, I. J., B. G. Reguero, F. J. Méndez, S. Castanedo, A. J. Abascal, and R. Mínguez  
2013. Long-term changes in sea-level components in latin america and the caribbean. *Global and Planetary Change*, 104:34–50.
- Lott, F. and C. Millet  
2009. The representation of gravity waves in atmospheric general circulation models (gcms). In *Infrasound Monitoring for Atmospheric Studies*, A. Le Pichon, E. Blanc, and A. Hauchecorne, eds., Pp. 685–699. Dordrecht: Springer Netherlands.
- Lowe, J. A.  
2009. *Marine & coastal projections*. [Exeter]: [Met Office Hadley Centre].
- Lowe, J. A. and J. M. Gregory  
2005. The effects of climate change on storm surges around the united kingdom. *Philosophical transactions. Series A, Mathematical, physical, and engineering sciences*, 363(1831):1313–1328.
- LSBG  
2012. *Gewässer und Hochwasserschutz in Zahlen*, volume 14 of *Berichte des Landesbetriebes Straßen, Brücken und Gewässer*. Hamburg, GE: Freie und Hansestadt Hamburg im Auftrag

der Behörde für Stadtentwicklung.

LSBG

2014. Die sturmflut nach dem tief xaver vom 5. bis 7. dezember 2013.

Ludwig, W. and J.-L. Probst

1998. River sediment discharge to the oceans; present-day controls and global budgets. *American Journal of Science*, 298(4):265–295.

Luijendijk, A., G. Hagenaars, R. Ranasinghe, F. Baart, G. Donchyts, and S. Aarninkhof

2018. The state of the world's beaches. *Scientific reports*, 8(1):6641.

Magnusson, L., J.-R. Bidlot, S. T. K. Lang, A. Thorpe, N. Wedi, and M. Yamaguchi

2014. Evaluation of medium-range forecasts for hurricane sandy. *Monthly Weather Review*, 142(5):1962–1981.

Malcherek, A.

2010. *Gezeiten und Wellen: Die Hydromechanik der Küstengewässer*, 1. aufl. edition. s.l.: Vieweg+Teubner (GWV).

Manabe, S. and K. Bryan

1969. Climate calculations with a combined ocean-atmosphere model. *Journal of the Atmospheric Sciences*, 26(4):786–789.

Marcos, M., G. Chust, G. Jordà, and A. Caballero

2012. Effect of sea level extremes on the western basque coast during the 21st century. *Climate Research*, 51(3):237–248.

Marcos, M., G. Jordà, D. Gomis, and B. Pérez

2011. Changes in storm surges in southern europe from a regional model under climate change scenarios. *Global and Planetary Change*, 77(3-4):116–128.

Marks, F. D.

2003. Hurricanes. In *Encyclopedia of atmospheric sciences*, J. R. Holton, ed., volume 1, Pp. 942–966. Amsterdam: Academic Press.

Marsigli, C., F. Boccanera, A. Montani, and T. Paccagnella

2005. The cosmo-leps mesoscale ensemble system: Validation of the methodology and verification. *Nonlinear Processes in Geophysics*, 12(4):527–536.

Martínez-Alvarado, O., S. L. Gray, J. L. Catto, and P. A. Clark

2014. Corrigendum: Sting jets in intense winter north-atlantic windstorms (2012 environ. res. lett. 7 024014). *Environmental Research Letters*, 9(3):039501.

Mastrandrea, M. D., C. B. Field, T. F. Stocker, O. Edenhofer, K. L. Ebi, D. J. Frame, H. Held, E. Kriegler, K. J. Mach, P. R. Matschoss, G.-K. Plattner, G. W. Yohe, and F. W. Zwiers

2011. Guidance note for lead authors of the ipcc fifth assessment report on consistent treatment of uncertainties: Ipcc cross-working group meeting on consistent treatment of uncertainties: Jasper ridge, ca, usa 6-7 july 2010. *IPPC*, 2011:1–7.

Matthies, H. G.

2007. Quantifying uncertainty: modern computational representation of probability and applications", extreme man-made and natural hazards in dynamics of structures. *NATO Security*

- through Science Series - C*, 1(1):105–135.
- Mawdsley, R. J., I. D. Haigh, and N. C. Wells  
2015. Global secular changes in different tidal high water, low water and range levels. *Earth's Future*, 3(2):66–81.
- Meier, H. E., B. Broman, and E. Kjellström  
2004. Simulated sea level in past and future climates of the baltic sea. *Climate Research*, 27:59–75.
- Meier, H. E. M.  
2006. Baltic sea climate in the late twenty-first century: A dynamical downscaling approach using two global models and two emission scenarios. *Climate Dynamics*, 27(1):39–68.
- Met Office  
2011. Climate observations, projections and impacts.
- Met Office  
2013. St jude's day storm - october 2013.
- Michaelis, A. C., J. Willison, G. M. Lackmann, and W. A. Robinson  
2017. Changes in winter north atlantic extratropical cyclones in high-resolution regional pseudo-global warming simulations. *Journal of Climate*, 30(17):6905–6925.
- Milliman, J. D. and R. H. Meade  
1983. World-wide delivery of river sediment to the oceans. *The Journal of Geology*, 91(1):1–21.
- Milliman, J. D. and J. P. M. Syvitski  
1992. Geomorphic/tectonic control of sediment discharge to the ocean: The importance of small mountainous rivers. *The Journal of Geology*, 100(5):525–544.
- Muis, S.  
2016-06-22. Global tide and surge reanalysis (gtsr).
- Muis, S., M. Verlaan, H. C. Winsemius, Aerts, Jeroen C. J. H., and P. J. Ward  
2016. A global reanalysis of storm surges and extreme sea levels. *Nature communications*, 7:11969 EP –.
- MunichRe  
2014. *TOPICS GEO Naturkatastrophen 2013: Analysen, Bewertungen, Positionen: Hochwasser-jahr*, Topics Geo. Munich: Münchener Rückversicherungs-Gesellschaft.
- MunichRe  
2017. *TOPICS GEO Naturkatastrophen 2016: Analysen, Bewertungen, Positionen: Land unter*, Topics Geo. Munich: Münchener Rückversicherungs-Gesellschaft.
- MunichRe  
2018a. Teuerste winterstürme für die versicherungswirtschaft in europa von 1980 bis 2016 nach gesamtschäden und versichertem schaden: in mio. usd: Natcatservice. In *Katastrophenschäden der Versicherungswirtschaft*, statista, ed. Hamburg, London, New York: n.a.
- MunichRe  
2018b. *TOPICS GEO Naturkatastrophen 2017: Analysen, Bewertungen, Positionen: Ein Jahr der Stürme*, Topics Geo. Munich: Münchener Rückversicherungs-Gesellschaft.



Munk, W. H.

2005. Origin and generation of waves. *Coastal Engineering Proceedings*, 1(1):1.

Murphy, A. H.

1988. Skill scores based on the mean square error and their relationships to the correlation coefficient. *Monthly Weather Review*, 116(12):2417–2424.

Murphy, A. H. and E. S. Epstein

1989. Skill scores and correlation coefficients in model verification. *Monthly Weather Review*, 117(3):572–582.

NatCatSERVICE

2018. Natural catastrophe statistics online – the new natcatservice analysis tool. In *Katastrophen-schäden der Versicherungswirtschaft*, statista, ed., volume 1, P. 1. Hamburg, London, New York: n.a.

NDR

31/10/2017. Sturmflut: strand unter auf wangerooge.

Nerem, R. S., B. D. Beckley, J. T. Fasullo, B. D. Hamlington, D. Masters, and G. T. Mitchum

2018. Climate-change-driven accelerated sea-level rise detected in the altimeter era. *Proceedings of the National Academy of Sciences of the United States of America*.

Neu, U., M. G. Akperov, N. Bellenbaum, R. Benestad, R. Blender, R. Caballero, A. Coccozza, H. F. Dacre, Y. Feng, K. Fraedrich, J. Grieger, S. Gulev, J. Hanley, T. Hewson, M. Inatsu, K. Keay, S. F. Kew, I. Kindem, G. C. Leckebusch, M. L. R. Liberato, P. Lionello, I. I. Mokhov, J. G. Pinto, C. C. Raible, M. Reale, I. Rudeva, M. Schuster, I. Simmonds, M. Sinclair, M. Sprenger, N. D. Tilinina, I. F. Trigo, S. Ulbrich, U. Ulbrich, X. L. Wang, and H. Wernli

2013. Imilast: A community effort to intercompare extratropical cyclone detection and tracking algorithms. *Bulletin of the American Meteorological Society*, 94(4):529–547.

Nicholls, R. J., N. Marinova, J. A. Lowe, S. Brown, P. Vellinga, D. de Gusmão, J. Hinkel, and R. S. J. Tol

2011. Sea-level rise and its possible impacts given a 'beyond 4 degree celsius world' in the twenty-first century. *Philosophical transactions. Series A, Mathematical, physical, and engineering sciences*, 369(1934):161–181.

Niemeyer, H. D., G. Beaufort, R. Mayerle, J. Monbaliu, I. Townend, H. Toxvig Madsen, H. de Vriend, and A. Wurpts

2016. Socio-economic impacts—coastal protection. In *North Sea Region Climate Change Assessment*, M. Quante and F. Colijn, eds., Regional Climate Studies, Pp. 457–474. Cham: Springer International Publishing.

NLWKN

2004. *Jahresbericht 2004*, Jahresbericht. Norden: Bley Offset.

NLWKN

2005. *Jahresbericht 2005*, Jahresbericht. Norden: Bley Offset.

NLWKN

2006. *Jahresbericht 2006*, Jahresbericht. Norden: Bley Offset.

NLWKN

- 2007a. *Generalplan Küstenschutz Niedersachsen/Bremen -Festland-: Küstenschutz Band 1.* Norden, GE: NLWKN.
- NLWKN
- 2007b. *Jahresbericht 2007*, Jahresbericht. Norden: Bley Offset.
- NLWKN
2008. *Jahresbericht 2008*, Jahresbericht. Norden: Bley Offset.
- NLWKN
2009. *Jahresbericht 2009*, Jahresbericht. Norden: Bley Offset.
- NLWKN
2010. *Jahresbericht 2010*, Jahresbericht. Norden: Bley Offset.
- NLWKN
- 2011a. *Generalplan Küstenschutz Niedersachsen/Bremen -Ostfriesische Inseln -: Küstenschutz Band 2.* Norden, GE: NLWKN.
- NLWKN
- 2011b. *Jahresbericht 2011*, Jahresbericht. Norden: Bley Offset.
- NLWKN
2012. *Jahresbericht 2012*, Jahresbericht. Norden: Bley Offset.
- NLWKN
2013. *Jahresbericht 2013*, Jahresbericht. Norden: Bley Offset.
- NLWKN
- 2014a. *Deutsches Gewässerkundliches Jahrbuch: Weser- und Emsgebiet: 2014 (1.11.2013-31.12.2014)*, DGJ 2014. Norden, GE: Digitale Ausgabe - Version 4.0, Woköck Geotechnik, Braunschweig, GE.
- NLWKN
- 2014b. *Jahresbericht 2014*, Jahresbericht. Norden: Bley Offset.
- NLWKN
2015. *Jahresbericht 2015*, Jahresbericht. Norden: Bley Offset.
- NLWKN
2016. *Jahresbericht 2016*, Jahresbericht. Norden: Bley Offset.
- NLWKN
2018. *Jahresbericht 2017/2018*, Jahresbericht. Norden: Bley Offset.
- NMW
2016. Ergebnis machbarkeitsstudie jadeweserport ii liegt vor.
- NOAA, ed.
2018. *Climate Timeseries: AMO (Atlantic Multidecadal Oscillation) Index*. United States: Physical Science Division.
- NWO
2018. Daten und fakten: Bereits über 1 milliarde tonnen rohöl umgeschlagen.
- Otto, F. E. L., N. Massey, G. J. van Oldenborgh, R. G. Jones, and M. R. Allen



2012. Reconciling two approaches to attribution of the 2010 russian heat wave. *Geophysical Research Letters*, 39(4):n/a–n/a.
- Otto, F. E. L., R. B. Skeie, J. S. Fuglestedt, T. Berntsen, and M. R. Allen  
2017. Assigning historic responsibility for extreme weather events. *Nature Climate Change*, 7:757 EP –.
- Oumeraci, H., G. Gönnert, J. Jensen, A. Kortenhaus, P. Fröhle, B. Gerkenmeier, T. Wahl, C. Mudersbach, M. Naulin, G. Ujeyl, E. Pasche, D. R. Dassanayake, and A. Burzel  
2012. Xtremrisk: Extremsturmfluten an offenen küsten und ästuarge-bieten - risikoermittlung und -beherrschung im kli-mawandel (xtremrisk): Abschlussberichr.
- Pall, P., T. Aina, D. A. Stone, P. A. Stott, T. Nozawa, A. G. J. Hilberts, D. Lohmann, and M. R. Allen  
2011. Anthropogenic greenhouse gas contribution to flood risk in england and wales in autumn 2000. *Nature*, 470(7334):382–385.
- Parker, H. R., E. Boyd, R. J. Cornforth, R. James, F. E. L. Otto, and M. R. Allen  
2016. Stakeholder perceptions of event attribution in the loss and damage debate. *Climate Policy*, 17(4):533–550.
- Partheniades, E.  
1965. Erosion and deposition of cohesive soils. *Journal of the Hydraulics Division*, 91(1):105–139.
- Pawlowicz, R., B. Beardsley, and S. Lentz  
2002. Classical tidal harmonic analysis including error estimates in matlab using t\_tide. *Computers & Geosciences*, 28(8):929–937.
- Pelling, H. E., J. A. Mattias Green, and S. L. Ward  
2013. Modelling tides and sea-level rise: To flood or not to flood. *Ocean Modelling*, 63:21–29.
- Petroliagkis, T. I., E. Voukouvalas, J. Disperati, and J. Bidlot  
2016. *Joint probabilities of storm surge, significant wave height and river discharge components of coastal flooding events: Utilising statistical dependence methodologies & techniques*, volume 27824 of *EUR, Scientific and technical research series*. Luxembourg: Publications Office.
- Pfahl, S., P. A. O’Gorman, and E. M. Fischer  
2017. Understanding the regional pattern of projected future changes in extreme precipitation. *Nature Climate Change*, 7(6):423–427.
- Phillips, N. A.  
1956. The general circulation of the atmosphere: A numerical experiment. *Quarterly Journal of the Royal Meteorological Society*, 1956(Vol. 82 No. 352):123–164.
- PIANC  
2004. *Dredging of marinas: RecCom report of WG 13: RecCom Working Group 13*, volume 13 of *The World Association for Waterborne Transport Infrastructures*, 1 edition. Bruxelles, Belgium: PIANC Secrétariat Général.
- PIANC  
2008. *Minimising harbour siltation: MarCom report 102*, volume 102 of *The World Association for Waterborne Transport Infrastructures*, 1 edition. Bruxelles: PIANC Secrétariat Général.



- Pickering, M. D., N. C. Wells, K. J. Horsburgh, and J. Green  
2012. The impact of future sea-level rise on the european shelf tides. *Continental Shelf Research*, 35:1–15.
- Pietrzak, J. D., G. J. de Boer, and M. A. Eleveld  
2011. Mechanisms controlling the intra-annual mesoscale variability of sst and spm in the southern north sea. *Continental Shelf Research*, 31(6):594–610.
- Pinto, J. G., U. Ulbrich, G. C. Leckebusch, T. Spanghehl, M. Meyers, and S. Zacharias  
2007. Changes in storm track and cyclone activity in three sres ensemble experiments with the ecam5/mpiom1 gcm. *Climate Dynamics*, 29(2-3):195–210.
- Pinto, J. G., S. Zacharias, A. H. Fink, G. C. Leckebusch, and U. Ulbrich  
2009. Factors contributing to the development of extreme north atlantic cyclones and their relationship with the nao. *Climate Dynamics*, 32(5):711–737.
- Planck, M.  
1899. Über irreversible strahlungsvorgänge. *Sitzungsberichte der Königlich Preussischen Akademie der Wissenschaften zu Berlin - Erster Halbband (Verl. d. Kgl. Akad. d. Wiss., Berlin 1899)*. Seite 479–480., 1899(Erster Halbband (Verl. d. Kgl. Akad. d. Wiss., Berlin 1899)):479–480.
- Plass, G. N.  
1956. The carbon dioxide theory of climatic change. *Tellus*, 8(2):140–154.
- Plüß, A.  
2003. Das nordseemodell der baw zur simulation der tide in der deutschen bucht. In *Die Küste*, P. Hupfer, ed., volume 67, Pp. 84–127. Karlsruhe: Bundesanst. für Wasserbau (BAW).
- Ponce de León, S. and C. Guedes Soares  
2014. Extreme wave parameters under north atlantic extratropical cyclones. *Ocean Modelling*, 81:78–88.
- Pontee, N.  
2013. Defining coastal squeeze: A discussion. *Ocean & Coastal Management*, 84:204–207.
- Postma, H.  
1967. Sediment transport and sedimentation in the estuarine environment. In *Estuaries*, G. H. Lauff, ed., volume 83 of *Estuaries*, Pp. 158–179. Washington, DC: American Association for the Advancement of Science Publication.
- Puls, W., T. Pohlmann, and J. Sündermann  
1997. Suspended particulate matter in the southern north sea: Application of a numerical model to extend nerc north sea project data interpretation. *German Journal of Hydrography*, Volume 49(Number 2/3):307–327.
- Quante, M. and F. Colijn, eds.  
2016. *North Sea Region Climate Change Assessment*, Regional Climate Studies. Cham: Springer International Publishing.
- Rahmstorf, S. and D. Coumou  
2011. Increase of extreme events in a warming world. *Proceedings of the National Academy of Sciences of the United States of America*, 108(44):17905–17909.

- Ranasinghe, R.  
2016. Assessing climate change impacts on open sandy coasts: A review. *Earth-Science Reviews*, 160:320–332.
- Rasmussen, D. J., K. Bittermann, M. K. Buchanan, S. Kulp, B. H. Strauss, R. E. Kopp, and M. Openheimer  
2018. Extreme sea level implications of 1.5, 2.0, and 2.5 degree celsius temperature stabilization targets in the 21st and 22nd centuries. *Environmental Research Letters*, 13(3):034040.
- Reistad, M., A. K. Magnusson, S. Haver, O. T. Gudmestad, and D. Kvamme  
2005. How severe wave conditions are possible on the norwegian continental shelf? *Marine Structures*, 18(5-6):428–450.
- Rhein, M., S. R. R. S. A.-E. C. D. C. R. A. F. S. G. G. C. J. S. A. J. A. K. C. M. D. R. L. D. T. and F. Wang  
2013. Observations: Ocean. *IPCC, AR5(Chapter 3)*:255–316.
- Roberts, J. F., A. J. Champion, L. C. Dawkins, K. I. Hodges, L. C. Shaffrey, D. B. Stephenson, M. A. Stringer, H. E. Thornton, and B. D. Youngman  
2014. The xws open access catalogue of extreme european windstorms from 1979 to 2012. *Natural Hazards and Earth System Sciences*, 14(9):2487–2501.
- Rockel, B. and K. Woth  
2007. Extremes of near-surface wind speed over europe and their future changes as estimated from an ensemble of rcm simulations. *Climatic Change*, 81(S1):267–280.
- Roelvink, D., A. Reniers, A. van Dongeren, J. van Thiel de Vries, R. McCall, and J. Lescinski  
2009. Modelling storm impacts on beaches, dunes and barrier islands. *Coastal Engineering*, 56(11-12):1133–1152.
- Romero, R. and K. Emanuel  
2017. Climate change and hurricane-like extratropical cyclones: Projections for north atlantic polar lows and medicanes based on cmip5 models. *Journal of Climate*, 30(1):279–299.
- Ross, S. M.  
2014. *Introduction to probability and statistics for engineers and scientists*, 5. ed. edition. Amsterdam: Elsevier Acad. Press.
- Roudier, P., J. C. M. Andersson, C. Donnelly, L. Feyen, W. Greuell, and F. Ludwig  
2016. Projections of future floods and hydrological droughts in europe under a +2 degree celsius global warming. *Climatic Change*, 135(2):341–355.
- Rovere, A., P. Stocchi, and M. Vacchi  
2016. Eustatic and relative sea level changes. *Current Climate Change Reports*, 2(4):221–231.
- Rudeva, I., S. K. Gulev, I. Simmonds, and N. Tilinina  
2014. The sensitivity of characteristics of cyclone activity to identification procedures in tracking algorithms. *Tellus A: Dynamic Meteorology and Oceanography*, 66(1):24961.
- Ruttimann, J.  
2006. Milestones in scientific computing. *Nature*, 440:399 EP –.
- Salas, J. D., J. H. Heo, D. J. Lee, and P. Burlando

2013. Quantifying the uncertainty of return period and risk in hydrologic design. *Journal of Hydrologic Engineering*, 18(5):518–526.
- Sanders, F. and J. R. Gyakum  
1980. Synoptic-dynamic climatology of the “bomb”. *Monthly Weather Review*, 108(10):1589–1606.
- Santo, H., P. H. Taylor, and R. Gibson  
2016. Decadal variability of extreme wave height representing storm severity in the northeast atlantic and north sea since the foundation of the royal society. *Proceedings of the Royal Society A: Mathematical, Physical and Engineering Sciences*, 472(2193):20160376.
- Schmidt, H. and H. von Storch  
1993. German bight storms analysed. *Nature*, 365(6449):791.
- Schmitz, H. P.  
1965. Ein differenzgleichungssystem zur ermittlung instationärer bewegungen in einem meer mit geringer turbulenzreibung. *Deutsche Hydrographische Zeitschrift*, 18(3):97–113.
- Schmitz, H.-P., D. Habicht, and H. Volkert  
1988. Barotropic numerical experiments on external surge generation at the edge of the north-western european shelf. *Gerlands Beiträge zur Geophysik*, 1988(97):422–437.
- Schneidereit, A., R. Blender, K. Fraedrich, and F. Lunkeit  
2007. Icelandic climate and north atlantic cyclones in era-40 reanalyses. *Meteorologische Zeitschrift*, 2007(1):1–3.
- Schrottke, K., M. Becker, A. Bartholomä, B. W. Flemming, and D. Hebbeln  
2006. Fluid mud dynamics in the weser estuary turbidity zone tracked by high-resolution side-scan sonar and parametric sub-bottom profiler. *Geo-Marine Letters*, 26(3):185–198.
- Schrum, C., J. Lowe, H. E. M. Meier, I. Grabemann, J. Holt, M. Mathis, T. Pohlmann, M. D. Skogen, A. Sterl, and S. Wakelin  
2016. Projected change—north sea. In *North Sea Region Climate Change Assessment*, M. Quante and F. Colijn, eds., Regional Climate Studies, Pp. 175–217. Cham: Springer International Publishing.
- Schultz, D. M. and K. A. Browning  
2017. What is a sting jet? *Weather*, 72(3):63–66.
- Seager, R., M. Hoerling, S. Schubert, H. Wang, B. Lyon, A. Kumar, J. Nakamura, and N. Henderson  
2015. Causes of the 2011–14 california drought\*. *Journal of Climate*, 28(18):6997–7024.
- Shapiro, M. A. and D. Keyser  
1990. Fronts, jet streams, and the tropopause.
- Shepherd, T. G.  
2015. Climate science: The dynamics of temperature extremes. *Nature*, 522(7557):425–427.
- Shepherd, T. G.  
2016. A common framework for approaches to extreme event attribution. *Current Climate Change Reports*, 2(1):28–38.
- Shutts, G.



2005. A kinetic energy backscatter algorithm for use in ensemble prediction systems. *Quarterly Journal of the Royal Meteorological Society*, 131(612):3079–3102.
- Shutts, G., M. Leutbecher, A. Weisheimer, T. Stockdale, L. Isaksen, and M. Bonavita  
2011. Representing model uncertainty: stochastic parameterizations at ecmwf. *ECMWF Newsletter*, 2011(129):19–24.
- Siegismund, F. and C. Schrum  
2001. Decadal changes in the wind forcing over the north sea. *Climate Research*, 18:39–45.
- Simmonds, I. and I. Rudeva  
2014. A comparison of tracking methods for extreme cyclones in the arctic basin. *Tellus A: Dynamic Meteorology and Oceanography*, 66(1):25252.
- Slangen, A. B. A., J. A. Church, X. Zhang, and D. Monselesan  
2014. Detection and attribution of global mean thermosteric sea level change. *Geophysical Research Letters*, 41(16):5951–5959.
- Small, C. and R. J. Nicholls  
2003. A global analysis of human settlement in coastal zones. *JOURNAL OF COASTAL RESEARCH*, 2003(19 (3)):584–599.
- Smeaton, J. F.  
1759. An experimental enquiry concerning the natural powers of water and wind to turn mills, and other machines, depending on a circular motion. *Philosophical Transactions*, 1759(51):100–174.
- Smith, T. M., R. W. Reynolds, T. C. Peterson, and J. Lawrimore  
2008. Improvements to noaa’s historical merged land–ocean surface temperature analysis (1880–2006). *Journal of Climate*, 21(10):2283–2296.
- Smits, A., A. M. G. Klein Tank, and G. P. Können  
2005. Trends in storminess over the netherlands, 1962-2002. *International Journal of Climatology*, 25(10):1331–1344.
- Sparrow, S., R. J. Millar, K. Yamazaki, N. Massey, A. C. Povey, A. Bowery, R. G. Grainger, D. Wallom, and M. Allen  
2018. Finding ocean states that are consistent with observations from a perturbed physics parameter ensemble. *Journal of Climate*, 31(12):4639–4656.
- Stachnik, J. P. and C. Schumacher  
2011. A comparison of the hadley circulation in modern reanalyses. *Journal of Geophysical Research*, 116(D22):n/a–n/a.
- statista, ed.  
2018. *Katastrophenschäden der Versicherungswirtschaft: Dossier*. Hamburg, London, New York: n.a.
- Stendel, M., E. van den Besselaar, A. Hannachi, E. C. Kent, C. Lefebvre, F. Schenk, G. van der Schrier, and T. Woollings  
2016. Recent change—atmosphere. In *North Sea Region Climate Change Assessment*, M. Quante and F. Colijn, eds., Regional Climate Studies, Pp. 55–84. Cham: Springer International Publishing.

- Sterl, A., A. M R Bakker, H. W. van den Brink, R. Haarsma, A. Stepek, I. L. Wijnant, and R. C. d. Winter  
2015. Large-scale winds in the southern north sea region: The wind part of the knmi'14 climate change scenarios. *Environmental Research Letters*, 10(3):035004.
- Sterl, A., H. van den Brink, H. de Vries, R. Haarsma, and E. van Meijgaard  
2009. An ensemble study of extreme storm surge related water levels in the north sea in a changing climate. *Ocean Science*, 5(3):369–378.
- Stewart, H., T. Bradwell, J. Bullard, S. J. Davies, N. Golledge, and R. D. McCulloch  
2017. 8000 years of north atlantic storminess reconstructed from a scottish peat record: Implications for holocene atmospheric circulation patterns in western europe. *Journal of Quaternary Science*, 32(8):1075–1084.
- Stocker, T., ed.  
2014. *Climate change 2013: The physical science basis : Working Group I contribution to the Fifth assessment report of the Intergovernmental Panel on Climate Change*. Cambridge: Cambridge University Press.
- Stott, P. A., D. A. Stone, and M. R. Allen  
2004. Human contribution to the european heatwave of 2003. *Nature*, 432(7017):610–614.
- Sturmflutwarndienst  
2013a. Die nordsee-sturmflut vom 28.10.2013: Erste nordseesturmflut des herbstes 2013.
- Sturmflutwarndienst  
2013b. Die nordseesturmfluten vom 5. und 6.12.2013: Xaver.
- Sündermann, J. and T. Pohlmann  
2011. A brief analysis of north sea physics. *Oceanologia*, 53(3):663–689.
- Sutherland, J., A. H. Peet, and R. L. Soulsby  
2004. Evaluating the performance of morphological models. *Coastal Engineering*, 51(8-9):917–939.
- SwissRe Sigma  
2017. *Natural catastrophes and man-made disasters in 2016: a year of widespread damages*, volume 2/2017 of 270 0217 en. Zurich, Swiss: Swiss Re Institute.
- Tabea Brodhagen, Natacha Fery, Lidia Gaslikova, Iris Grabemann, Elisabeth Rudolph, Birger Tinz, and Ralf Weisse  
2017. Analyse extremer sturmfluten an der deutschen nordseeküste und möglicher verstärkungen.
- Taylor, K. E., R. J. Stouffer, and G. A. Meehl  
2012. An overview of cmip5 and the experiment design. *Bulletin of the American Meteorological Society*, 93(4):485–498.
- Trenberth, K. E., J. T. Fasullo, and M. A. Balmaseda  
2014. Earth's energy imbalance. *Journal of Climate*, 27(9):3129–3144.
- Trenberth, K. E., J. T. Fasullo, and T. G. Shepherd  
2015. Attribution of climate extreme events. *Nature Climate Change*, 5(8):725–730.

TU Delft

2018. Swan: Simulating waves nearshore: User manual swan cycle iii version 41.20a.

Ulbrich, U., G. C. Leckebusch, J. Grieger, M. Schuster, M. Akperov, M. Y. Bardin, Y. Feng, S. Gulev, M. Inatsu, K. Keay, S. F. Kew, M. L. Liberato, P. Lionello, I. I. Mokhov, U. Neu, J. G. Pinto, C. C. Raible, M. Reale, I. Rudeva, I. Simmonds, N. D. Tilinina, I. F. Trigo, S. Ulbrich, and Wang  
2013. Are greenhouse gas signals of northern hemisphere winter extra-tropical cyclone activity dependent on the identification and tracking algorithm? *Meteorologische Zeitschrift*, 22(1):61–68.

Ulbrich, U., J. G. Pinto, H. Kupfer, G. C. Leckebusch, T. Spanghel, and M. Meyers

2008. Changing northern hemisphere storm tracks in an ensemble of ipcc climate change simulations. *Journal of Climate*, 21(8):1669–1679.

UNESCO

1981. *Tenth report of the joint panel on oceanographic tables and standards*, volume 36 of *UNESCO technical papers in marine science*, 10 edition. Paris, France: United Nations Educational, Scientific and Cultural Organization.

United Nations

12/1988. Protection of global climate for present and future generations of mankind: A/res/43/53.

United Nations

2015. Paris agreement: Unfccc.

United Nations

2017. *World Population Prospects: The 2017 Revision, Key Findings and Advance Tables: Working Paper*, No. ESA/P/WP/248. United Nations.

Universität Siegen, Forschungsinstitut Wasser und Umwelt

2012. Kleine dokumentation historischer sturmfluten.

U.S. Department of Energy

31/12/2012. Hurricane sandy situation report: Office of electricity delivery and energy reliability.

Valerius, J., F. Kösters, and M. Zeiler

2015. Erfassung von sandverteilungsmustern zur großräumigen analyse der sedimentdynamik auf dem schelf der deutschen bucht. In *Aufbau von integrierten Modellsystemen zur Analyse der langfristigen Morphodynamik in der Deutschen Bucht*, KFKI, ed., volume 83 of *Die Küste*, Pp. 39–63. Karlsruhe: Bundesanstalt für Wasserbau.

van Rijn, L. C.

1993. *Principles of sediment transport in rivers, estuaries and coastal seas*. Amsterdam: Aqua Publications.

van Rijn, L. C., J. S. Ribberink, J. van der Werf, and D. J. Walstra

2013. Coastal sediment dynamics: Recent advances and future research needs. *Journal of Hydraulic Research*, 51(5):475–493.

Vilibić, I. and J. Šepić

2010. Long-term variability and trends of sea level storminess and extremes in european seas. *Global and Planetary Change*, 71(1-2):1–12.

- Vlaamse Overheid  
2018. Sigmoplan.
- von Storch, H.  
2014. Storm surges: Phenomena, forecasting and scenarios of change. *Procedia IUTAM*, 10:356–362.
- von Storch, H. and H. Reichardt  
1997. A scenario of storm surge statistics for the german bight at the expected time of doubled atmospheric carbon dioxide concentration. *Journal of Climate*, 10(10):2653–2662.
- von Storch, H. and R. Weisse  
2008. Regional storm climate and related marine hazards in the northeast atlantic. In *Climate Extremes and Society*, H. F. Diaz and R. J. Murnane, eds., Pp. 54–73. Cambridge: Cambridge University Press.
- Vörösmarty, C. J., M. Meybeck, B. Fekete, K. Sharma, P. Green, and J. P. Syvitski  
2003. Anthropogenic sediment retention: Major global impact from registered river impoundments. *Global and Planetary Change*, 39(1-2):169–190.
- Vousdoukas, M. I., L. Mentaschi, E. Voukouvalas, M. Verlaan, and L. Feyen  
2017. Extreme sea levels on the rise along europe’s coasts. *Earth’s Future*, 5(3):304–323.
- Vousdoukas, M. I., E. Voukouvalas, A. Annunziato, A. Giardino, and L. Feyen  
2016. Projections of extreme storm surge levels along europe. *Climate Dynamics*, 47(9-10):3171–3190.
- Vuik, V., S. N. Jonkman, B. W. Borsje, and T. Suzuki  
2016. Nature-based flood protection: The efficiency of vegetated foreshores for reducing wave loads on coastal dikes. *Coastal Engineering*, 116:42–56.
- VYNOVA  
2018. Wilhelmshaven, germany.
- Wahl, T., I. D. Haigh, R. J. Nicholls, A. Arns, S. Dangendorf, J. Hinkel, and A. B. A. Slangen  
2017. Understanding extreme sea levels for broad-scale coastal impact and adaptation analysis. *Nature communications*, 8:16075.
- Wahl, T., I. D. Haigh, P. L. Woodworth, F. Albrecht, D. Dillingh, J. Jensen, R. J. Nicholls, R. Weisse, and G. Wöppelmann  
2013. Observed mean sea level changes around the north sea coastline from 1800 to present. *Earth-Science Reviews*, 124:51–67.
- Waldemar, R.  
1979. *Küstenentwicklung und Deichbau: während des Mittelalters zwischen Maade, Jade und Jadebusen*, Sonderdruck. Aurich, GE: Ostfriesische Landschaft.
- Walling, D. E.  
1983. The sediment delivery problem. *Journal of Hydrology*, 65(1-3):209–237.
- Walling, D. E.  
2009. *The impact of global change on erosion and sediment transport by rivers: Current progress and future challenges*. Paris, France: Unesco.



- Walstra, D., R. Hoekstra, P. K. Tonnon, and B. G. Ruessink  
2013. Input reduction for long-term morphodynamic simulations in wave-dominated coastal settings. *Coastal Engineering*, 77:57–70.
- Walstra, D. J. R., J. A. Roelvink, and J. Groeneweg  
2001. Calculation of wave-driven currents in a 3d mean flow model. In *Coastal Engineering 2000*, B. L. Edge, ed., Pp. 1050–1063, Reston, VA. American Society of Civil Engineers.
- Wan, H., X. L. Wang, and V. R. Swail  
2010. Homogenization and trend analysis of canadian near-surface wind speeds. *Journal of Climate*, 23(5):1209–1225.
- Ward, S. L., J. A. M. Green, and H. E. Pelling  
2012. Tides, sea-level rise and tidal power extraction on the european shelf. *Ocean Dynamics*, 62(8):1153–1167.
- WCRP, G.-S.-L.-B.-G.  
2018. Global sea-level budget 1993-present. *Earth System Science*, 10(1):1551–1590.
- Weisse, R., D. Bellafore, M. Menéndez, F. Méndez, R. J. Nicholls, G. Umgiesser, and P. Willems  
2014a. Changing extreme sea levels along european coasts. *Coastal Engineering*, 87:4–14.
- Weisse, R., L. Gaslikova, B. Geyer, N. Groll, and E. Meyer  
(2014)b. coastdat – model data for science and industry. In *Die Küste*, volume 81, Pp. 5–18. Karlsruhe: Bundesanst. für Wasserbau (BAW).
- Weisse, R. and I. Meinke  
2011. Nordseesturmfluten im klimawandel. In *Küstenmentalität und Klimawandel*, L. Fischer, ed., Pp. 131–140. München: oekom-verl.
- Weisse, R. and A. Plüess  
2006. Storm-related sea level variations along the north sea coast as simulated by a high-resolution model 1958–2002. *Ocean Dynamics*, 56(1):16–25.
- Weisse, R. and H. Storch  
2010. *Marine Climate and Climate Change: Storms, Wind Waves and Storm Surges*, Springer Praxis Books. Berlin, Heidelberg: Springer-Verlag Berlin Heidelberg.
- Weisse, R., H. von Storch, and F. Feser  
2005. Northeast atlantic and north sea storminess as simulated by a regional climate model during 1958–2001 and comparison with observations. *Journal of Climate*, 18(3):465–479.
- Weisse, R., H. von Storch, H. D. Niemeier, and H. Knaack  
2012. Changing north sea storm surge climate: An increasing hazard? *Ocean & Coastal Management*, 68:58–68.
- Wilhelm, von Gottes Gnaden Deutscher Kaiser, König von Preußen  
29/06/1883. Gesetz, betreffend die reichs-kriegshäfen und die feststellung eines nachtrages zum reichshaushalts-etat für das etatsjahr 1883/84: No 1497.
- Winter, C.  
2011a. Macro scale morphodynamics of the german north sea coast. *JOURNAL OF COASTAL RESEARCH*, 64(ICS2011, Proceedings of the 11th International Coastal Symposium):706–710.



- Winter, C.  
2011b. *Observation- and Modelling of Morphodynamics in Sandy Coastal Environments*. Habilitationsschrift, Universität Bremen, Bremen, GE.
- Winter, C. and A. Bartholomä  
2006. “coastal dynamics and human impact: South-eastern north sea”, an overview. *Geo-Marine Letters*, 26(3):121–124.
- Winter, R. C. d., A. Sterl, J. W. de Vries, S. L. Weber, and G. Ruessink  
2012. The effect of climate change on extreme waves in front of the dutch coast. *Ocean Dynamics*, 62(8):1139–1152.
- WMO  
2011. *Guide to storm surge forecasting*. Geneva: World Meteorological Organization.
- Wong, P. P., I. J. Losada, J. P. Gattuso, J. Hinkel, A. Khattabi, K. L. McInnes, Y. Saito, and A. Salenger  
2014. Coastal systems and low-lying areas. In *Climate Change 2014 Impacts, Adaptation, and Vulnerability*, C. B. Field, V. R. Barros, D. J. Dokken, K. J. Mach, and M. D. Mastrandrea, eds., Pp. 361–409. Cambridge: Cambridge University Press.
- Woodworth, P. L.  
2010. A survey of recent changes in the main components of the ocean tide. *Continental Shelf Research*, 30(15):1680–1691.
- Woollings, T., J. M. Gregory, J. G. Pinto, M. Meyers, and D. J. Brayshaw  
2012. Response of the north atlantic storm track to climate change shaped by ocean–atmosphere coupling. *Nature Geoscience*, 5(5):313–317.
- Wright, L. D. and B. G. Thom  
1977. Coastal depositional landforms. *Progress in Physical Geography: Earth and Environment*, 1(3):412–459.
- WSV  
2006a. Projektgruppe weseranpassung: Teil b (aw) erläuterungsbericht: zum plan für die anpassung der bundeswasserstraße außenweser von weserkilometer 65 bis weserkilometer 130.
- WSV  
2006b. Projektgruppe weseranpassung: Teil b (uw) erläuterungsbericht: zum plan für die anpassung der bundeswasserstraße unterweser von weserkilometer 8 bis weserkilometer 65.
- WSV  
2018a. Zentrales datenmanagement (zdm) küstendaten: Portal tideweser.
- WSV, W.  
2016. Schifffahrtsstraße jade: Wasserstraßen.
- WSV, W.  
2018b. Jade data base [personal communication with a. götschenberg].
- Xue, Y., M. J. Fennessy, and P. J. Sellers  
1996. Impact of vegetation properties on u.s. summer weather prediction. *Journal of Geophysical Research*, 101(D3):7419–7430.



XWS

2015. Extreme wind storms catalogue: Xws.

Zimmermann, C. and S. Mai

2004. Klimawandel und präventives risiko- und küstenschutzmanagement an der deutschen nordseeküste (krim): (teilprojekt 2 - klimaänderung und küstenschutz) ; endbericht ; (01.04.2001 - 31.05.2004).

Zitscher, F.-F., R. Scherenberg, and U. Carow

1979. Die sturmflut vom 3. und 21. januar 1976 an den küsten schleswig-holsteins: Empfehlungen für die ausführung von küstenschutzwerken. In *Sturmfluten 1976*, KFKI, ed., volume 33 of *Die Küste*, Pp. 71–99. Heide: Westholsteinische Verl.-Anst. Boyens.

Zorndt, A. C.

2014. *Impacts of climate change on hydrodynamic conditions and salinity of the Weser estuary*. Dissertation, Gottfried Wilhelm Leibniz Universität Hannover, Hannover, GE.

Zorndt, A. C., T. Schlurmann, and I. Grabemann

2012. The influence of extreme events on hydrodynamics and salinities in the weser estuary in the context of climate impact research. *Coastal Engineering Proceedings*, 2012(33):1–12.

Zorndt, A. C., A. Wurpts, and T. Schlurmann

2011. The influence of hydrodynamic boundary conditions on characteristics, migration, and associated sand transport of sand dunes in a tidal environment. *Ocean Dynamics*, 61(10):1629–1644.



## A Appendix



## A.1 Curriculum Vitae

### Personal Details

First Name, Name, acad. titles: Oliver, Lojek, Dipl.-Ing. (FH), M.Sc.  
DOB & POB: 22.05.1986, Siegburg, Nord-Rhein-Westfalen, DE  
Nationality: German

### Studies

10/2010 - 10/2012 LEIBNIZ UNIVERSITY HANNOVER, Lower Saxony, DE  
Faculty of Civil Engineering and Surveying  
Water Resources and Environmental Management  
Major: Water Resources Management  
Degree: M.Sc. Civil Engineering

10/2006 - 9/2010 LEUPHANA UNIVERSITY LÜNEBURG, Lower Saxony, DE  
Faculty III, Environmental Campus Suderburg  
Water Resources and Soil Management  
Major: Water protection and river basin management  
Degree: Dipl.-Ing. FH Civil Engineering

### Professional experience

since 3/2013 PhD. Civil Engineering at the Ludwig-Franzius-Institute  
for, Hydraulic Estuarine- and Coastal Engineering  
Lower Saxony, DE

1/2011 - 3/2012 Researcher at EPEA Int. Environmental Research Inc.  
Hamburg, DE

7/2009 - 3/2010 Student research assistant at EPEA Int. Environmental  
Research Inc., Hamburg, DE

7/2008 - 9/2008 Technical assistant with Prof. Dr.-Ing. H. Wittenberg,  
Leuphana University Lüneburg

### Educational training

7/2002 - 5/2006 German section of the AFNORTH International School, NL  
Degree: Higher educational entrance qualification

7/1999 - 6/2002 Ludwig-Meyn-Schule (Secondary school), Uetersen, DE

7/1996 - 6/1999 Deutsche Schule El Paso (Secondary school), TX, USA

## A.2 Model in- and outputs and featured resolutions

Table A.2.1: Model in- and outputs given for the various model components with their respective spatial and temporal resolution and source.

	Input	Output
FLOW (2DH Hydrodynamics)	Tidal water levels 1. min. resolution based point observations (WSV Wilhelmshaven, 2018; WSV Bremerhaven, 2018; WSV Bremen, 2018; WSV Brake, 2018)	26 hydrodynamic quantities (e.g. bed shear stresses, current velocities and directions) on a curvilinear grid comprising 4.5 mio. vertices; saved every 10 min. for the whole FLOW domain
	Discharge volumes daily mean values and long-term means from point observations (WSV Bremen, 2018; WSV Brake)	21 time series extracted at positions of observations stations (tide gauges, current meters) for subsequent evaluation of tidal constituents saved with a 10 min resolution
	Salinity and temperature 1. min resolution point based observations (WSV Bremerhaven; WSV Wilhelmshaven, 2018)	3 atmospheric quantities on the curvilinear grid discretizing the domain saved at 10 min resolution
	Wind velocities and mean sea level pressure both with 60 min resolution on 0.22° regular grid spacing from coastDat2 reanalysis data (HZG, 2014)	
	Bathymetry DTMW of 2012 of the lower and outer Weser (incl. Jade) with a 1x1m resolution (WSV, 2012) and North Sea floor with a 50x50m resolution (BSH, 2018)	
	Structures based on geo-data for training walls and terminals (WSV Wilhelmshaven, 2018; WSV Bremerhaven, 2018) implemented as <i>thin dams</i> and <i>porous plates</i>	
	↓      Direct bi-directional coupling on 0.05 min time step      ↓	
MOR/SED	Surface sediment information based on 520858 samples containing 14 sieve classes each (AufMod, 2015)	3-Dimensional sediment inventory eight morphodynamic quantities (e.g. bed load transport) Updated bathymetry during simulations saved every 10 min
	Sequentially layered bed with five different fractions	
	↓      Bi-directional coupling on 30 min intervals      ↓	
WAVE	Wave buoy observations with 15 min resolution from the station ELBE in the North Sea (BSH, 2018)	23 quantities characterizing the sea state on the WAVE domain saved every 10 min

### A.3 Reclassified sediment sample distribution

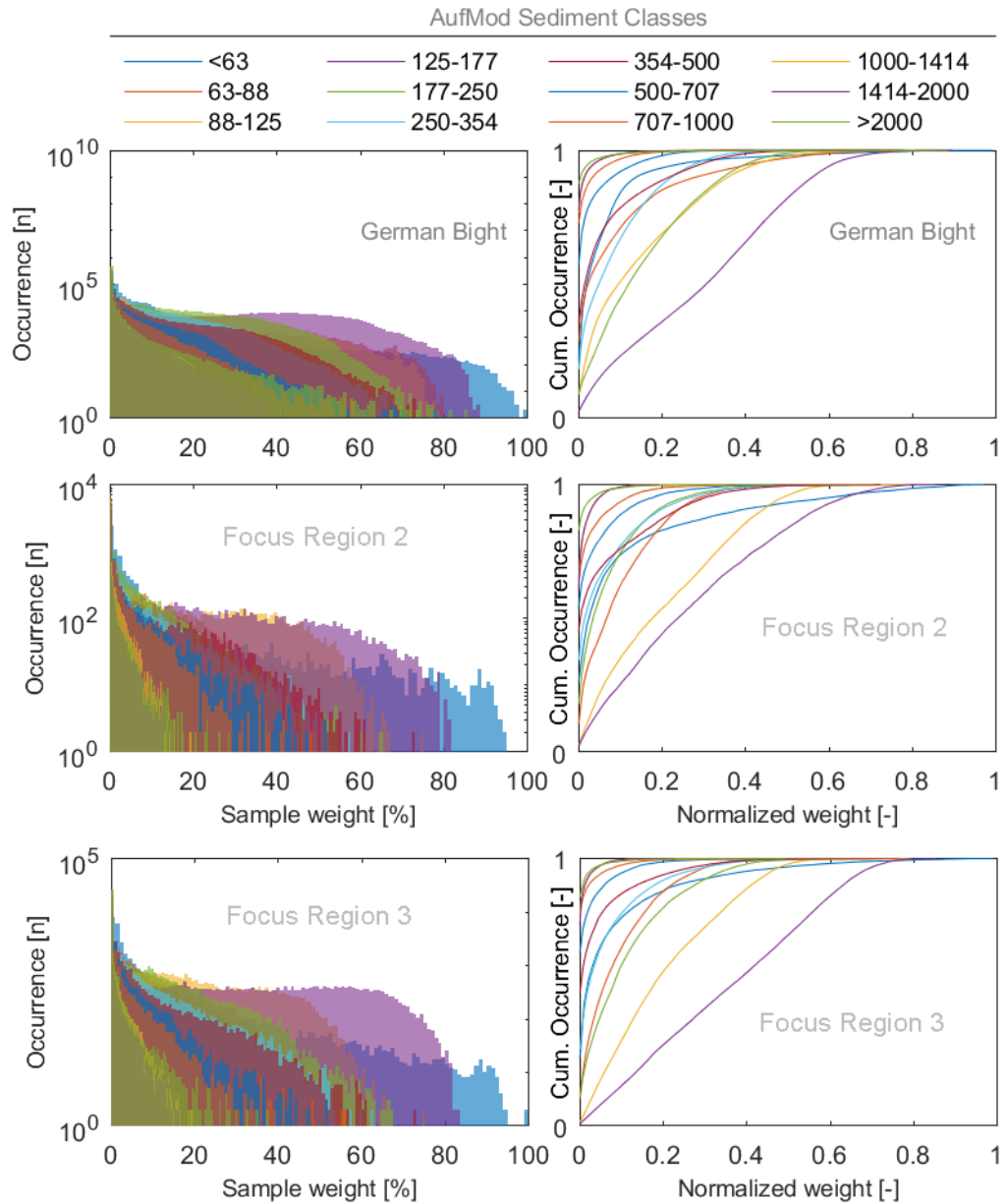


Figure A.1: Sediment sample distributions in the German Bight (top panels), focus region two (mid panels) and focus area three (bottom panels)



#### A.4 Decomposition of tide gauge signal for storm surge events

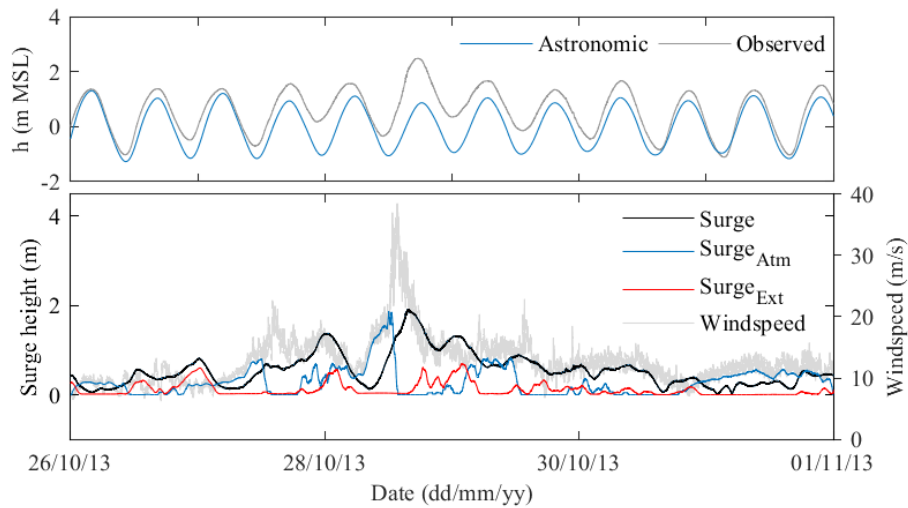


Figure A.2: Tidal water level observation during Christian (upper panel) and single components (lower panel) comprising astronomic constituents, wind related surge, external surge and residual set up as well as wind speed

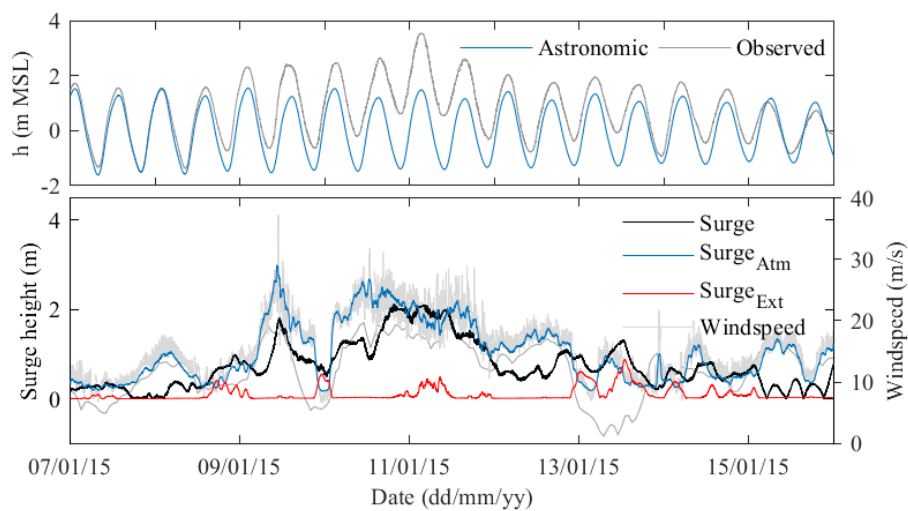


Figure A.3: Tidal water level observation during Elon (upper panel) and single components (lower panel) comprising astronomic constituents, wind related surge, external surge and residual set up as well as wind speed

## A.5 Barometric deep sea surge potential

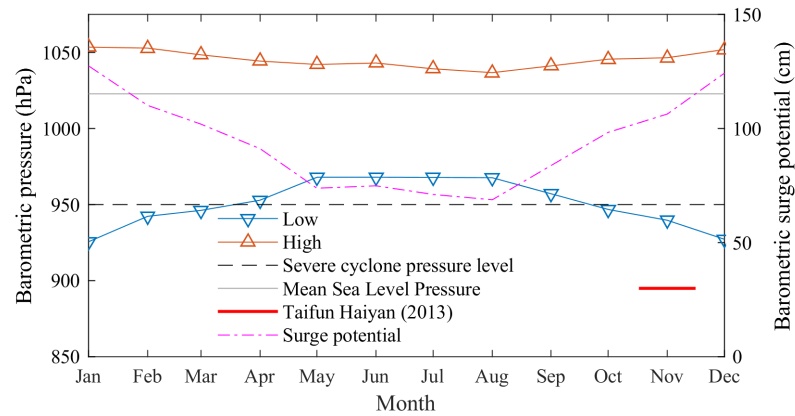


Figure A.4: Barometric pressure and external surge potential based on observations in the United Kingdom (Burt, 2007). The extreme low pressure Tayphoon Haiyan in 2013 is given as reference



### A.6 Sectional Weser fairway

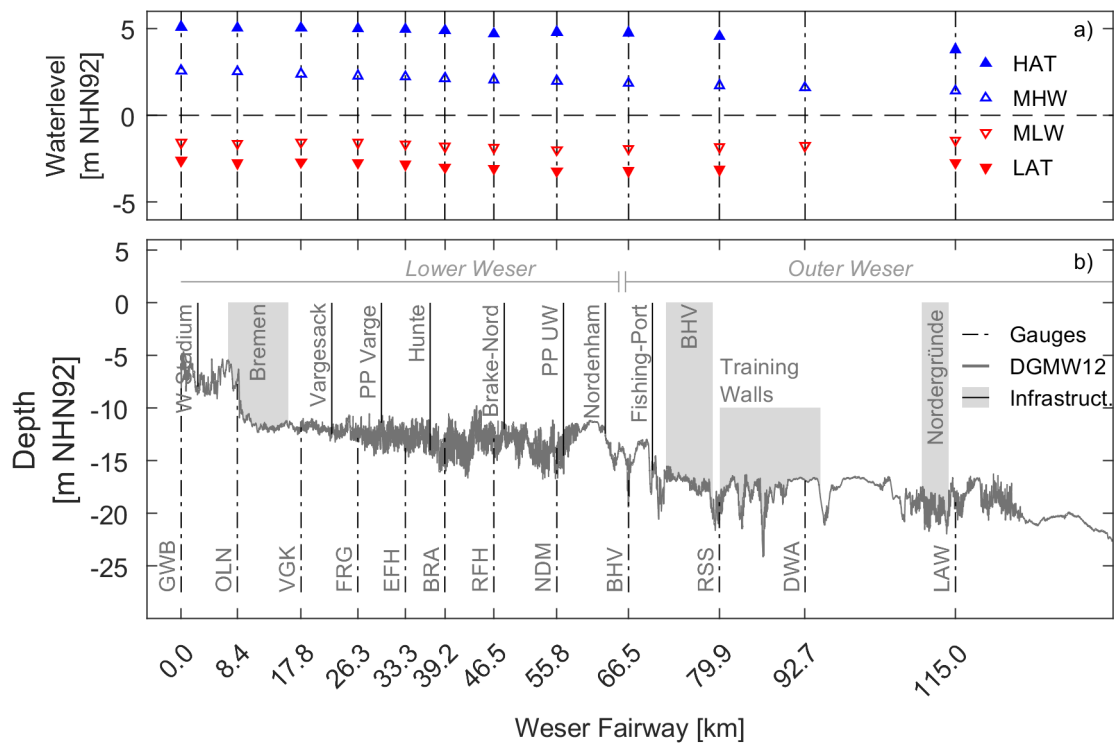


Figure A.5: Outer and Lower Weser fairway with hydraulic works a) and associated tidal-parameters b). Bulk-terminals, Ports and other critical infrastructure are marked below the fairway in a). Gauges are marked above the bed, with islands marked in *italic*. Depth is based on the Digital terrain model of the waterbody (DTMW) 2012. Tidal parameters in b) are derived from tide gauge data of the WSV (2018b).

### A.7 Multibeam survey of Wilhelmshaven New Outer Harbour

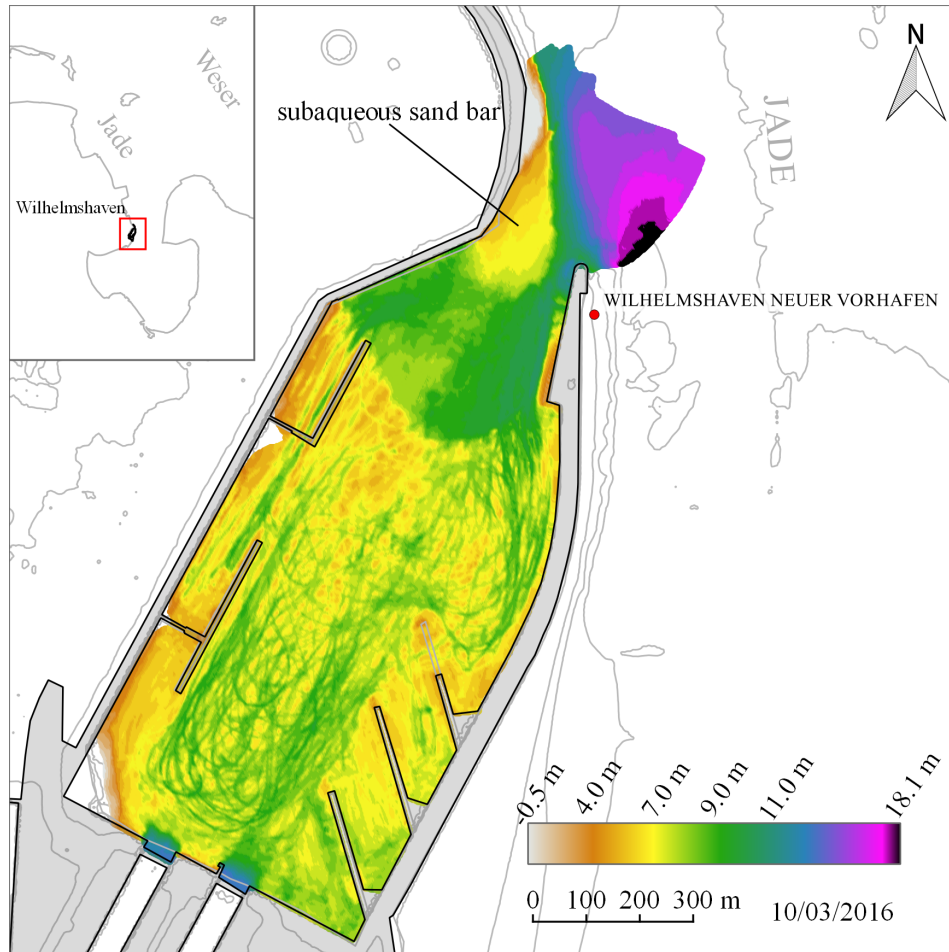


Figure A.6: Wilhelmshaven New Outer Harbour survey of 10/03/2016 revealing the formation of a subaqueous bar in the harbor entrance.

### A.8 Scour measurement between the ECTW and the BTW

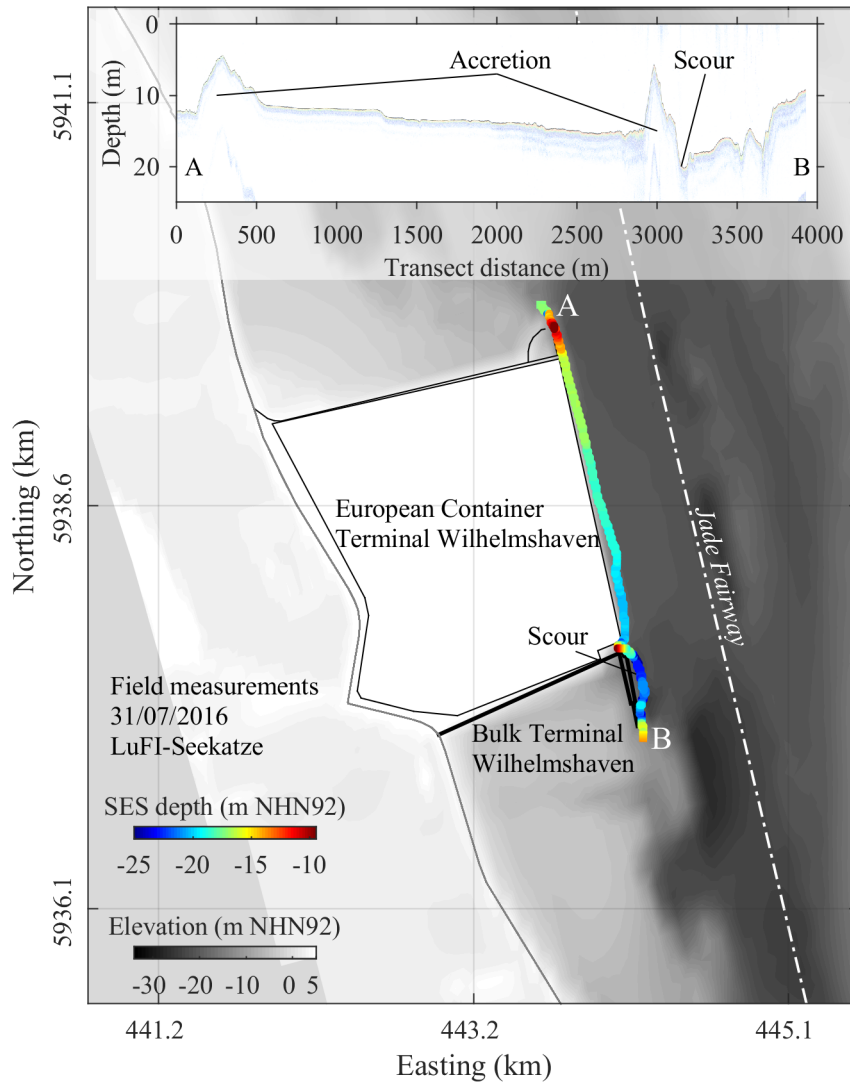


Figure A.7: European Container Terminal Wilhelmshaven survey conducted with the research vessel *Seekatze* of the Ludwig-Franzius-Institute for Hydraulic, Estuarine and Coastal Engineering deploying a sub-bottom profiler of type Innomar SES-2000 compact for depth measurements. The survey reveal a local scour between the ECTW and the adjacent BTW dropping 4.5 m. Data was provided by the WSV (2018b).

## A.9 Simulation results for Wilhelmshaven

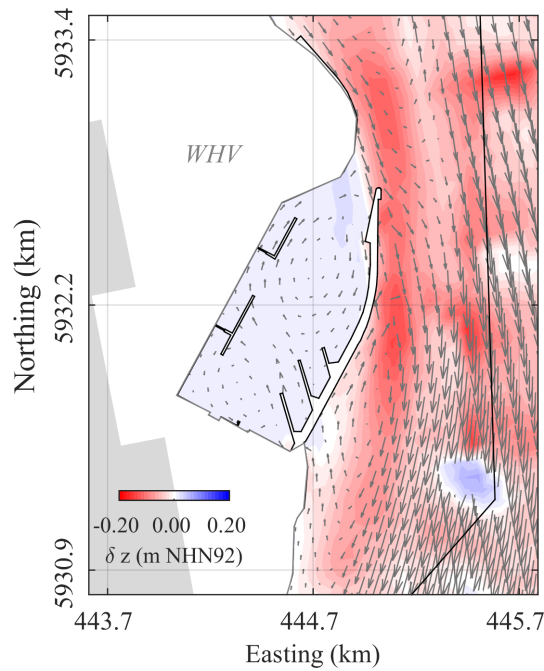


Figure A.8: New Outer Harbour Wilhelmshaven simulation results for Xaver under extreme compound scenario conditions. Areal accretion of 0.15 m with a sub-aqueous overslaugh at the entrance.

## A.10 Summary terms for evidence and agreement

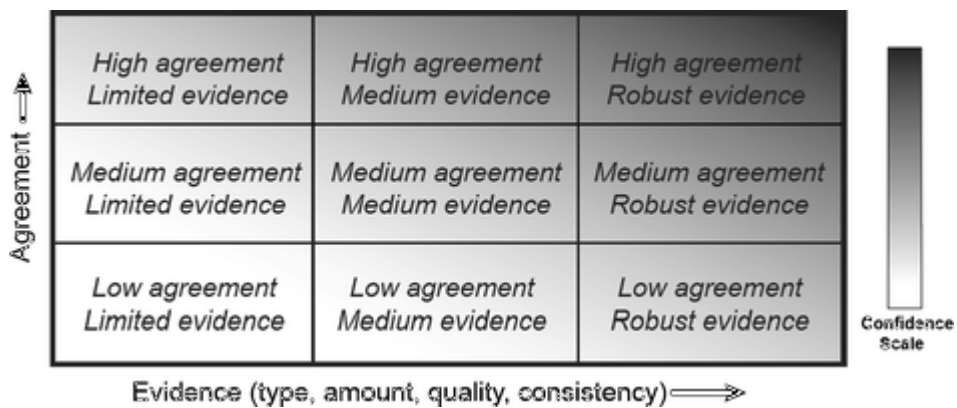


Figure A.9: A depiction of evidence and agreement statements and their relationship to confidence. The nine possible combinations of summary terms for evidence and agreement are shown, along with their flexible relationship to confidence. In most cases, evidence is most robust when there are multiple, consistent independent lines of high-quality evidence. Confidence generally increases towards the top-right corner as suggested by the increasing strength of shading. Figure reproduced and legend adapted from Mastrandrea et al. (2011).

## A.11 KRITIS threshold definitions

### Energy supply (oil & coal)

The threshold for oil refinery volume is calculated according to:

$$420,000t = 0.84\text{tyr}^{-1}\text{PE}^{-1} \cdot 500,000\text{PE} \quad (\text{A.11.1})$$

and is based on an average annual consumption of  $0.84\text{tyr}^{-1}$  per PE (BSI 2017, p.7, para. 10). The value is applied as threshold for the Wilhelmshaven Refinery Terminal (WRT) in table 2.4.1.

The threshold for oil terminal turnover volume is calculated according to:

$$4,400,000t = \frac{620,000\text{tyr}^{-1}}{0.14\text{tyr}^{-1}\text{PE}^{-1}} \quad (\text{A.11.2})$$

and is based on the assumption that approximately 1.4 t are needed to produce enough medium fuel oil to supply one PE for one year resulting in 620,000t for 500.000PE and the conversion factor of 0.14 t medium fuel oil per ton crude oil (BSI 2017, p.7, para. 12). This threshold is also applied to the bulk coal terminal Wilhelmshaven.

### Logistics (maritime trade)

The volume threshold for traffic centers of maritime trade (major ports) is calculated as follows:

$$1,875,000\text{tyr}^{-1} = 3.75\text{tyr}^{-1}\text{PE}^{-1} \cdot 500,000 \quad (\text{A.11.3})$$

taking into consideration the average annual freight supply volume per PE of 3.75 t in combination with a defined norm population number of 500,000 (BSI 2017, p. 27, para. 8). This value is applied to the Port of Wilhelmshaven in table 2.4.1.

The critical threshold for maritime goods traffic infrastructure (container terminals) is calculated according to:

$$17,000,000\text{tyr}^{-1} = 34\text{tyr}^{-1}\text{PE}^{-1} \cdot 500,000\text{PE} \quad (\text{A.11.4})$$

utilising the assumption of annually required  $34\text{tPE}^{-1}$  of goods to supply any one person with a base value of 500.000 people as reference (BSI 2017, p. 27, para. 10).

## A.12 Residual storm surge currents

Christian

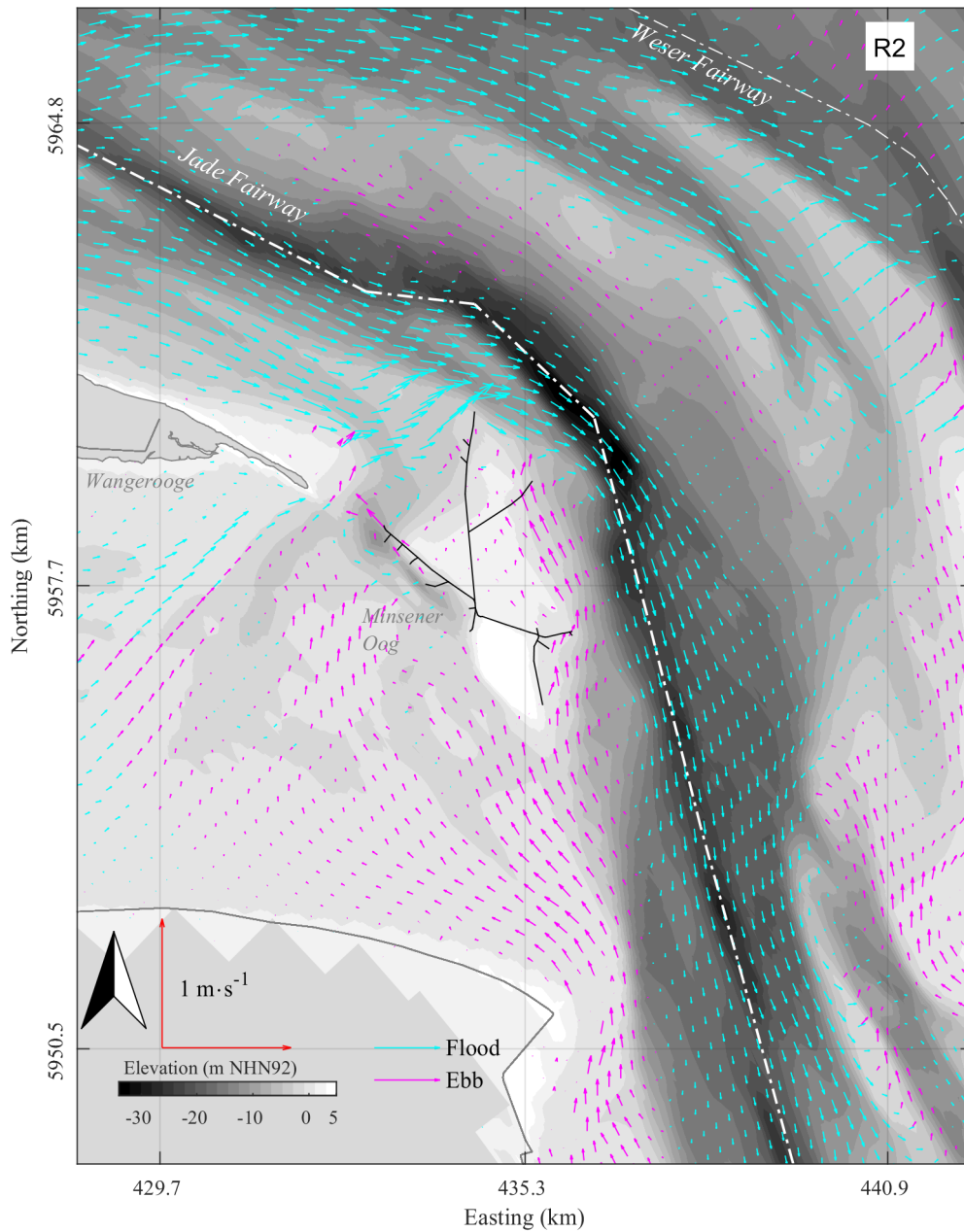


Figure A.10: Simulated residual depth averaged currents for European Windstorm Christian with all metocean processes for the reference scenario focus area 1.

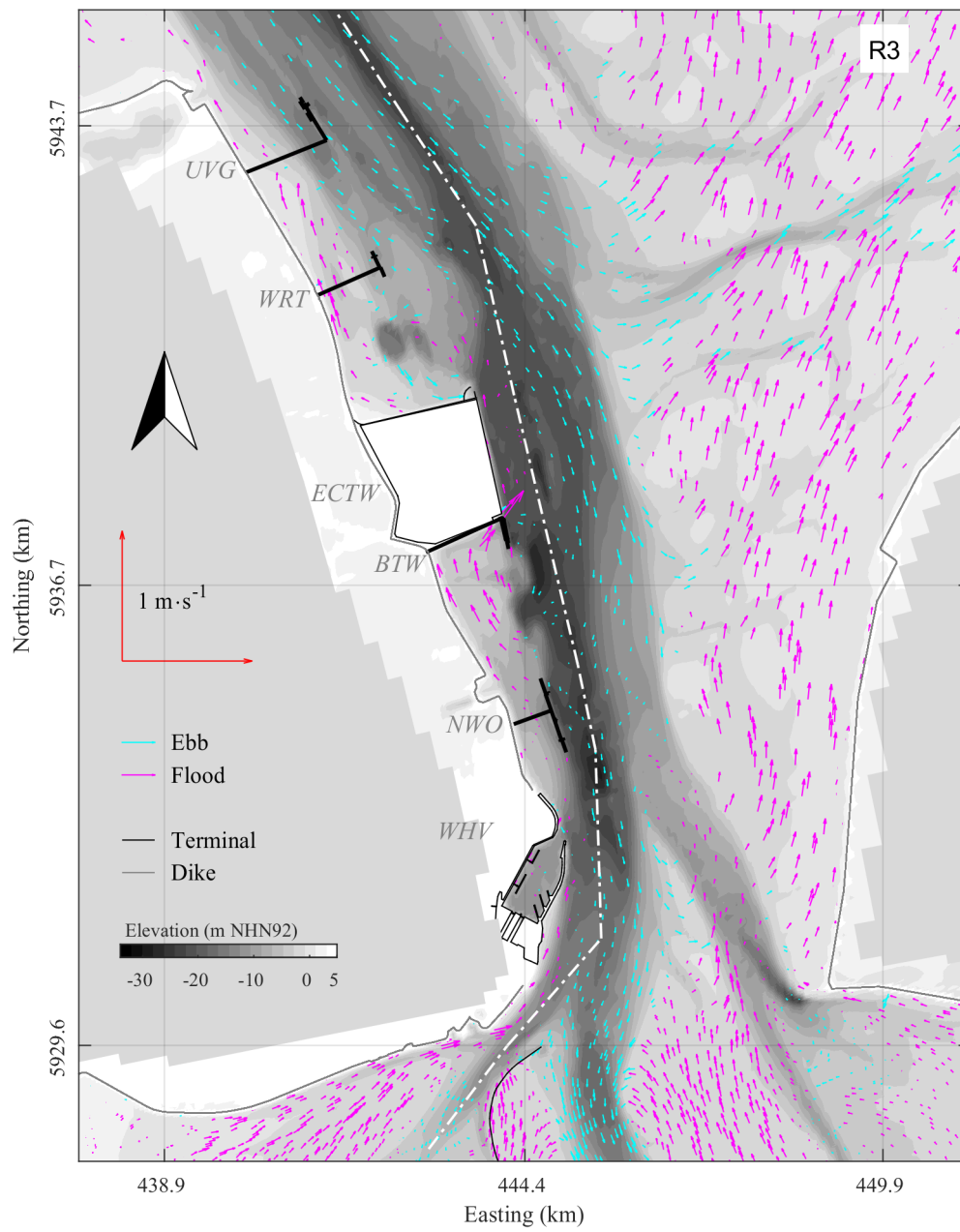


Figure A.11: Simulated residual depth averaged currents for European Windstorm Christian with all metocean processes for the reference scenario focus area 2.

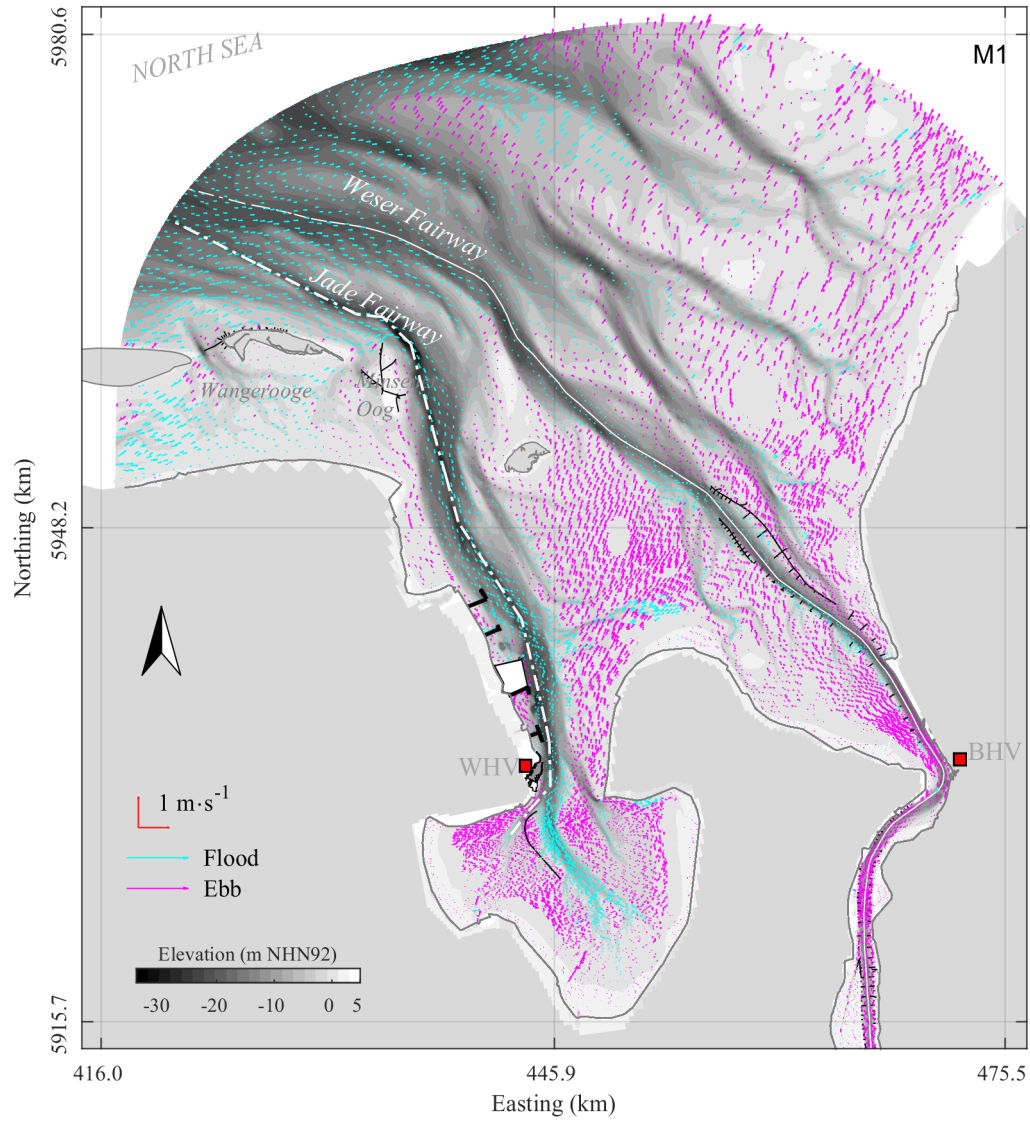


Figure A.12: Simulated residual depth averaged currents for European Windstorm Christian with all metocean processes for the medium scenario.



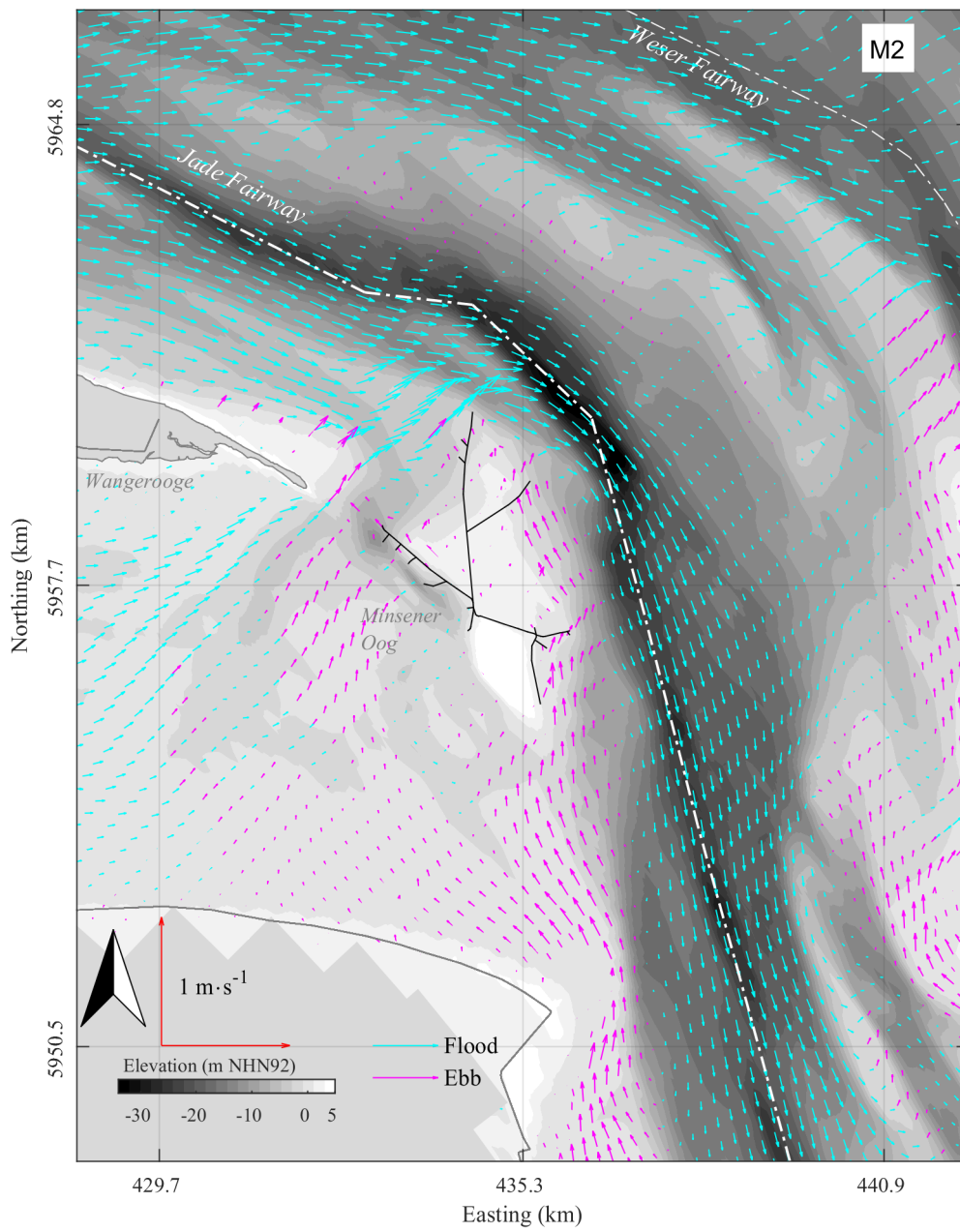


Figure A.13: Simulated residual depth averaged currents for European Windstorm Christian with all metocean processes for the medium scenario focus area 1.

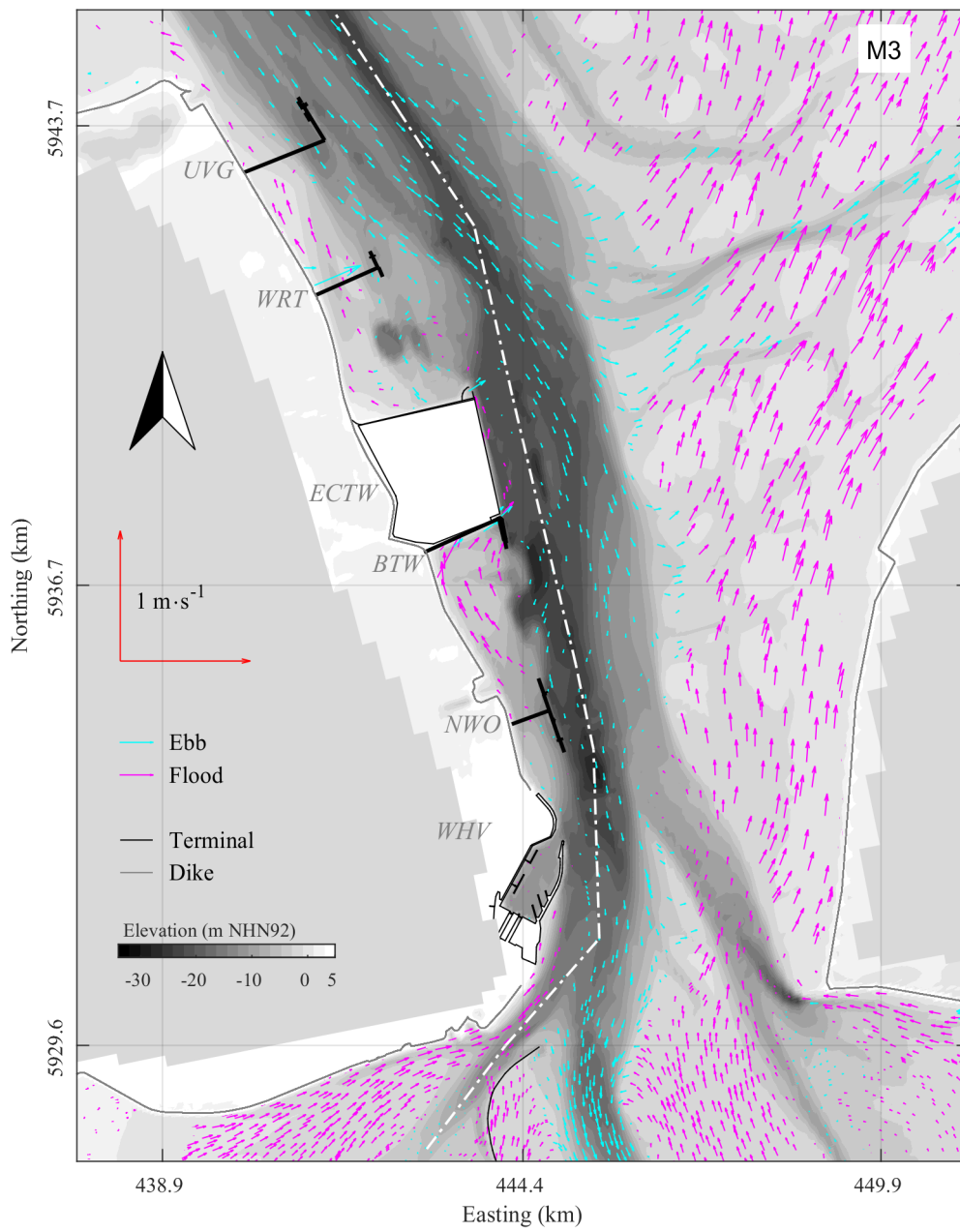


Figure A.14: Simulated residual depth averaged currents for European Windstorm Christian with all metocean processes for the medium scenario focus area 2.

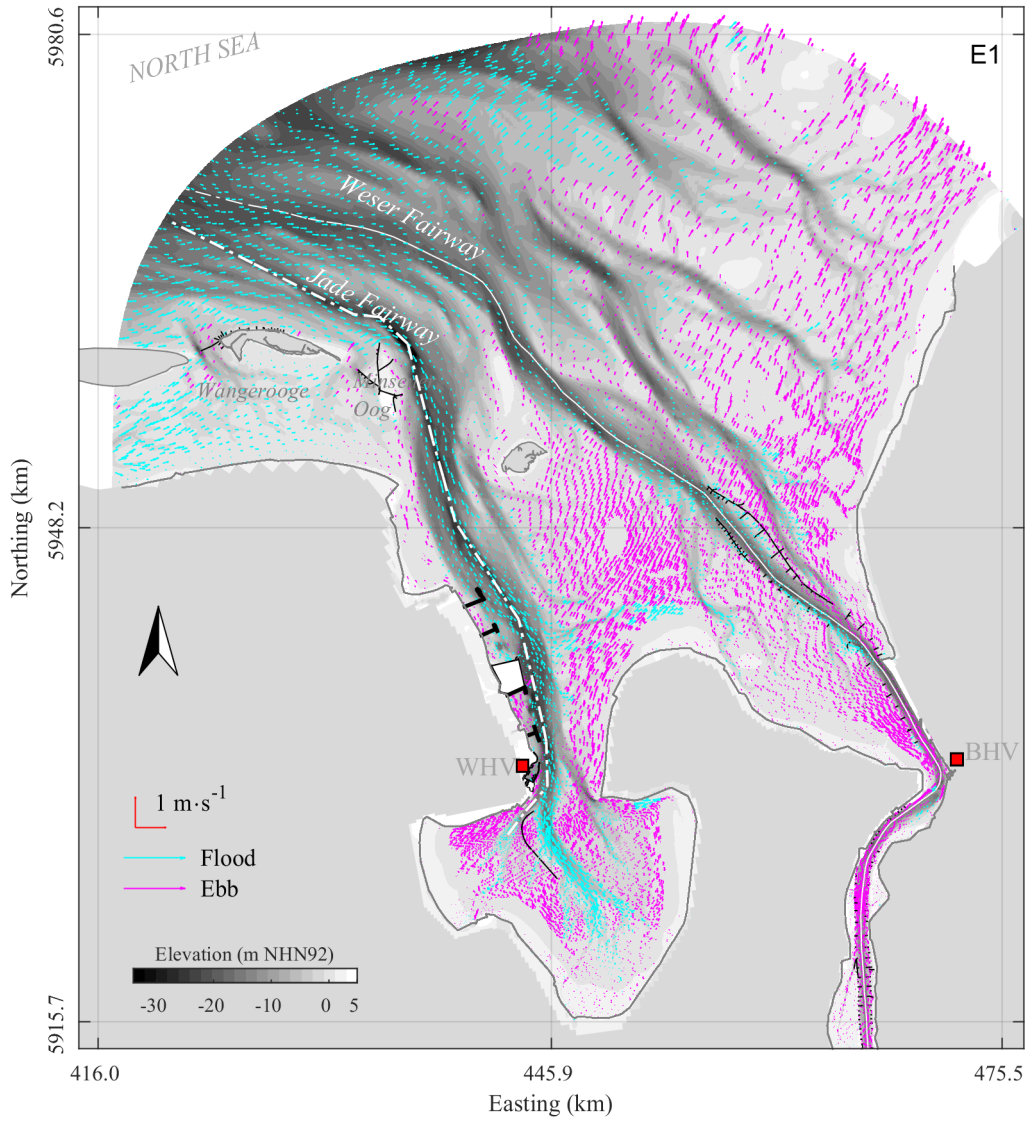


Figure A.15: Simulated residual depth averaged currents for European Windstorm Christian with all metocean processes for the extreme scenario.

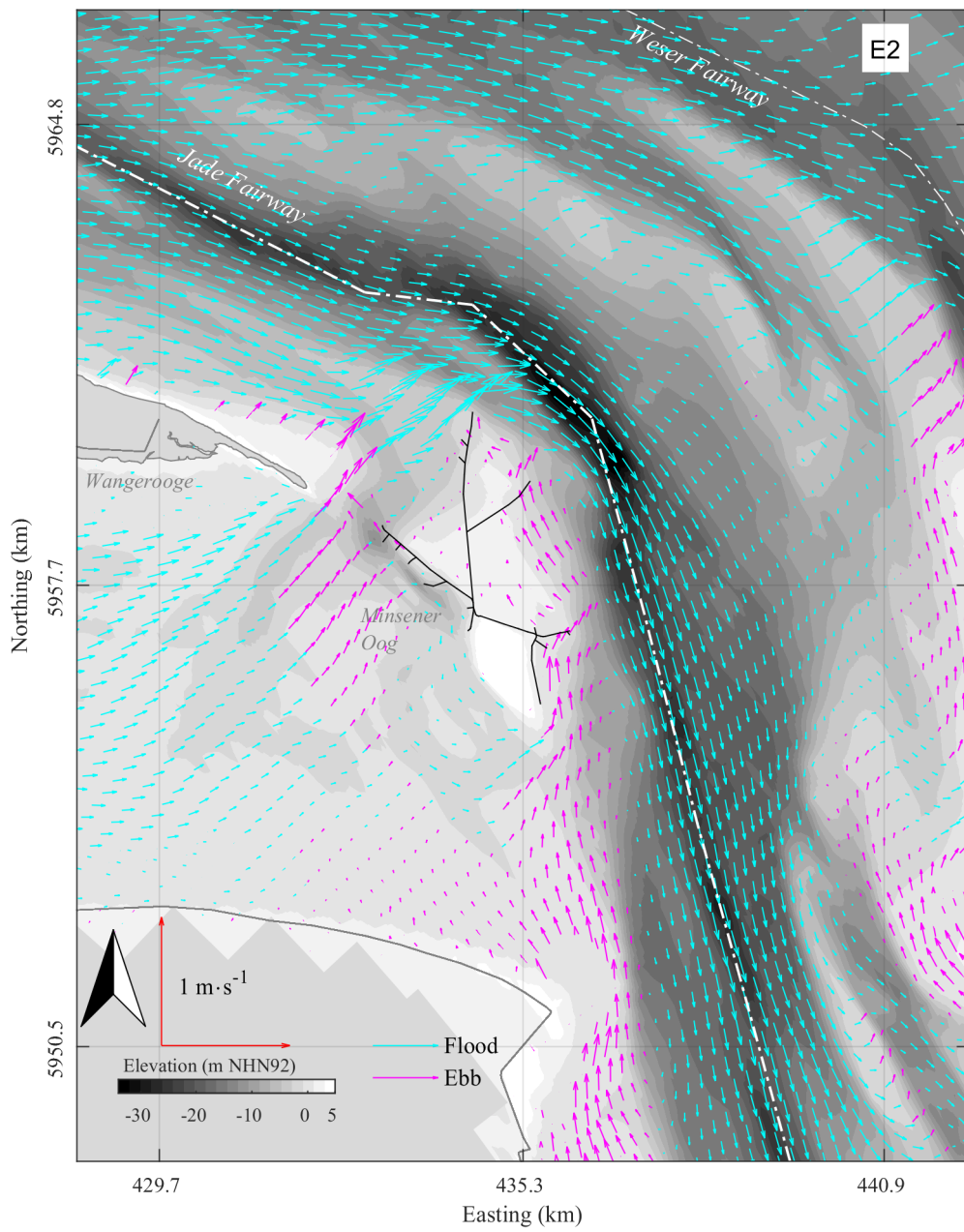


Figure A.16: Simulated residual depth averaged currents for European Windstorm Christian with all metocean processes for the extreme scenario focus area 1.

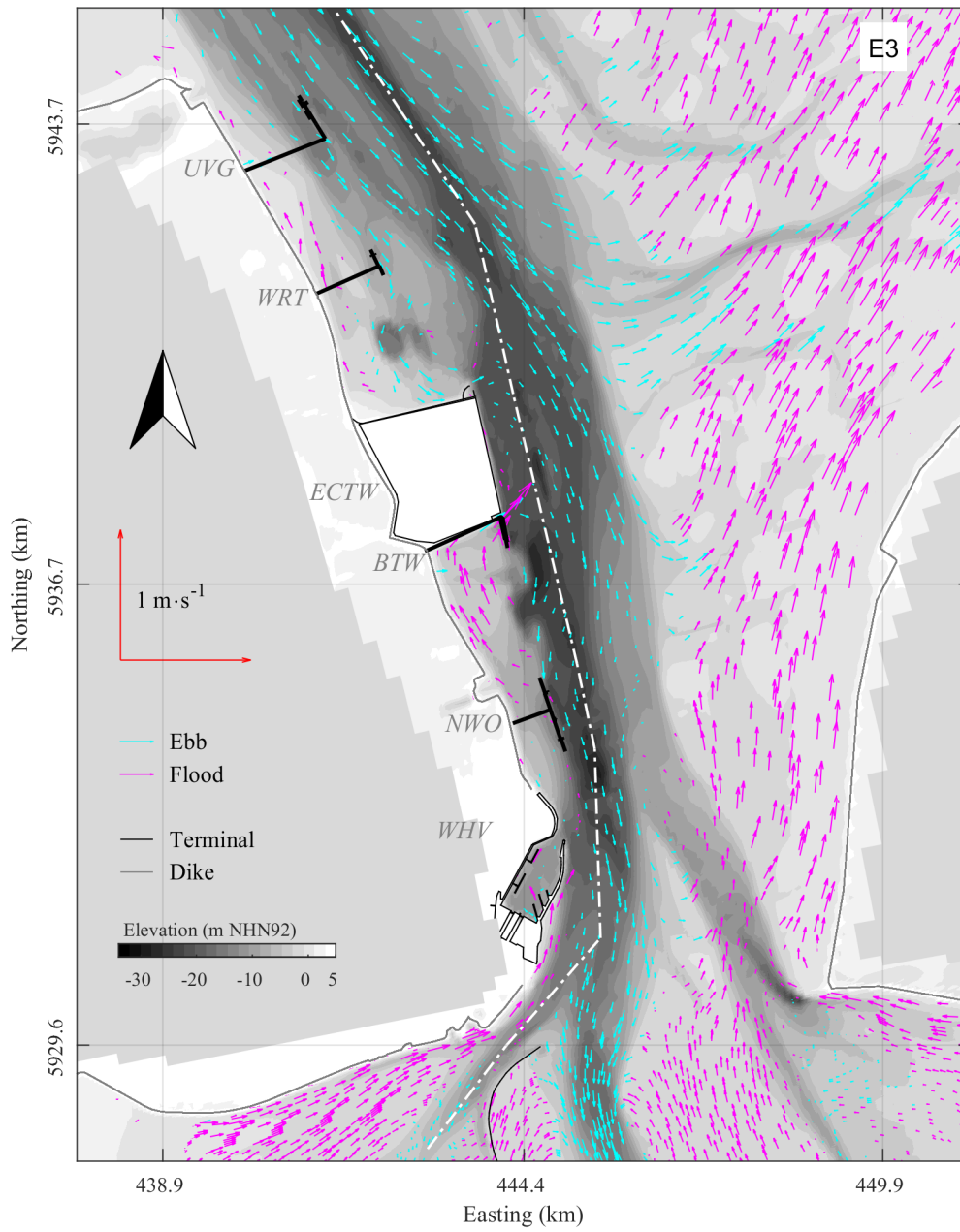


Figure A.17: Simulated residual depth averaged currents for European Windstorm Christian with all metocean processes for the extreme scenario focus area 2.

Xaver

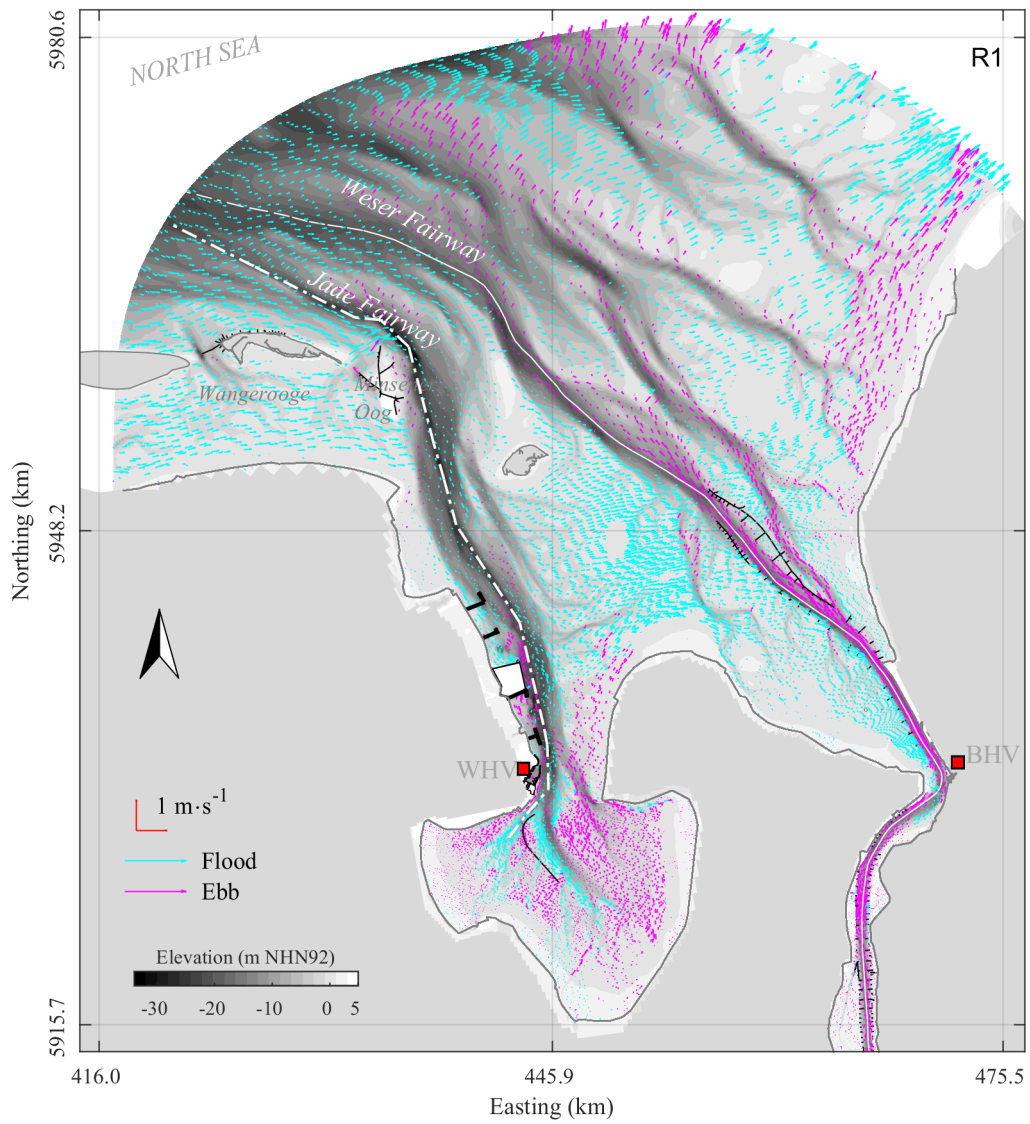


Figure A.18: Simulated residual depth averaged currents for European Windstorm Xaver with all metocean processes for the reference scenario.

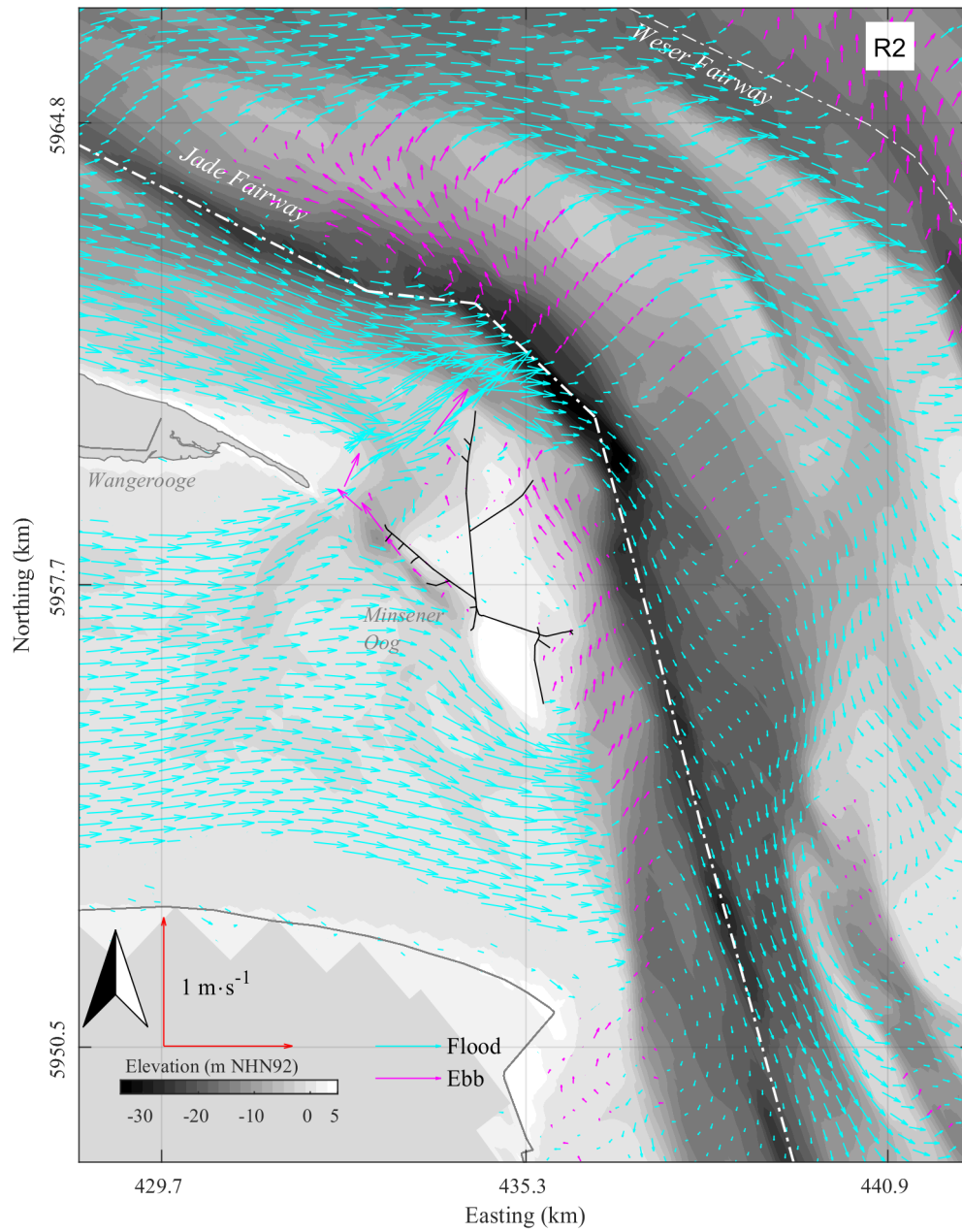


Figure A.19: Simulated residual depth averaged currents for European Windstorm Xaver with all metocean processes for the reference scenario focus area 1.

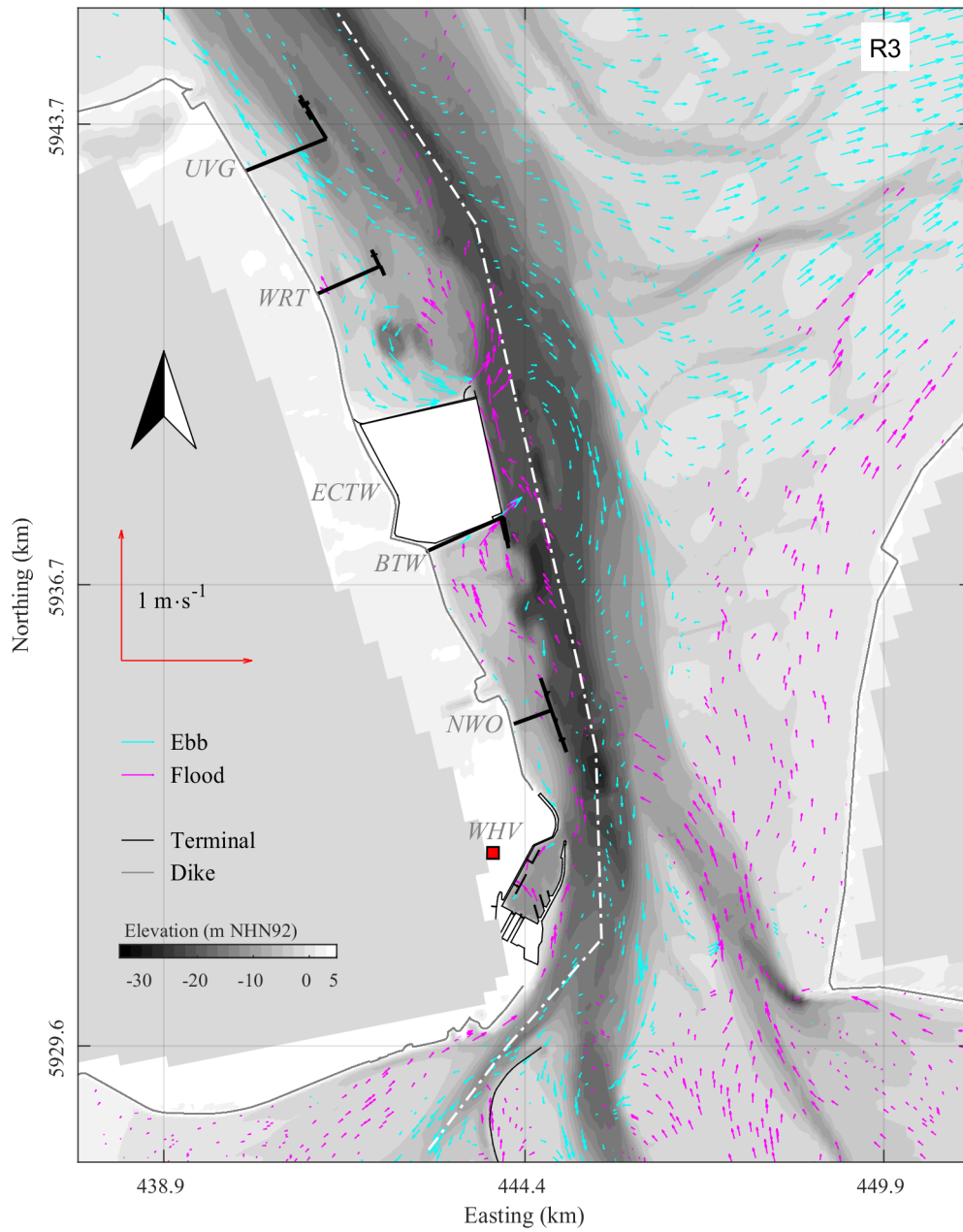


Figure A.20: Simulated residual depth averaged currents for European Windstorm Xaver with all metocean processes for the reference scenario focus area 2.



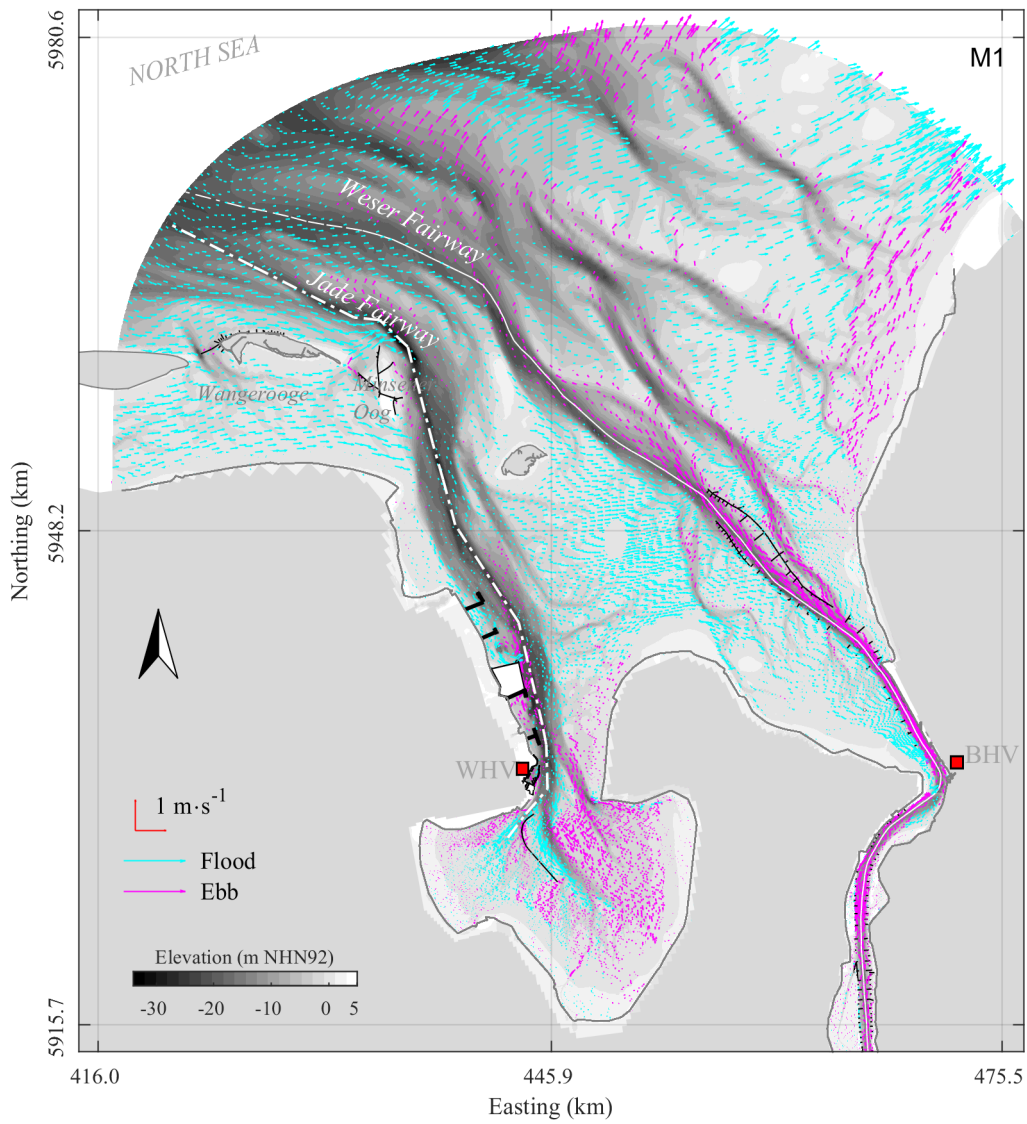


Figure A.21: Simulated residual depth averaged currents for European Windstorm Xaver with all metocean processes for the medium scenario.

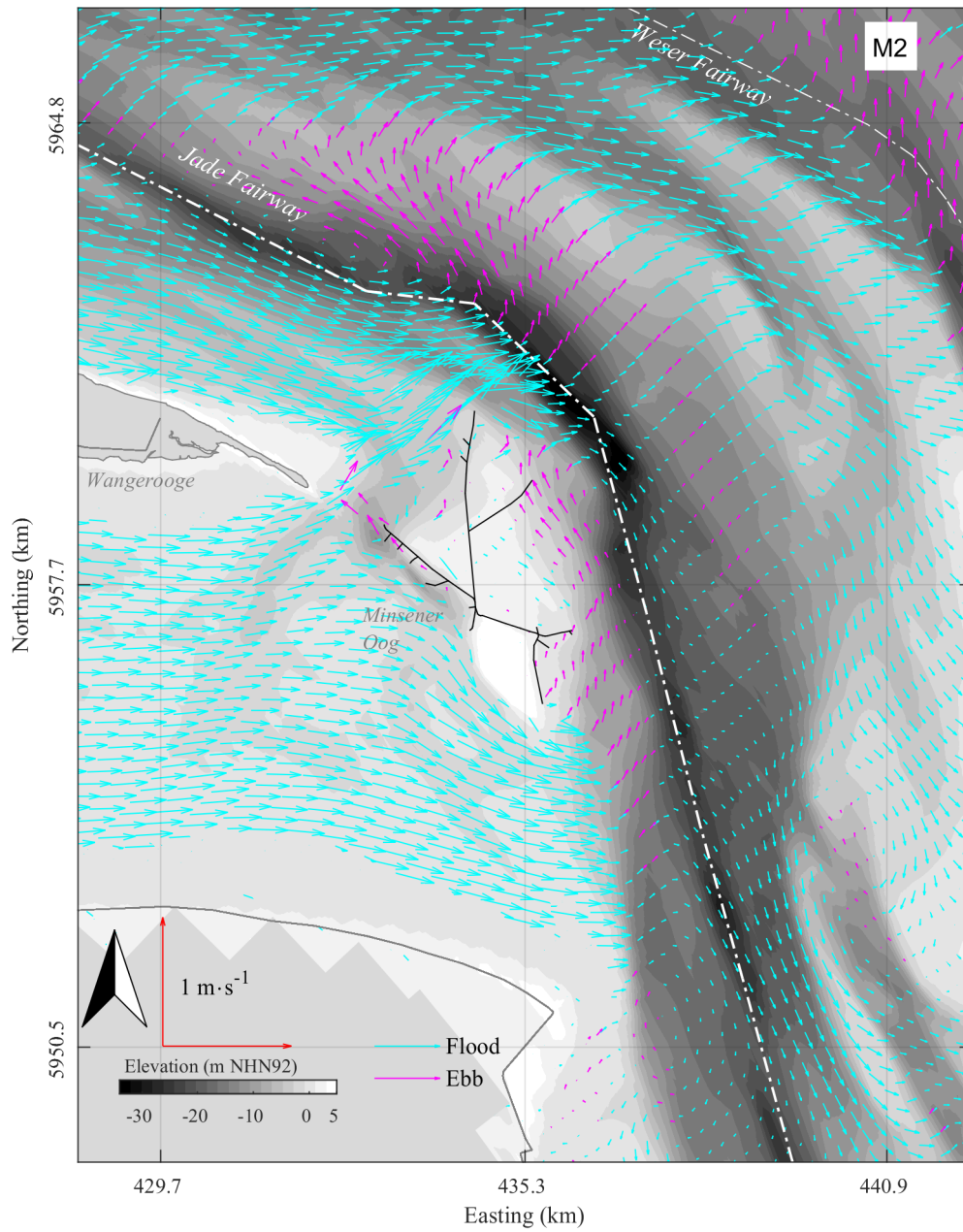


Figure A.22: Simulated residual depth averaged currents for European Windstorm Xaver with all metocean processes for the medium scenario focus area 1.

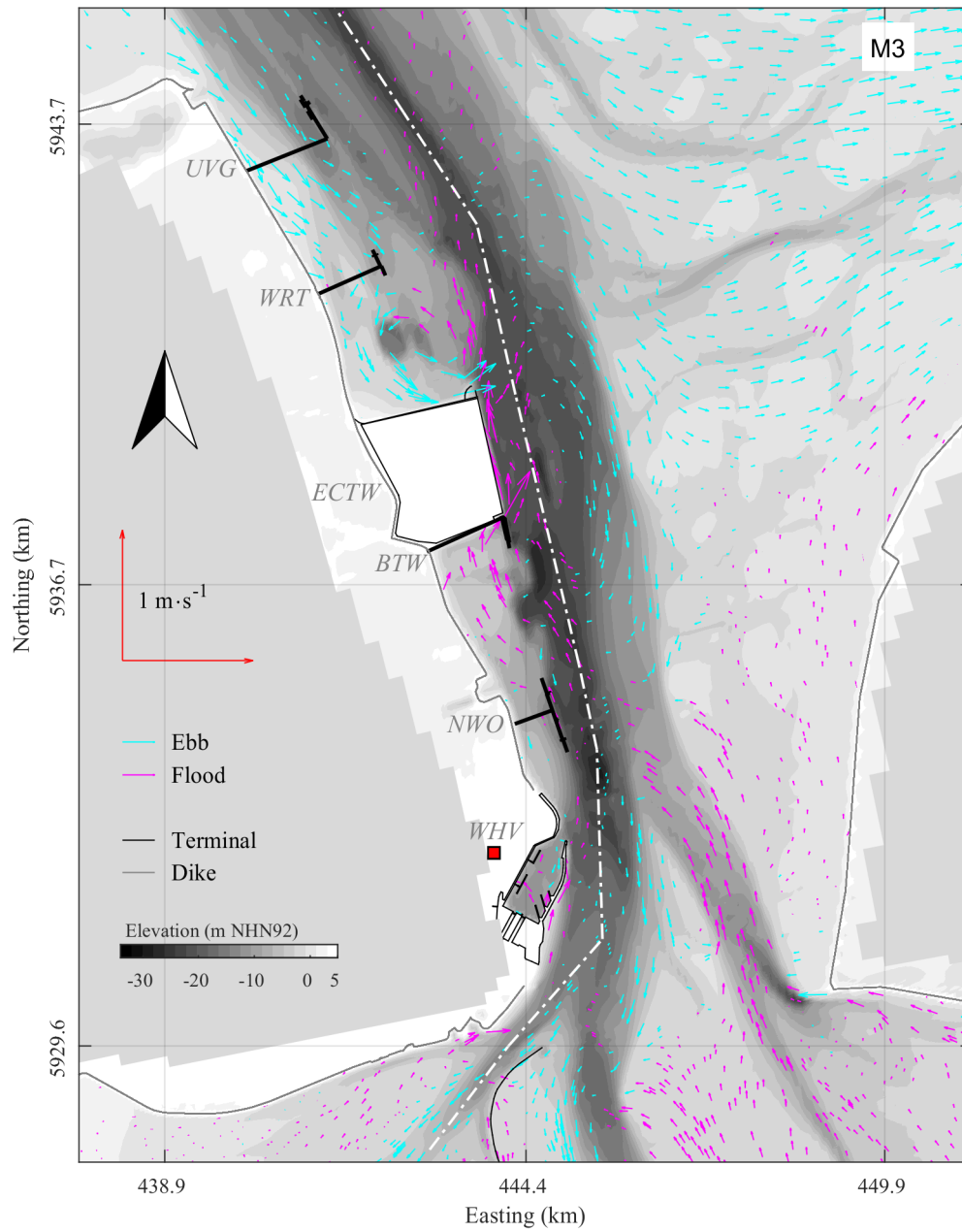


Figure A.23: Simulated residual depth averaged currents for European Windstorm Xaver with all metocean processes for the medium scenario focus area 2.

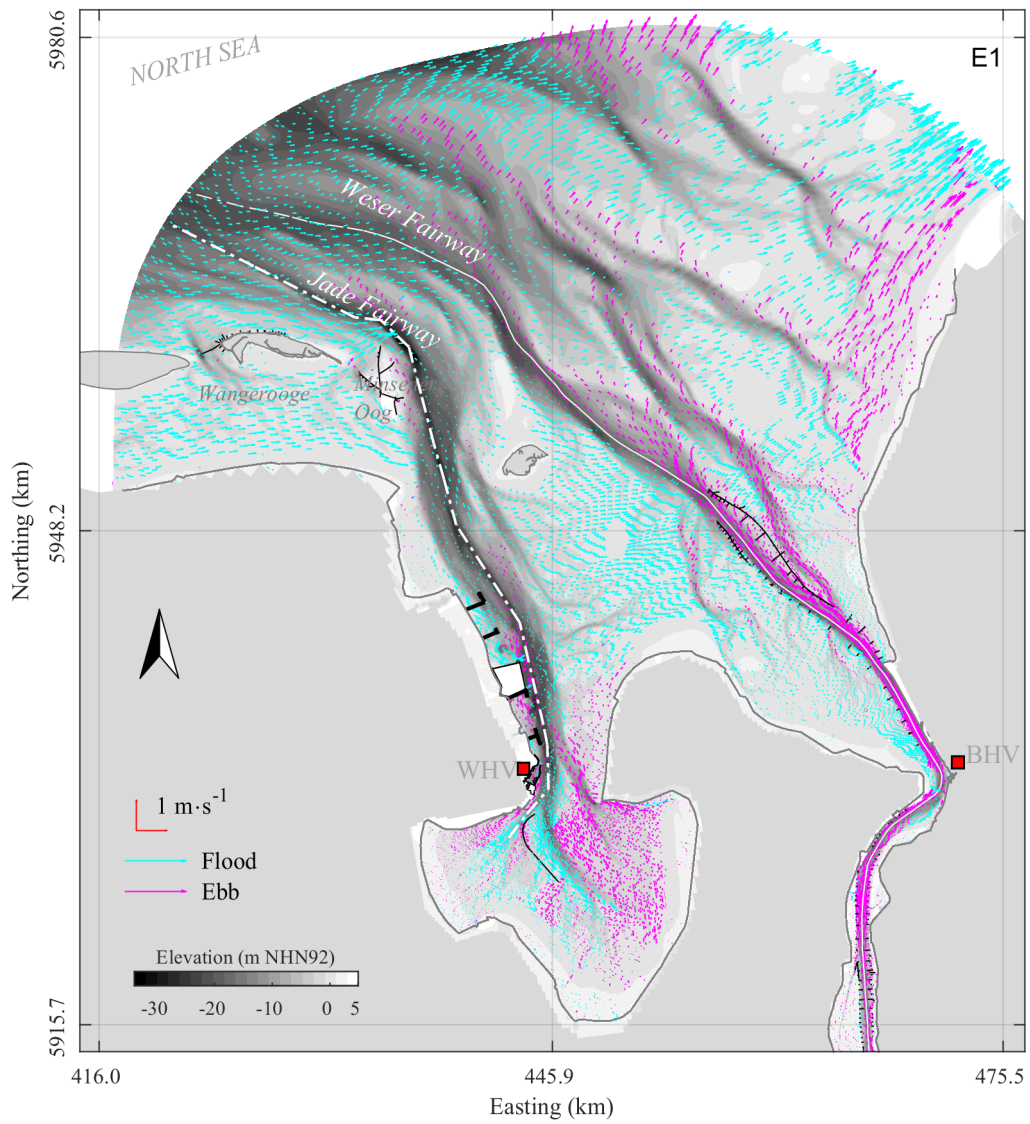


Figure A.24: Simulated residual depth averaged currents for European Windstorm Xaver with all metocean processes for the extreme scenario.

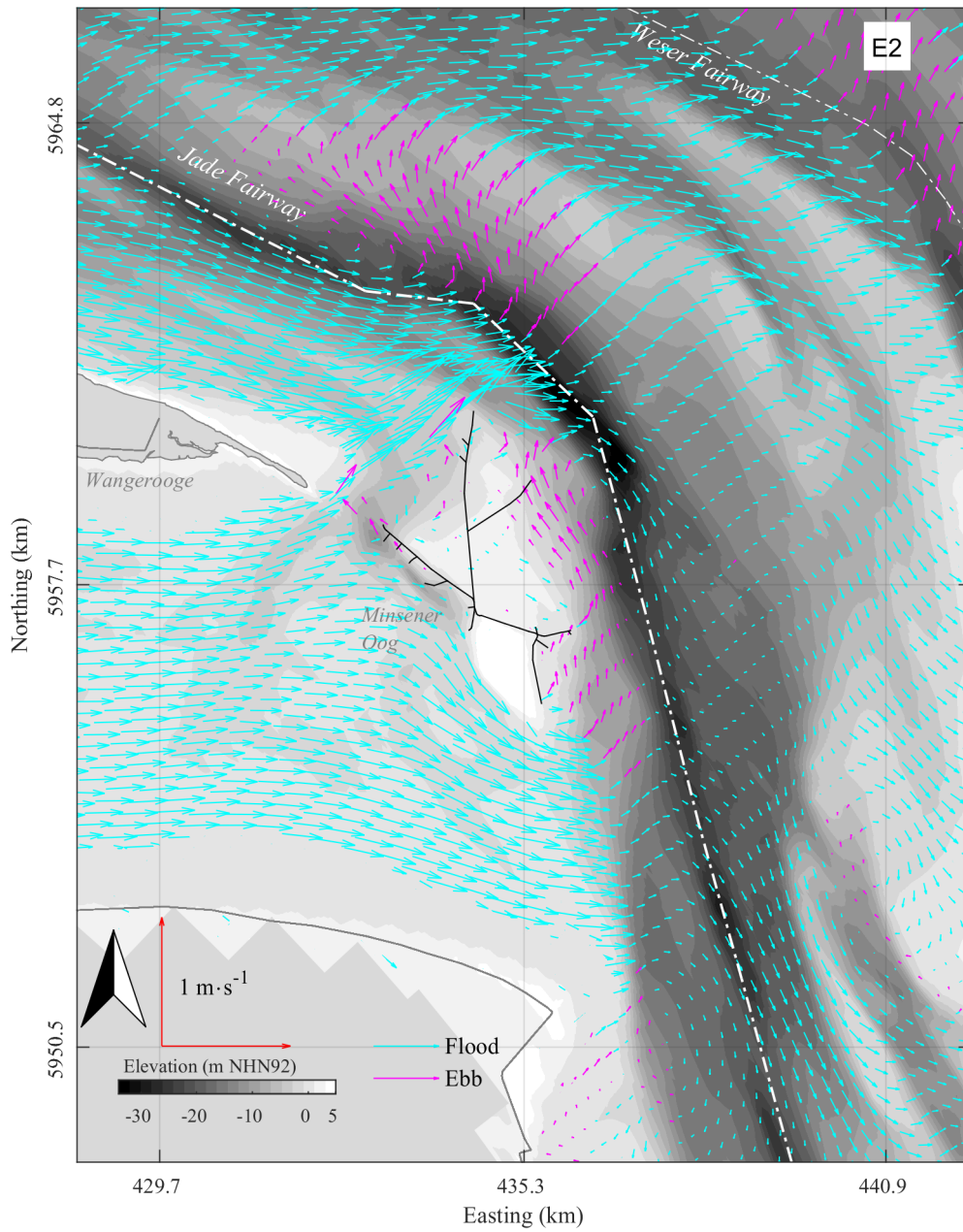


Figure A.25: Simulated residual depth averaged currents for European Windstorm Xaver with all metocean processes for the extreme scenario focus area 1.

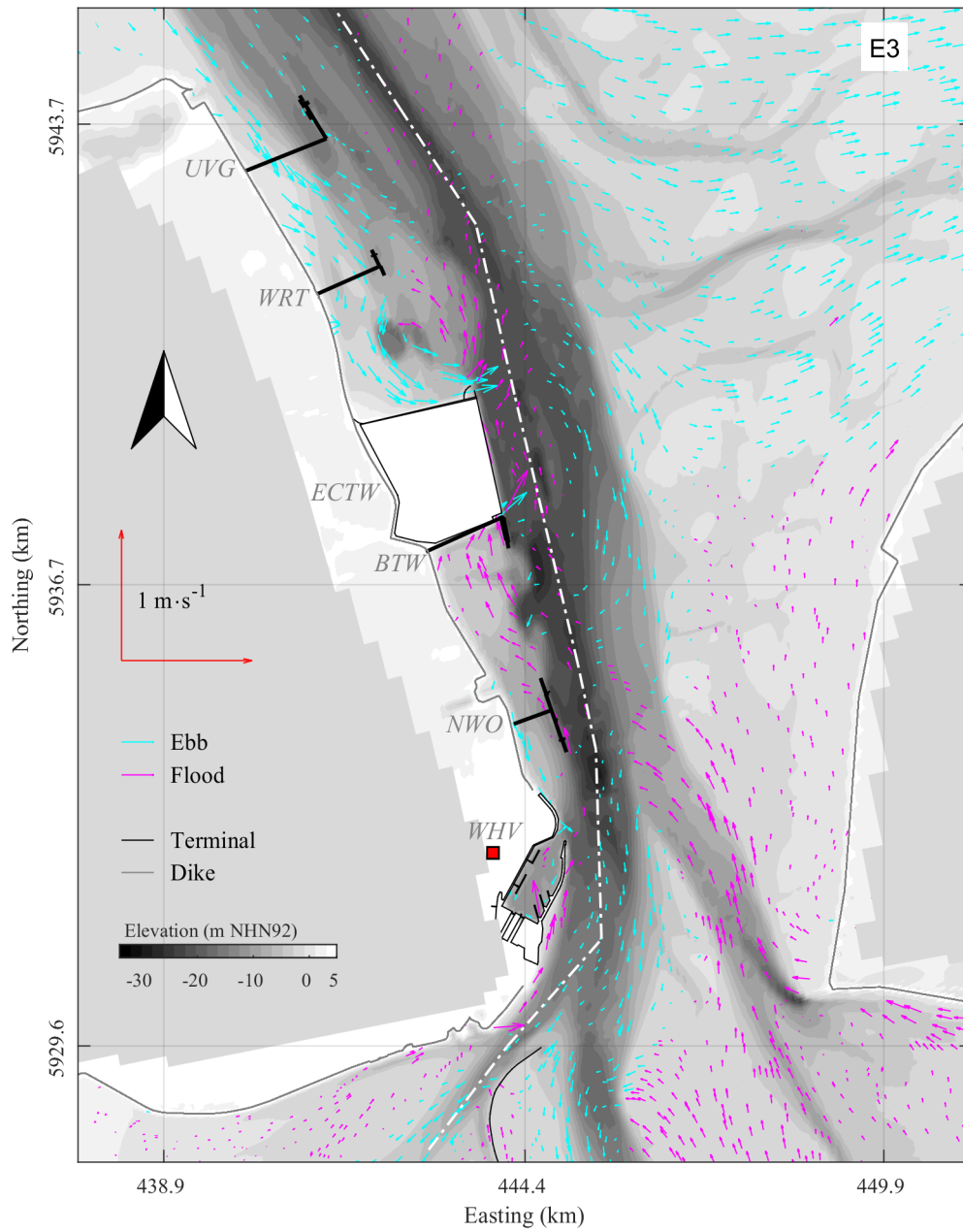


Figure A.26: Simulated residual depth averaged currents for European Windstorm Xaver with all metocean processes for the extreme scenario focus area 2.

### A.13 Hydraulic intervention scenario

#### Christian

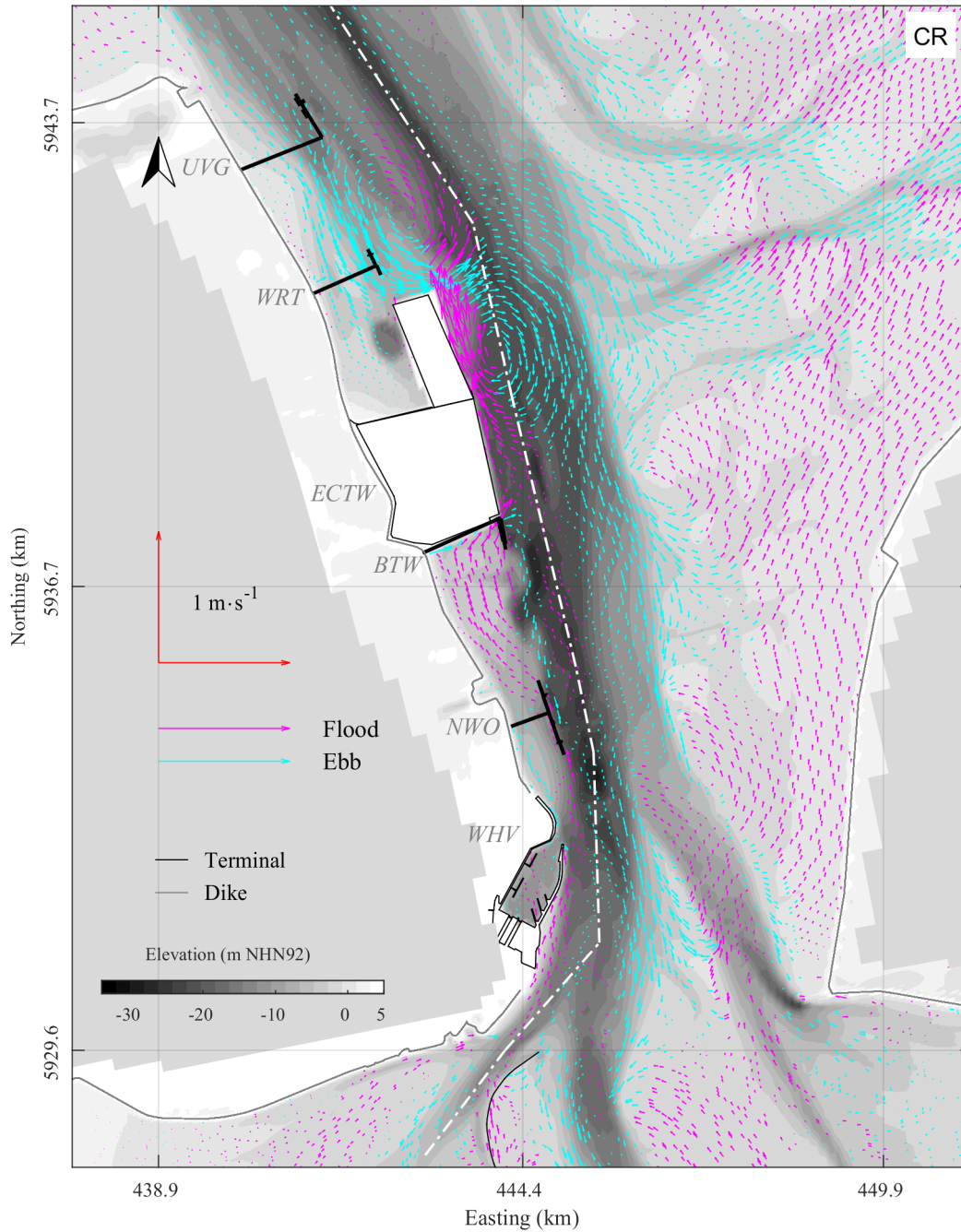


Figure A.27: Residual currents in the hydraulic intervention scenario for European Windstorm Christian for the reference scenario.

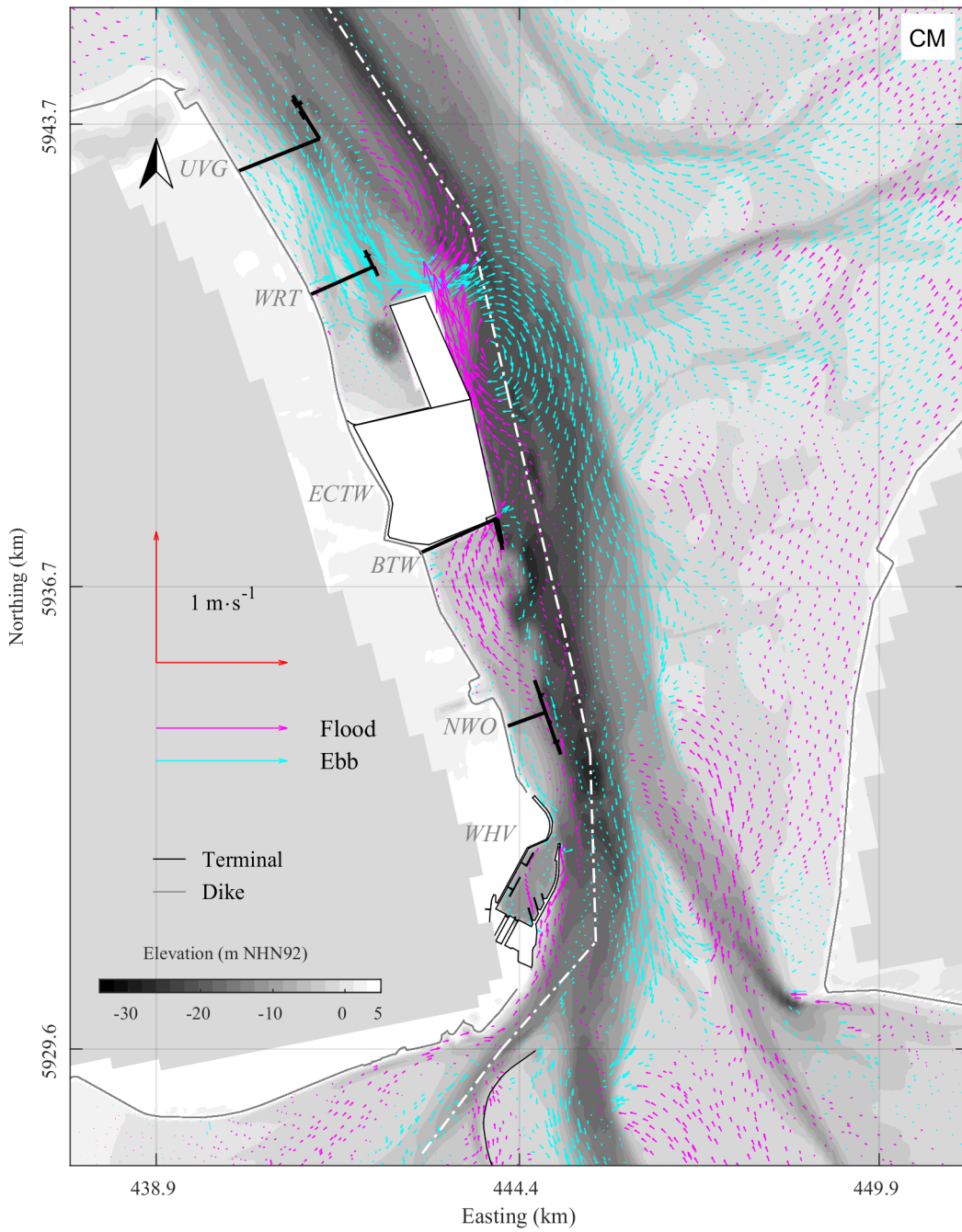


Figure A.28: Residual currents in the hydraulic intervention scenario for European Windstorm Christian for the medium scenario.



Xaver

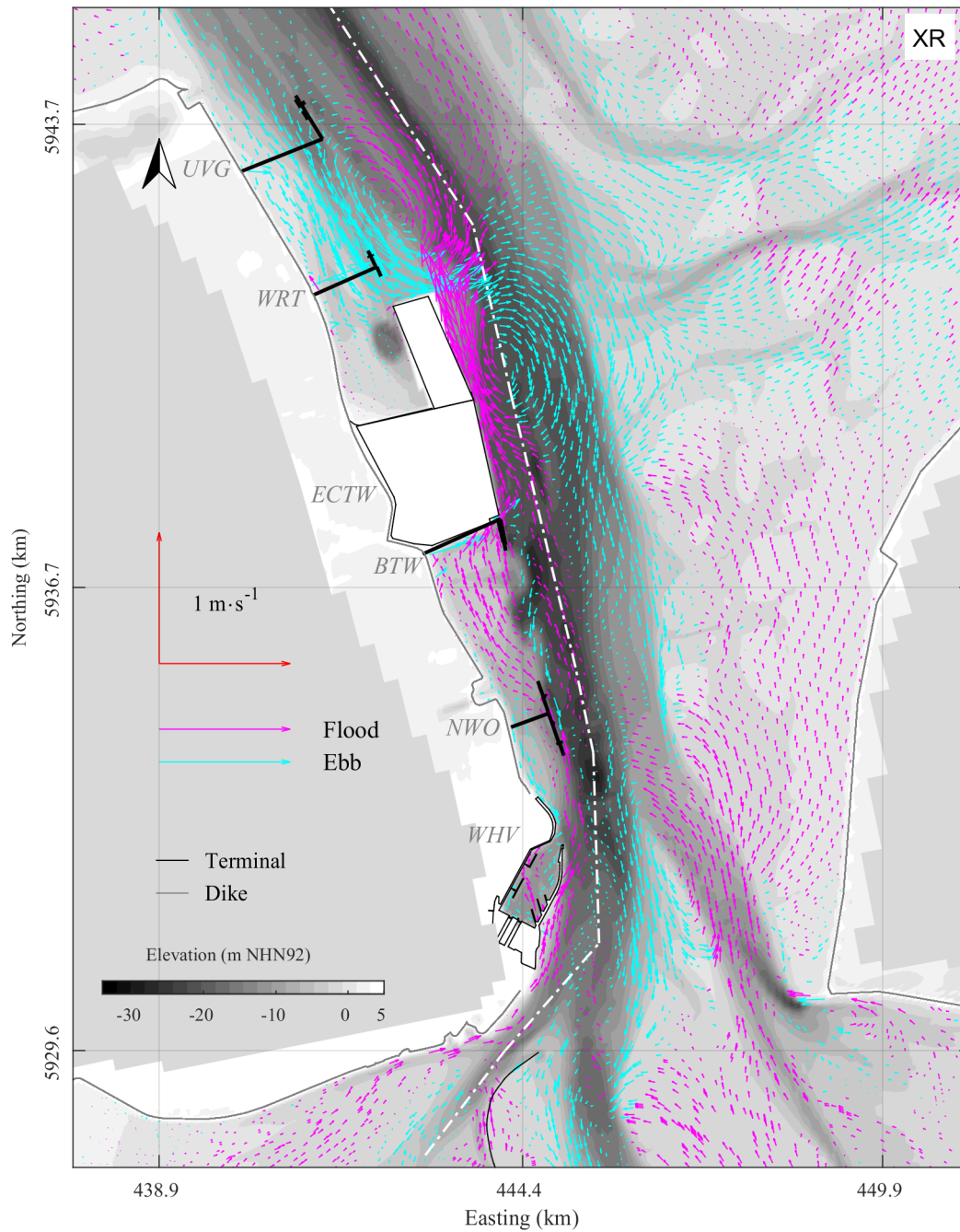


Figure A.29: Residual currents in the hydraulic intervention scenario for European Windstorm Xaver for the reference scenario.

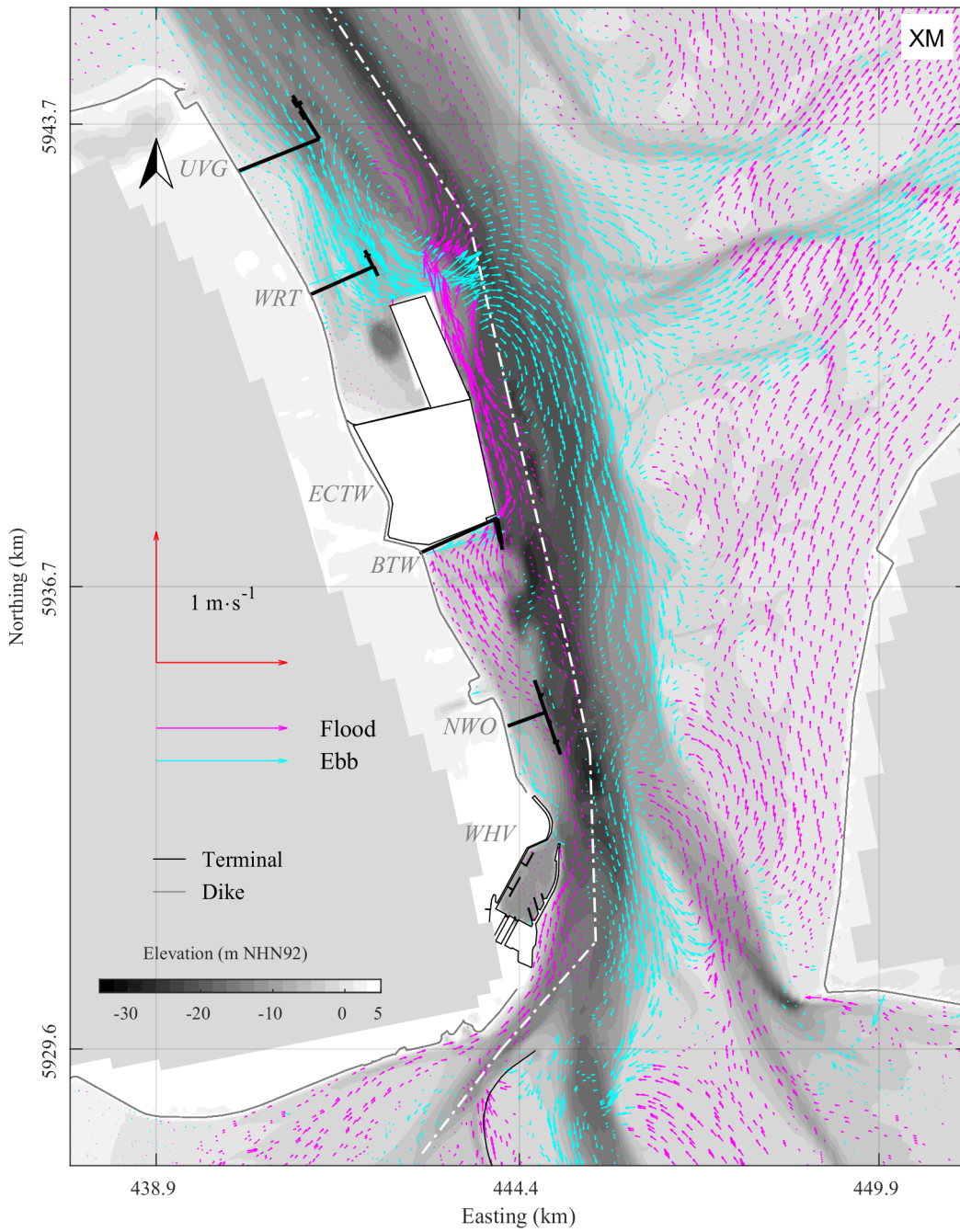


Figure A.30: Residual currents in the hydraulic intervention scenario for European Windstorm Xaver for the medium scenario.